I am among those who think that science has great beauty. A scientist in his laboratory is not only a technician: he is also a child placed before natural phenomena which impress him like a fairy tale.

– Marie Curie (1867-1934)

There are in fact two things, science and opinion; the former begets knowledge, the latter ignorance.

– Hippocrates (460 BC - 377 BC)

University of Alberta

VISCOELASTIC INSTABILITY IN ELECTRO-OSMOTICALLY PUMPED ELONGATIONAL MICROFLOWS

by

Robert Mark Bryce

A thesis submitted to the Faculty of Graduate Studies and Research in
partial fulfillment of the requirements for the degree of

Doctor of Philosophy.

Department of Physics

Spring 2010
Edmonton, Alberta

Examining Committee

Dr. Mark Freeman, Physics

Dr. Jed Harrison, Chemistry

Dr. Richard Sydora, Physics

Dr. Ying Tsui, Electrical and Computer Engineering

Dr. Lorenz Sigurdson, Mechanical Engineering

Dr. Kari Dalnoki-Veress, Physics, McMaster University

Abstract

The focus of this thesis is on electro-osmotically pumped flow of viscoelastic fluids through microchannels.

Fluid transport in microscaled structures is typically laminar due to the low Reynolds numbers involved. However, it is known that viscoelastic polymeric liquids can display striking instabilities in low Reynolds number flows.

The motion of polymer doped solutions electrically pumped through microchannels is studied at low Reynolds number. It is found that extensional instabilities can be excited in such microflows with standard electro-osmotic pumping ($\approx$ mm/s flow rate regime), occurring at the viscoelastic instability threshold. The existence of these instabilities must inform design as microfluidic applications move beyond simple fluids towards using biological materials and other complex suspensions, many of which display elasticity. It is further found that discrete and persistent microgels are formed at sufficiently high current densities.

Prior work has found up to orders of magnitude increase in mixing rates, however additional fluid deformation effects (notably shear) exist in other studies and high viscosity solvents are used. The flows here exclude shear, a ubiquitous feature in mechanically driven cavity flows, and low viscosity solvents typical in microfluidic applications are used. The device is also highly symmetric minimizing Lagrangian chaos deformation and mixing of fluids. It is demonstrated that viscoelastic instabilities *reduce* mixing relative to low viscosity polymer-free solutions. The decrease in mixing found is consistent with the understanding that viscoelastic flows progress towards Batchelor turbulence, and demonstrates that, in contrast to common expectations, viscoelastic flows are effectively diffusion limited. Electro-osmotic pumped devices are the

ideal platform to study isolated viscoelasticity and elastic turbulence, where additional effects (such as shear, or Lagrangian deformation manipulations) can be introduced in a controlled manner allowing fundamental studies of viscoelasticity and mixing.

Besides the viscoelastic experimental observations it is shown that (1) a recently discovered instability due to density fluctuation has an analogue in polymeric fluids corresponding to the viscoelastic instability threshold, (2) inspection of correlations in microparticle image velocimetry (μ-PIV) data in unstable polymer flows reveals the relaxation time of polymer solutions, and (3) poly(ether sulfone) polymer films can act as negative electron beam resist.

Acknowledgements

We have about a pound of bacteria in our gut. Human DNA is shot through with code from other species. There is a type of mite that is thought to only live in our eyebrows. What we think of as distinctly human is often better thought of as a part of an ecosystem. And so it is with our lives and successes. What is "us" is often just the tip of the iceberg, with many people and events behind the scenes, often not even known to ourselves.

I am grateful most of all to my family - I thank Natasha and Max for bringing so much joy to my life. I thank my brother Jonathan for being one of a kind. I owe a lot to Dr. Mark Freeman, I have learned much about thinking, science, and life from you. You have helped me through hard times with understanding; to you I own the greatest gratitude. Likewise I have grown tremendously due to Dr. Ying Tsui's mentoring - seeing how you think and approach life has changed and deepened me. I thank everyone who was a member of "the Freeman group" with me (and a special thanks for Gigi!), Bahrad, Tyler, Torin, James, John, Katie, Mantonio, Danielle, and many more for interesting conversations, arguments, and plain old fun. I thank you all.

In addition to the people who have changed me I am thankful for the sponsors who made my studies financially viable. The Department of Physics, the National Institute for Nanotechnology, NSERC, Micralyne, and Mark have provided me with support through my studies; NIH, iCORE, and CIPI funded workshops while CMC provided microfabrication services. The University of Alberta Nanofab was a great environment to learn and work in. In addition, iCORE has provided wonderful retreats at Banff, a beautiful environment in which to learn, reflect, and recharge, one of the many benefits of studying in Alberta.

Table of Contents

List of Figures

List of Symbols

$\approx$	approximately
$\dot{\gamma}$	shear rate
ϵ	dielectric constant
$\dot{\epsilon}$	elongation rate
$\dot{\epsilon_{cr}}$	critical elongation rate
ζ	zeta potential, coefficient of friction
η	viscosity of liquid
η_0	viscosity of solvent
η_*	viscosity at polymer overlap concentration
$[\eta]_0$	intrinsic viscosity of polymer solution
λ	relaxation time
λ_{LJ}	Lennard-Jones relaxation time
λ_p	p-th relaxation time
λ_{Zimm}	Zimm relaxation time
μ_{EOF}	electro-osmotic mobility
$\mu - PIV$	microparticle image velocimetry
μTK	microtoolkit
ν	kinetic viscosity of liquid, (Flory) polymer-solvent interaction parameter
Π	osmotic pressure
ρ	density of liquid
σ	standard deviation, stress, conformation tensor
τ	shear, stress in McKinley, Pakdel, Oztekin work
τ_{11}	normal stress in flow direction (elongational stress) in McKinley, Pakdel, Oztekin work
τ_{elong}	elongational stress
τ_{shear}	shear stress
ϕ	electric potential, volume fraction
Ω	number of states
b	(Kuhn) monomer length
BEM	boundary elements method
BCC	body centered cubic
c	(weight) concentration
c_*	overlap concentration of polymer solution (polymer coils impinge)
c_{**}	concentrate concentration of polymer solution
CCD	charge coupled device

CFD	computational fluid dynamics
D	diameter, diffusion coefficient
d	diameter
$D_{*\%}$	dosage for $*$% film retention
D_h	hydrodynamic diameter
D_{tr}	translational diffusion coefficient
De	Deborah number
De_*	critical Deborah number
DFA	detrended fluctuation analysis
$DMAc$	dimethylacetamide
$DMDCS$	dimethyldichlorosilane
DNA	deoxyribonucleic acid
E	electric field
EDL	electric double layer
EHD	electrohydrodynamic
EKI	electrokinetic instability
EOF	electro-osmotic flow
EP	electro-phoresis
f	force, frequency
F	Helmoltz free energy
FCC	face centered cubic
$FENE$	finite extensible nonlinear elastic
G	modulus
GUI	graphical user interface
HMW	hight molecular weight
$HWNP$	high Weisenberg number problem
I	intensity
IPA	isopropyl alcohol
IV	current-voltage
K	spring constant
kT	thermal energy
L	characteristic dimension
l_D	Debye layer thickness
L_e	entrance length (distance for uniform profile to develop in laminar flow)
LJP	liquid junction potential
LMW	low molecular weight
LTM	linked twist map
M	molecular weight
M_{cr}	critical threshold for McKinley, Pakdel, and Oztekin model
$M1$	first moment mixing index
N	degree of polymerization (monomer number)
N_A	Agravado's number
N_b	buckling number (viscous diffusive time over elastic buckling time)
N_{mix}	mixing length (in number of constrictions)
p	pressure

$PAA, PAAm$	polyacrylamide
$PDMS$	polydimethylsiloxane
PEO	poly(ethylene oxide)
PES	poly(ether sulfone)
$PMMA$	poly(methyl methacrylate)
PMT	photomultiplier tube
ppm	part-per-million
Q	sensitivity
R	radius
$\dot{R}$	time rate of change of position
R_a	surface roughness
R_{cm}	radial position of center of mass
R_G	radius of gyration
R_H	hydrodynamic radius
R_{HS}	hard sphere radius
R_i	radius of i-th monomer in a polymer chain
Re	Reynolds number (inertial over viscous force)
RHS	right hand side
$R.M.S., rms$	root mean square
rpm	revolutions per minute
S	entropy
St	Strouhal number
T	temperature
t_ν	viscous diffusive time
t_B	elastic buckling time
T_g	glass transition temperature
t_{mix}	mixing time
$TAMRA$	tetramethylrhodamine
TBE	tris-borate-ethylenediaminetetraacetic acid
U	internal energy
v, V	velocity, voltage
We, Wi	Weissenberg number
wt	weight
xt	space-time
Z	friction coefficient

Chapter 1

Introduction

We are all familiar with microfluidics - everytime we receive an injection the fluid is pushed through a narrow metal pipe (the needle) into our blood stream.

Ouch. Why not make it narrower, and therefore less painful? Can we use "small pipes" for other uses? What is the nature of microflows? These questions are being addressed in the field of microfluidics, which aims to explore the physics and applications of microflows.

One of the salient characteristics of microflows is their creeping laminar nature - smooth, steady flows. When large deformable molecules, such as polymers, are added to flows they can be stretched and distorted. In turn they can distort the fluid they are suspended in, leading to unsteady and even turbulent flows. As microfluidics moves from liquids consisting of solutions of simple and small molecules to those with complex and large particles these effects will become increasingly important. The unsteady flows may, potentially, also be purposely harnessed to promote mixing.

In this thesis the motion of polymer solutions in microchannels will be explored, with a focus on electrical pumping ("electro-osmotic" flow, EOF). Several items are of interest: Flows of polymer solutions in microchannels, electro-osmotic flows, characterization of polymers, prediction of when polymer instabilities will arise, and mixing.

Needles cannot be arbitrarily reduced in size, for frictional resistance increases as channel diameters decrease. This increases the pressure required to push fluids through a channel, and these pressures quickly become impractically large. For this reason use of electro-osmotic pumping is favorable. Just how this works and experimental results of electro-osmotic microflows of polymer solutions will be described. Mechanically driven polymer solutions have been well studied, the investigation of electro-osmotic driven flow of polymeric solutions is a key contribution presented here.

It turns out that polymers underlying chemical structure is often of little interest, and the most important feature of polymers in flows is captured by the polymers relaxation time. A new method for finding this relaxation time from experimental (or numerical) data of tracer particles in polymer solutions is presented.

If flow is slow and has mild velocity gradients, as compared to the polymer relaxation time, polymers act as passive tracers whose main effect is to increase viscosity. If flow rates are increased so that polymers are stretched and distorted the interaction with the fluid becomes more complicated and interesting behaviour can result. The demarkation between these regimes is the coil-stretch transition. Fluids above the transition are no longer isotropic due to the stretching, "hoop-stresses" arise and polymers move across stream lines, "memory" effects arise as a polymers past history becomes important in its current conformation, and instabilities can occur. A difficulty in understanding polymer flows is the lack of robust constitutive models describing the fluid behaviour, and the trade-off between fidelity to experimental observations and computational tractability is strongly present in nonNewtonian fluid dynamics. Recently it has been noted that instabilities can arise in Newtonian fluids due to density effects, and here it is shown that an analogous concentration instability may occur in polymeric solutions; this instability occurs at the same nominal threshold as the classic viscoelastic coil-stretch transition instability, and may contribute to the numerical tractability problems.

The aim of the thesis is to explore polymers and viscoelastic fluids, with a particular focus on the instability behaviour of polymeric solutions. The touchstone work investigated pumping lightly polymer-doped solutions through microchannels with elongational flow fields using electro-osmotic pumping, a flow regime previously unstudied and of interest as electro-osmotic pumping schemes as well as viscoelastic fluids are important for microfluidic applications. The following were found

- thin films of poly(ether sulfone), PES, can act as negative electron resist, as PES is a robust polymer it can be used as an etch mask and may be suitable for direct fabrication of devices (section 3.3)
- by doping liquids with high molecular weight polymer, instabilities can be excited for flow through sudden constrictions/expansions (section 5.6)
- the observed instabilities arise above the classic viscoelastic instability criteria, indicating an elastic mechanism (section 5.6)
- no instability is seen for polymer-free flows, and reduced fluctuations are seen for smaller polymers when flows are tagged with passive dye for visualization of instabilities, supporting an elastic instability mechanism (section 5.6)
- the imposed flow rates are typical (O(1 mm/s)) for electro-osmotic flow - care must be taken in driving complex fluids as perturbation from laminar flow may be readily achieved (section 5.6)
- high current density effects can lead to formation of globular "rafts", discrete and persistent gels (sections 5.6, and 5.9)
- it has recently been discovered that variation in local density can lead to instabilities in simple liquids, it is found that for polymers the predicted corresponding concentration instability threshold corresponds to the classic viscoelastic instability value (section 4.5)
- by inspecting the correlations in fluctuations in particle tracer movement in unstable polymer flow the relaxation time of polymer solutions can be obtained - this allows for "in-situ" and parameter/model-free measurement of relaxation time (section 4.6)
- the electro-osmotic flow, EOF, device excites viscoelastic instabilities in the absence of shear (for the first time in cavity flows) and it is shown

that viscoelastic instabilities do not lead to enhanced mixing, as commonly expected, a consequence of viscoelastic flows progressing towards Batchelor turbulence which is a particularly smooth type of turbulence (chapter 6, in particular section 6.8)

- doping with polymer does not improve mixing in electro-osmotic flows; however, EOF provides an ideal platform for studying "pure" viscoelastic instabilities and optimizations may lead to useful schemes for enhancing mixing (chapter 6)

It is hoped the reader gains an appreciation of the beauty and utility of microflows and polymer solutions. I did.

Chapter 2

Fluids and Microsystems

2.1 General overview

Fluids in motion can be visually arresting.

A wide range of flows can occur - we are familiar with irregular clouds, waves on a lake, dripping taps, and turbulence in our coffee visualized by the motion of added cream. The range and beauty of flow patterns has lead to several "picture books" on fluids in order to illustrate, and give intuition of, various fluid phenomena [35, 36, 37, 38].

In our daily lives we are used to readily made unstable flows - smoke shedding off a cigarette breaks into vortices, we trail our hand through water to make eddies, we mix up a drink without a thought. In our macroscopic world inertial effects are large, and can lead to instabilities. These instabilities are both beautiful and useful; rapid mixing allows for quicker processing of fluid mixtures.

Given the wide range of flows it is impressive that a general mathematical description of fluids exists. By treating fluids as a continuum the Cauchy momentum equation, which balances the forces on a "fluid particle"[1], describes an incompressible fluid

$$\rho(\frac{\partial}{\partial t} + \boldsymbol{v} \cdot \boldsymbol{\nabla})\boldsymbol{v} = -\boldsymbol{\nabla} p - \boldsymbol{\nabla} \cdot \boldsymbol{\tau} + \boldsymbol{f}; \tag{2.1}$$

---

[1] A fluid particle is a parcel of fluid of an intermediate and indeterminate size such that fluid properties are uniform in the parcel - if we reduce the size too much molecular effects will result in statistical variation, if we take a too large size there will be a significant variation in properties due to external forces.

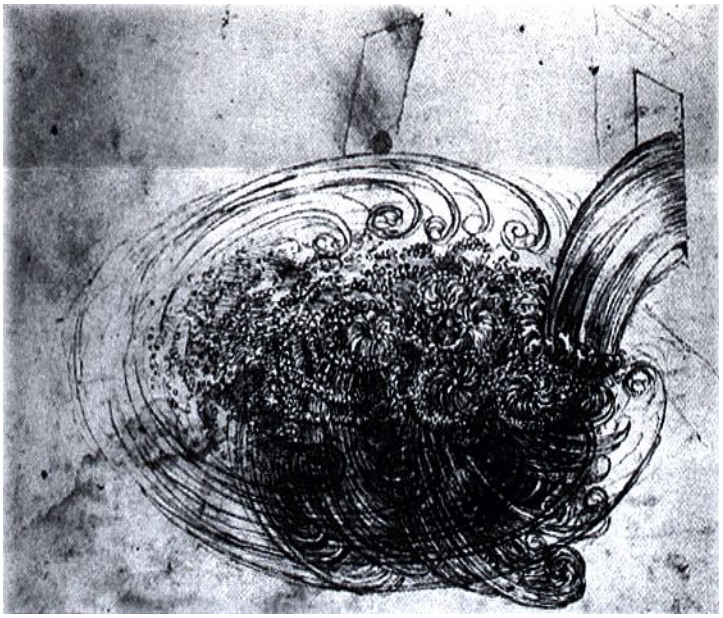

Figure 2.1: Leonardo da Vinci's "turbolenza", 1500. Sketch of a free water jet flowing into a pool. This study is thought to be the first detailed flow visualization, notice the eddies and vortices which result in rapid mixing. Image obtained from eFluids and used with permission.

where ρ is the fluid density, $\boldsymbol{v}$ is the velocity of a fluid particle, p is the pressure, $\boldsymbol{\tau}$ is the shear force on a fluid particle, and $\boldsymbol{f}$ are externally imposed forces; $\boldsymbol{\nabla}$ is the del operator (in Einstein notation: $\nabla = \vec{e_i}\partial_i$, where the $\vec{e_i}$'s are basis vectors and ∂_i the corresponding differential operator).

There are three basic regimes of equation 2.1, the Euler (viscous free), Newtonian (viscosity described by a positive constant), and nonNewtonian (nonconstant viscosity) regimes.

In general fluids are nonNewtonian but key fluids such as air and water can be treated as Newtonian over most "normal" conditions simplifying analysis dramatically[2]. Despite this good fortune many liquids of import do require nonNewtonian description: polymers, biofluids, foods, crude oil, suspensions, emulsions, etc.

The assumption of a constant linear relationship between shear and stress is an important simplification that captures the Euler and Newtonian regimes

---

[2] However, solution of the Navier-Stokes equation is a difficult problem; even showing that nondivergent solutions exist in general is one of the Clay prizes.

of interest (the Euler regime is mostly of use as a limiting case allowing analytic solution):

$$\tau = \eta \frac{\partial v}{\partial x}; \tag{2.2}$$

where τ is the shear stress, η is the (here constant) dynamic viscosity, v is the velocity and x is the spatial dimension perpendicular to the velocity; See Fig. 2.2.

Using equation 2.2 in equation 2.1 leads to the Navier-Stokes equation:

$$\rho(\frac{\partial}{\partial t} + \boldsymbol{v} \cdot \boldsymbol{\nabla})\boldsymbol{v} = -\boldsymbol{\nabla} p - \nu \boldsymbol{\Delta v} + \boldsymbol{f}; \tag{2.3}$$

where $\nu = \eta/\rho$ is the kinetic viscosity and $\boldsymbol{\Delta v}$ is Laplacian of the velocity. Various simplifications (ν=0 for the Euler case, LHS=0 for the steady slow flow case, etc.) allow analytic or more rapid numerical solution.

The continuum assumption for fluids is surprisingly robust, and molecular dynamics simulations have shown that the Navier-Stokes equation, which is built under the continuum assumption, performs quite well[3]. Molecular dynamics simulations demonstrate [39] that a breakdown of the Navier-Stokes equation occurs in shear flows over a critical value of

$$\dot{\gamma}\lambda_{LJ} \approx 1.4; \tag{2.4}$$

where $\dot{\gamma}$ is the shear rate and λ_{LJ} is the characteristic molecular time for simple Lennard-Jones liquids; as characteristic molecular times are on the picosecond scale, this indicates that relevalistic velocities are required before a breakdown would be observed if shear was created by sliding two plates seperated by 1 μm. We will see that this numerically found breakdown is due to viscoelastic effects, with the threshold in close agreement with many experimental, numerical, and theoretical studies of numerous test fluids. Briefly, if a fluid is forced at a rate approaching or exceeding the characteristic internal time scale describing a fluid molecules movement there can be a strong coupling between external

---

[3] A note on "nanofluidics" - Steve Wereley promotes the use of continuum and subcontinuum fluid mechanics, versus the widely used nanofluidics, for just this reason - fluids are often observed to conform to continuum behavior even at nanometer scales.

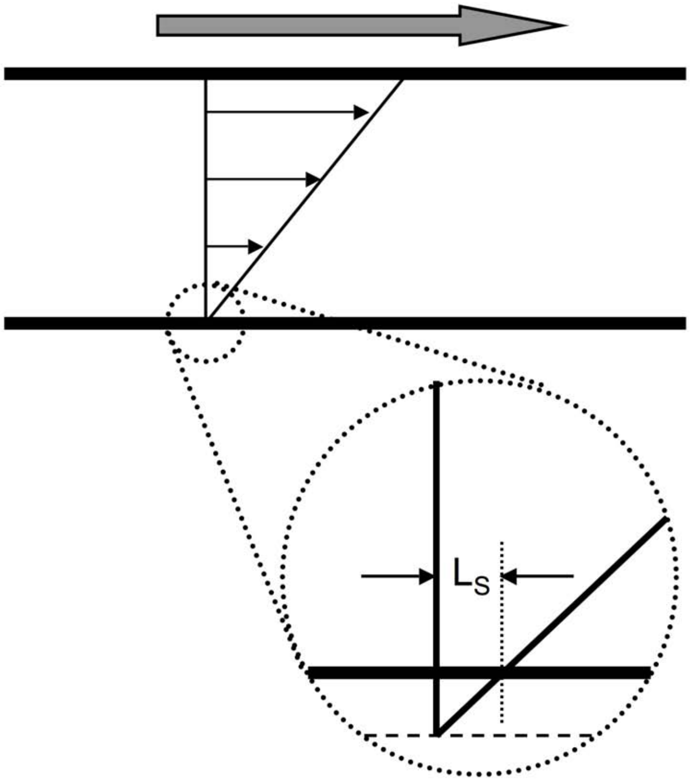

Figure 2.2: If liquid is placed between two plates and one (top plate here) is moved relative to the other (bottom plate stationary here) a shearing flow is set up. Due to molecular interactions and "stickiness" (cohesive forces) a nominal no-slip boundary condition occurs at liquid-solid boundary at the plates. By forcing the top plate at a velocity v fluid immediately nearby will be entrapped and dragged along. Via cohesive interactions with nearby fluid further from the wall that fluid will also be pulled along, and a linear velocity profile will be set up with no movement at the bottom plate and a velocity v at the top. No-slip is an idealization, and partial slip may occur at the wall – depending on molecular details. If slip occurs one imagines that beyond the plate there will be a location where velocity will be zero, and by projecting the velocity profile to this zero velocity location a slip length $\mathrm{L_S}$ and a slip velocity v_S at the wall is defined. For large systems with simple fluids any slip is insignificant and the system is well described by no-slip boundary conditions [1]; for complex fluids [2] and small scaled channels [3] the suitability of no-slip is more questionable and care must be taken. Note that a shear flow can be considered a "slanting" map that preserves area and consists of rotation and elongation (see Fig. 2.8 for more discussion). Consider the horizontal line as a bolus of dye that can move with the flow, under shear it will rotate and elongate (compare to the line at an angle that defines the velocity field).

and internal motions leading to new stresses and energy storage mechanisms that can disrupt flow.

In addition to the nonNewtonian viscoelastic effects predicted under extreme conditions, granularity effects are experimentally observed [40, 41] when fewer than roughly 10 molecular layers (e.g. $\approx$ a few monolayers) exist in a wetting liquid between close surfaces. Studies have also shown that no-slip conditions breakdown when liquid density dramatically drops near surfaces, i.e. under non-wetting conditions [42, 43]. Finally, compressibility become significant when flow velocities are close to the speed of sound which requires more careful use of the Navier-Stokes equations as, for example, flow can couple to acoustic fields. However, for most flows of simple liquids the Navier-Stokes equations with constant density accurately captures the relevant physics [44]; the Navier-Stokes becomes inaccurate for simple liquids only under high velocity or in highly confined environments.

While the Navier-Stokes describes simple liquids well, "complex", or non-Newtonian, liquids[4] are not well described by the Navier-Stokes equations, as will be described shortly, and as foreshadowed by equation 2.4.

2.2 Fluid instabilities: the buckling transition

Reynolds visualized flow by adding a dye stream to the center of fluids flowing through a pipe. As the flow velocity was increased instabilities were observed as unstable motion in the dye stream, and eventually highly unstable rapid transverse motion and mixing was found [4]. In general as a fluid is forced to move rapidly eventually instabilities occur.

The Reynolds number, Re, is a dimensionless number that characterizes flows

$$\mathrm{Re} = \frac{\rho v \mathrm{L}}{\eta}; \tag{2.5}$$

where v is the velocity of the fluid, L is a characteristic dimension of the flow,

---

[4] Complex liquids are *structured* liquids, which have structures that are similar in size to the flow fields within the liquid.

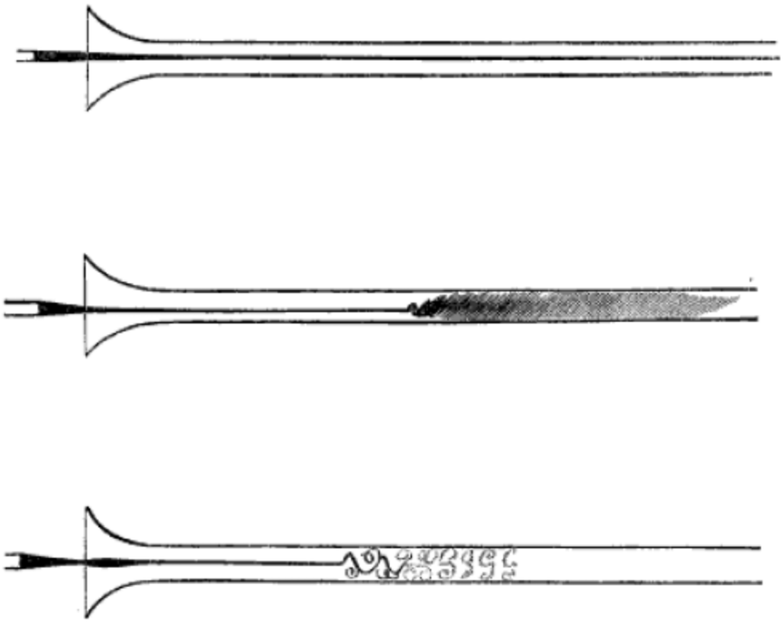

Figure 2.3: Sketches of laminar and unsteady flow from Reynolds classic work. Dye added to the center of pipe flow allowed visualization of flow regimes. Reynolds observed smooth straight flow at low velocities (top sketch), and upon raising the velocity a sudden transition to well mixed flow occurred downstream (middle sketch). Viewing the flow using spark light (stroboscopic imaging) resolved distinct eddies (bottom sketch). Composite image from Ref. [4], this material has passed out of copyright.

ρ is the fluid density, and η is the fluids viscosity. Essentially Re captures the competition between the fluids inertia which tends to cause instabilities, due to the $\boldsymbol{v} \cdot \boldsymbol{\nabla v}$ term in the Cauchy equation, and the "smoothing" effects of internal friction of the fluid which is described by the viscosity ν. Empirically it is found that when Re is greater than some critical value instabilities arise, and as Re is further increased turbulence is observed where flows are unsteady and fluid particle trajectories are chaotic in space and time [45].

The study of turbulence remains one of the outstanding challenges of classical physics, with much research effort focusing on various aspects and continual new findings being uncovered. For example, recent evidence strongly indicates that, in contrast to the prevailing view, turbulence is *transient* and will spontaneously and abruptly collapse back to laminar flow [46] and is therefore a chaotic "repeller" state. Elastic turbulence, a new type of turbulence (see section 4.2), has recently been established [47], as has the fluctuation instability where thermal fluctuation induced modification of density couples through the viscosity to create flow instabilities, given strong enough forcing [48].

The empirical observation of fluid instability at high Re number is classically conceptually explained in terms of inertial effects - given a high enough velocity the inertia of a fluid particle becomes large, and the flow tends to cross field lines and a breakdown occurs. Here a slightly different perspective is outlined, as developed by Bejan[5] [45]. Bejan takes the view that global minimization principles, such as least action, describe much of observed physics and proposes the minimization of flow time to all points in a flow system[6] as one such principle. From this principle a transition from laminar to instabilities, a "buckling" transition, is found to occur and nominally predicts the critical Reynolds numbers observed in practice. Bejan defines a buckling number as the ratio between buckling time t_B (e.g. related to the effective bending elasticity of a jet column) and the viscous diffusion time t_v:

---

[5] Of Bejan number fame, another dimensionless number.

[6] i.e. maximum "mixing", if the diffusion time across a stream is slower than the time of rolling (vortex) motion then rolling - instabilities - will occur.

$$N_b = \frac{t_v}{t_B}. \tag{2.6}$$

Bejan notes that for a dimensionless group to be relevant the transition delineation should be of order one, as this reflects the balance between the competing mechanisms, and finds that for free jets the predictions accurately reflect observations (i.e. instabilities occur near $N_b \approx 1$). It should be noted however, that the argument is somewhat ill defined for general use, with the buckling time difficult to estimate for a given flow. Nevertheless, Bejan's method is promising and can help explain why such high Re numbers are required before pipe flow becomes unstable, namely buckling is prevented by the solid boundaries, and can be conceptually checked against flow through a sudden expansion. In such flows the entrance length, the distance for the flow to fully develop, is $L_e \approx 0.035DRe$ for intermediate and high Reynolds number flows[7]. If the entrance length becomes large the stream will behave more and more like a free jet, and one imagines that if the entrance length becomes much larger than the buckling length that instabilities will be possibly excited. Taking the buckling wavelength from the Strouhal number $St = \frac{D}{\lambda_B}$ and using the estimate of $St \approx 0.2$ one finds that if $Re \approx 570$ instability would be expected, under the assumption that the entrance length should be roughly twice the buckling wavelength[8]. This is roughly what is found numerically, where a transition near Re = 625 is found [49], which indicates that an *elastic* mechanism is behind instabilities in both free jets and sudden expansions, which approximate free jets at high Re.

2.3 Low Re limit

As one scales down from the familiar macroscopic environment to the microscopic level inertial effects become irrelevant compared with viscosity - the liquid environment is effectively a billion times sticker than we are used to

---

[7] "Intermediate" flows are for Re on the order of 10, as here inertial effects can become important, such as centrifugal liquid motion occurring around bends.

[8] This rough estimate is motivated by the fact that the "jet" expands to fill the expanded channel over L_e, so will very roughly maintain its diameter for half this distance.

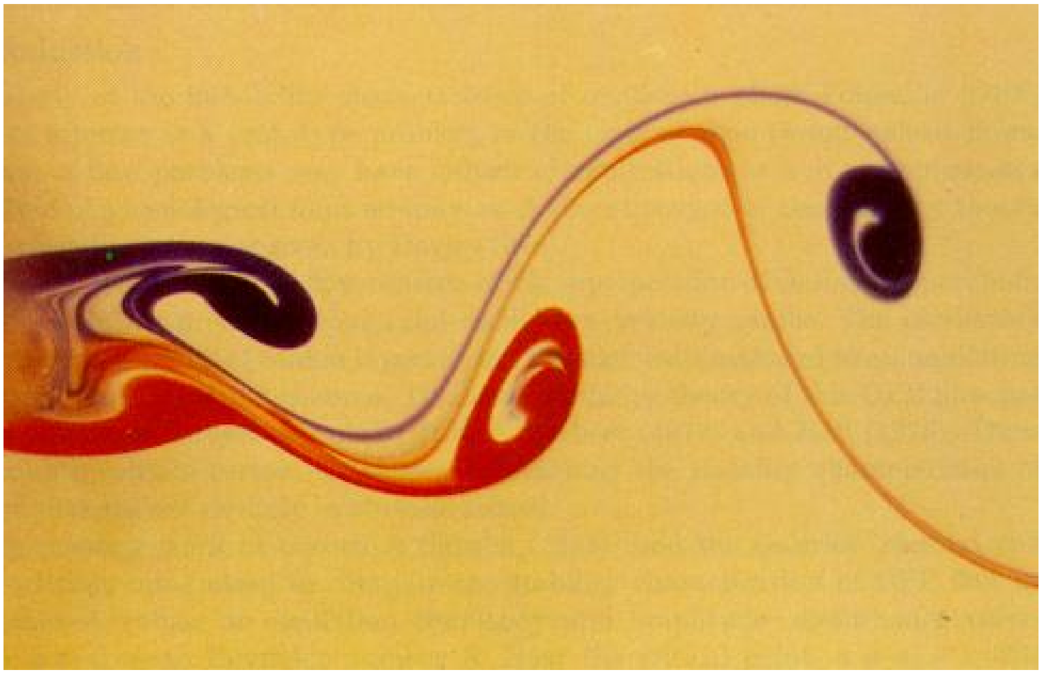

Figure 2.4: von Karman vortex. Flow past solid bodies causes rhythmic vortex shedding before the onset of turbulence (Re = 80 here). Instabilities allow for improved mixing and are suppressed at microscales due to the low Reynolds numbers involved, often leading to diffusion *limited* mixing (for a counter example see Fig. 2.5). Image obtained from eFluids and used with permission.

[50].

For creeping laminar motion of Newtonian fluids steady flows occur and the LHS of equation 2.3 can be set to zero, leading to Stokes equation for inertial-free flows:

$$\nu \boldsymbol{\Delta v} = -\boldsymbol{\nabla} p + \boldsymbol{f}. \tag{2.7}$$

Simply put, force is dissipated through diffusion and mixing becomes diffusion dominated. Due to the $t_{mix} \sim x^2$ scaling diffusion is slow for large scales (where advection can play a large role, dramatically promoting mixing rates) and rapid at small (nm) scales. Microfluidic systems are typically on the order of 10-1000 μm and fall between these two regimes were fast mixing can occur. Microfluidics systems are therefore diffusion *limited*: mixing is dominated by diffusion, due to lack of convective instabilities which are suppressed by the small scales, but the size is too large for this process to be rapid.

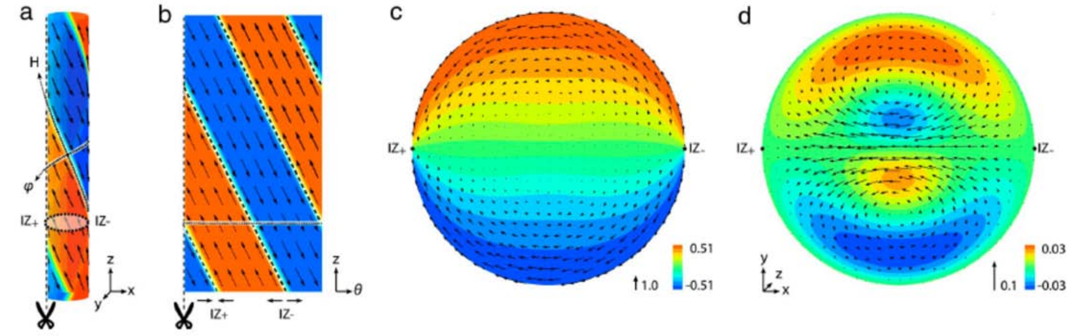

Figure 2.5: Model of fluid flow in a giant plant cell. Mixing at low Reynold numbers is difficult. Giant (≈ 1 mm by 10 cm) alga cells promote internal mixing by driving fluids at the inner cell surfaces with molecular motors. An effective slip velocity "at the wall" is created, similar in action to electro-osmotic flow: in both cases details in the layer near the wall are not well known, but outside this thin (≈ O(1-1000nm) for EOF flows) layer a simple slip condition can be utilized. For the alga cell (a,b) two counter flowing banded regions are separated by a thin "indifferent zone" (IZ) with no flow forcing. These boundary conditions induce (c,d) counter rotating vortices that twist along the cell axis. In (c) the velocity projection along the twisting band (H) is shown, and in (d) the (order of magnitude smaller) velocity projection perpendicular to the band (ϕ) is shown. The resulting flow fields consists of a global flow moving up/down along the stem and counter rotating vortices that rotate perpendicular to the stem, leading to enhanced mixing due to the interaction of the two flow fields (see discussion of the Linked Twist Map in section 6.5); this enhanced mixing is an example of "Lagrangian Chaos" where good mixing occurs in smooth flows and allows the cell to move food, waste, and other chemicals in an environment where diffusion is slow and limiting. Image from Ref. [5] and copyright of the Proceedings of the National Academy of Sciences of the United States of America, used with permission.

This diffusion dominated regime is characteristic of microfluidics and has the advantage of simple description and the disadvantage of slow reaction rates.

Creating fluid flows requires some pumping mechanism. The two most widely used pumping schemes for microflows are (1) pressure driven flows, and (2) electro-kinetically driven flows. Pressure driven flows can use a piston (syringe pump) or height differentials (gravity pump) to cause movement. The key advantage is ease of use, however due to scaling issues[9] pressure pumping

---

[9] Nominal no-slip at the walls creates a shear profile across a channel, as the thickness

becomes increasingly difficult as channel diameters are reduced and eventually becomes impractical. In electro-kinetically driven flows electric fields are used to move charged particles, which couple to the fluid by drag. In electro-osmotic flows polar liquids in contact with ionizable surfaces[10] produces an electric double layer (EDL) where ions of opposite charge are attracted to the wall [53]. This electrically non-neutral EDL sheaths surfaces, allowing electric fields to produce flows by driving the sheath, which in turn viscously couples to the bulk fluid away from the wall [53]. The key advantage here is effectively having a slip condition at the wall; shear is confined to the EDL in uniform channels, so scaling down the channel does not effect the effort required for pumping, and a flat velocity front is created in uniform channels. The disadvantages are related to the electrical aspect - electrochemistry, Joule heating, sensitivity to ion concentrations. See Figure 2.5 for a brief description of a natural system similar to electro-osmotic systems and Figure 2.6 for a visualization of velocity fronts in pressure and electro-osmotic microflows.

2.4 Basic electro-osmotic flow theory

When a solid is immersed in liquids an electrode double-layer often forms at the surface, as surface groups can become solvated (such as OH^- on polymers, glass surfaces, etc.) or due to polarization of a metallic surface. A simple model of the resultant charged interface is the electric double layer, or Debye layer, which consists of a strongly absorbed layer (Stern layer) of charged ions close to the surface, and a secondary diffuse layer of counter ions which has an exponential drop off in charge, see Fig. 2.7. It is empirically found that double-layer capacitance is often on the order of 10-40 μF/cm^2 [54], and that the Debye layer l_D is 1-1000 nm thick.

The double layer thus constitutes a sheath of charge that exists at the

---

is decreased the shear stress increases. See Fig. 2.2 for a discussion of slip; also see [51] for discussion relevant to polymers and [42] for simple liquids.

[10] "Solid-liquid interfaces tend to develop surface charge, which attracts oppositely charged counterions and repels similarly charged co-ions." [52]; interfaces become charged for various, ultimately quantum mechanical, reasons but the general tendency is towards a charged interface for many solid-liquid interfaces. See Fig. 2.7 for a schematic and some discussion on the electric double layer.

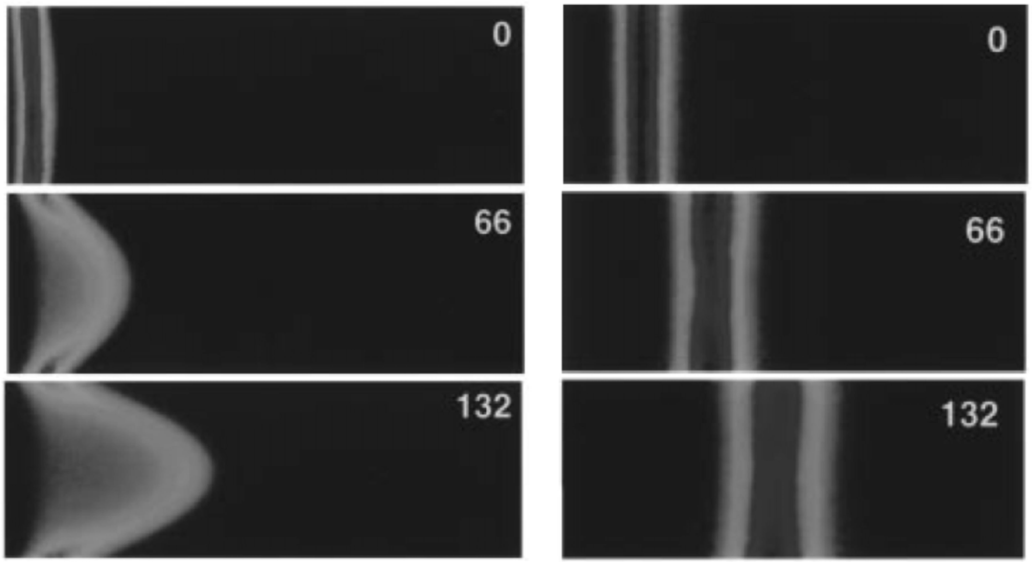

Figure 2.6: Pressure and electro-osmotic flow fronts. By using a pulsed planar ultraviolet laser sheet cutting perpendicular to fused silica capillaries caged fluorescent dye is released allowing the effect of velocity fields to be visualized by subsequently exciting the dye with a delayed pulse of light tuned to the dyes absorption peak. The laser sheet is $\approx 20\ \mu$m thick and impinges perpendicular to a cylindrical micro-capillary. On the left we see the no-slip boundary conditions in pressure flow leads to a parabolic or Poiseuille velocity profile; on the right we see that slip at the wall leads to a flat or plug velocity profile. Labels correspond to time (ms) after uncaging. All mechanically pumped cavity flows will have a significant shear component to the flow fields, due to the no-slip condition. The channel diameter will set the shear in Poiseuille flows, making flows sensitive to channel size. In contrast EOF flows have shear confined to the Debye layer near the wall, and changing the channel dimensions will not modify the flow details (until dimensions become close to the Debye layer thickness). Note that the broadening of the dye profile with time is due to diffusion, allowing the diffusion coefficient of the dye to be extracted from the images. Composite image reproduced with permission from Ref. [6]. Copyright 1998 American Chemical Society.

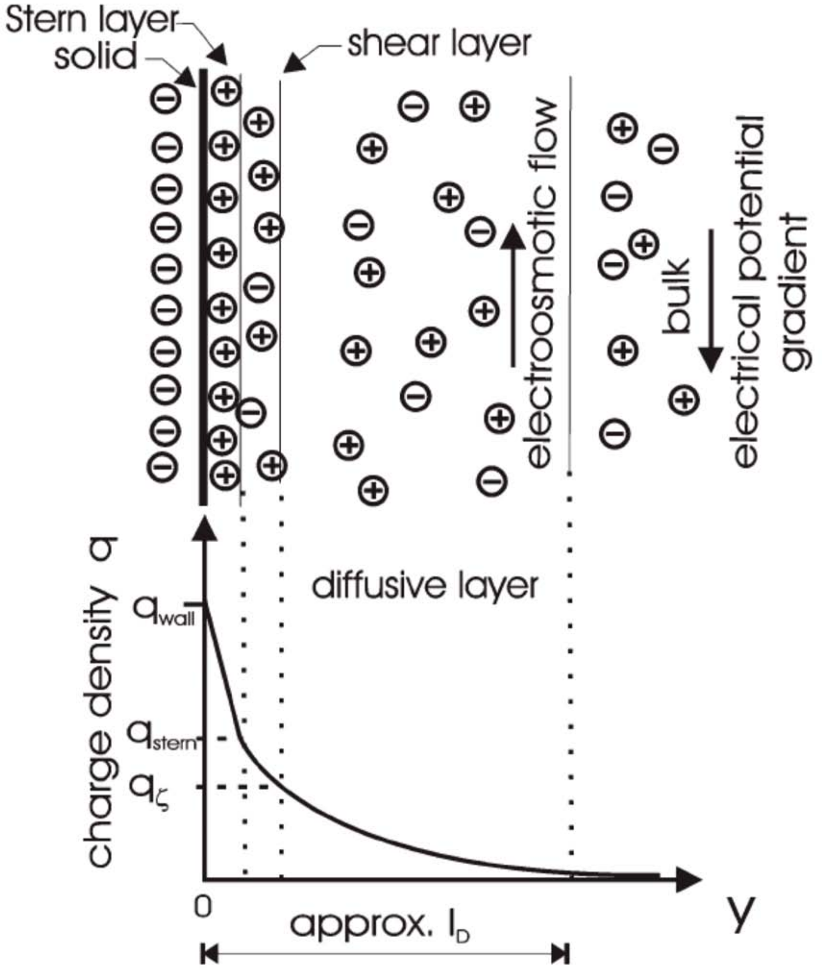

Figure 2.7: Simple double layer model of charged solid-liquid interface. The solid is charged at the surface with an absorbed layer of opposite charges. A secondary layer of diffuse counter charges surrounds the absorbed charge layer. The strongly absorbed Stern layer is considered to be static, although charges dynamically exchange with the fluid, and just past the Stern layer motion along the surface can occur ("shear layer"). With an imposed electric field the diffuse charged layer can move, setting up a velocity gradient across the Debye layer of thickness l_D and which viscously couples to the "bulk" fluid pulling it along with effective slip boundary conditions. See Fig. 5.21 and related discussion on oscillatory forcing, which can be used to promote mixing. Figure from Ref. [7], http://dx.doi.org/10.1039/b503696h. Reproduced by permission of The Royal Society of Chemistry.

interface between a solid and a liquid. If an electric field is set up parallel to the surface the diffuse charge layer will migrate under the influence of the field and viscously pull the liquid. The resultant motion is termed electro-osmotic flow. As shear is confined to the Debye layer which is much smaller than the channel sizes (10-100 μm), and as the Debye layer is constant for a given liquid/solid, "plug" flow (constant flow front velocity) is observed for arbitrary cross-sectional shaped channels with uniform cross-section [53]; scaling the channel dimensions does not change the required pumping effort. This is in contrast to pressure driven flow, where the no-slip conditions at the wall[11] leads to a parabolic[12] velocity profile ("Poiseuille flow") with a shear dependent on channel dimensions and cross-sectional shape, and thus viscous losses depending on channel size. For this reason (independence of channel dimension in practice) electro-osmotic pumping is desirable for microfluidics, the programmability of flow conditions via electronic control of forcing E-fields is an additional benefit.

As the Debye layer which establishes flow and the channel dimensions are usually well separated ($< \mu$m and $> \mu$m) the flow behaviour can be simplified with the flow dynamics within the Debye layer ignored and the effects approximated by the an effective slip velocity at the wall. This approximation leads to the classic Helmhotz-Smoluchowski equation for electro-osmotic flow.

The Helmhotz-Smoluchowski velocity is given by:

$$v = -\frac{\epsilon\zeta}{\eta}E = \mu_{EOF}E; \tag{2.8}$$

where ϵ is the dielectric constant, ζ is the zeta potential, η is the viscosity, and μ_{EOF} is the electro-osmotic mobility. The zeta potential is defined as the voltage between the shear layer in the Debye layer (see Fig. 2.7), where fluid no longer strongly sticks to the boundary, and the bulk of the fluid; note that the zeta potential is not directly measured, but is instead inferred from

---

[11] No-slip conditions are an empirical finding, that occasionally fail, for example for hydrophobic or other surfaces with poor liquid-solid contact. For most flows no-slip is an excellent approximation [1].

[12] The parabolic shape holds for circular or slot channels, other cross-sectional shapes will have modified parabolic "like" velocity profiles.

other measures and, due to difficulty in determining physical properties near the liquid-surface boundary, the inferred ζ should be considered an "effective" zeta potential [55].

Most often μ_{EOF} is experimentally determined. By monitoring the flow of dyed solution downstream the apparent mobility, μ, can be found by timing flow over a known distance. If the dye is uncharged μ_{EOF} is equal to the apparent mobility, if the dye is charged an electrophoretic mobility, μ_{ER}, due to the charge must be accounted for with $\mu = \mu_{EOF} + \mu_{ER}$ [56]. In this work TAMRA (carboxytetramethylrhodamine) dye is used as a visualization agent, as TAMRA is a zwitterionic fluorophore it is neutral [57] allowing direct determination of μ_{EOF} by monitoring movement [58].

Electro-osmotic flows are often used in the remediation of polluted soils, for loose soil $\mu_{EOF} \approx 0.5$ cmμmV^{-1}s^{-1}, which is about an order of magnitude less than those for in microchannels [59, 60].

One of the beneficial attributes of EOF flow is the insensitivity of the dissipated energy with the characteristic width of the channel, which is in contrast to pressure flows were the dissipation is linked to the width of the channel. This distinction is due to the confinement of shear to the Debye layer in EOF flows, whereas the shear profile exists throughout the flow in pressure flows. The Debye layer is determined by ionic considerations, and thus the dissipation is confined to the sheathing layer *independent of the channels width.* This is in sharp contrast to the pressure driven case where the shear is dictated by the channels width, and thus dissipation in pressure flows is intimately related to the channel width. Note that if electrochemical processes lead to a change in ionic conditions during EOF pumping then the Debye layer will change in size and the *dissipation rate and thus flow velocities will change.*

The use of EOF pumping is widely investigated and put to use, however some of the suggested superiority is moderated by the fact that electrochemistry can modify flow rates over time, a change in working fluids requires experimental verification of flow velocities, microchannels are (at the present) fairly large allowing pressure pumping to be often appropriate, Joule heating effects can be significant, and costly equipment is required. In short, EOF pumping is sensitive to sample details[13]. The attractive features of EOF - insensitivity to channel size (down to micron scales), flat velocity profiles, and possibility for rapid modification of flow conditions - remain highly desirable and often make the costs worth bearing.

In considering properties of fluids near surfaces bulk behaviour is often assumed, for example the viscosity and density is typically assumed to be equal to that in the bulk. This assumption underlies many calculated properties of “hidden” variables, i.e. those variables not directly measured, such as the zeta potential in equation 2.8 where the velocity is measured for a given applied electric field and the zeta potential calculated using bulk values for ϵ and η. This will lead to *incorrect*, albeit consistently incorrect, values. The interface between the solid and liquid remains a research frontier, with both the solid and liquid phases having properties differing from the bulk and not well characterized and with possible slip effects, ionic concentrations, nanobubbles, and possibly modified ordering and density of solvent [55]. Understanding of the interface remain elusive, and there is contention on issues such as possible “interfacial water”, the inferred existence of which is currently not experimentally supported and features attributed to interfacial (ordered) water may be due to nanobubbles at hydrophobic surfaces [55]. Ignoring such known surface effects will lead to significant error in calculated values, however the errors are consistent and largely affect “hidden” values. As bulk properties are used in the literature their use will allow estimates to be found, however the use of this persistently incorrect procedure should be kept in mind.

Electro-osmosis is characterized by a length scale, the thickness of the Debye layer, which is typically on the order of 10-1000 nm versus the typical scale of 10-1000 μm for microchannels. This wide range in scales of interest makes full numerical simulations difficult due to a need to track both small and large scales, requiring the use of fine meshes to describe the geometry. In addition to this numerical issue the details of what physically happens within the Debye layer is not well understood. By effectively ignoring the detailed

---

[13] This sensitivity is typically put to use in EP flows, but is normally an inconvenience in EOF flow.

physics of what happens within the Debye layer simulations can be performed by imposing slip boundary conditions.

2.5 Potential electro-osmotic flow: a laminar creeping flow regime

Electro-osmotic flow of simple liquids is a potential flow[14] [61, 62], provided the following conditions are met: the E-field is steady, the fluid/interface is homogeneous, the Debye layer is thin relative to the channel dimensions (i.e. Helmholtz-Smoluchowski, or slip boundary conditions, are appropriate), there is an absence of pressure effects, and flows are parallel to surfaces.

Given these conditions the velocity is proportional to the electric field and the flow is irrotational. Note that the electric field, and hence flow field, being irrotational necessitates a *shear-free* and purely elongational flow [63], as shear fields consist of both rotational and elongational components (see Fig. 2.8) [1]:

$$\begin{aligned} \boldsymbol{\nabla} \times \boldsymbol{E} = 0 \implies \boldsymbol{\nabla} \times \mu_{EOF} \boldsymbol{E} = \boldsymbol{\nabla} \times \boldsymbol{v} = 0 \\ \implies \text{shear-free flow (shear} = \textbf{rotation} + \text{elongation).} \end{aligned} \tag{2.9}$$

A given shear can always be decomposed into deformation (elongation) and rotation components ("vorticity") [1]. As such a shear necessarily includes a rotational component and a rotationally-free (curl-free) field is therefore shear-free [64]. Note however that one can have rotation without shear so the converse is not true, that is, shear-free does not necessarily mean rotationally-free. In studies of vortices the underlying presence of rotation in shear presents difficulty as calculating the curl of a flow field will not discriminate between pure shearing and vortex motion, making measurement and identification of vortices difficult [64].

Below the coil-stretch transition polymer liquids should meet the similarity conditions, while above the transition the inhomogeneous fluid properties will break the homogeneity requirement opening up possibility for rotational (and

---

[14] A similarity between gas slip flows and electro-osmotic flows has been noted by Steffen Jebauer in 2008, but detailed comparisons have not yet been completed.

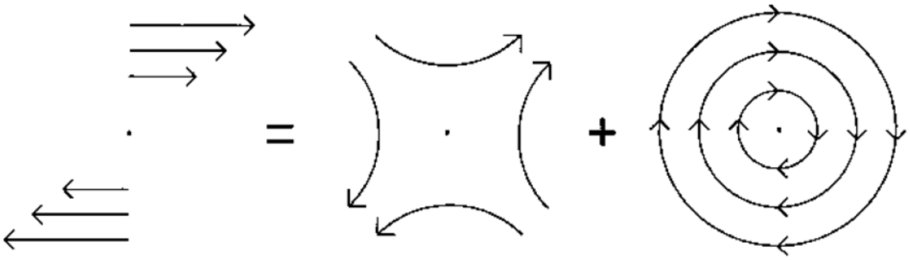

Figure 2.8: Shear consists of both rotational and elongational components. It is known that shear fields can be decomposed into rotational and elongational elements, as schematically shown here. As the E-field is irrotational ($\nabla \times \boldsymbol{E} = 0$) electro-osmotic pumped flow fields are also irrotational, due to the similarity condition ($\boldsymbol{v} = \mu_{EOF}\boldsymbol{E}$), and therefore shear-free. Note, however, that entrance effects are expected at sudden constrictions (or any other rapid change in boundary geometry) which will break similarity. As entry effects are thought to be a pure pressure effect [8] the Helmholtz decomposition theorem should apply and the flow fields will remain irrotational (shear-free), indicating that changes from potential flow will be solely (rigid) translational and elongational [9]. Image from [10]. Reprinted with permission from AAAS.

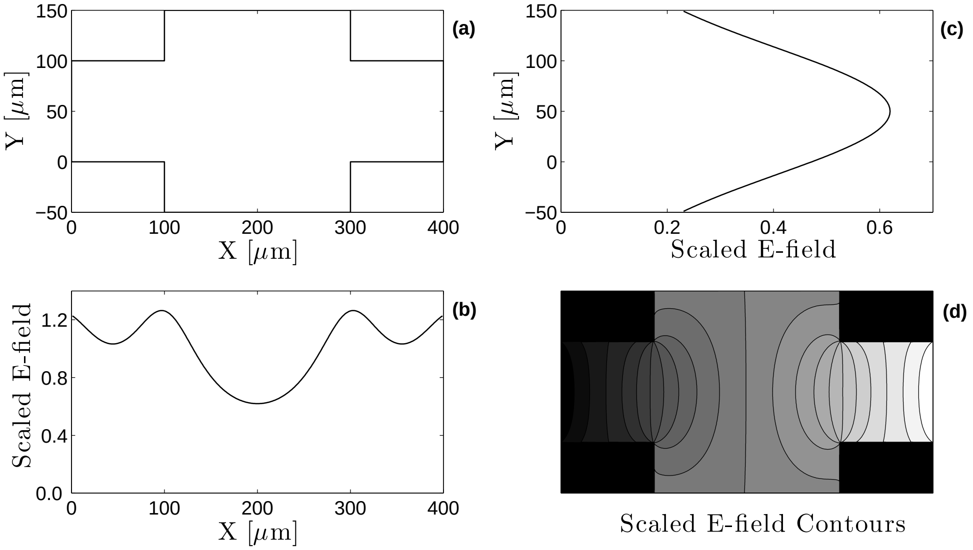

Figure 2.9: Representative expansion unit in a microchannel. Extensional flow is imposed with 2:1 constrictions/expansions along the microchannels (a). The E-field show in (b) is of a cut along the center of the channel and all fields are scaled by the average field along this center cut though the channel. The field along the flow axis varies through the channel, with a ratio of maximum (peak) to minimum (trough) field of 2.04; using the similarity condition allows the velocity to be directly related to the E-field. Based on conservation of mass the flow velocity is expected to change by a factor of two between the constricted and expanded regions; numerical checks of computed flow fields demonstrate conservation of flow within 3% of theoretical expectation, however large discretations of the boundary results in distortion of field lines (see d). The E-field cut transverse across the flow direction and in the center of the expansion is shown in (c). Note that despite a change in the E-field (and hence velocity) across the channel the flow is shear-free as it remains irrotational. In (d) the flow front (contour of the scaled E-field) is shown, flow moves perpendicular to the contours. The boundary element method is used to solve Laplace's equation here; this allows a rough approximation of flow, however both the entrance effect of the sudden expansion and the presence of polymers (above the coil-stretch transition) in flow break the similarity condition.

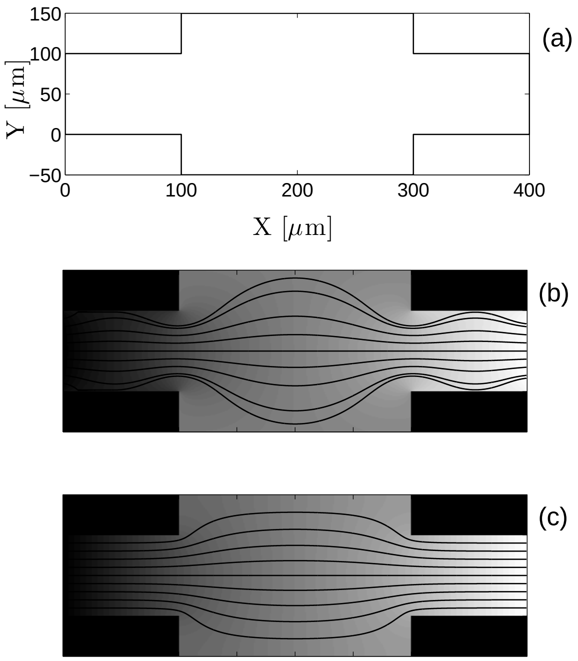

Figure 2.10: Fluid flow lines in expansion unit. Extensional flow is imposed with 2:1 constrictions/expansions along the microchannels (a). Using the boundary element method, rapid solution to Lapace's equation was achieved in Matlab. However due to minimal pre-processing in the code used - geometry creation is done "by hand" - it is difficult to create and modify geometries, and large discretization elements were used (with each boundary face in (a) used as a single discretized unit). Taking slices across the channel confirms that volume flow is conserved within 3%. Despite the bulk flow being correct discretization leads to distortion of precise flow lines, as the midpoint value of the voltage field is used to represent the boundary condition on each face; see Fig. 2.9.d for the flow front and (b) here which shows the distorted flow lines. Using a well developed toolbox for solving Laplace's equation by the Schwarz-Christoffel conformal map [11] allows discretization error to be reduced with relative ease, enabling precise flow lines to be found as in (c). Using the Schwarz-Christoffel toolbox error is reduced relative to the BEM method (with an estimated flow rate change between the wide and narrow region that is 1% less than the predicted value of 2X) and the flow lines follow gross expectations; the toolbox has been compared with test cases to confirm accuracy [11]. In (b) and (c) the voltage gradient that drives flow is represented with a grey colour map. Note that intuitively it *appears* that shear exists in the flow, however see Fig. 2.8 and discussion. For the flows in (b) and (c) the curl was numerically calculated and found to be zero within machine accuracy.

unsteady) flows. Maintaining potential flow conditions is advantageous, as it simplifies numerical simulations, but prevents instabilities - the irrotational condition of potential flows is correspondent with steady laminar flow.

Assuming irrotational conditions allows the Laplace equation to be used to model the (potential) flows, giving the steady flow base case. The Laplace equation with mixed boundary conditions describes the fluid geometry, with Neuman boundary conditions ($\frac{\partial \phi}{\partial n} = 0$) describing the walls and Dirichelet boundary conditions ($\phi = V$) the imposed electric potential (ϕ). Solving the Laplace equation with mixed boundary conditions is a well studied problem with many techniques available. One excellent approach is the boundary element method (BEM) [65], which is well suited for linear, elliptic, homogeneous partial differential equations defined on the boundary. The BEM discretizes and solves *solely* on the boundary, thereby effectively reducing the solution space dimension by one relative to physical space, and values taken in the solution domain are evaluated post-determination of the solution on the boundary[15]. For the Laplace equation BEM is vastly superior[16] to domain discretization methods in both accuracy and efficiency[17], and can implemented with relative ease in MatLab [66].

For a given expansion unit (Fig. 2.9) the E-field can be found by solving the Laplace equation, and finding the derivative of the found potential. This E-field is proportional to the velocity, allowing flow dynamics to be found. In Fig. 2.9 and Fig. 2.10 the electric field is shown for a sudden expansion. In addition to this variation a pressure drop will also occur, with an associated entrance length [8] on the order of the hydrodynamic diameter ($\approx 0.6 D_H$). This pressure drop effect has been shown to be important to the flow dynamics for electro-osmotic flows [67, 68], and the associated entrance length can be taken as the characteristic dimension of flow change. Many studies ignore this

---

[15] To do so the relevant Green's functions are fit to the given boundary conditions, allowing direct evaluation using the Green's functions post fitting.

[16] Another excellent way to solve Laplace's equation is to use the Schwarz-Christoffel transformation [11].

[17] To the extent that "[problems solved with] a laptop computer using the boundary-element method may require the use of a supercomputer by finite-different and finite-element methods for the same level of accuracy" [65].

entrance length effect, for example the excellent dispersion investigation in Ref. [69], and more detailed investigations and comparison with experiment[18] are required to determine the extent of systematic error introduced by the exclusion of this effect.

The potential flow often found in electro-osmotic flow is homologous with smooth laminar flow, and the conditions for potential flow therefore must be broken in order to obtain instabilities. At sudden constriction/expansion entry length effects will "break" the potential flow[19]; above the coil-stretch condition stretching of polymers will also break potential flow, due to an additional (elastic) force perturbing flow.

The entry length of a channel is the distance over which the perturbation to the fluid imposed by a sudden change in geometry will take to decay and is identified with a pressure drop. The distance is somewhat arbitrary, and is typically taken as the distance for the flow profile to reach 99% of the final maximum velocity in the channel [3]. The entrance length at a sudden contraction for creeping pressure driven flows is $\approx 0.63D$ [3], where D is the diameter of the channel, and has been found to be $\approx 0.57D$ for creeping electro-osmotic flows [67]. The entrance length can therefore be taken to be $\approx$ 0.6D for either pressure driven or electro-osmotic flows; in high aspect ratio channels D should be the smaller diameter, as diffusion of momentum and interaction between the fluid and the wall will be the mechanism leading to eventual convergence to steady-state profiles.

The E-field determined flow field is shear-free (irrotational), however the entrance effect may conceivably break this condition and allow shear to exist. One way to determine if flow remains shear-free in the presence of the entrance effect is via a full 3D multi-physics simulation where the E-field at the boundary sets a slip-condition[20] and the Cauchy equation (or Navier-Stokes for simple liquids) is solved where the pressure term allows entrance effects to

---

[18] Or use of simulations that can turn the entrance effect on and off; for example by using the Laplace equation versus the full Navier-Stokes equations.

[19] Although this breaking of the similarity condition does not lead to instability, as experimentally instabilities are not seen.

[20] Including the Debye layer physics would vastly increase the numerical efforts required, and slip boundary conditions allow a good approximation.

be included[21]. The solved flow field would then have to be numerically found irrotational to demonstrate flows remain shear-free. Alternatively, recognizing that pressure is identical[22] to the gradient component of the advection and diffusion terms of the Navier-Stokes equation [9], and that the curl of a gradient is zero, one can see that despite the entrance effect the flow should remain irrotational and shear-free. This is an application of the Helmholtz decomposition theorem that decomposes vector fields into solenoidal (divergent free) and irrotational (curl-free, and thus shear-free) components, for the Navier-Stokes equation the pressure captures the curl-free aspect of the flow.

Electro-osmotic pumping is the pumping scheme investigated in this thesis.

2.6 Summary

Microflows are of fundamental and practical interest:

- The Reynolds number Re characterizes flows and is given by the ratio of inertial to viscous effects; for $\mathrm{Re} \lesssim 1$ in Newtonian fluids inertia is often insignificant and creeping laminar flows occur, this is the typical condition for microfluidics. As Re increases instabilities, and eventually turbulent flows, arise.

- In microfluidics there are two main pumping mechanisms used: mechanical pumping and electro-osmotic pumping. Due to no-slip boundary conditions mechanical pumped cavity flows have significant shear and as shear is set by dimensions the flows are also sensitive to channel dimensions. EOF flows in contrast have shear confined to a thin layer near the confining surfaces (Debye layer) and have effective slip boundary conditions.

---

[21] A danger of dropping terms in equations/numerics for expediency, such as pressure or time variation, is that this excludes the possibility of various effects associated with those terms from being seen.

[22] This pressure-gradient identity strictly holds only for incompressible fluids, and as Chorin cautions [9] “pressure” can mean different things in different contexts and is a subtle topic; note that this insight into the pressure has lead to a class of numerical solvers for the Navier-Stokes equation (projection methods).

- Electro-osmotic pumping is the pumping scheme investigated here.
- For EOF flows in uniform channels potential flow exist, enabling Laplace's equation to describe the flows. This potential flow does *not* hold near rapid changes in confining boundaries, where pressure effects will lead to "entrance" effects which perturb flow over a distance given by the entrance length. In low Re flows the entrance length is roughly 0.6D, where D is smallest cross channel dimension.
- EOF flows are shear-free in uniform channels; for sudden changes in the channel geometry there will be a pressure effect that breaks the similarity conditions that dictate shear-free flow. The Helmholtz decomposition theorem suggests that that while similarity will not hold the flow will remain shear-free.

Chapter 3

Polymers Below and at the Coil-Stretch Transition

Polymers are a class of materials consisting of macromolecules that are covalently bonded elementary units (monomers). The 1920's were the defining decade of polymers, and between 1920 when Staudinger first proposed the macromolecular hypothesis and 1929 when Carothers has synthesized a number of polymers the field of polymer science was created [70].

Polymers in solution are of prime interest - at large dilutions interpolymer interactions can be excluded leaving a model system, molecular simulations can be attempted, radiation scattering can probe structure and dynamics, and volatile solvents can be used to move and deposit polymers. Below the *coil-stretch transition* polymers act as mostly passive "cargo" that move with fluid flows, with the major effect being a change (increase) in viscosity, while above this coil-stretch transition significant stretching of the polymer occurs and elastic effects and back-reaction on the flow can occur [71]. The transition is defined by the relaxation time of a polymer, the characteristic time for a stretched polymer to relax back to the random-coil structure taken by many polymers under stagnant fluid conditions. In this chapter polymers below the coil-stretch transition are considered in order to lay out the basic groundwork of polymers.

While polymers below the coil-stretch transition are thought to be similar to passive colloidal objects it should be noted that these objects are *soft*, and the same forces that leads to their collapse (i.e. thermal agitation) into globular random coils leads to deformations in the coils, as can be seen by fluorescently labeling DNA and optically observing motion in static fluid, Fig. 3.1. The coils are dynamic and “breath” on a timescale defined by their relation time.

3.1 Polymer structure

Poly-mer, literally many-parts. Polymers are large macromolecules created from a small set of monomers, basic building blocks. For example, proteins are biological polymers which make up the basic molecular machines of known life forms that are built up out of 22 amino acids[1]. The -mer’s of a polymer are repeatedly used as building blocks, often to create linear structures with sidechains off the main backbone. There are 1000’s to millions of monomers making up polymers, so that end effects (the difference in chemical structure of monomers in the backbone versus at the end where only one side is connected to the chain) are not observed; in limited monomer chains, oligomers, end effects are often observable. The molecular weight of polymers is huge in contrast with simple chemicals, with weights on the order of 1000’s to millions of Daltons[2] (Da).

Synthetic polymers typically have a handful of monomers (1 or 2 monomers is common) and are linear due to the difficulty in finding synthesis routes [70]. In theta-solvents, defined as solvent conditions where the monomers have equal attraction/repulsion to both the solvent and other monomers, the linear chain undergoes thermal agitation and “collapses” into a random coil that is well described by Gaussian statistics [70].

Solvents will span from “poor” solvents, where monomers have a relative attraction to other monomers versus the solvent which leads to the polymer coil collapsing in relative to theta-solvents, to theta-solvents where monomer-monomer and monomer-solvent interactions are perfectly balanced, to “good” solvents where monomers preferentially interact with the solvent which leads to polymer coils expanded relative to the theta-solvent. The theta-solvent

---

[1] As always there are complications, in addition to the 22 standard amino acids there are many nonstandard amino acids that are occasionally used.

[2] A Dalton is the molar mass of ^{12}C.

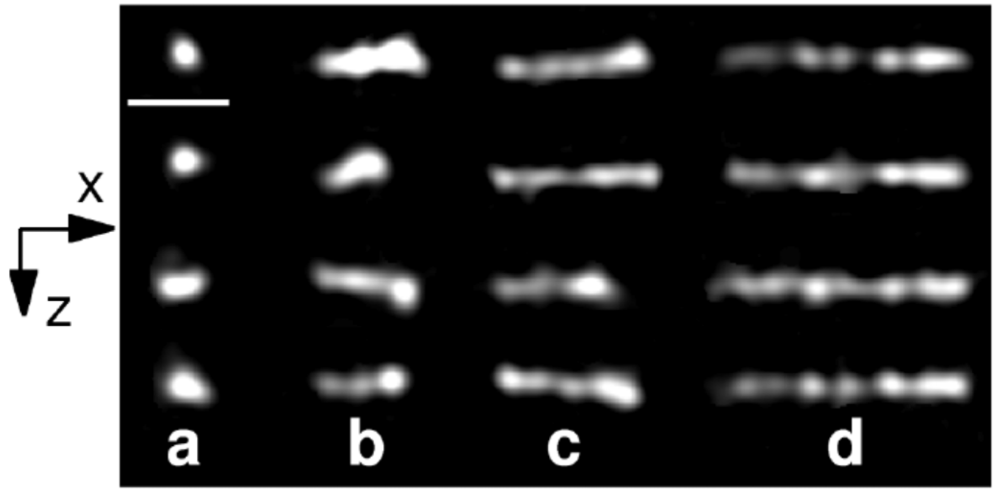

Figure 3.1: Conformations of dyed DNA polymer with one end tethered to a surface. Images are separated in time by one relaxation time. From (a)-(d) flow rates increase from static to highly deforming shear flow. Note that even with no flow the polymer is dynamic and "breaths", displaying change over time periods on the order of the relaxation time. The scale bar is 5 μm. Dyed DNA is in many senses an ideal system, allowing conformation of individual polymers to be investigated and being mono-disperse (although genetic differences between DNA samples should lead to subtle differences in properties), and as such many numerical and experimental investigations are being focused on DNA. λ-DNA, such as shown here, is similar to the high molecular weight polyacrylamide polymer studied in this work. Reprinted figure with permission from Ref. [12], http://prl.aps.org/abstract/PRL/v84/i20/p4769_1. Copyright 2000 by the American Physical Society.

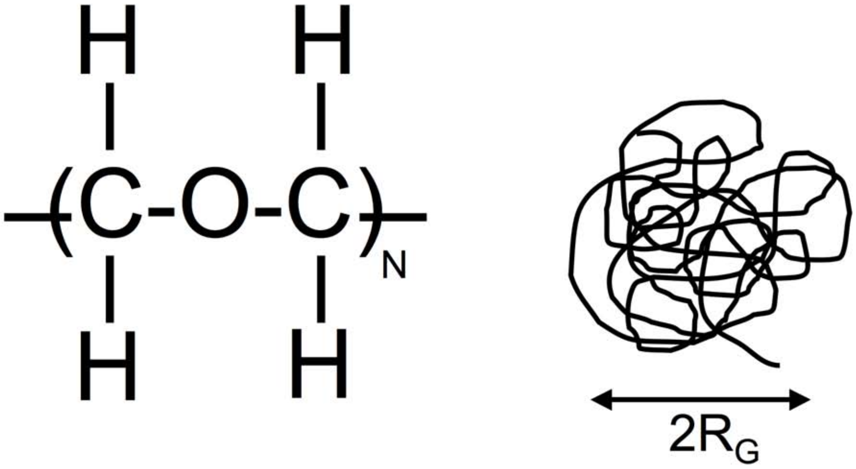

Figure 3.2: Polymers are made up of many repeat units. Polyethylene Oxide (PEO) is a well studied water soluble polymer. The basic repeat unit, which is repeated N times, and globule random coil structure typically taken by synthetic polymers with a radius R_G is shown. The random coil is well described as a (entropic) spring and thermal agitation will tend to relax a stretched spring/polymer coil back to the globule state with a characteristic relaxation time λ.

condition leads to Gaussian statistics, and hence tractable mathematics, and is therefore used as a simple model to describe polymers in solution. In practice the specific solvent conditions must be considered. The idealized theta-solvent conditions leads to the Gaussian random coil [70]:

$$P(N,R) = (\frac{1}{4\pi R_G^2})^{\frac{3}{2}} e^{-\frac{R^2}{4R_G^2}}; \tag{3.1}$$

where P(N,R) is the radial probability distribution for a polymer with degree of polymerization (number of monomers) N, with radius of gyration $R_G^2 = \frac{1}{N}\sum_{i=0}^{N}(R_i - R_{cm})^2$, where R_i is the radial position of the i^{th} monomer and R_{cm} is the radial position of the center of mass. For an ideal linear chain $< R_G >^2 = \frac{b^2 N}{6}$, where b is the monomer length.

Polymers are often chemically inert under most conditions and are stable molecules, this inertness allows them to be viewed as mechanical objects under many conditions and their approximate Gaussian coil shape results in fairly simple mechanical properties.

In volatile solvent suspended random coils go from dilute and well separated, to coil-overlap, to concentrated, and finally to a solvent-less melt (or glass below T_g, the temperature demarking the transition between a liquid flowing state to a glass) as the solvent evaporates away. The individual coils mark their presence in resulting solid films by the roughness associated in line patterns defined in films that can be patterned: instead of sharp precise lines roughness remains due to the discrete polymer coil units forming small aggregates which are selectively etched away by solvents [72, 73].

3.2 Thin Films

Solid thin films are the elemental building blocks of microdevices.

Polymers are often solvated not for their properties or use in solution, but rather as a means to transport polymers for deposition on surfaces. Spin or dip casting polymers allows for deposition of a solid film on a substrate, if a volatile solvent is used. Evaporation of the solvent will increase the polymer to solvent ratio until only solute is left, by rapidly rotating a substrate or by uniformly pulling a substrate out of a liquid a quasi-uniform coating can be achieved. The thin films that result are the basic building block used in microdevices and microlithography. Polymers are routinely used as resists, which can be selectively damaged or strengthened by exposure to radiation (photons or electrons being the most commonly used radiation sources).

Here patterning of poly(ether sulfone) polymer film patterning using electron beams (see Fig. 3.4 and next section for details) was undertaken. Unlike other sulfone polymers it was found PES acted as a negative resist, making PES suitable for mask applications but less desirable for direct rapid prototyping of microchannels.

3.3 Patterning poly(ether sulfone) films

Poly(ether sulfone) thin films were created and patterning of the films with electron beam lithography was undertaken[3].

The sulfone containing polymer poly(butene sulfone) has long been used as positive electron beam resist due to the high scission rate of sulfone under electron irradiation. Here it is demonstrated that poly(ether sulfone) acts as a high resolution negative electron beam resist which displays good chemical and dry-etch resistance. The electron beam exposure sensitivity at 10 kV was found to be approximately 230 μC/cm^2 for poly(ether sulfone), roughly 2.3X that of poly(methyl methacrylate). As poly(ether sulfone) is a robust engineering polymer that can withstand etching this polymer is a suitable mask material, and has properties of interest for direct incorporation in devices.

Electron-beam lithography is currently the principle technique for high resolution patterning of nanodevices and can in principle reach near atomic resolution, with resolution limited in practice by electron optics and resists used [76, 77]. Several electron-beam resists are available including poly(methyl methacrylate) (PMMA) [76], a benchmark polymeric resist, and ring-molecules such as calixarenes [78], a negative resist which displays ultrahigh resolution.

---

[3] A version of this section has been published as “Poly(ether sulfone) as a negative resist for electron-beam lithography” in Applied Physics Letters and was also selected for publication in the Virtual Journal of Nanoscale Science and Technology [74, 75].

Negative resists are often limited by a low sensitivity to electron exposure and the tendency to swell and buckle when developed [79]. Here it is demonstrated that thin films of poly(ether sulfone) (PES) act as a negative electron-beam resist with a reasonable sensitivity and good etch resistance.

PES is an engineering polymer that displays many desirable properties: low synthesis cost, good thermal character including a high glass transition temperature ($\approx$ 220 °C), resistance to chemicals including glass, silver, and aluminum etchants (although ketones, such as acetone, attack PES). As PES is transparent and is hydrophilic there is potential for microfluidic applications, and PES has already found use in optical applications [80]. PES is available in thin sheets, and can be spun cast into thin films on substrates. PES coatings are food grade and commonly used in cookware, electronics, and medical equipment as well as finding widespread use as a fluid separation filter - applications that demonstrate the robustness of PES. These attributes suggest that PES is a good polymer for use in microdevices; as PES acts as a negative resist, as shown here, devices can be directly fabricated, and the resistance of PES to chemicals allows etch mask applications.

Films of PES (Radel A-104P, Solvay) were formed by solvating in N,N-dimethylacetamide (DMAc) at a concentration of 4 wt %. Solutions were filtered with $\approx$ 1 μm pore filter paper and spun cast at 2000 rpm. Films were immediately soft baked on a hot plate at $\approx$ 100 °C for 5-10 minutes. Using a profilometer[4] (Alpha Step 100, Tencor) film thicknesses were measured to be nominally 80 nm near the edge of wafers, where film thickness is maximal due to the spinning process. Extremely smooth films were formed, with film roughness (R_a) of $\approx$ 1 nm over 100 μm profilometer line scans. Bare glass (pyrex), (100) Si, and $\approx$ 30 nm Au surfaces (with $\approx$ 5 nm Cr adhesion layers) were used as substrates for spin coating, with good quality films obtained in all cases (few observable defects on the 4" wafers used). Electron beam patterning was performed at 10 kV using a RAITH150 direct write e-beam lithography system [81]. Patterned films were developed at room temperature in DMAc

---

[4] Contact profilometers are essentially phonographs where a stylus is moved relative to a surface and vertical surface undulations are measured.

for 30 s, rinsed in isopropyl alcohol (IPA) for 30 s, and blown dry in nitrogen.

Varying dosage was used to pattern 40 μm squares to find the response of PES to electron exposure. The exposed squares were separated by 40 μm gaps to ensure no proximity effects occurred. After dosing and development the remaining film thickness was measured with a profilometer, as shown in Fig. 3.3. The sensitivity Q of a electron resist is defined as the dosage required to retain 50% of the film thickness, and was found to be $\approx 230\ \mu\text{C/cm}^2$ for PES at 10 kV, roughly 2.3X the value [82] for PMMA 950k ($\approx 100\ \mu\text{C/cm}^2$). The contrast of negative resists is defined as $log_{10}[D_{100\%}/D_{0\%}]^{-1}$, where $D_{100\%}$ and $D_{0\%}$ are the doses for full and no film retention, as extrapolated from the dosage curve. For PES the contrast is ≈ 0.8. A contrast of < 1 is not typically desirable due to electron scattering causing thick film patterns to lose aspect ratio, but is useful for creating holographic masks and 3-D lithography, or for use with thin ($< 1\ \mu$m) resist layers. Using DMAc as a developer distortion occurred in long thin features below approximately 100 nm in width, as seen for the 30 nm wide gate in Fig. 3.4, which can be attributed to swelling and buckling due to solvent absorption. Such swell induced effects are commonly observed in polymeric negative resists [76, 79].

To discern the suitability of PES for creating etch masks, both wet and dry (plasma) etching were performed. Patterned features in PES were developed on Au films, with wet etching done by standard gold and chrome etchants diluted by deionized water to reduce the etch rate of the metal films to reasonable time scales ($\approx$ 30 s). The patterned PES films withstood the Au and Cr adhesion layer etchants, allowing features to be defined (Fig. 3.4.b, inset). Isotropic reactive ion dry etching was done using PES as a mask on Si wafer pieces in a Trion Phantom, using a brief O_2 etch followed by a SF_6 etch. Typical results are shown in Fig. 3.5. A dry-etch selectivity of $\approx$ 4:1 (Si:PES) was found at room temperature by etching the PES mask away and measuring the resulting etch depth. This dry etch resistance is roughly four times higher than calixarene and sixteen times higher than PMMA in a similar gas [78] (SF_4), acceptable for many applications. Low temperature dry etching is know to increase selectivity of organic resists by $>$ 5X by suppression of

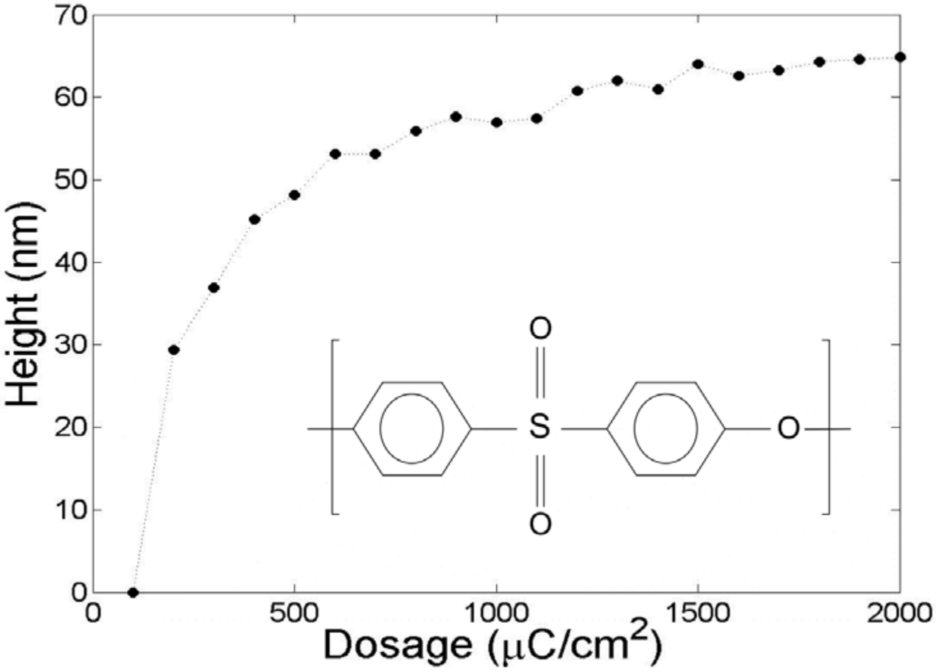

Figure 3.3: Exposure response of PES on a Si wafer to 10 keV electron beam. Thickness is measured with a profilometer after electron exposure and development with DMAc. The sensitivity was found to be ≈ 0.2 mC/cm^2, while the contrast was ≈ 0.8. The basic repeat structure of PES is inset.

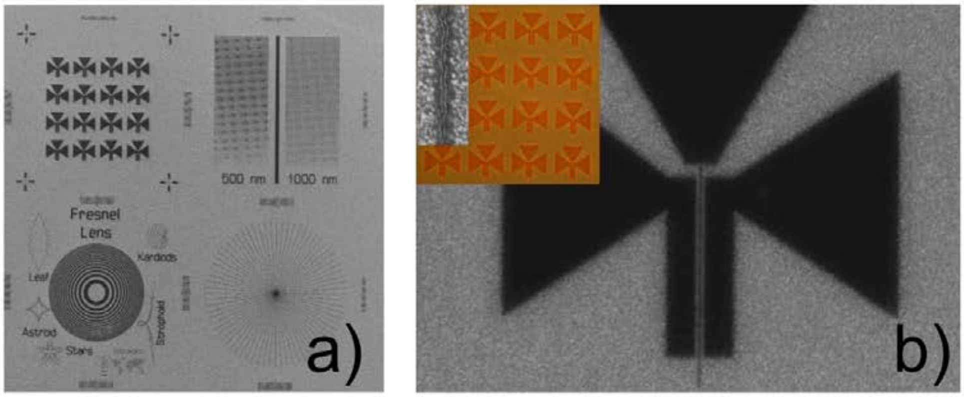

Figure 3.4: Patterned PES on Au. Patterning at 10 kV and 200 μC/cm^2 defined a wet etch mask for Au patterning. (a) Large scale features are well defined, (b) as dimensions fall below 100 nm solvent induced swelling can cause buckling of thin features as seen for the $\approx$ 30 nm gate of a field effect transistor structure (see inset for enlargement of 30 nm line feature). PES withstood Au and Cr etching of the $\approx$ 30 nm Au and $\approx$ 5 nm Cr adhesion layer (inset, b).

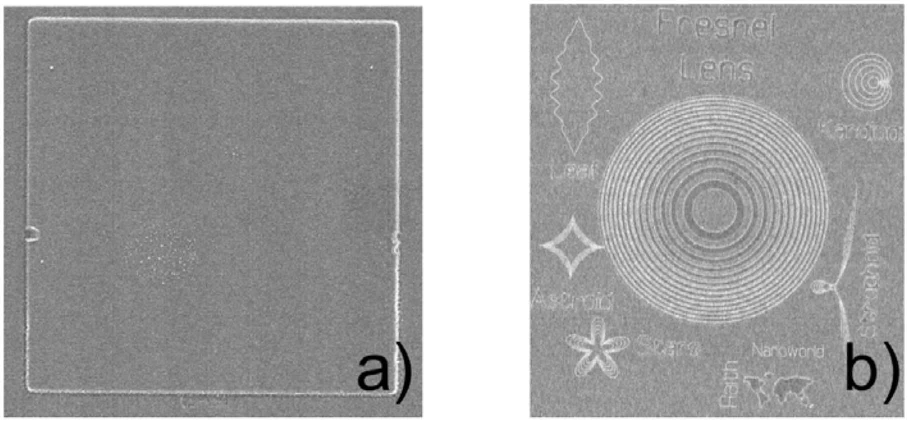

Figure 3.5: SEM images of dry etched PES. (a) 40 μm squares were defined in PES on Si and over-etched in a SF_6 plasma at room temperature, sidewall roughness is due to etching away the mask and notched stitching errors can be seen on the edges. A selectivity of $\approx$ 4:1 was found. (b) Lightly etched Si ($\approx$ 25 nm) with PES mask in place. A power of 30 W and 50 sccm flow of SF_6 were used.

surface diffusion allowing anisotropic features to be defined [83], and this is expected to hold for PES allowing improved etch characteristics.

Statistical cross-linking models and experimental evidence establishes that the product of sensitivity and average molecular weight is a constant in negative resists [84]. As the sensitivity-weight product is a constant it can be used to estimate dosages for differing molecular weight samples. Reducing polydispersity, for example by fractionation, will therefore improve the contrast and increasing the molecular weight will reduce the dosage required to define features. The molecular weight of the polymer stock used is 48,500 ± 2,500 with a polydispersity of 3.62 ± 0.35; where the error indicates variability between batches and the resolution of gel permeation chromatography used for measuring values [85]. For PES it is found that the sensitivity-weight product is 11 ± 1 Cg/cm^{2}mol, roughly double the value [84] for polystyrene (6.3 Cg/cm^{2}mol). For PES to have sensitivity better than PMMA 950k a molecular weight above 110,000 is required.

Resolution is limited by swelling, and swell induced buckling typically becomes a factor for features smaller than approximately the films thickness [86] due to mechanical instability (this rule of thumb is consistent with the buckling observed for 30 nm features here). As swelling occurs when solvent interpenetrates the cross-linked polymer network reducing solvent uptake becomes critical in achieving ultrahigh (nm) resolution. Using cold ($\approx$ 5°C) development [86] can reduce uptake; alternatively the chain network connectivity can be made dense by use of low molecular weight chains or increasing the number of cross-links per chain in high weight polymers, e.g. increasing the dosage, which should reduce the tendency to deform and swell.

Sulfone containing polymers are recognized as positive electron beam resists, as their scission rates are much higher than in other degrading polymers [87] due to the C-S bond being relatively weak and radical S-O chemistry leading to additional cleaving [88]. For example, poly(butene sulfone) is a positive electron beam resist with high sensitivity that led to its routine use in photomask production [87, 89]. The cross-linking response of PES is therefore surprising. Contamination writing or carbonization of polymer films can induce negative resist behavior but is discounted, as the corresponding activation dosages [76] are several orders of magnitude larger than the applied dosages here.

Cleaving at sulfone sites radicalizes the aromatic ring and subsequent modification and cross-linking at the aromatic ring is a mechanism that could be causing PES to act as a negative electron beam resist [88]. Inclusion of styrene (an aromatic ring) as a side-chain to sulfone polymer has been studied to improve etching characteristics of sulfones, and found to act as a positive electron resist [90] suggesting that the location of the radical site after cleaving is crucial for cross-linking to take place (on the aromatic ring here, versus off the ring in the case of poly(styrene sulfone)). These examples indicate that sulfone polymers are a promising avenue for developing electron beam resists, as the competition between scission and cross-linking can lead to both positive and negative resists. As sulfur is known to form stable bonds with every element (excluding noble gases, under most conditions [91]), in general, sulfur-containing polymers should display electron beam sensitivity as broken sulfur bonds can "glue" to close-by material.

In previous work, PES was used as the support layer in a low temperature nanodevice [92], due to its good thermal characteristics. Slight negative electron sensitivity was reported but not considered significant [92]. While a 40 nm Si layer and an 85 nm PMMA layer shielded the PES film the range of electron penetration is greater than 1 μm for these materials at standard electron beam voltages [76]. Further, the PES polymer used (Victrex 5003P, ICI) was similar to the one employed in the present work. As electron exposure would define the same features in the top (PMMA) and bottom (PES) layers, observable effects of PES electron sensitivity would be limited mainly to modified etch rates, which may explain the very small (and not quantified) sensitivity noted but not investigated further.

In summary, Poly(ether sulfone) can be used as a negative resist. A sensitivity-weight product of 11 ± 1 Cg/cm^{2}mol was found, corresponding to the sensitivity of 230 μC/cm^2 measured at 10 kV. Features were well defined when larger than the thickness of the film and PES displayed a high durability to sulfur hexafluoride reactive ion etching and withstood Au/Cr wet etchants. As PES is optically transparent and, in porous membrane form, widely used as a filter for fluids, electron beam patterned PES could be used to directly make optical [93] and microfluidic [82] devices, in addition to acting as a mask as shown here. However, as the film acts as a negative resist and works best on thin films ($< \mu$m) due to scattering direct prototyping of large scale devices such as standard microchannels would take long continuous writing making PES more suitable for "nanofluidic" (sub-μm channel dimensions and short lengths) devices.

3.4 Solutions: dilute to melts

Polymer solutions are formed by dissolving a polymer into a suitable solvent. The separation of polymer coils defines the type of solution. Selection of suitable solvents is essentially an art, and is mostly achieved through trial and error and educated guesses.

At the *overlap* concentration c_* near by polymer coils just begin to impinge on each other and overlap. As the concentration of polymer increases past overlap the solution is *semidulute* and becomes *concentrated* when coils interpenetrate to the point that thermal fluctuations are hindered when concentration passes a certain threshold c_{**}, which is on the order of 0.2-0.3 g/mL for polymers with molecular weight on the order of 10^6 Da [94]. In the absence of solvent the "solution" is termed a melt, when the polymer is above its glass transition temperature T_g and is a glass below T_g. Below the overlap concentration the solvent is *dilute*. Each regime of concentration shows scaling properties, e.g. for viscosity, that change as concentration moves past each demarkation. Due to reduced inter-coil interactions dilute solutions are most often studied as models and experimental studies are easier to control.

Diffusion in dilute polymeric solutions will have two basic regimes - an unhindered regime where a diffusing particle travels distances shorter than the distance between neighboring polymers and a regime where the particle travels farther than this interpolymer distance. Below the neighbor-neighbor distance diffusion will be unhindered and approximated by free solution diffusion, above this distance a "renormalized" background viscosity will be seen by the diffusing particle. The diffusion coefficient is given by the classic Nernst-Einstein equation

$$D_{tr} = \frac{kT}{Z}; \tag{3.2}$$

where D_{tr} is the translational diffusion coefficient, kT is the thermal energy, and Z is the friction coefficient for the diffusing particle. The Sokes equation for a spheres friction coefficient $Z_{sphere} = 6\pi\eta R$, with η being the solvent viscosity and R the (hydrodynamic) radius of the sphere[5], gives an estimate accurate for many solutes.

One can estimate the renormalized viscosity of polymers by using the Einstein viscosity equation for colloidal spheres [95]

$$\eta = \eta_0(1 + 2.5\phi); \tag{3.3}$$

where η is the effective viscosity, η_0 is the solvents viscosity, and ϕ is the hard sphere volume fraction. As more and more polymer is added to the solution it will tend towards the overlap concentration where all polymer coils begin to touch.

Experimentally $\frac{\eta}{\eta_0} = 2$ is often used as the defining condition for the overlap concentration [21], and conversion from the hard sphere volume to the concentration gives

$$\eta \approx \eta_0(1 + \frac{c}{c_*}); \tag{3.4}$$

where c is the concentration and c_* is the overlap concentration.

3.5 Towards dynamics: relaxation time and elasticity

.

In this thesis the behaviour of liquid polymers in microchannel is also investigated. In a certain sense almost nothing is “solid” or “liquid”, and these labels correspond to limiting cases where relative time scale of a materials characteristic response to an observation time allows good description of a simplified “solid” or “liquid”. Given enough time most materials will flow (rocks plastically deform in the earth), and on short enough time scales liquids act like solids (rapidly slap the surface of water). Polymers tend to sit at the boundary of the solid-liquid divide in practice, with their characteristic time scales close to time scales of interest in technology or normal life. Polymers are

---

[5] The hydrodynamic radius is often experimentally found and is believed to consist of the particles radius plus a shell of bound water, for hard particles.

huge molecules which can deform making their liquid behaviour more complex than in simple (small, essentially internally static) molecular liquids; polymer flows can be nonNewtonian.

When flows that carry polymer coils have sufficiently large velocity gradients [71] the coil will transition to stretching. At this point polymer coils will begin to stretch out and act as entropic springs that acts back against the flow, and various effects such as normal and second normal stresses results. The Weissenberg effect is a visually interesting effect where viscoelastic fluids will climb up[6] a rotating cylinder due to these normal stresses making the fluid “cling” to the rod, which is the opposite of the centrifugal “throw” Newtonian fluids experience[7].

The demarkation of the coil-stretch transition is defined by the *relaxation time* of the polymer coil, and this relaxation time is the single most important characteristic of polymers in solvent.

From the Gaussian model of a polymer random coil, equation 3.1, one can find [70] the entropy S

$$S = k_B ln(\Omega); \tag{3.5}$$

where k_B is the Boltzman constant and Ω is the number of conformations, as well as the Helmholtz free energy

$$F = U - TS; \tag{3.6}$$

where U is the internal energy and T is the absolute temperature. The internal energy is independent of the conformation, for ideal chains (where polymer conformations make random walks), while the entropy will be dependent on the conformation (equation 3.1). The free energy will reduce to

$$F = \frac{1}{4} k_B T \frac{R^2}{R_G^2} + C; \tag{3.7}$$

---

[6] Hence the alternative name of “rod climbing”.

[7] Bird *et al.* [2] note that viscoelastic secondary flows tend to be opposite to inertial secondary flows.

where C is a constant. The force f_x required to separate a chain by a distance R_x is

$$f_x = \frac{\partial F}{\partial x} = \frac{1}{2} k_B T \frac{R}{R_G^2}. \tag{3.8}$$

The form of this equation is that of a simple elastic spring, and as entropy is at the root polymer coils are said to be entropic springs. It must be noted that this entropic spring model is developed under theta-solvent conditions, and should be considered an approximate model. In practice deviation from this model will occur, to the extent that coils deviate from Gaussian coils.

One consequence of the entropic spring nature of polymer coils is that the coil is quite dynamic, and if one estimates the energy that is driving the spring as varying by $\frac{1}{3} k_B T$ in each direction one finds that[8] the dimension of the coil changes by roughly $\sqrt{\frac{2}{3}}$, as can be observed in Fig. 3.1.

As polymer coils act as entropic springs they can store energy, and they impart a “bending” or hoop-stress force (normal stress) when flow fields stretch them quicker then the polymer naturally relaxes back to a random globular state (see Fig. 3.6). As such polymeric fluids have a characteristic relaxation time. This characteristic relaxation time λ is a fundamental parameter describing polymer solutions and is approximately given by the Zimm relaxation time [96, 97, 70] for many dilute polymer solutions

$$\lambda \approx \frac{\eta_s R_G^3}{k_B T} \approx \frac{[\eta]_0 M \eta_s}{N_A k_B T}; \tag{3.9}$$

where η_s is the solvent viscosity, $[\eta]_0$ is the intrinsic viscosity of the polymer solution, and N_A is Agravado’s number. The radius of gyration can be found from a random walk model for the case of theta-solvents; in practice, however, theta-solvent conditions are often not satisfied, and R_G is experimentally found, for example using Dynamic Light Scattering or by finding the intrinsic viscosity through fitting viscosity-molecular weight data and obtaining Mark-Houwink fit parameters [70] ($[\eta]_0 = KM^a$, where K and a are fit parameters and M is the molecular mass of the polymer). In this work polyacrylamide

---

[8] by taking $E = f_x < x >= \frac{k_B T}{3}$

polymer is used in water-methanol solutions, which acts as a good solvent, and both Dynamic Light Scattering and Mark-Houwink parameters are used.

It is interesting to note that the approximate radius of gyration of 18×10^6 polyacrylamide, which is used here, is roughly 0.4 μm (see section 5.7), while the theta-condition random walk predicts a size of roughly 0.06 μm. This large difference between theta and good solvent radius of gyration is due to the large molecular size of polymer coils, allowing even small differences in solvent-monomer and monomer-monomer interaction energies to build-up leading to significant expansion of coils in good solvents relative to theta solvents [70].

In addition to this approximation the relaxation time can be found by fitting measured viscosity to models, such as the Oldroyd-B model that is found to describe dilute solutions [98]

$$\eta = \eta_s + N k_B T \lambda; \tag{3.10}$$

where N is the number density of the polymer molecules, or by watching dynamics in oscillatory shear experiments.

In the ultradilute limit various precise prefactors < 1 are often used in the Zimm estimate, however an unity prefactor has long been used in estimates [96, 70] and for nominally dilute solutions recent systematic rheological [97] experiments demonstrate that the ≈ 1 prefactor describes relaxation time in elongational flows. Additionally, FENE dumbbell models, a simple model that takes finite extension into account and offers reasonable agreement with experiments, gives a similar estimate, again with a prefactor of ≈ 1, for example see equation (13.5-30) and discussion in Ref. [2]. There is growing evidence that "dilute" solutions must be separated into dilute (below overlap in a stagnant liquid, but with possible hydrodynamic interactions, and even steric interactions due to coil stretching, in flowing fluids) and ultradilute [99] (displaying true molecular independence, even in flows) regimes.

Theoretical investigations of polymeric solutions indicate there is a spectrum of relaxation times, although experimental investigations and models seem to be well described (to the accuracy of investigations) by the "first

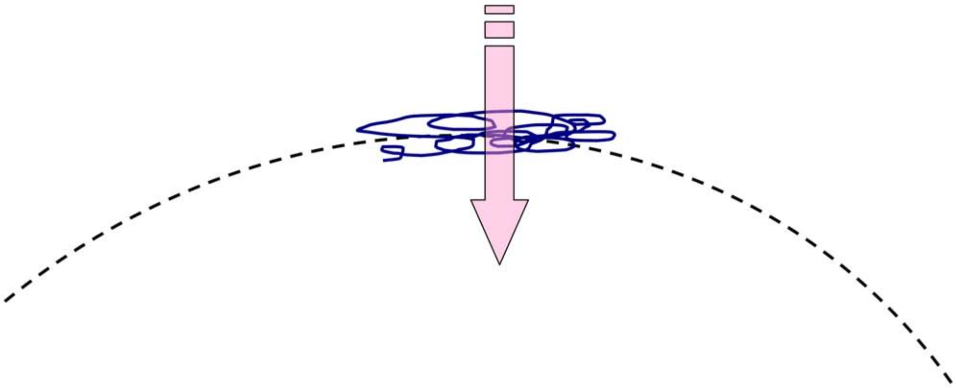

Figure 3.6: Stretched polymers can lead to instability. Polymers relax into random sphere-like coils, however stretching (normal force) can lead to a coil-stretch transition where polymers become elongated several times their equilibrium size. The resulting anisotropic fluid can lead to instabilities if stretched polymers move along curved flow lines - like a stretched elastic band pulled against an object an inward force is exerted which can cause polymers to cross stream lines [13], as illustrated in the schematic here, and lead to instability. Note that, in general, there can be a huge mismatch in dimensions of an elongated polymer relative to the curvature of flow lines. For example a polymer that has a maximal extension of roughly 20 μm, and which has a radius of gyration of roughly 0.5 μm at equilibrium, may experience a radius of curvature on the order of 3 mm [14] making for a weak inward force. However the distance over which this force is exerted can be significant (see equation 3.16 and discussion), and for the $\lesssim$ 20 μm polymer moving along a 3 mm radius of curvature flow line the distance the polymer travels while relaxing is roughly 0.8 times the radius of curvature [14]; this *sustain* allows for polymers to cross flow lines, despite the large mismatch between polymer elongation and curvature scales that may exist in a given arrangement. This *curvature plus normal forces* mechanism for instability was phenomenologically found [15, 16] and shows both empirical success in prediction of instability and can be interpreted in terms of physical mechanisms and now forms the conceptual underpinning of viscoelastic instabilities [17].

order" relaxation time [2].

Numerous models of *viscoelastic* fluids exist in addition to the Zimm and Oldroyd-B models [2]. The simplest conceptual model is the Maxwell model, the combines a viscous element in series with an elastic element in a simple chained spring-dashpot (see Fig. 3.7). Taking the shear viscosity η of the fluid

$$\eta = \frac{\tau}{\dot{\gamma}}; \tag{3.11}$$

where τ is the shear stress and $\dot{\gamma}$ is the shear rate, and the shear modulus G of the solid

$$G = \frac{\tau}{\gamma}; \tag{3.12}$$

where γ is the shear strain, defines a time scale for relaxation

$$\lambda = \frac{\eta}{G}; \tag{3.13}$$

where, for dilute solutions, it is seen that $G \approx \frac{k_B T}{R_G^3}$. Experimentally it is found that Maxwell's model does not accurately describe observations, and this divergence between theory and experimental is traced to the time derivative[9] [2].

3.6 Dimensionless number marking viscoelastic flow instability

The relaxation time describes the timescale for which polymers are no longer simply passive cargo in a fluid, but instead interact in a complex way with the flow fields causing secondary flows and even instabilities [2]. The dimensionaless number that demarcates this transition is most often termed the Deborah number [2], although there is inconsistent and somewhat confused use in the literature [100]. The Deborah number De is defined as

---

[9] Namely, the quantities are not scalars, but tensors, which require further constraints on the derivative - much like the vector quantities in fluid flow leads to the substaitative derivative; various models deal with constraining the time derivative in different ways.

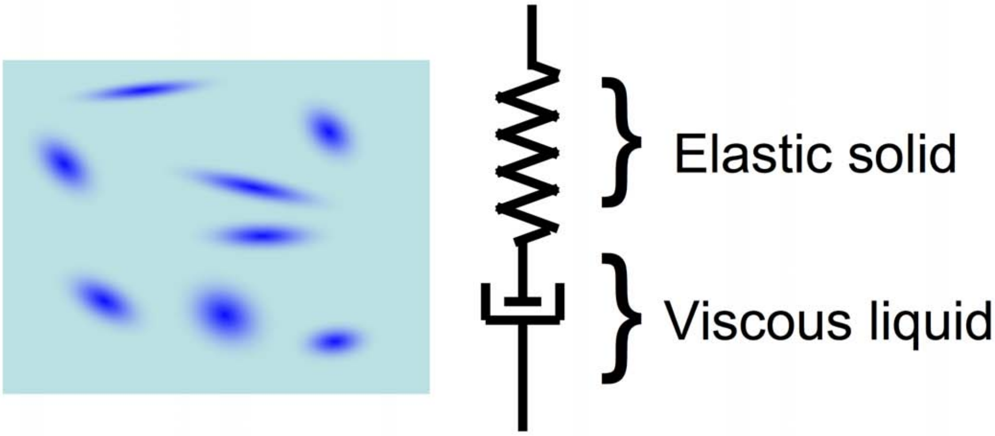

Figure 3.7: Polymer coils suspended in liquid solvent add elasticity to the viscous solution, when polymers are stretched. A model of polymeric liquids is the Maxwell model that assumes an elastic solid (Hookean spring) in linear series with a viscous liquid (dashpot) to obtain a simple viscoelastic composite material. The time derivative is not well described by the implicit scalar assumption in the Maxwell model, and to better characterize viscoelastic fluids various more complicated time derivatives are used. It is empirically found that the continuum models using the more accurate time derivatives are numerically unstable at high Weissenberg numbers close to physical instability limiting detailed numerical investigations, a persistent problem that is termed the HWNP (high Weissenberg number problem). Note that the bulk fluid has elasticity that arises from the polymeric component, the composite fluid is elastic in the sense that energy can be stored in, and later released from, the polymer coils within the fluid and a "bulk" spring-like object – for example due to a percolation network of entangled polymer coils connected throughout the fluid – is not required or thought to underlie elasticity [2]; see Fig. 3.6 for discussion on flow instabilities that can arise from the elasticity imparted by polymers.

$$De = \frac{\lambda}{t_{flow}}; \tag{3.14}$$

where t_{flow} is the normally taken as "time interval during which a typical fluid element experiences a significant sequence of kinematic events" [2], a definition that is somewhat vague and imprecise. The Weissenberg number Wi (or We) is a secondary dimensionaless number that is defined as

$$Wi = \lambda\kappa; \tag{3.15}$$

where κ is the characteristic strain rate in the flow. These definitions and labels are used interchangeably [100] and, due to Bird *et al.*'s [2] influence, De is normally taken as the label used when there is one dominant flow time. Despite the imprecise definition, and the somewhat imprecise relaxation time[10] instabilities are often seen when the De/Wi number is of O(1), with transition values scattering between roughly 0.5-10 in the literature.

It should be noted that there is another dimensionless number that can be used to predict instability for no-slip boundary condition (mechanically driven) cavity flows, where both shear and elongation effects occur, which was developed by McKinley, Pakdel, and Oztekin [15, 16] and is given by

$$\left(\frac{\lambda U}{R}\frac{\tau_{11}}{\eta_0\dot{\gamma}}\right)^{1/2} \geq M_{cr}; \tag{3.16}$$

where λ is the relaxation time of the liquid, U the characteristic streamwise fluid velocity, R is the radius of curvature of flow lines, τ_{11} the normal stress in the direction of flow (elongational stress), η_0 the zero shear viscosity[11], and $\dot{\gamma}$ is the shear rate. The parameter λU is the characteristic length a perturbation travels before decaying, and scaled by the radius of curvature R this gives a relative perturbation travel distance. M_{cr} is observed, either experimentally or via numerical simulations. One can recognize $\eta_0\dot{\gamma}$ as the shear viscosity, and thus the general form of

---

[10] Which is often found by a fit to a model, with different models giving somewhat different values of the relaxation time [101].

[11] Shear thinning, or thickening, can modify the viscosity as shear changes - most often the zero shear rate viscosity is used to characterize a fluid.

$$\text{(Relative Perturbation Travel Distance)}\left(\frac{\tau_{elong}}{\tau_{shear}}\right) \geq M_{cr}. \tag{3.17}$$

This result can be molecularly interpreted using Chu *et al.*'s work on direct optical observation of single molecules in elongational and shear flows [102, 10], which demonstrate that elongation stretches out polymers ("stretching springs" and storing elastic energy) and shear will lead to tumbling and polymers "resetting" to the globular coil state (see Fig. 3.8 for an example of direct observation of single molecules). At high elongation rates elastic stretching will occur, while at high shear rates tumbling will tend to reduce the likelihood of elastic storage, and the relative perturbation travel distance will increase likelihood of streamline crossing. It should be noted that while this criteria has been developed by inspecting a number of different canonical flow geometries, and can be intuitively explained, the advantage of this criteria over the classic De/Wi number is not obvious. As the De/Wi number is both simpler, more widely used, and more general[12] the De/Wi number is considered here.

3.7 Coil-stretch transition: Instability, theory, models

When polymer coils stretch in strong enough flow a sharp transition can occur, and the conformation of the polymer goes from approximately a spherical shape to an elongated stretched out object that can be completely unraveled and even stretched. The transition in elongational flows occurs nominally at Wi = 0.5, as predicted with the Zimm model [103] (i.e. for dilute solutions). It should be noted that this threshold value is considered "the" threshold for polymers, despite the fact that varying polymeric systems should be described by slightly differing constitutive equations. The 0.5 value has been determined for dilute polymers, and has also be reported to hold for melts [104] - a sys-

---

[12] For example, the McKinley *et al.* condition has been explicitly found, and investigated, for no-slip flows, and therefore in the regime of significant shear; additionally, for a given geometry the McKinley *et al.* condition can be cast into a De/Wi condition.

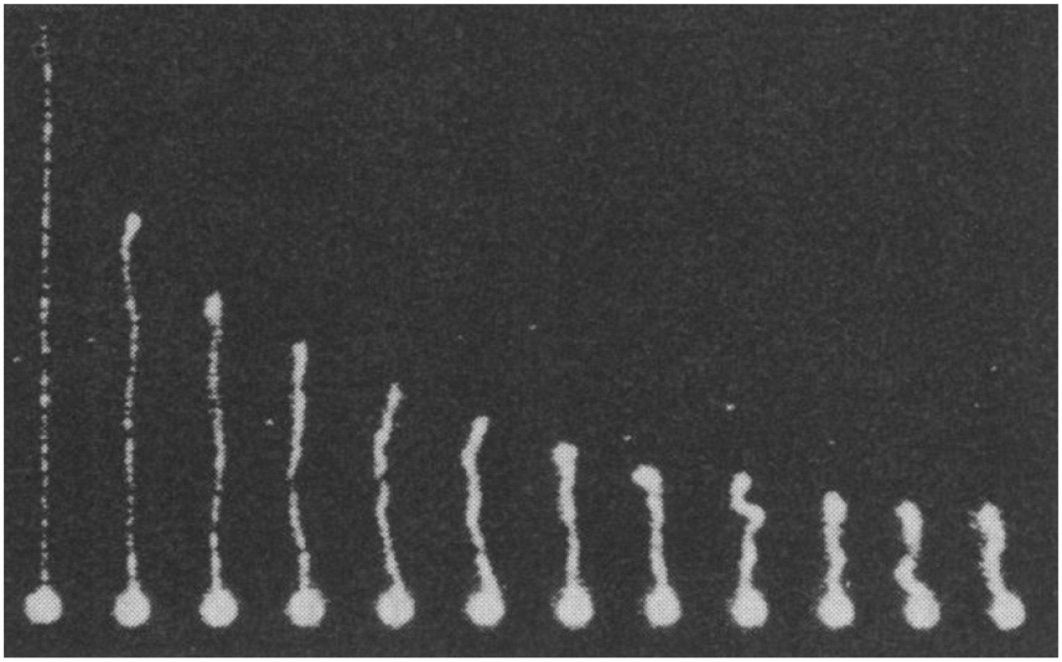

Figure 3.8: Relaxation of a stretched polymer. Fluorescently labeling DNA molecules has revolutionized polymer studies as investigation of *molecular individualism* and direct observations of single molecules are now possible. Here a DNA polymer stretched to its full 39 μm length shows rapid initial recoil, followed by exponential relaxation. Figure from Ref. [18]. Reprinted with permission from AAAS.

tem that is at the opposite concentration limit - which indicates the threshold may be universal. As various models are selected to describe real systems this possible universality may simply indicate the central role of the coil-strech transition and an insensitivity of the transition to specific environmental details; while the particular stability analysis of a given theoretical model should change dependent on theoretical details if the nominal threshold is too far from that described by the coil-stretch value the model would be considered inaccurate[13]. It should be noted that the high Weissenberg number problem (HWNP), a problem where numerical simulations fail near Wi = O(1) for *all* analytical (continuum) models of polymers [105], is consistent with all theoretical models describing an physical coil-stretch transition near the same value (hence the generic coincidence of numerical failure, which is though to be ultimately due to a physical instability in flow [105]).

Direct measurements done via optically labeling DNA molecules [102] have found a transition threshold of 0.4 versus the predicted 0.5, however, due to experimental uncertainty, this value is consistent with the theoretical value of 0.5. Larson points out [96] that project-to-project error for the high viscosity solvents used to create Boger fluids (such as in Ref. [102]) can be up to 100%, due to viscosity being sensitive to temperature and evaporation effects, making it plausible that the 0.4 threshold is due to measurement inaccuracy within a given experimental project rather than indicating a threshold differing from theory. Later experiments on larger DNA molecules, done by the same group to probe predicted hysteresis effects due to conformation[14] find a "from below" transition at 0.5 [106] versus the earlier 0.4 threshold found for smaller molecules [102]. They note that for the smaller molecules [102] a single transition (e.g. no hysteresis) is observed, however they do not discuss

---

[13] Of course a "toy-model", i.e. one that gives qualitative insight, has differing selection criteria (namely ease of manipulate and the belief that qualitative features are correct); for example the de Gennes's dumbbell model has a threshold of 0.275 versus 0.5, however this value is not expected to be correct and the model is used to provide general insight [103].

[14] Approaching the coil-stretch transition from below will result in spherical conformations, versus elongated conformations which will occur from above, which results in hysteresis for very large molecules (e.g. larger than explored in the experiments carried out in this thesis, see [106])

the 0.4 threshold value found in the earlier work in regards to the new experiments. From above the coil-stretch transition occurs at 0.4 for the larger molecules [106], however in that work the smaller molecules (i.e. those with a threshold previously identified at 0.4) relax back to the coiled state from a pre-streched state at Wi = 0.4 - clearly the threshold is higher in the second experiment for the same molecule. Additionally, work by a different group (the Steinberg group) on the same polymer as in Ref. [102] finds a transition near 0.5 [107]. In short, due to the extreme sensitivity of the solvent used in direct visual experiments, which give the clearest evidence on the coil-stretch threshold, experimental error is sizable and experiment is consistent with theory; theoretical analysis and bead-model simulations (e.g. Brownian Dynamics simulations) currently offer the most precise insight into the location of the transition, which is identified at 0.5 for dilute solutions [103].

Since roughly the 1970s there has been significant efforts at simulating polymer flows, with much work focusing on continuum approaches [105]. This focus on continuum work is due to various factors, for example the possibility of modifying Navier Stokes computational fluid dynamic packages, the hope to bridge the scale issue (small molecules in a fluid system that can have dimensions hundreds, thousands, millions of times larger, making full a computational approach impossible), and the ability to glean insights from analytical forms are key reasons. However, despite strong and sustained efforts such work has remained sharply limited by the HWNP, which is now thought to be fundamentally due to an inability of standard approaches to capture exponentially growing stresses and diverging trajectories near instabilities [108]. However, despite this sharp limitation a general overview of the constitutive equation (see Vol. 1 of Ref. [2] for a solid discussion on various particular models) is in order as these models have driven much of the insight and understanding of polymer flows.

A simple dumbbell model (known as the Oldroyd-B model) is outlined here, loosely following Larson [109] and drawing on Ref. [110] and Ref. [111].

Considering a polymer coil in suspension as a Hookean elastic dumbbell, e.g. as two beads connected by a linear spring, the Langevin equation describing the balance of forces is

$$\dot{\boldsymbol{R}} = \boldsymbol{R} \cdot \boldsymbol{\nabla v} - \frac{1}{\lambda}\boldsymbol{R} + N\xi; \tag{3.18}$$

where the stretching of one of the beads making up the polymer is due to the stretching of the fluid element (first term on the RHS), which relaxes back due to the spring force with a relaxation time λ (second term on the RHS), and is also driven by thermal noise Nξ (final term on the RHS). The thermal noise here is somewhat subtle, as handling the thermal movement involves a stochastic process[15] - a "random" process is sampled at discrete times in order to emulate the thermal motion. To implement this a Brownian Dynamics simulation is often used in practice [111], which involves interplay with the computational time step being imposed resulting in a motion of $\sqrt{2D\Delta t}\xi$, where ξ is a Gaussian random number, sampled every Δt. The diffusion coefficient D of the bead, in turn, is often estimated by the Nerst-Einstein equation 3.2, where the Stokes equation for spheres friction coefficient is used.

Equation 3.18 is an approximation that uses only 2 beads connected by a spring (dumbbell), ignores hydrodynamic interaction between "beads" making up the polymer, assumes an uniform velocity gradient over the polymer, and often simply uses Stokes' law to find the coefficient of friction; each of which adds some error and more accurate terms and assumptions can be used to extend this approach. Never-the-less this general approach conceptually describes how the polymers themselves are forced by the fluid, and by *simultaneously* solving the Cauchy equation 2.1 and a constitutive equation describing the stress-deformation relationship of polymers in the liquid - such as equation 3.18 - flow dynamics can be obtained[16].

---

[15] Stochastic modeling is phenomenological, and discriminates between "fast" and "slow" processes. By "integrating out" and then reintroducing the fast motions (e.g. thermal forces here) a simplified system is created, however the reintroduction of the fast motions is somewhat tricky and the details, such as the size of the artificial time step used to evaluate and introduce thermal forces, affect the final equation.

[16] Traditionally the conformation tensor $\sigma_{ij} = \frac{\langle R_i R_j \rangle}{R_G^2}$ is used to describe the polymers in the liquid versus the R used here; to introduce the back-reaction of the polymers on the fluid flow the stress tensor in the Cauchy equation is split between a solvent (e.g. Newtonian) component and a polymeric part given by nK$\langle R_i R_j \rangle$, with n being the number of polymers in a fluid element, the angle brackets averages conformation over the element, and K is the

Various modifications to equation 3.18 lead to different constitutive equations, for example using finite extensible nonlinear elastic (FENE) spring potentials allows for more realistic modeling of finite extensibility and "hardening" of polymers as they reach their full extension [2]. Here a differential approach was outlined, but an integral approach can also be taken opening up even more constitutive models [2]. Note that instead of explicitly following every discrete polymer coil in solution (which also can be done, at a cost of numerical effort) the constitutive equation, for example equation 3.18, is considered a field and the discrete polymers are treated as a continuum. Often in making this continuum approximation from underlying discrete components various averages and approximations are made to simplify the resultant equations.

Different details lead to various models, but the basic approach is to create a coupled system of equations: one (the Cauchy equation) which describes the flow of the fluid, and a constitutive equation used to "close" the Cauchy equation by describing the polymeric stress-deformation relationship in order to determine the stress tensor. These equations are coupled together - the fluid forces the polymers which act back on the fluid - and there are two different aspects that can cause nonlinearity in flows. First, there is the familiar inertial component in the Cauchy equation which is nonlinear in velocity, leading to high Reynolds number instability, and secondly there is the modified (polymeric part of the) stress tensor. This stress tensor is nonlinear due to the elastic nature of polymers and can create unstable flow when polymers are driven above the coil-strech transition, as large changes in stress occur small perturbations can become amplified. This is seen both experimentally and in the models themselves [2].

In Fig. 3.1 it can be seen that even in stagnant liquids polymer coils "breath", and as pointed out in Ref. [102] in a discussion of behaviour of individual polymers in elongational flows, "Some molecules deformed only slightly, whereas others rapidly reached a steady-state extension", "This large and

---

Hookean spring constant; again, various ways of averaging, different spring constant, etc. can be incorporated in the polymeric component of the stress tensor previously unobservable heterogeneity was perhaps unexpected because these molecules were identical in size and had experienced the same [conditions]" [102] and that "Polymers do not undergo a simple, collective and simultaneous unwinding as soon as $\dot{\epsilon} > \dot{\epsilon_{cr}}$." Polymeric liquids therefore display a *molecular individualism* where apparently the precise conformational state dynamically changes (due to thermal agitation) and small differences introduced can be "amplified" during the coil-stretch process. These mechanisms (thermal perturbation of polymers and "amplification" of noise/conformational differences) are deeply embodied in the conceptual and theoretical models which have long been used (e.g. Brownian forces make polymers "springs" and nonlinear stress causes elastic instability in polymer flows), but the efforts spearheaded by the Chu group only recently demonstrated just how dynamic the individual molecules behave.

In summary:

- Polymers tend to form random coils in solution,
- The coil-stretch transition demarcates when polymer coils experience significant stretching, and therefore behave as elastic springs which transforms the flow from one of viscous to viscoelastic,
- Polymer coils can be, and are, often conceived as inert entropic springs; note, however, that the model development depends on theta-solvent conditions, where the polymer interacts with itself and the solvent equally resulting in random walk dynamics and tractable mathematical structure, in practice the polymer may "prefer" itself (bad solvent) or the solvent (good solvent) and the entropic-spring model should be considered a qualitative and highly simplified approximation for non-theta-solvent conditions,
- Polyethersulfone films can be patterned with electron beams; however its negative resist properties and electron scattering make PES promising for masking but not for direct rapid prototyping of standard microchannels; for this reason PES microfluidic devices are not investigated here,

but they remain a promising option to investigate for sub-μm wide microchannels and smaller devices ("nanofluidics") as these films are hydrophilic, transparent, robust, and - as seen here - patternable,

- Below the overlap concentration where polymers begin to impinge on each other the coils are nominally independent, and the low concentration and lack of (reduced) polymer-polymer interactions simplifies both experimental and theoretical investigations,
- The solution viscosity is $\eta \approx \eta_0(1+\frac{c}{c_*})$ in the dilute concentration regime,
- Polymer coils are not static rigid spheres, but instead are quite dynamic with change in physical dimension of up to $\approx \sqrt{\frac{2}{3}}$ over the time-scale of the relaxation time,
- The Deborah number De (and/or Weissenberg number Wi) is a dimensionless number that indicates when elastic instabilities are expected - when De/Wi is of order 1 instabilities can occur,
- Viscoelastic fluids are often described with a continuum model that incorporates solid (spring) and liquid (viscosity) models in series; due to tensor quantities the time derivative is not a simple scalar and various more complex forms have been found to describe various polymer solutions; for these continuum models numerical instabilitity will effect simulations close to physical instability which limits numerical study of instability. This problem is so persistent that it has earned the acronym HWNP ("the high Weissenberg number problem"), and addressing this problem is a key concern in polymeric studies. Currently the precise[17] nature of instabilities, such as scaling properties, near and past physical instability threshold is not known,
- The constitutive equations for polymers (to fully describe the Cauchy equation with a polymeric component to the stress tensor a constitutive, or stress-deformation relationship, is required for the polymers) describes

---

[17] Or even general shape.

a secondary source of instability, in addition to the inertia aspect familiar in Newtonian liquids a nonlinear aspect to the stress tensor is introduced by the elastic nature of polymers,

- The direct observations of polymer dynamics spearheaded by the Chu group provide clear and striking evidence of molecular individualism, a finding that is latent in the conceptual and theoretical framework of polymers.

Chapter 4

Instabilities: Overview

4.1 Are inertial instabilities viscoelastic in origin?

Traditionally instabilities in fluids are described as being inertial in origin, with instabilities arising when fluid “particles” have sufficient momentum to cross stream lines thereby destroying laminar flow and setting up unsteady, chaotic, and eventually turbulent flow. However, despite having a simple common origin the critical Reynolds number which signals the onset of instability in a flow is neither precise nor accurate, in the sense of being a well defined universal number. For a given experimental system instabilities can arise at critical Reynolds numbers that are orders of magnitude different from another system (compare pipe flow, with $\mathrm{Re} \approx 2000$, with flow past a cylinder or sphere with $\mathrm{Re} \sim O(10^5)$). In contrast viscoelastic flows, where elasticity is the simple common mechanism that gives rise to instability, onset of instabilities is fairly well described by the Deborah/Weissenberg numbers, and these numbers give accurate prediction of unstable conditions. Further, it is known that *all* fluids are viscoelastic, and it is simply the large separation in characteristic fluid and flow time-scales that allow fluids to be approximated by elastic free conditions. The non-universality of the critical Reynolds number and inherent viscoelastic nature of fluids suggests that what is commonly thought to be an inertia instability mechanism may be viscoelastic in origin.

To test the plausibility of a viscoelastic mechanism behind “inertial” instability an instability in flow past a sphere is considered.

The Strouhal number is a dimensionless number which relates the frequency of oscillating flows, such as the oscillations in the wake of a blunt object moving relative to a fluid (such as a large truck on the highway). For a sphere the Strouhal number St is

$$St = \frac{fD}{V} \approx 0.2; \tag{4.1}$$

where f is the frequency of oscillation, D the diameter of the sphere, and V the relative velocity of fluid. The Deborah number is

$$De = \lambda \frac{V}{D}; \tag{4.2}$$

with λ being the relaxation time, V the velocity, and D the diameter of the sphere. In the wake of the sphere a pocket, or "bubble", of lower density fluid exists. It is known that bubbles act as (viscoelastic) Hookean springs [112], with the spring constant being approximately equal to the surface tension. Taking this known viscoelastic nature of bubbles, we can interpret the observed frequency as a measure of the relaxation time of the trapped low pressure bubble in the wake of the sphere. Under this assumption one finds that

$$\lambda = \frac{1}{f} = \frac{D}{0.2V} \implies De_* = \frac{D}{0.2V}\frac{V}{D} = \frac{1}{0.2} = 5, \tag{4.3}$$

which is above the critical number of De_* of approximately 2 found for viscoelastic flows past spheres in containing cylinders [113]; however the critical value in these experiments will be reduced due to the wall effects. In dye coated ball dropping experiments where wall effects are excluded a qualitative difference was found between fluids with De = 1.44 and 3.95, which showed "dual-wake" effects (a primary and a delayed separation of flow lines), and fluids with De = 8 and 30 which showed single wake (separation of flow lines) [114], demonstrating a change in qualitative behaviour between De ≈ 4-8, consistent with the estimated $De_* = 5$ here. More recent and more detailed experiments [115] show instability of dropping spheres starting to appear at De ≈ 4, where occasional instability would be observed despite stable movement for the majority of the experiment, and clear instabilities at next highest De of

≈ 7, again consistent with the prediction of $De_* = 5$ for "inertial" instabilities in the wake of a sphere, reinterpreted with a viscoelastic mechanism.

The similarity of the critical De number estimated for a "pressure bubble" trapped in the wake of a sphere, and the critical De number of the flow of a classic viscoelastic fluid past a sphere is consistent with the hypothesis of a viscoelastic mechanism for what is classically thought to be due to inertial effects.

In the literature of bubbles in viscous liquids further support can be found for this bubble mechanism. It is found that bubbles will cusp in highly viscous flow. Comparing the estimated Deborah number for when cusping occurs in Reference [116] one finds[1] that $De_* = 3.1$ which is roughly half the value estimated here for the inertial instability. This off by a factor of two with regard to the stationary bubble case - but almost exactly the same value as viscoelastic fluids in a similar experimental set up where a critical value of 3.2 was found [20]. The similarity gives further evidence that bubbles act like (viscoelastic) springs. One can speculate that a bubble trapped in the wake of an object would experience an enhanced Deborah number relative to a free-flowing bubble, however the estimation of Deborah numbers are inexact and the arguments here are rather heuristic.

In addition to providing an possible explanation of von Karman votex shedding that appears to be consistent with both flow of pure viscoelastic fluid past a sphere, as well as free flows of deforming bubbles, the "viscoelastic bubble" model is an attractive mesoscale model for polymer flows. By modeling polymer coils of radius R_G with equivalently sized bubbles (R_{HS}) and selecting the surface tension to model the relaxation time of the polymer a tractable computational model can be developed. Each individual polymer with its ever changing conformation is replaced by a bubble of an equivalent size and with the surface tension tuned to match the relaxation time of the polymer, in this manner a simple approximation of the system which retains

---

[1] To estimate the relaxation time one finds that $\lambda = \frac{3\eta R}{K}$, which using K $\approx \sigma$, allows $\lambda =$ 2 s to be found for the experimental liquid-bubble mixture. The authors give the condition where cusping occurred, which corresponds to a shear rate of 1.55 /s, which allows De = 3.1 to be estimated for the roughly 0.8 mm wide bubbles.

discrete "polymers" is obtained. In exchange for simplicity two key losses occur - loss of thermodynamic (fluctuation) motions, which are significant (with polymers "breathing" at the relaxation time (see Fig. 3.1)), and the analytic niceties of continuum models which allow special cases to be solved in order to gain insights. As the analytic approach is somewhat intractable [105] and as comparison can be made with solved test cases and experiments the computational nature of the model is relatively a minor tradeoff, while the loss of fluctuation dynamics is bound to be significant under some conditions. Additionally bubble-bubble repulsion will be large at close ranges, whereas polymer coils will be able to interpenetrate each other, which will lead to the model becoming unrealistic unless quite dilute solutions are considered.

We have seen that Bejan accurately predicts the instability in free jets based on jet bending elasticity, and that elasticity associated with pressure "bubbles" in the wake of a blunt object appears to predict the observed von Karman votex street. Both these cases suggest that at least some instabilities classically considered to be inertial in origin may be instead due to elasticity.

4.2 Elastic instabilities and elastic turbulence

Numerous elastic instabilities have been noted in polymers due to their widespread industrial use [109]. Since the 1970's increasing scientific study of viscoelastic fluids and their instabilities have been undertaken, and several technical advances have been made: (1) direct imaging of optically labeled DNA molecules which allows the underlying components to be observed, (2) uniform and steady filament stretching apparatus which enables elongation studies in addition to high quality shear apparatus[2] which have long been available, (3) creation of model dilute polymer solutions (Boger fluids) allowing theory and experiment to be better compared, and (4) increase in computational speed allowing still limited but realistic numerical investigations [109]. In addition to these technical advances the discovery that elastic instabilities can develop into a true *elastic turbulence* [19] as the Deborah/Weissenberg number increases,

---

[2] Elongation and shear being two key distortion mechanisms imposed on fluid flows.

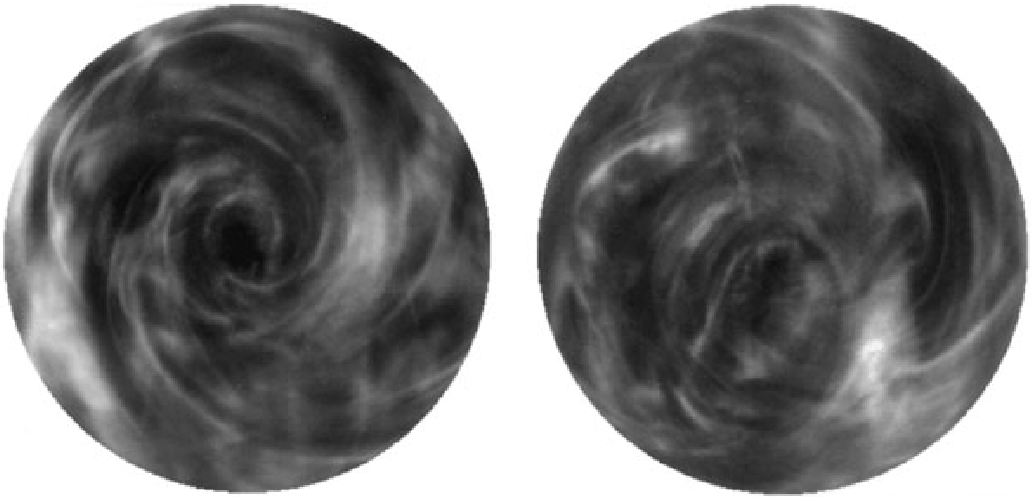

Figure 4.1: Elastic turbulence in shear geometry. Doping highly viscous (via inclusion of sugar) polymeric liquid with reflective flakes allows irregular flows to visualized. The two images are two separate snapshots taken of the unsteady flow. Here the flow is creeping (Re=0.7), but has a high Wiessenberg number (Wi=13). It has long been known that polymeric solutions can undergo instabilities and studies of this flow allowed determination that elastic turbulence is a true form of turbulence, and established this form of turbulence as a type of Batchelor turbulence. Due to favorable scaling (increased tendency to instability with reducing system dimensions) viscoelastic instabilities and elastic turbulence is of interest to microfluidics. Reprinted by permission from Macmillan Publishers Ltd: Nature Ref. [19], copyright 2000.

much like the steady, unstable, turbulence advancement in Newtonian fluids with Reynolds number, has peaked fundamental interest in polymeric fluid instabilities.

Elastic turbulence has many of the main characteristics of Newtonian developed turbulence, and has been shown to be Batchelor turbulence[3] [31].

Groisman and Steinberg demonstrated that elastic turbulence is a true type of turbulence in their early work [19, 20, 31] and the Steinberg group also showed that chaotic flows exist in microchannel [21] replica of serpentine Dean flows that had earlier been studied on a macroscopic scale [20]. In addition to these flows were precise quantitative description of instabilities were established it has long been know that rapid constriction/expansions can lead to instabilities (see chapter two of [2] for a general overview), for example

---

[3] Batchelor turbulence exists in the regime below the “Kolmogorov dissipation scale” in high Re turbulence, a regime that is normally difficult to access.

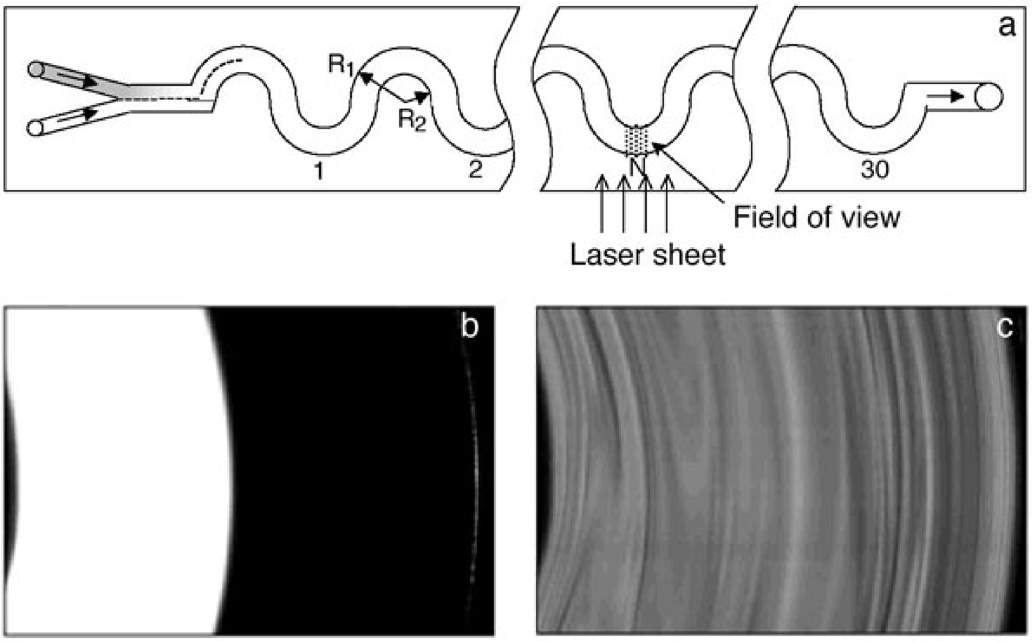

Figure 4.2: Demonstration of turbulent mixing in serpentine Dean flow. Dyed and undyed liquids are brought together (a) and gravity pumped through the curvilinear geometry. For no polymer (b) and polymer doped (c) liquids at the 29^{th} half-ring either little (b) or enhanced (c) mixing occurs at $\mathrm{Re} = 0.16$ (and $\mathrm{Wi} = 6.7$ in (c)). The observed enhancement in mixing was orders of magnitude improved over the polymer-free sample. Note that both here and in Fig. 4.1 the solution viscosity is made much higher than in most lab on a chip applications, where aqueous solutions are typically used. Reprinted by permission from Macmillan Publishers Ltd: Nature Ref. [20], copyright 2001.

modification of serpentine microchannels [21] to add asymmetric corrugation (triangular constrictions followed by sudden expansions along the channel) demonstrates the formation of unstable vortices [117] when polymeric fluid is pumped through the channel at sufficiently high rates. These unstable vortices are excited in linear channels as well and display apparent random growth and decay dynamics [118] which, due to the corrugation asymmetry, display differing dynamics depending on flow direction. The unstable vortices arise at Re < 1 for highly elastic polymeric liquids; in the same device Newtonian flow (water) also displays vortices at intermediate Reynolds numbers (Re ≈ 5) due to inertial effects.

The seminal efforts of Steinberg *et al.* has spawned various studies of of elastic turbulence and other highly unstable viscoelastic flows. The schematic process that leads to elastic instability is the stretch-coil transition that elongates polymer coils which then act like stretched springs that can cross curvilinear laminar flow lines via "hoop stress", or the normal stress[4], and this stress will induce a secondary flow that moves polymers across flow lines and which can lead to instability. This basic mechanism of crossing curved flowlines is thought to be the main cause of polymer instabilities [119], and all work appears to support this model[5].

Viscoleastic instabilities follow a $\frac{1}{d}$ scaling, making microfluidic (small d) devices a natural consideration, and various efforts have been undertaken to investigate viscoelastic flows in microdevices. Experimentally pressure or other mechanically driven flows are the pumping schema previously studied experimentally, while some numerical work has investigated electro-osmotic flows of viscoelastic fluids (see the next section). Zig zag flows, similar to microchannel

---

[4] Pull an elastic band tight around an object, and it will exert a force against the object. Likewise there will be a force that will pull a stretched polymer coil inwards was it flows along a curvilinear path [13].

[5] There is at least one exception to the rule that curvilinear flows are required - in Ref. [120] instabilities have been numerically found in a non-curvilinear (Kolmogorov) flow at high Wi numbers. An experimental realization or independent numerical work has not yet confirmed the finding, however the instability is consistent with expectations: high stretch of polymers will eventually lead to sensitivity to perturbations, the roughly order of magnitude increase in critical Wi number versus those seen in curvilinear flow geometries is consistent with the "requirement" for curvilinear flows and is perhaps the proverbial exception that proves the rule.

Dean flows [21], have been studied [121] and instabilities were found to allow high flow rates to be used (reduced diffusive mixing at high flow rates normally prevents use, if mixing is required). Nguyen *et al.* (see Ref. [122] and subsequent work) have investigated fast flows of viscous polymer liquids through a sudden constriction/expansion, where they find a "whipping" filament structure that leads to mixing. Studies of cross-slot flow have found asymmetric flow followed by instabilities [101]. H-filter flow of saliva was found to have interfacial instabilities, negatively affecting performance, [123], demonstrating unintended viscoelastic fluid effects. "Flow focusing" of particles [124] was demonstrated for viscoelastic fluids moving through straight channels. Entry flow of elastic fluids in microdevices have been systematically investigated [125]. In addition to interest in physical flow it has been demonstrated that memory and control can be achieve with viscoelastic fluid flows in microdevices [126].

4.3 Electro-osmotic flows of viscoelastic fluids

The majority of microfluidics research has investigated simple fluids. As the core understanding of various mechanisms, operating conditions, and key limitations and strengths has grown increasingly complex fluids are being investigated. The investigation of electro-osmoticallly driven viscoelastic fluids has been partially investigated. Numerical computation of EOF flow in square microchannels was investigated (Ref. [127]), for *explicitly steady state* flows. In later work the authors appear to retain the time derivative, however do not observe instabilities despite the enormous Deborah numbers that would be present in the Debye layer. Flow velocity is reduced for viscoelastic fluids, however the viscoelastic fluids have higher viscosity[6] which will account for some of the observed shift. In the approach used a continuum model is assumed, which limits the approach to small polymers which will not be entropically repelled from the Debye layer [128]. Afonso *et al.* also investigate EOF

---

[6] Both solvent and polymer contributions occur, and seem to be contrasted with the solvent only case versus a solvent with an identical overall viscosity - rough estimates indicate that the majority of the differences is due to this increased overall viscosity.

flows in microchannels, and also find that plug profiles exist as for Newtonian liquids and, again, they also do not see any instability due to their analytical approach which eliminates the time derivative. Experimentally entropic depletion near the surface is seen [128, 129], unless surface binding occurs such as in the case of H-bonding with the surface [129].

4.4 Viscoelastic instabilities in electro-osmotically pumped viscoelastic fluids?

The presence of viscoelastic instabilities in microdevices has been demonstrated for pressure driven flows. As electro-osmotic pumping is a widely used alternative to pressure driven flows the possibility of exciting viscoelastic instabilities with electro-osmotic pumping is of interest for (1) intentionally driving instabilities for fundamental studies or improved mixing, and (2) the possibility of unintended exciting instabilities which may affect device performance, as has been seen in pressure driven flows of saliva in an H-filter [123].

Viscoelastic instabilities arise due to elastic stretching and bending of the underlying polymer in solution (see Fig. 3.6, enabling instability in low Reynolds numbers. In mechanically driven flows it has been found that the instabilities lead to irregular flow patterns (Fig. 4.1) and can improve mixing (Fig. 4.2), and for channel flow mixing visually appears like repetitively folded and kneaded material (Fig. 4.2)

As is seen in the next chapter viscoelastic instabilities can be excited under steady electro-osmotic pumping through elongational flow fields, it is found that unlike pressure driven channel flows that stretching ("kneading") of material is not visually apparent and instead soley large scale movement of material occurs (see Fig. 6.8 and discussion in chapter 6). This distinction can be understood by no-slip boundary conditions that lead to shear, and thus stretching, in pressure driven flows and a slip boundary condition and the absence of strong stretching in electro-osmotic flows.

4.5 Complicating a complex fluid - concentration fluctuation instability?

It should be noted that relaxation time of solutions is taken to be equal to that of the underlying polymer molecules. Recent studies have found that density fluctuations can give rise to instabilities [48] in simple liquids, and the analogue with polymeric solutions was pointed out where concentration fluctuations could play the role of density fluctuations. The 'density fluctuation instability is essentially due to fluid becoming structured, with small regions having different viscosity due to fluctuations changing density, and one effectively has a break down of the continuum assumption. Rather than having a smooth fluid granularity is introduced, and if the granularity occurs on a scale over which velocity gradients are set finite -sized effects will become possible with unstable flows.

Using standard simple models results in an instability criteria that is nominally identical to the Zimm relaxation time (see below for a detailed development of this relationship), suggesting that *two concurrent* and different instability mechanisms exist in polymer solutions. In simple liquids density fluctuations lead to viscosity fluctuations, and thus local fluctuation in fluid motion - in high enough velocity fields the fluctuations can lead to instabilities, as given by the criteria

$$\dot{\gamma}_{cr} = \left(\frac{\partial \eta}{\partial p} \right)_T^{-1} ; \tag{4.4}$$

where η is the density dependent viscosity and p is the pressure. In complex fluids *concentration* instability should play a similar role, where fluctuation in local concentration will lead to viscosity differences, and a possibility for instability.

It has only been recently discovered that density fluctuations in sheared Newtonian fluids can lead to instability, and only a few studies exist - see Ref. [48] and Ref. [130] for the original efforts.

In Newtonian fluids the shear rates required to drive these instabilities are large making them difficult to excite, allowing this instability mechanism to go unnoticed until recently. The theory developed [48] predicts the observed critical shear rate for instabilities in lubricants for over three orders of magnitude, compelling evidence of the theories validity, as well as predicting observed instability in a fluid simulation. Later work [130] further developed the theory and noted instabilities are observed in dusty plasmas in experiments conducted above the predicted threshold, providing additional support for validity.

Detailed, and the original, development of the density instability theory can be found in [48]. Briefly, viscosity dependence on density is taken into account for shear flow in the Navier-Stokes equation. Linear analysis reveals a coupling between density fluctuations and the shear flow and that above a critical shear rate the fluid becomes unstable. The resulting prediction for the critical shear rate for the onset of fluctuation instability is

$$\dot{\gamma}_{cr} = \left(\frac{\partial \eta}{\partial p}\right)_T^{-1}; \tag{4.5}$$

where η is the density dependent viscosity and p is the pressure.

There is an analogy between density and concentration fluctuations in Newtonian and complex fluids [48], respectively. For the case of complex fluids the critical shear rate for concentration fluctuation driven instabilities is given by

$$\dot{\gamma}_{cr} = \left(\frac{\partial \eta}{\partial \Pi}\right)_T^{-1}; \tag{4.6}$$

where $\eta = \eta(\phi)$ is the concentration dependent viscosity dependent on the volume fraction ϕ and Π is the osmotic pressure. It was noted in Ref. [48] that complex fluids display various phase separations in flow conditions [48], however exploration of expected thresholds in polymeric or other structured fluids was not done. We do so here for dilute polymer solutions.

To investigate the predicted threshold given by (4.6) one can take derivatives with respect to concentration [48], in order to make use of functional relationships for the osmotic pressure and viscosity

$$\dot{\gamma}_{cr} = \left(\frac{\partial \eta}{\partial \Pi}\right)_T^{-1} = \left(\frac{\partial \eta}{\partial \phi}\frac{\partial \phi}{\partial \Pi}\right)_T^{-1} = \left(\frac{\frac{\partial \eta}{\partial \phi}}{\frac{\partial \Pi}{\partial \phi}}\right)_T^{-1}, \tag{4.7}$$

this rearrangement casts the equation in terms of the viscosity dependence on concentration and on the osmotic modulus of the liquid ("concentration compressibility").

The threshold for concentration instability is estimated by using (1) the van't Hoff approximation for osmotic pressure in a polymeric liquid [70]

$$\Pi \approx \frac{kT\phi}{b^3 N}; \tag{4.8}$$

where kT is the thermal energy, N is the number of monomers in a polymer chain, b is the Kuhn length, and ϕ is the volume fraction of polymers, and (2) the solution viscosity as estimated from the Zimm model [70]

$$\eta \approx \eta_s \left(1 + \phi N^{3\nu - 1}\right); \tag{4.9}$$

with η_s being the solvent viscosity and ν the dimensionless scaling parameter describing the polymers interaction with the solvent. Using these approximations it is found the threshold for concentration instability is

$$\dot{\gamma}_{cr} \approx \left(\frac{\eta_s b^3}{kT} N^{3\nu}\right)_T^{-1}. \tag{4.10}$$

The term with in the bracket is the nominal Zimm relaxation time [70] of a polymer, λ_{Zimm}. The critical shear rate for concentration fluctuation instability in shear is seen to be the same as for elastic instability for sheared viscoelastic flows [2] (e.g. the critical Deborah number condition)

$$\dot{\gamma}_{cr} = \frac{1}{\lambda}; \tag{4.11}$$

where λ is the polymer relaxation time, often approximated by λ_{Zimm} for dilute polymer suspensions.

The coinciding instability criterion for concentration and elastic instabilities cannot be taken to suggest a reinterpretation of the mechanism that leads to instabilities in viscoelastic fluids from elasticity based to purely concentration fluctuation based. Elastic fluids have long been investigated, with Maxwell giving an early model, and during this time numerous simulations and theoretical models [2] have been studied and interpreted as verifying the role of elasticity in driving the instability. Direct observation of individual DNA polymers [131] confirms significant polymer stretching above the classic viscoelastic instability threshold, as numerical simulations also demonstrate [2, 109], and as is visually observed in the rod-climbing effect.

The evidence that elasticity plays a strong role in instability is ample and convincing, in particular the numerical and experimental demonstrations of *single* polymer instability in flows above predicted threshold where inter-polymer effects are absent (i.e. concentration effects being absent), while purely elastic models lead to instabilities in simulations [2]. Instead, these coinciding instability criterions suggests the existence of two different, yet concurrent, instability mechanisms. This is somewhat surprising, however for different fluids their viscoelastic instability and "fluctuation" instability threshold will be at different values, and it is unsurprising that for *some* liquid they would be the same.

The apparent correspondence of predicted elastic and concentration fluctuation instabilities may help explain the insensitivity towards modeling viscoelastic fluids as a bulk liquid or considering an individual polymer: in the literature relaxation times of viscoelastic fluids are used interchangeably with relaxation times of the polymers within the fluid, and no clear distinction appears to be made [2], yet good agreement with experimentally observed instabilities is often found [2].

If concentration mediated instability coincides with elastic instability the apparent insensitivity between bulk and molecular perspectives becomes more understandable. The close agreement between the proposed "fluctuation instablity" and viscoelastic instability in polymeric liquids also would explain why it has taken so long for fluctuation instabilities to be discovered - in a fluid that easily displays them in an experimentally accessible setting the instability is masked by an concurrent instability that is immediately and conceptually sought, the elastic instability. Given that full quantitative understanding of scaling properties or other detailed information is lacking the elastic instability mechanism can be taken to (fully) explain observations; Occam's razor cuts deep and alternative or additional mechanisms are not sought unless there is a plausible need or possibility.

Consideration of hard colloidal suspensions using equation (4.7) leads to similar threshold predictions and can act as a control with no internal dynamics. Concentration instability in colloidal solutions may underlie the chaotic motion recently demonstrated in sheared colloidal suspensions [132]. Experiments done on sheared suspensions with an oscillatory flow with a rms shear of roughly 0.3 s^{-1} demonstrate chaotic particle trajectories, the predicted concentration fluctuation threshold[1] for the experimental setup is $\approx 10^{-10}s^{-1}$ which is well below the experimental conditions. The experimental setup in Ref. [132] would be a particularly effective test of the threshold predicted here, as both microsphere and polymer suspensions can be independently probed and compared as a function of concentration.

In summary, with simple models it is found that the threshold for concentration instability for sheared viscoelastic flows is nominally the same as the viscoelastic threshold. The models used both here and in the literature are approximate but as different mechanisms (intra- versus inter- particle) underlie the instabilities distinction between these mechanisms should be observable in controlled experiments and with rigorous theoretical investigations. This possible second and concurrent mechanism for instability is an intriguing possibility.

4.6 Relaxation time estimates using detrended fluctuation analysis

An approach that estimates the relaxation time from tracer particle data, which uses no model assumptions, is described here.

Using the Zimm relaxation time estimate is simple and is thought to accurately describe dilute solutions [2, 133]. However it is based on a model, which

---

[1] The threshold is strongly dependent on particle size, and by scaling from the nominally 230 μm microspheres used to $\approx$ 100 nm spheres the threshold predicted (using the Einstein relation for viscosity and the van't Hoff approximation for osmotic pressure) becomes close to the shear rate used in the experiment, allowing for the experimental probing of an instability onset.

introduces assumptions. While these assumptions are not overly strict, as evidenced by the utility of the Zimm time in describing experimental results, it is useful to have methods to estimate relaxation time without relating to a model in order to help verify theory and give independent estimates. Rheological measurements, for example of shear, also use model fitting of data to find relaxation times.

By following the fluctuations of tracer particles in viscoelastic flows above the instability threshold one should be able to find the relaxation time by studying correlations. There should be two regimes of correlations, with different dynamics below and above the relaxation time. Based on this concept the analysis of particle motion in viscoelastic flows using Detrended Fluctuation Analysis (DFA) should allow the relaxation time to be found.

It is found that for unstable polymer flows in microchannels that DFA can find the relaxation time. The key limitation of this technique for finding relaxation times is, in addition of capturing microparticle trajectories[7], the requirement to sample at a rate higher than the inverse relaxation time.

The general idea behind DFA is that of "fractal" analysis where one selects a window size setting a resolution for analyzing a time series, for D**F**A the analysis involves measuring fluctuations, and if the time series is scale invariant a power-law will relate the measure taken with different window sizes (see Appendix A for more discussion and details on DFA). DFA analyses data by looking at increasingly large time binning of time series data, fitting a best fit line to the data, and finding the fluctuation of the data as a function of time bin size[8]. This "boxing and fitting" detrends the data, allowing effects of drift and other nonstationary effects to be reduced[9], and correlation of data as a function of bin size (in time) can be found. It is often found that different

---

[7] This is not merely a technical issue, but the microparticles presence themselves will modify the fluid.

[8] In the DFA literature the bin size is denoted n, as n points are in a time period of length T which is sampled every Δt, and this notation is retained in Appendix A on DFA; in the discussion here $\frac{T}{\Delta t}$ is used.

[9] DFA was originally introduced to deal with physiological data, such as heart rate or EEG data, which is often nonstationary. Most time series approaches assumes stationary underlying parameters, DFA is a limited approach but with the advantage of not assuming stationary conditions.

regimes exist, each of which display a characteristic scaling law with sharp "kinks" between these regimes, these kinks define crossover points between different scaling regimes. More precisely, the log-log plot of fluctuations versus bin size is used with linear regions being considered a sign of power-law scaling.

Characteristic times t_{Char} are determined by finding the crossover c_x between power law scaling regimes on the log-log plot of the fluctuations versus box size and mapping it to the time domain:

$$t_{Char} = \Delta t 10^{c_x}; \tag{4.12}$$

where $1/\Delta t$ is the sampling rate of the times series. The process is thus one of transforming time-series data into fluctuation-box size data, and looking for well defined regimes and crossovers.

DFA of the velocity data (Fig. 4.3) shows, for large time bins, power-law (linear on the log-log plot) scaling, while for smaller time bins some nonlinear curvature is seen. Simply inspecting "by-eye" gives[10] a crossover between the linear-nonlinear regions at (1.2 ± 0.1) s, and possibly another crossover at (0.36 ± 0.04) s within the nonlinear region, with error due to discrete data points and difficulty in discerning precise locations of crossovers. The experimentally determined [21] relaxation time is 1.1 s, agreeing within error with the crossover between linear and nonlinear scaling. A slight divergence from power law like scaling can be seen between 2.0 and 2.5 in Fig. 4.3, and is likely a weak sinusoidal signal (see Appendix A and Ref. [134]) which may be due to vibrations in the experimental setting [135].

The first order (slowest mode) relaxation time is normally used to characterize polymeric liquids, due to difficulties in extracting higher order relaxation times from observations, however a spectrum of relaxation times are expected. Zimm polymer theory [70] predicts that the p-th mode relaxation time λ_p is given by:

$$\frac{\lambda_p}{\lambda_1} = (\frac{1}{p})^{3\nu}; \tag{4.13}$$

---

[10] Both the direct plot, and the difference plot between the linear fit for the "large bin" region and the data (e.g. residual plot), were inspected; the residual plot did not significantly clarify the data over the raw data.

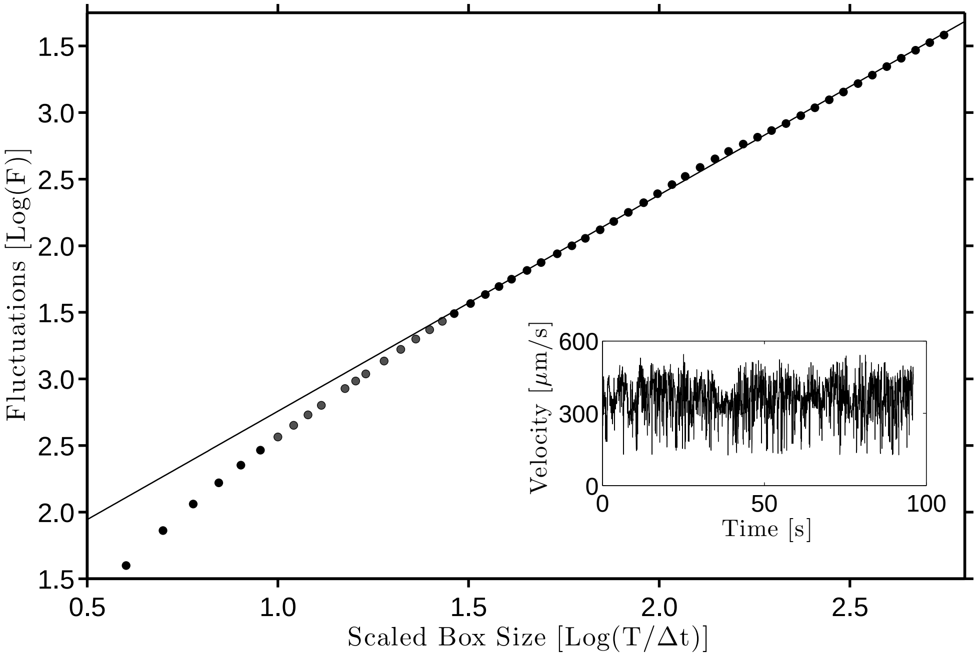

Figure 4.3: Unstable fluid flow. Chaotic flow is exhibited by polymeric liquid flowing through a serpentine microchannel [21] under steady forcing conditions. The fluid velocity (inset), as measured by particle tracking every 40 ms, demonstrates large velocity fluctuations. Visual inspection of Detrended Fluctuation Analysis "filtered" velocity data displays a linear region for larger time bins that crossovers to a nonlinear region at roughly 1.2 s. Within the nonlinear region there is some suggestion of a crossover at 0.36 s. The experimentally determined [21] relaxation time is 1.1 s, agreeing with the nonlinear-linear crossover. Zimm theory predicts a second mode relation time of 0.35 s for good solvents, coinciding to the possible crossover in the nonlinear region; note, however, that it is difficult to discern if this is a visual artifact or a true crossover. The potential for "in-situ" use and the lack of fitting parameters make DFA relaxation time estimates desirable as systematic (and hard to estimate) error will be reduced. A key limitation is the requirement to seed the fluid of interest with microparticles, which will modify the liquid, and the need to sample more rapidly than the relaxation time, which will limit the polymeric solutions that can be studied. Velocity fluctuation data kindly provided by Dr. T. Burghelea [21].

where λ_1 is the first order relaxation time and ν is the Flory solvent parameter (0.588 for a good solvent, and 0.5 for a theta solvent [70]). Assuming good solvent conditions [21], and using the first order relaxation time determined here, the second order relaxation time is calculated to be 0.35 s, in close agreement with the 0.36 s value found for the possible crossover in the nonlinear region. This agreement demonstrates the potential ability of DFA to find higher mode relaxation times. The theta solvent case of 0.42 s is outside of the estimated error range here, and theta conditions are not expected to apply for PAA in water [136]. The third order and higher relaxation times cannot be determined here due to the sampling rate and limited resolution.

Note that although the possible crossover corresponding to the second order relaxation time was visually extracted and then found to correspond to the second order relaxation time the data this could simply be a coincidence, with the apparent crossover and change in scaling behaviour a perception artifact [22]. The curvature between the supposed regimes appears to be different, for some viewers, however the increasing space between data points may be misleading. Looking at the residual between the data and the power-law fit (made for times larger than the relaxation time) does not clarify over the raw data plot. Inspecting the numerical derivative indicates only one flat region, which corresponds to linear scaling. As the bin size is reduced scatter first occurs in the numerical derivative and with more reduction in bin size the numerical derivative starts to sharply change. The crossover from the "scatter region" to the "rapid change region" occurs at ≈ 0.36 s, however as no sharp change occurs there is a possibility that this purported crossover is simply a perceptual artifact that happens to correspond to a physically meaningful relaxation time by coincidence.

The Zimm relaxation time, or other estimate, and Detrended Fluctation Analysis of tracer probe fluctuations are complementary and useful approaches. Using the Zimm formula is simple and available for essentially any experiment, the DFA approach is simple to apply to data and directly estimates relaxation time from data, but requires data collection which not all setups allow limiting its use and, in addition, tracer particles themselves will change the solution.

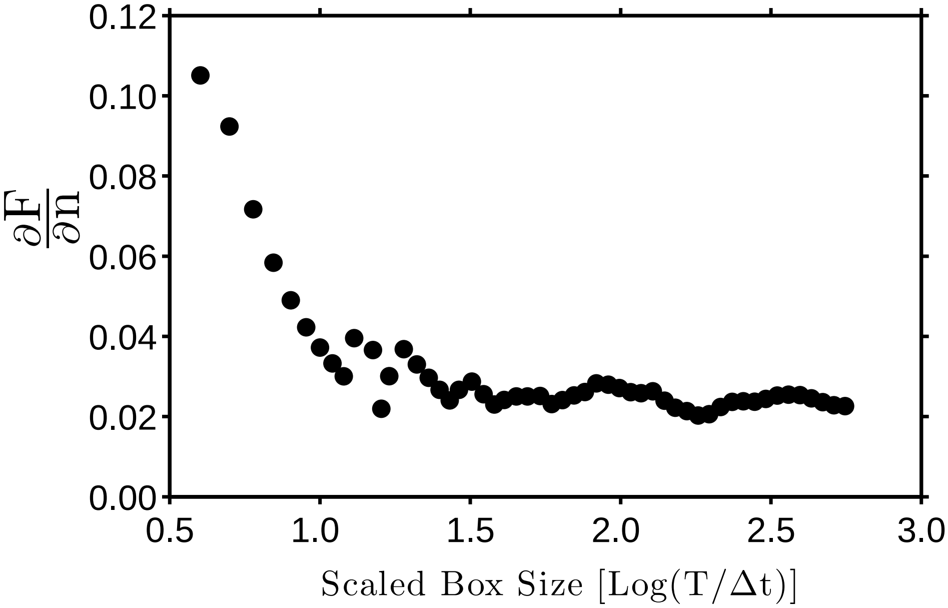

Figure 4.4: Numerical derivative of fluctuation scaling in unstable fluid flow. Visual inspection of Detrended Fluctuation Analysis “filtered” velocity data indicates two and possibly three time correlation regimes, with a crossover at roughly 1.2 s and possibly 0.36 s (see Fig. 4.3). For time bins smaller than the relaxation time there appears to be possibly two correlation regimes, however as power-law (linear on log-log plots) scaling is absent and data points start to become more sparse for small box sizes perceptual artifacts are possible [22]. Inspecting the numerical derivative, $\frac{\partial \mathrm{F}}{\partial \mathrm{n}}$, where F is the DFA fluctuations (see Fig. 4.3) and n is the bin size given by $\frac{T}{\Delta t}$, shows that three distinct constant steps are not observed, as expected if three linear regimes existed. Within the limited resolution it is seen that a flat “tail” exists for large time bins (with a signature of a sinusoidal signal perturbing the data here) and that a region with significant scatter separates this tail from a rapidly changing region. The purported crossover in the nonlinear region corresponds to the point where the data with scatter changes into rapid change. Due to limited resolution and the absence of visually clear linear-linear or linear-nonlinear transition, this possible crossover may be an artifact.

A key advantage of DFA of tracer probe data in finding relaxation time is "in situ" use, allowing fluid behaviour to be probed in the precise experimental conditions of interest. As rheological measurements make use of simplified experimental setup in order to facilitate contact with theory the validity of measurements can sometimes be in doubt [2] - as a simple example shear measurements may not always be accurate estimates of elogational flows. Additionally rheological measurements will often make use of a given model in order to estimate relaxation time, which can introduce systematic error.

4.7 Summary

It is noted that

- Bubbles, like polymers, act like springs and are analogous and may be used to shed insight on polymer and other flows (such as, possibly, flow past blunt objects).
- The analogy between polymer coils and bubbles indicates that a mesoscopic model, where bubbles are used to represent polymer coils and setting the surface tension allows the relaxation time to be accounted for, may allow numerical simulations. Difficulty in implementing viscoelastic codes and the high Weinsenberg number problem that plagues such codes once set up make this of interest[11].
- *Elastic turbulence* is a recently discovered turbulence that can be excited at arbitrarily low Reynolds numbers in polymeric flows. While it has long been known that instabilities occur in viscoelastic fluids detailed understanding is lacking. In addition to establishment of turbulence in viscoelastic fluids, efficient mixing was demonstrated in mechanically pumped elastic turbulent flows through curvilinear channels in both large and microscaled geometries.
- Electro-osmotic flows of viscoelastic fluids have not been well studied; as EOF pumping is one of the two main pumping schemes in microfluidics

---

[11] Bubbles can be included in many CFD codes.

further investigation of EOF pumped viscoelastic fluids is warranted. Simulations have been done, but focus on explicitly steady flows due to reduction of the Cauchy equation which prevents instability from arising.

- Following Ref. [48] the similarity between density fluctuations in simple liquids and concentration fluctuations in complex fluids was considered for dilute polymer solutions - it is found that the instability condition *corresponds to the classic viscoelastic instability condition*; in Ref. [48] the possibility of a viscoelastic origin of the instability described was excluded for simple liquids, however it appears that for polymeric solutions the instability threshold coincides.

- This possible concurrent instability mechanism complicates the physics, and careful investigation (e.g. comparison of colloidal versus polymeric solutions, and varying concentration) will be required to determine if this proposed concentration instability exists. Currently the elastic instability is assumed to be the sole mechanism, and lack of knowledge on precise scaling properties or other details prevents either confirming or excluding the concentration instability at present.

- By inspecting the correlations between fluctuations in tracer particle velocimetry data a parameter free means of measuring the relaxation time for viscoelastic fluids "in-situ" can be found; as the technique is simple to perform it is a valuable alternative means for measuring the relaxation time. The lack of free parameters and possibility for use in a specific environment will reduce systematic error in determining relaxation time. Note that not only was the dominate (first order) relaxation time found, but also - possibly - the second order relaxation time, which agreed with the (Zimm) predicted value.

Chapter 5

Polymer Instabilities in Elongational Flow

5.1 Experimental motivation

There are three main ingredients that motivated the experimental work here. (1) It has long been known that inclusion of polymers in working fluids allows secondary flows and instabilities to be excited in mechanically driven flows [2], and a new form of turbulence, *elastic turbulence*, in polymeric solutions has recently been discovered [19] which can be excited at arbitrarily low Reynolds numbers, (2) as fluid flow in microfluidic systems is typically laminar due to the low Reynolds numbers that characterize the flows it is difficult to achieve rapid mixing, and finally, (3) electro-osmotic pumping is one of the key means of driving fluids in microfluidic systems. Motivated by these factors the possibility of exciting elastic instabilities and elastic turbulence in electro-osmotically driven microflows, both as to document possible unintended departure from laminar flow in complex fluids[1] and to intentionally promote instability, was undertaken.

5.2 Preliminary efforts: viscous solutions

Highly viscous liquids are often used in viscoelastic fluid studies as (1) diffusion is reduced, allowing for diffusive mechanisms to be small relative to convec-

---

[1] As lab on the chip applications are pursued concentrated cell, DNA, microparticle, or other complex fluids are increasingly used.

tive instabilities, simplifying studies[2], and (2) the relaxation time is increased, making fluids more elastic allowing higher Wi numbers to be explored. Initially highly viscous sugar solutions were used, however several issues became apparent

- sample preparation took long setup, which did not cause problems for focused experiments but would result in an undesirable protocol for experimental studies making use of the high viscosity solutions or in lab on a chip diagnosis applications (i.e. if time is of the essence, as in proposed medical uses of microfluidics, long preparation times limit use)
- filling and cleaning microchips was difficult, with bubbles often becoming trapped and removal of viscous liquids being difficult
- velocities obtained were quite low, and transient effects long
- viscosity of the sugar solutions used appeared to undergo significant viscosity changes during experiments, most likely a Joule heating effect[3]

In short, using highly viscous solutions was problematic for high throughput rapid testing, one of the desirable factors for possible microfluidic lab on a chip applications. Further, reflection on two of the key aspects of the experiment (1) the relaxation time, and (2) the EOF flow rate, suggested that high viscosity fluids would not provide a significant gain in Wi number: the viscous enhancement of relaxation time ($\lambda \propto \eta$) is offset by viscous depression of velocity in EOF ($v \propto \frac{1}{\eta}$), limiting achievable enhancement of the Wi number for EOF pumped liquids.

Simply putting polymers in low viscosity liquids should, to first order, lead to the same Wi number; low viscosity liquids are easier to work with experimentally and are what most lab on the chip applications use; and if rapid mixing is the aim diffusion should not be suppressed. For these reasons suspending polymers directly into low viscosity liquids (i.e. aqueous solutions)

---

[2] e.g. by increasing contrast between dyed and un-dyed liquids and time windows for study

[3] Glycerin, an alternative means of increasing viscosity, experiences the same difficulty.

was pursued instead of artificially increasing viscosity by the inclusion of concentrated small molecules.

5.3 Initial design and experiments

It has been shown that chaotic instabilities can arise in Dean flow (curvilinear serpentine channels) in pressure driven microflows [21], where characterization of macroscopic equivalent flows [19] demonstrates elastic turbulence enhances mixing. A curvilinear chip design was undertaken and high viscosity solutions were used. Two liquid streams, a dyed stream and an undyed stream, were brought together in a y-branch constriction which feed the following curvilinear section; a visual overview and brief description of the y-branch component can be seen in Fig. 5.1.

It was noted that, as described above, highly viscous liquids did not seem promising for lab on a chip applications. Moving towards low viscosity solutions, first in the semi-dilute regime (where it was speculated that relaxation time would be increased, yet - due to entropic repulsion from the wall - the EOF flow rate would not be substantially reduced) and then in the dilute region showed that instabilities would occur within the y-branch.

Based on the results in the y-branch, a microchannel with a series of sudden constrictions/expansions was fabricated in order to observe the effect of stacking elongational regions.

Curved “zig-zag” approximation to serpentine streamlines were investigated in Ref. [121] with electro-osmotic flow in mind but instead utilizing pressure driven flows due to low volumetric flow rates found for EOF of the working fluid, consisting of a high molecular weight polymer in a viscous sugar solution. In EOF through curved channels there will be some stretching acting on polymer coils due to electric field lines concentrating on inside curves, resulting in more rapid flow on inside corners which results in shear [53]. This effect leads to dispersion but is relatively weak [53] limiting the effective Deborah number achievable in the channels. This weak effect for EOF flow is in contrast to pressure flows where parabolic flow profiles across channels can im-

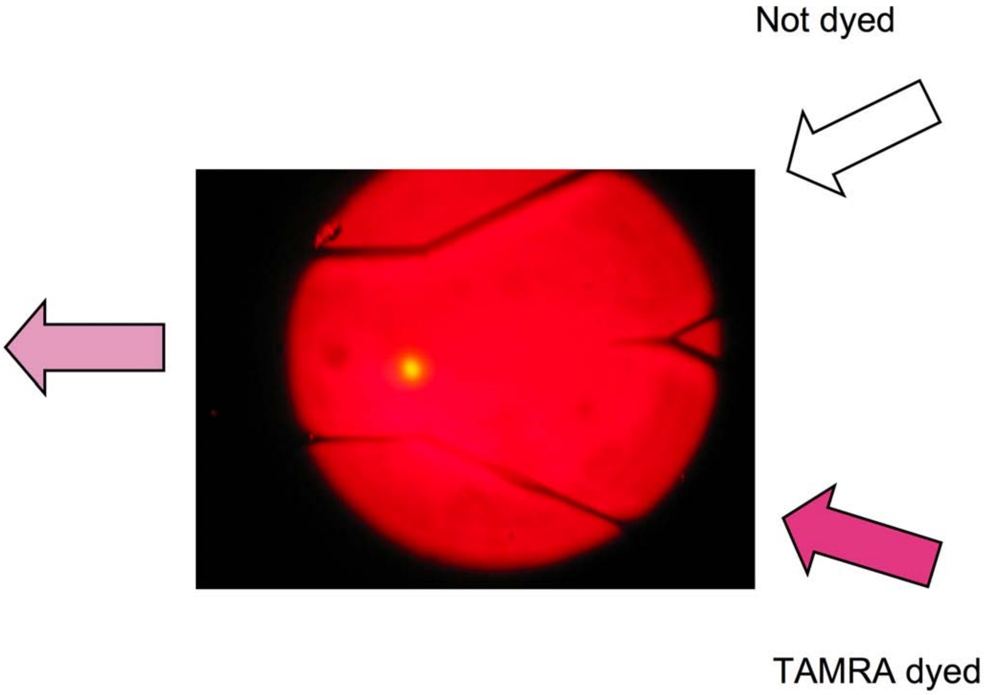

Figure 5.1: Y-branch geometry. Elongational flow is created by merging two streams of fluid into a single stream of half the input cross-section. One of the streams is labeled using TAMRA, a fluorescent dye (dark pink arrow in figure), while the other stream is dye free (white arrow), as the fluids move downstream they mix (light pink arrow). A laser is focused exciting the dye (yellow dot in image), allowing the amount of dye to be optically observed. For laminar steady flows diffusive action mixes the dye, which is observed as a steady optical signal, and it is found that addition of high molecular weight polymer leads to instabilities leading to a time varying optical signal. For long runs drift in the interface occurred, possibly due to Joule heating resulting in differential flow rates suggesting that heating effects may be present. The glass microchannels are 100 μm wide and 20 μm deep.

pose significant shear in the channel that stretches coils, polymers then move into bends and cross streamlines much like rubber bands impart force when stretched around an object. A lack of observed instability for EOF Dean flows in Ref. [121] indicates that, at least for viscous solvents, such instabilities are difficult to excite; the experimental observations here show that, in contrast, elogational flows can excite instablities with relative ease (i.e. with standard EOF flow rates).

5.4 Instrumentation: the μTK

The Microfluidic Tookit, or μTK, from MicraLyne Inc. is[4] a platform for electrokinetic microfluidics, used for driving electrophoretic and electro-osmotic flows. The apparatus consists of an high voltage power supply that supplies a voltage (up to 6 kV) to platinum electrodes located on a lowerable assembly. A microchip can be set in a machined plexiglas holder below the electrode assembly, below which a 40X microscope objective is positioned allowing imaging of microchannels. The optics module consists of an epiluminescent confocal microscope allowing fluorescent excitation and either visual inspection by eye or by a photomultiplier tube (PMT)[5] which can be swung and held in the optical path; the PMT data collection frequency can be selected between[6] 25 and 50 Hz. Removing the eyepiece allows a camera to be attached using a custom machined connector and an optical adaptor (camera-to-microscope).

The optical module has an internal 532 nm diode laser[7], a beam splitter, and various lenses in an enclosure. The internal laser can be either focused into an ≈ 10 μm beam waist focal spot, or expanded to ≈ 300 μm wide beam for broad illumination of channels. Due to dust on the expansion lens of the μTK's available for use, lens imperfections, and high modulation of the Gaussian-like field use of an external laser for illumination of channels was used to take images of the entire flow field.

---

[4] or, was, MicraLyne has discontinued the μTK

[5] Hamamatsu H5773-03 PMT

[6] higher rates are possible, however the PMT only outputs at 50 Hz making the higher rates irrelevant

[7] Alternatively, an 635 nm laser option option existed

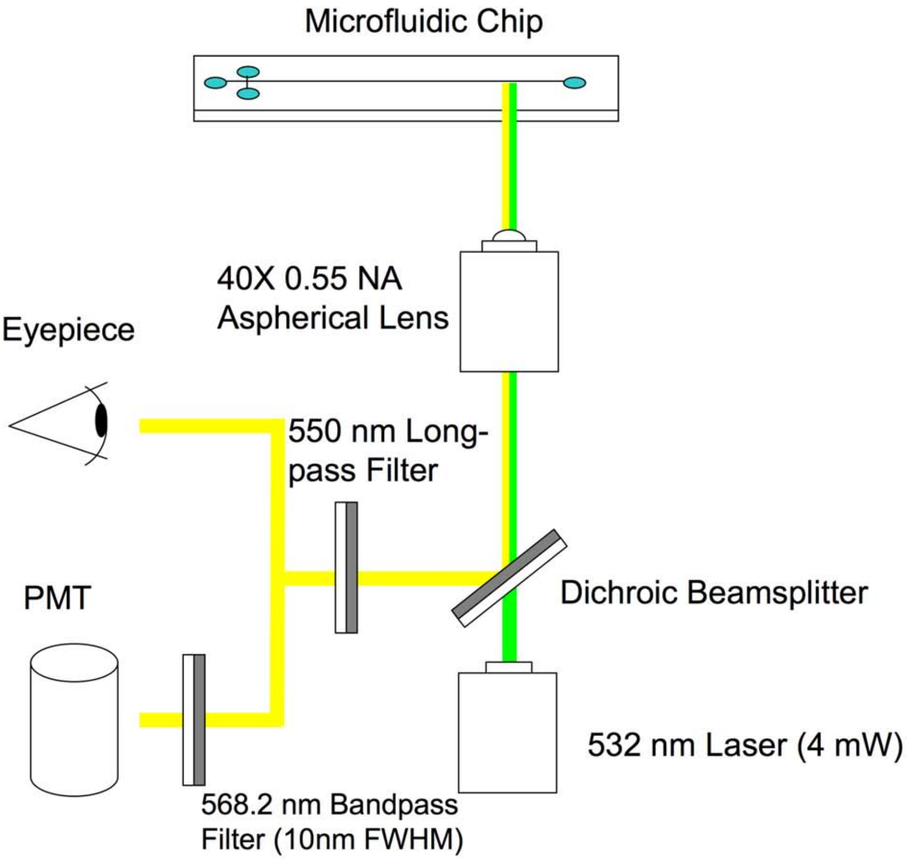

Figure 5.2: MicroTool Kit Optics Diagram. The MicraLyne Inc. μTK allows optical observation either by eye piece or with a PMT.

See Appendix C for more discussion of the μTK apparatus.

5.5 "Slow" expansion: y-branch

Elogational flow into an y-branch was set up and semi-dilute solutions were electro-osmotically pumped though the device component. Instabilities were observed and investigated and found to persist in the dilute regime[8].

Microchannels with 100 μm width and 20 μm depth with the characteristic D chemical etch cross section were formed in glass. A y-channel geometry with two input channels of unequal length and a single output created extensional flow at the channel intersection (see Fig. 5.3, inset).

Polymer solutions were made by adding high[9] (18×10^6) molecular weight polyacrylamide (PAAm) from Polysciences Inc. to standard tris- borate-ethylenediaminetetraacetic acid (TBE) buffer[10], at 2500 ppm PAAm in 1XTBE. The overlap concentration c_* is $\approx$ 300 ppm, placing the solution in the semi-dilute regime.

The glass microchips were loading into a μTK and flow was electro-osmotically driven with electric fields of up to $\approx$ 600 V/cm. The interface between the two input streams was observed by fluorescently tagging one input stream with a small amount ($\approx$ 2 μM) of tetramethylrhodamine (TAMRA) dye and exciting with the internal 532 nm diode laser. Laser induced fluorescent profiles were collected for various flow rates by focusing the laser to 1/10th of the channel width (10 μm beam waist) close to the dyed-undyed fluid interface at the output of the extensional region (see Fig. 5.3, inset) and collecting emitted light with a photomultiplier tube (PMT) at 25 Hz. This approach to monitoring the flow will capture movement of the interface perpendicular to the flow direction, if the sampling point is close enough to the interface to observe movement. As one moves away from the interface less of the fluctuating interface will

---

[8] Results of the instabilities observed for the semi-dilute polymer were presented at the 2007 APS March Meeting, in the Micro and Nano Fluidics section, talk "L30.00014 : Instability in extensional microflow of aqueous gel".

[9] This polymer appears to be the highest molecular weight polymer soluble in aqueous media that is commercially available, for the current time.

[10] TBE is selected as it is widely used in biology experiments.

be observed which makes this technique sensitive to the precise placement of the monitoring spot; alignment accuracy is roughly 5 μm and for the samples investigated error of $\approx 10\%$ was empirically found (see section 5.7).

It was found that at the highest electric fields applied bubbles would occasionally form at the electrodes, for both polymer/TBE solutions and pure TBE buffer. Bubble formation was not significant under the operating conditions studied, but demonstrates an upper voltage for bubble free operation when using TBE buffer. The bubbles would form at the input reservoirs and occasionally break free of the electrode and flow into the microchannels and flow downstream; as bubbles would change the amount of fluid that would flow through the channels, would interact with each other and the walls, and would not be deterministically created and moved downstream complicated flow would occur. Bubbles formed and captured by the microchannels in this manner where large in size, spanning the entire channel. The presence of bubbles can be seen in PMT signals by the presence of "notches" that occur when bubbles move past the sampling spot (see Fig. 5.4), as the optical thickness of dye would be reduced[11]. In the wake of bubbles good mixing was visually observed, as has been previously noted, studied, and applied (e.g. Ref. [23]).

Fig. 5.3 shows PMT time traces at two driving potentials, and it is apparent that for sufficiently large driving electric fields large fluctuations exist. This is interpreted as instability of the fluid causing the dye intensity to spatially flicker across the channel, which could be observed by eye by increasing dye concentration and defocusing the laser to a diameter of 200 μm.

It is not readily apparent in Fig. 5.3, but an ≈ 9.5 Hz signal was present in some PMT traces collected independent of experimental parameters, which is attribute to environmental vibrations as this signal is in the range of the natural resonance frequencies of buildings floors [137] (see Fig. 5.6, where this signal is more readily visible).[12]

---

[11] Additionally, inspection by eye indicates that deflection of the beam occurred which can be attributed to the change in refractive index and non-perpendicular beam-surface interactions.

[12] A vibration isolation table was later used to prevent this spurious signal and it was also found that the stage was not tightly locked down which resulted in higher sensitivity; tightening the stage and using vibration isolation tables resulted in no observable 9.5 Hz

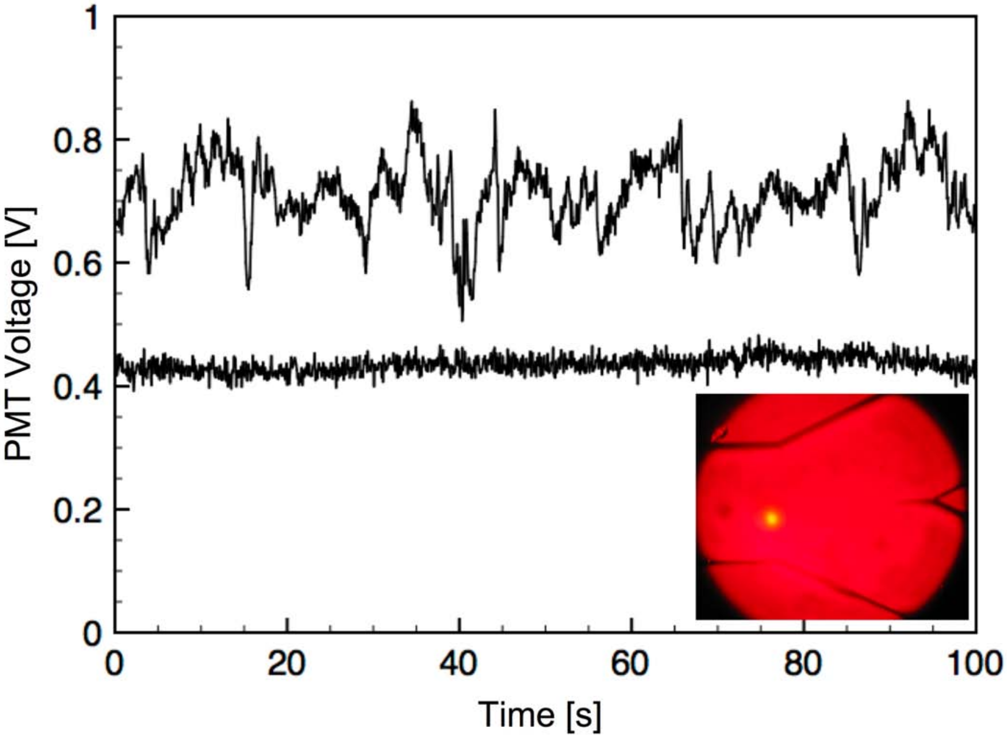

Figure 5.3: Photomultiplier tube time trace for concentrated polymer solution. 1XTBE buffer with 2500 ppm (semi-dilute) PAAm was electro-osmotically driven through an y-branch. When the driving electric field is increased sufficiently significant fluctuations arise, as can be seen comparing the PMT traces at ≈ 100 V/cm (lower) and ≈ 410 V/cm (upper) curves. The curves have been artificially offset for visibility. Note the significant noise in the low voltage signal; this noise creates a noise floor blelow which flow instability properties cannot be determined with the PMT. Inset: Micrograph (40X lens) of y-branch channel with (yellow) excited focal spot visible; the micrograph was captured by holding a camera up to the eyepiece, and the off center focal spot is an optical artifact due to non-perpendicular alignment (i.e. by eye the focal spot is seen to be centered; visual alignment was confirmed by noting equal stage displacement from the apparent center to the side walls). Flow is from right to left, with the fluid in the bottom channel dyed with TAMRA dye.

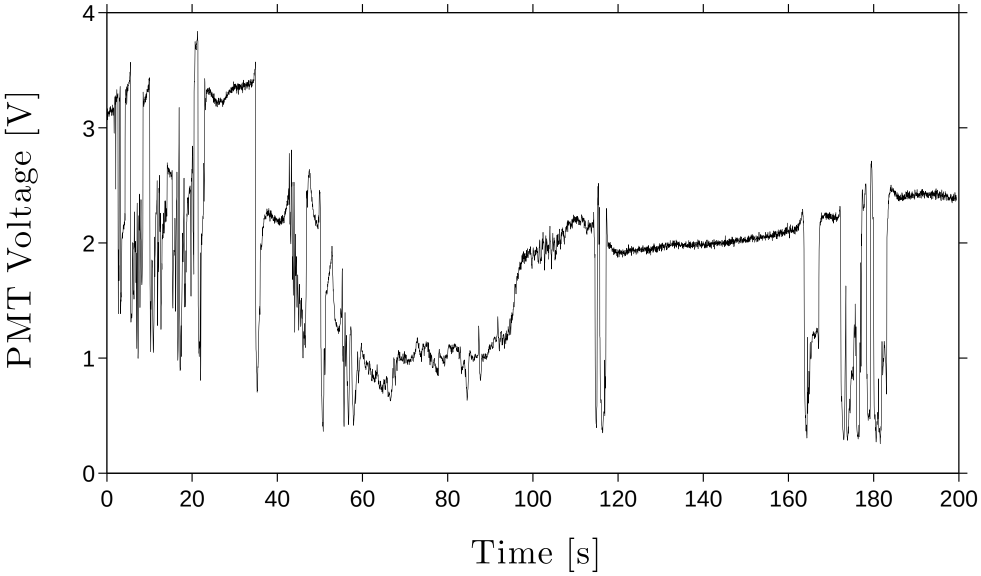

Figure 5.4: Photomultiplier tube time trace for bubble train in TBE buffer. At the highest applied voltages (6 kV here) bubbles would occur at the electrodes after long runs; these bubbles could be captured by flow down the microchannels and create complicated flow conditions. As bubbles move past the PMT focal spot "notching" occurs as the bubbles would displace dyed liquid (reducing optical section and signal, as well as due to deflection of the beam from the curved interfaces. Between the bubbles good mixing was visually seen, as has previously been noted and studied (see, for example, Ref. [23]). The formation of bubbles is a clear indication that Joule heating is present for higher applied voltages.

The power spectrum has power law behavior (not shown, see Fig. 5.6 for similar spectra), which is indicative of chaotic flow [21]. The PMT voltage is dependent on dye concentration, specific PMT bias voltage, run-to-run variation in laser output, and, due to diffusion across the dye-undyed interface, the precise location of the excitation spot from the interface, possible thinning effects [138], and flow velocities. It is therefore difficult to compare absolute voltage levels in a precise manner, and a relative measure is required to better compare different experimental conditions. The relative PMT signal fluctuations, $\tilde{\delta}_{\mathrm{PMT}}$, defined as var $\left(\frac{\mathrm{V}}{\langle \mathrm{V} \rangle}\right)$, where var(V) is the variance of the PMT voltage signal from the average $\langle \mathrm{V} \rangle$, are measured for various driving potentials (Fig. 5.5) and found to have a threshold beyond which fluctuations grow in size and lift off the noise floor.

Inspection of Fig. 5.3 reveals significant noise in low velocity flows, this is due to inherent laser fluctuations. The onset of fluctutions observed in Fig. 5.5 is near the to the expected threshold of 360 V/cm, however the relatively large noise floor makes it difficult to determine if instability truly occurs there the > 400 V/cm that is apparent.

Using the current monitoring method [139] flow velocities were estimated. This estimate of flow velocity allows the extensional rate to be found in the y-branch (Fig. 5.5, inset) where the extensional rate is estimated as $\dot{\epsilon} = \frac{\Delta v}{L}$ with Δv equaling the input velocity v (as velocity will double through the y-branch) and L ≈ 100 μm is taken as the characteristic size of the expansion region. The critical extensional rate [102] $\dot{\epsilon} = \frac{0.5}{\lambda} \approx 17$ /s defined by the Zimm relaxation time [70] of $\lambda_{Zimm} = \frac{\eta_s R^3}{k_B T} \approx 0.03$ s , where the TBE based solution viscosity η_s is assumed to be that of water, the coil radius R is taken to be [21] 0.5 μm, and a thermal energy $k_B T$ corresponding to room temperature (22 °C) is used to find the critical E-field of 360 V/cm.

The Zimm relaxation time, strictly speaking, only describes dilute solution dynamics and it is surprising that an increased relaxation time is not observed in the entangled concentrate polymer solutions resulting from polymer-

---

noise.

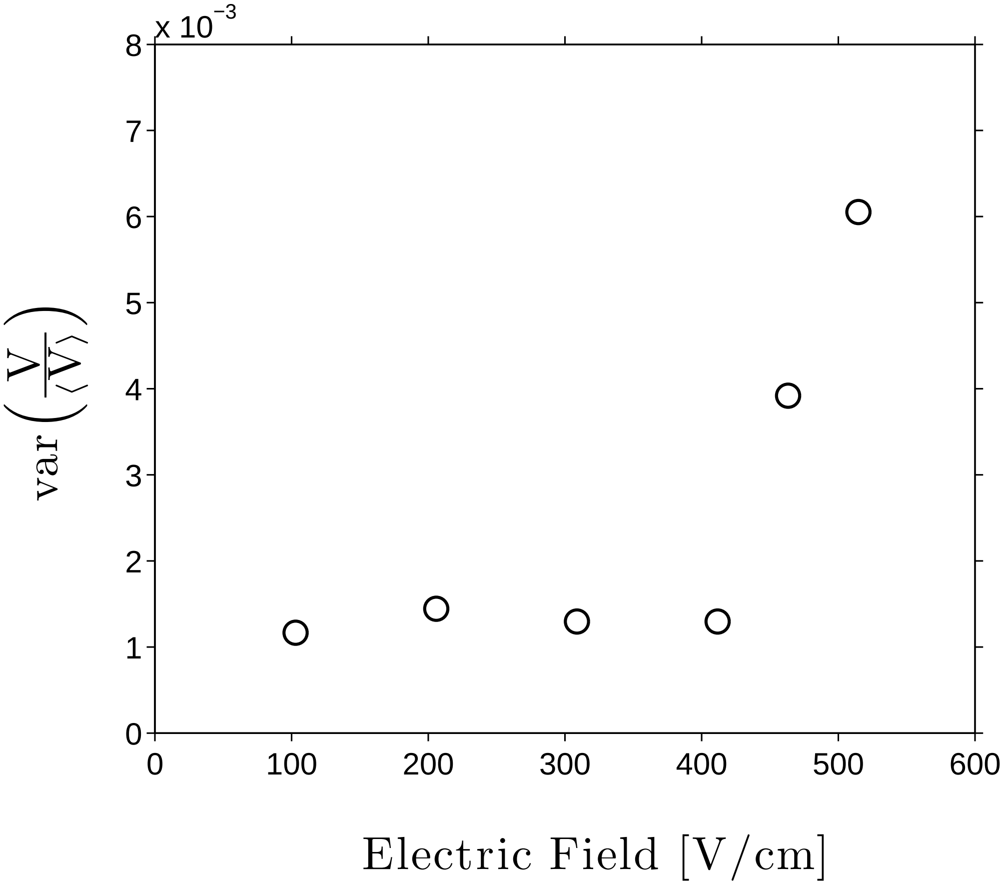

Figure 5.5: Fluctuations in photomultiplier tube time trace for semi-dilute polymer solution. Fluctuations were measured from 80 s PMT traces of 2500 ppm solution flow at various driving electric fields. Fluctuations rapidly grow in size beyond a predicted threshold corresponding to an electric field of roughly 360 V/cm; however the predicted threshold is below the noise floor not allowing determination if transition occurs earlier than the apparent value of roughly 400 V/cm where a rapid rise in fluctuations is seen.

polymer interactions [138]. The concentration is ≈10X the polymer coil overlap concentration [21], clearly no longer in the dilute regime. Two possible mechanisms suggest themselves as explanations. Measurements on a similar fluid [138] place the relaxation time around 2 s; while this value is significantly larger than the Zimm relaxation time thinning effects [138] in the y-branch will substantially reduce the relaxation time which may explain the depression of the relaxation time to the Zimm time. It is also well known that entropic repulsion of polymers at the walls will lead to a dilute region [140], if instabilities arise within this dilute region versus in the bulk away from the wall this can account for the Zimm relaxation time matching observations.

Entropic repulsion depletes the concentration of polymer near solid surfaces which will result in a dilute regime near the wall. Measured EOF mobilities, μ_{EOF}, which relate the driving electric field to the resulting velocity in the microchannels, are somewhat depressed for concentrated polymer solutions versus pure TBE buffer with a mobility reduced from $(6.0\pm0.4)\text{x}10^{-4}$ $\text{cm}^2\text{V}^{-1}\text{s}^{-1}$ to $(4.2\pm0.2)\text{x}10^{-4}$ $\text{cm}^2\text{V}^{-1}\text{s}^{-1}$. However, from bulk shear solution viscosity measurements [138] several orders of magnitude reduction is expected rather than the mild decrease, as viscosity is dependent on polymer concentration this limited decrease in flow is clear evidence of a significant depletion region near the wall. The depleted region may be the source of instabilities, however this does not exclude instabilities from arising in the bulk. In EOF flows fluid in the EDL is the primary flow that viscously couples to the fluid in the bulk of the channel. An upper bound of the time for viscous diffusion to the middle of the channel t_υ can be made by assuming waters kinematic viscosity υ describes the fluid, and is approximately three orders of magnitude smaller than the residence time t_{res} in the y-branch expansion for typical flow velocities (≈ 1 mm/s). As $\frac{t_\upsilon}{t_{res}} \ll 1$ the expansion is adiabatic, resulting in an uniform flow profile across the channel depth in the absence of secondary flows (i.e. before instabilities arise). As the relaxation time in the bulk will be greater or equal to the Zimm time the Weissenberg number will be at least as large as in the depleted region. As the Zimm relaxation time estimate describes experimental observations it appears that significant thinning occurs. Elongational thinning was qualitatively observed in a similar fluid [138], which is consistent with the possible thinning observed here, although reliable quantitative data is not available for elongation flows of the fluid used as the extensional character of polymeric fluids is not well known[13] in most cases [141].

It was found that drift in flow rates between input channels would eventually occur, likely due to Joule heating of the polymer solution asymmetrically effecting flow through the unequal input arm lengths, limiting the time over which data could be collected. This, as well as hindered diffusion in concentrated polymer solutions, increased time required to fully dissolve concentrate solutions, and more difficult theoretical and computational analyses, makes working with low concentrations desirable. To test the effect of concentration, a dilute solution (100 ppm) of PAA in 1XTBE buffer was made. To facilitate visual inspection increased TAMRA dye concentrations were used leading to increased visual and PMT signal; the increased dye concentration also dramatically reduced experimental noise. Instabilities were also observed for these solutions (see Fig. 5.6 inset for a representative PMT time trace) at the same approximate driving voltages as for concentrated solutions. Completely excluding polymer from the solution resulted in laminar flow (Fig. 5.6, inset), as expected, although a small drift in PMT voltage is apparent which is possibly due to joule heating affecting flow rates. Thinning at high concentrations is further supported, as instabilities occur at similar extensional rates in dilute and concentrate solutions within the same device despite the orders of magnitude difference expected if instabilities arose in the bulk *without* significant thinning occurring.

In summary, using a microchannel y-branch extensional instabilities were excited in electro-osmoticaly driven polymer flows for the first time. Polymer free solutions displayed laminar flow, while both concentrate (2500 ppm) and dilute (100 ppm) solutions of high molecular weight polymer added to standard buffer exhibited instabilities above a critical flow rate that appears to correspond to the Zimm relaxation time. As the Zimm relaxation time is

---

[13] Shear measurements are simpler to perform and are more reproducible, leading to the shear viscosity being the standard measure reported.

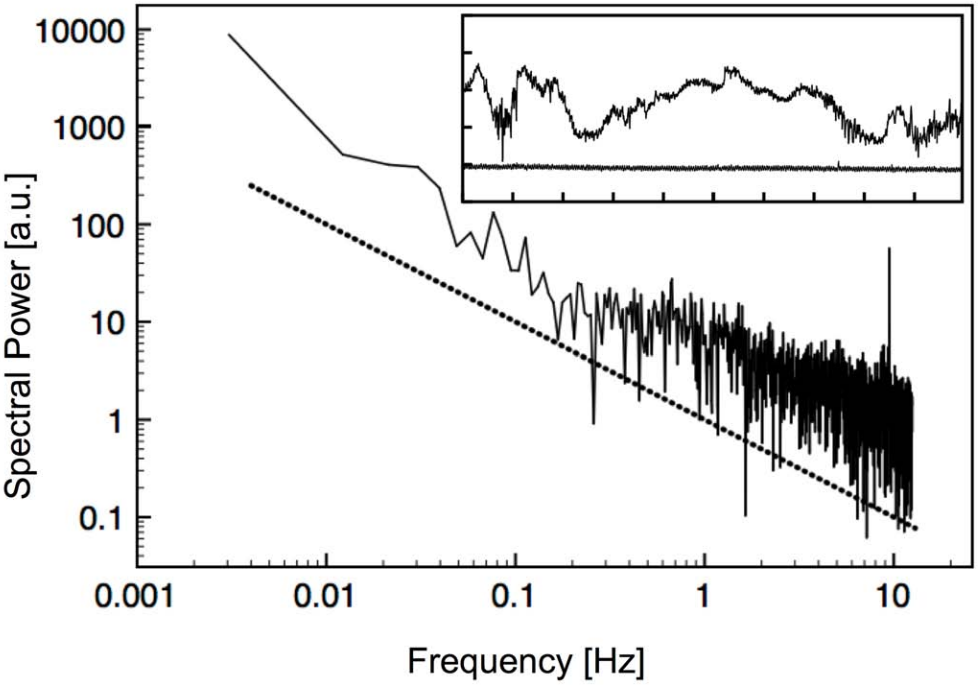

Figure 5.6: Power spectrum of dilute polymer solution instability. 1XTBE buffer with 100 ppm PAA driven at ≈ 410 V/cm. Instabilities have approximate power law spectra (compare to dotted line with power $\propto$ 1/frequency), characteristic of chaotic flow [21]. For steady flow there are no fluctuations, and thus the power spectra will consist of a noise floor. Rhythmic unstable flow, such as for von Karman instabilities (see Fig. 2.4) will result in sharp distinct peaks in the power spectrum. Chaotic flows will have a multitude of frequencies, which will result in an elevated power spectrum that drops off. Note the sharp peak at roughly 9 Hz, which corresponds to the resonance frequency of modern buildings – such as the one the experiments were done in. This peak is attributed to building resonance coupling into the experimental setup, a hypothesis supported by the exclusion of this ≈ 9 Hz peak by moving the apparatus to a vibration isolation table. Inset: PMT time trace (y-axis: 0-5V) over 200 s, 100 ppm PAA solutions driven at ≈ 410 V/cm (upper curve) are unstable while 0 ppm PAA (no polymer added) solutions driven at ≈ 515 V/cm (lower curve) are laminar, as is typical for flows in microfluidic devices. Instabilities in dilute solutions occurred at similar driving fields as for concentrated (2500 ppm) solutions indicating that Zimm relaxation dynamics describes both solutions.

easy to determine for given polymer solutions and extensional flows are simple to design addition of high molecular weight polymers to electro-osmotic microfluidic devices is a promising avenue to intentionally induce instabilities.

5.6 Instabilities in abrupt expansion : constriction units

As instabilities were observed in an y-branch investigating the effect of stacking multiple elongational units is a logical next step. By creating a series of sudden constriction/expansion units along a microchannel the effect on mixing can be probed. Again, for high molecular weight polymer chains it is found that flow velocities achievable by standard electro-osmotic pumping are sufficient to excite extensional instabilities in dilute solutions. The results show that electro-osmotic flows of complex fluids are perturbed from the steady regime, requiring care in considering and modeling the flow of liquids such as biopolymer suspensions.

5.7 Instabilities in extensional microflows of polymeric solutions

As before, microchannels were formed in glass, here with 100 μm and 200 μm channel width, and 20 μm depth to the bottom of the “D”-shaped chemically etched cross sections. Forming 2:1 constrictions (see Fig. 5.7.a) causes flow acceleration and deceleration as liquid transverses through the constricted regions, inducing extensional (stretching) flow fields. The sudden constriction/expansion unit was chosen as this is a canonical geometry used to excite elastic instabilities [2] and the “Manhattan” geometry is a natural choice for microdevices.

Polymer solutions were made by adding 18×10^6 Da high molecular weight (HMW) or 5×10^6 Da low molecular weight (LMW) polyacrylamide (PAAm) from Polysciences Inc. to a 20:80 vol.% methanol:water mixture, where methanol is used to prevent chain scission during storage [142]. The use of alcohol is not required for short term use of solutions[14] (i.e. $<$ months), but was chosen in order to allow solutions to be maintained during initial investigations and creation of protocols[15].

A concentration of 120 ppm was first investigated, as this is below the overlap concentration for both the HMW and LMW solutions when neighboring polymer coils impinge on each other ($\approx$ 300 ppm and $\approx$ 850 ppm, respectively). It was also found that concentrations of 60, 90, and 480 ppm of the HMW sample display similar behavior to the 120 ppm concentration (as seen in Fig. 5.10.b; see also Fig. 5.11).

The glass microchips are loaded into a Microfluidic Toolkit and flow is electro-osmotically driven with voltages of up to 0.4 kV (electric fields as high as $\approx$ 900 V/cm). The interface between the two input streams is observed by fluorescently tagging one input solution with a small amount ($\approx 21\ \mu$M) of tetramethylrhodamine (TAMRA) dye and exciting with a 532 nm (green) diode laser. Laser-induced fluorescence profiles are collected for various flow rates by focusing the laser to 1/10th of the channel width (10 μm beam waist) close to the dyed-undyed fluid interface centered in the first extensional region (constriction unit) (the focal spot indicated with a small circle in Fig. 5.7.a), and collecting light emitted from the dye at 570 nm (yellow) with a photomultiplier tube (PMT) at 50 Hz, after filtering with a 568 nm bandpass filter (10 nm FWHM).

Data runs were 100 s in duration, with the first 20 s removed prior to analysis to allow startup and transient behavior to attenuate. Care was taken to thoroughly clean and rinse microchannels before use to ensure clean surfaces and to prevent pH shifts or other effects from modifying flows. The cleaning protocol was to flush the channels with: water ($\times 2$), $\approx$ 1 M nitric acid, $\approx$ 1 M NaOH, water ($\times 2$), by first filling all the reservoirs and then pulling solutions through the channels by applying vacuum to the output reservoir (reservoir 4 in Fig. 5.7.a).

---

[14] Use of alcohol inhibits EOF flow relative to pure water, and may interact with a given sample, so is not desirable for general use.

[15] Aging effects on some samples were noted, motivating this precaution.

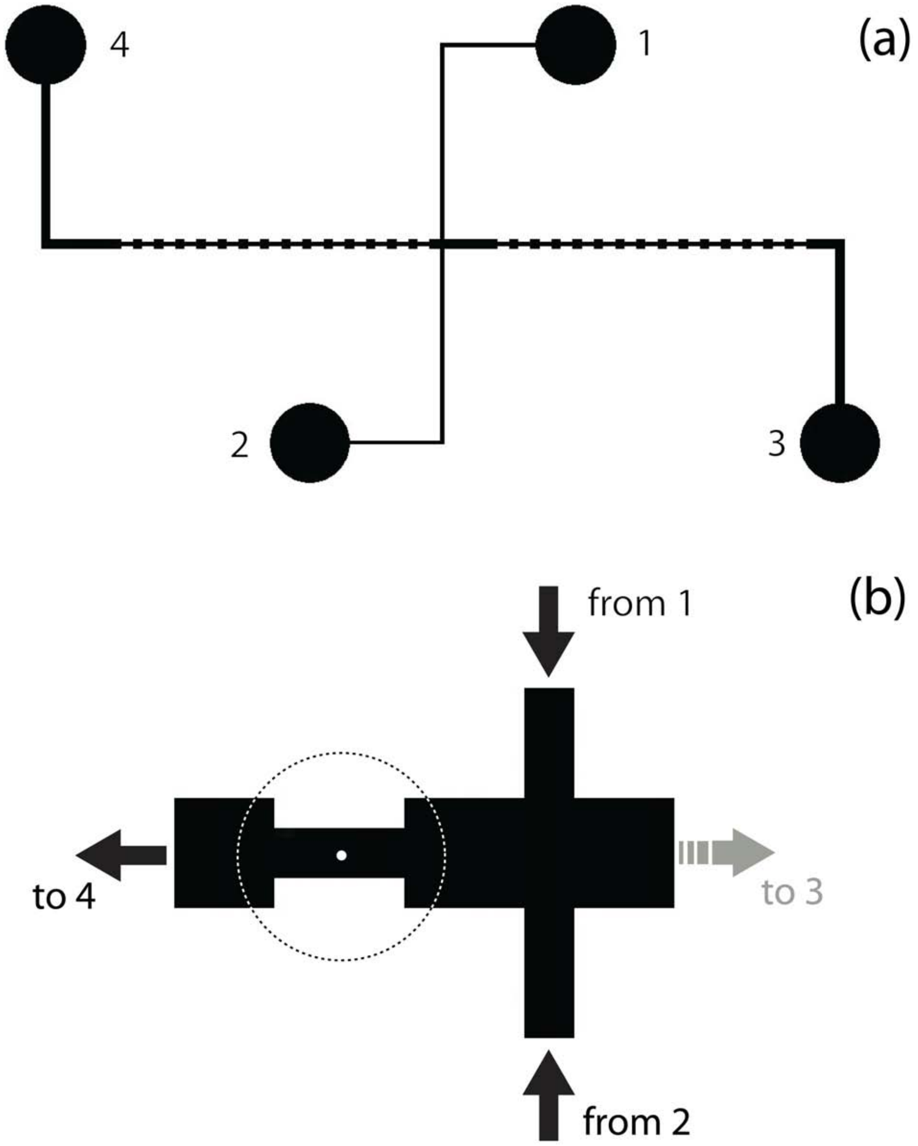

Figure 5.7: Device schematic. The microfluidic device (a) consists of four reservoirs connected via microchannels (two input reservoirs at positive voltage that flow into the grounded fourth reservoir, while the third reservoir floats during experiments described here). A dyed (reservoir 1) stream merges with an undyed (reservoir 2) stream and flows towards the ground (reservoir 4) through microchannels defined by a 20 μm deep chemical etch which results in the distinctive D-scooped profile associated with wet etching. Past the intersection that merges the two input streams 200:100 μm wide channel constrictions cause extensional flow fields. The small (not to scale) circle in (b) indicates the photomultiplier measurement spot ($\approx$ 10 μm focused waist of a 532 nm diode laser) used to measure fluorescence emitted by excited dye, while the large dashed circle outlines the field of view for microphotographs.

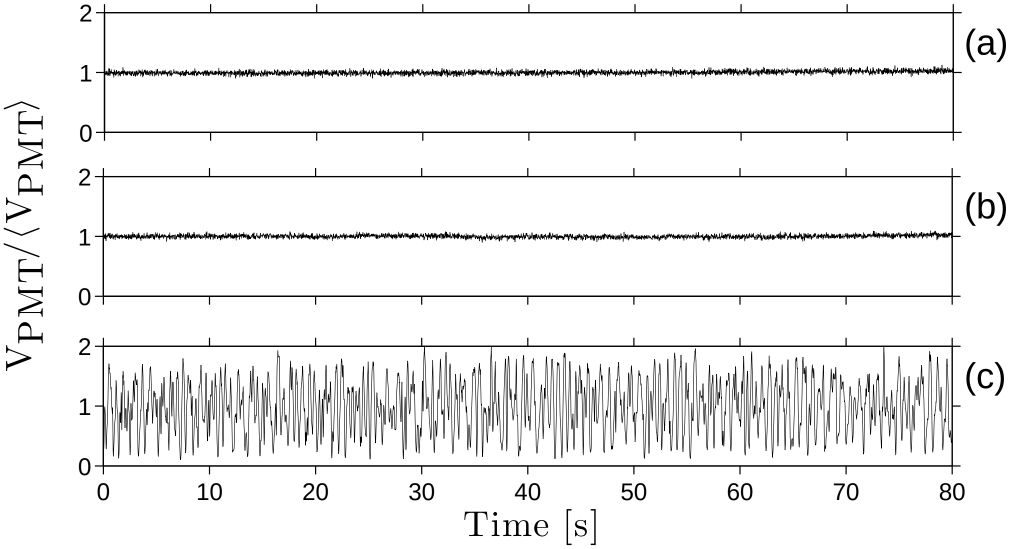

Figure 5.8: Normalized photomultiplier tube time traces. A PMT monitors the interface of the dyed/undyed streams of methanol-water solutions with (a) no driving voltage (no flow), (b) driven at 0.4 kV, and (c) driven at 0.2 kV with 120 ppm of HMW polymer added. With no polymer the PMT trace of the flow is smooth (b), albeit with noise from inherent laser diode instability as also seen for no flow (a), indicative of a stable interface and the laminar flow typical in microchannels. With polymer added rapid interface motion and instabilities are observed at moderate driving voltages, as evident by the dramatic fluctuations in the PMT signal (c).

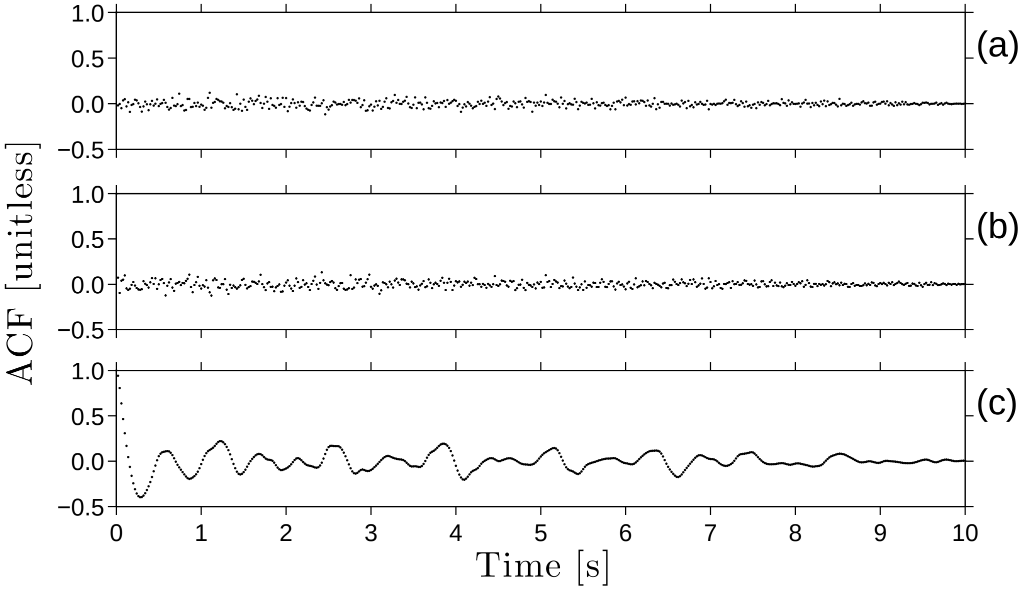

Figure 5.9: Autocorrelations of Fig. 5.8 photomultiplier tube data. Methanol-water solutions with (a) no driving voltage (no flow), (b) driven at 0.4 kV, and (c) driven at 0.2 kV with 120 ppm of HMW polymer added. The autocorrelations of polymer free fluid flow decay within a few sampling time steps and no substructure is apparent which is indicative of noise, while unstable polymer flows show rapid drop off followed by substructure without prominent peaks (i.e the ACF remains below 0.5), indicating no dominant frequencies [24].

Flow velocities in EOF are given by $v = \mu_{\text{EOF}} E$, where μ_{EOF} is the electro-osmotic mobility and E the applied electric field. By timing the movement of a marker of dye over a known distance the electro-osmotic mobility was measured to be $(5.6 \pm 0.5) \times 10^{-4}$ cm^2/Vs for polymer-free solutions, which agrees with the value of 6.00×10^{-4} cm^2/Vs reported in 50 μm diameter fused silica capillaries [143]. The HMW solution has a μ_{EOF} of $(5.7 \pm 0.7) \times 10^{-4}$ cm^2/Vs, indicating that for dilute solutions of large polymers the electro-osmotic mobility is not significantly modified from the pure solvent case. For the LMW solution the mobility is reduced to $(3.1 \pm 0.2) \times 10^{-4}$ cm^2/Vs. This reduced flow is possibly due to polymer coils interacting with the Debye layer, as has been previously observed in EOF pumped flows through uniform microchannels [128] – the Debye layer here is on the order of 100 nm thick [144] and comparable to the polymer coil hydrodynamic radii of roughly 300 (HWM) and 100 (LMW) nm. Note that polyacrylamide is synthesized by step-growth polymerization which results in a fairly broad tail of lower molecular weight chains for a given polymer sample; the polydispersity index of step-growth polymers is roughly 2. As such the HMW will have a tail in of smaller polymers which will interact with the Debye layer; however, as the HMW sample is simply the result of more steps in synthesis a similar *but shifted up in molecular weight* distribution to the LMW sample occurs, and relatively less weight fraction will occur for any given radii in the tail. This shift in molecular weight distribution will mean that although the HMW sample will experience increased interaction with the Debye layer relative to a monodisperse sample the interaction will be less than for the LMW sample. Additionally, it was found that use of a LMW sample from Polysciences Inc. which contained $\approx$ 1% ammonium chloride stopped electro-osmotic flow, even after dialysis. Pure LMW polymer from Polysciences Inc. was used, as noted above, and demonstrated normal flow. As PAAm is known not to adhere to channels [145], and $\approx$ 1% ammonium chloride solutions in water:methanol solvent demonstrated normal flow behavior, the mechanism preventing flow in the sample which included salt is not known. One possibility is the presence of a contaminant copolymer similar to poly-N-hydroxyethylacrylamide [146], which adheres to side-walls and significantly reduces the electro-osmotic mobility; this *specific* contaminant is not likely to be present, but as it is formed via radical chemistry modifying acrylamide based polymers in the presence of a radical. As ammonium can generate radicals the present of the ammonium chloride salt may lead to the formation of modified copolymers.

A visually observable fluid interface is created by flowing dyed fluid from reservoir 1 and undyed fluid from reservoir 2 to reservoir 4, Fig. 5.7.a. The channel geometry is designed with a 2:1 constriction in order to induce extensional flow and the fluid interface is monitored in the center of this region (at the white spot in Fig. 5.7.b). The Reynolds numbers here are < 0.01, below the nominal creeping flow limit of $Re < 1$. Without polymer creeping laminar flow persists to the highest applied voltages (Fig. 5.8.b), with the PMT traces appearing similar to the no-flow case (see Fig. 5.8.a). In contrast very large fluctuations arise, at sufficiently large driving electric fields, when polymer is added to the solution (Fig. 5.8.c). This arises from an instability of the flow causing the local dye concentration to vary under the green excitation spot. The polymer results in large movement of the dye/undyed interface relative to the illumination spot diameter generating order-unity fluctuations in Fig. 5.8.c. It was noted that extensional flow also exists in the cross-channel region, due to acceleration, which excites instabilities in polymeric fluids at high flow rates; the Deborah number in the cross-channel region is lower than in the designed constriction and these instabilities are eliminated at low flow rates.

No dominant oscillations were observed in PMT signals collected. The autocorrelation of PMT traces of polymer solution flows have quick decay times (≈ 0.1 s decorrelation time, taken as the e-folding time), and displayed substructure indicative of no distinct frequency components, i.e. not exhibiting sharp, large, repeated ringing which denote dominant sinusoidal frequencies. Autocorrelations of polymer-free fluid PMT signals decayed to the noise-floor in ≈ 2 sampling time steps and showed no substructure; indicating that fluctuations in the PMT trace are noise [24]. Fig. 5.9 shows the autocorrelation functions for the data presented in Fig. 5.8. Scatter and spectral plots (not shown) also did not show evidence of distinct sinusoidal frequencies [24] in unstable polymer flow, with the PMT signal showing correlated flow with substructure not consistent with the presence of sinusoidal oscillations [24]. Taken together these measures indicate that the flow is chaotic [21]. More detailed evidence is required in order to determine if the system investigated here displays true *elastic turbulence* [31], in particular measurement of velocity fluctuations and their spectral scaling properties to see if the scaling corresponds to the Batchelor regime [31].

The PMT signal is, again, dependent on dye concentration, possible thinning effects [138], and flow velocities. To reduce such effects the PMT signal is normalized by the average voltage. To study the development of the instability versus driving voltage, the PMT signal fluctuations, $\tilde{\delta}_{\mathrm{PMT}}$, defined as $\mathrm{var}\left(\frac{\mathrm{V}}{\langle \mathrm{V} \rangle}\right)$, where var(V) is the variance of the PMT voltage signal from the average $\langle \mathrm{V} \rangle$, are measured for various driving potentials. Polymer free solutions display laminar flow for all driving voltages (Fig. 5.10.a), as marked by an absence of increased fluctuation. In contrast to this laminar flow, fluctuations grow in size as the driving voltage increases for a concentration of 120 ppm of the HMW sample (Fig. 5.10.a). As seen in Fig. 5.10.b similar behavior occurrs at other concentrations of the HMW sample, both below (60, 90 ppm), and mildly above (480 ppm) the overlap concentration. Changing the concentration and investigating fluctuations at a constant (0.2 kV) voltage indicates that fluctuations rapidly grow from the noise floor and then plateau with increasing concentration, with fairly uniform measured fluctuations from $\sim \frac{1}{10}$X to $\sim$ 1X the overlap concentration, Fig. 5.11. The precise location of the excitation spot from the interface will affect the fluctuation measure $\tilde{\delta}_{\mathrm{PMT}}$. The positional accuracy is roughly 5 μm and, by measuring away from the interface on either side for a given experimental alignment[16], introduced error is estimated to be roughly 10% of the measured fluctuation for unstable flows at higher flow rates (e.g. 0.2 kV and above). This error agrees with the estimated error found by simply comparing run-to-run measurements, where

---

[16] We modified the μTK with a micrometer in order to obtain roughly 0.5 μm accuracy for relative movement

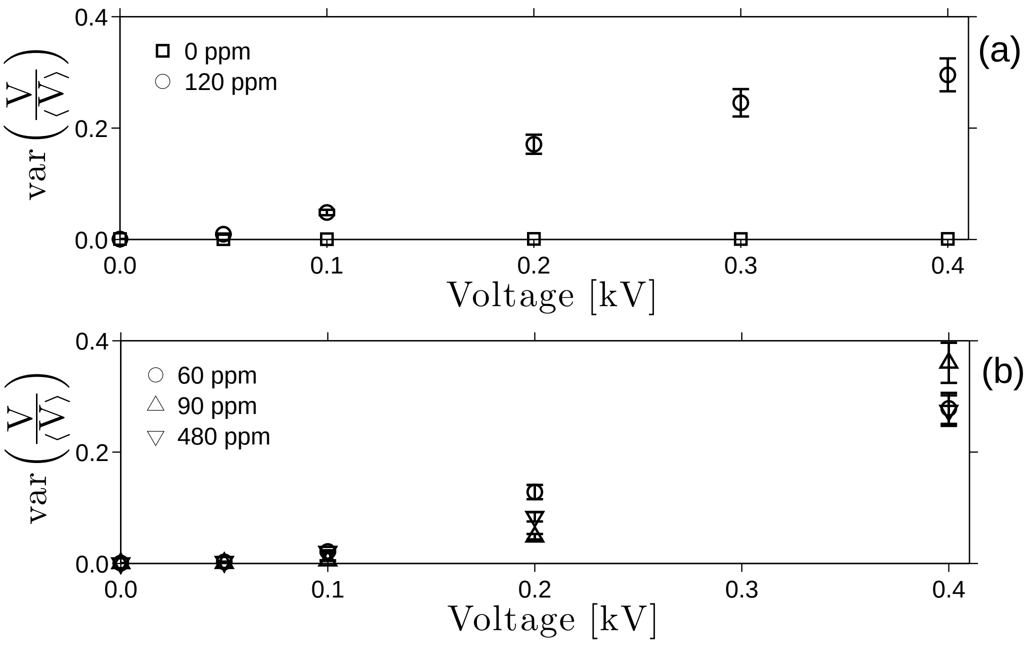

Figure 5.10: Fluctuation amplitude in normalized fluorescence signals. Fluctuations in the motion of the dyed/undyed fluid interface are measured with normalized PMT voltage for (a) 120 ppm of HMW polymer; the error is roughly on the order of 10% at higher flow rates in unstable flows. Control (polymer free) solution fluctuations are nominally zero (compare with Fig. 5.8.b). The instability threshold is predicted to be ≈ 0.01 kV here. Similar behavior (b) is displayed for 60, 90, and 480 ppm samples of HMW polymer.

realignment is required between runs. For lower values of fluctuation amplitude intrinsic system noise begins to dominate, and for no-flow conditions run-to-run differences in measured fluctuations is ca. 30%.

The viscoelastic instability condition (see section 2.8 in Ref. [2] and [103]) is given by

$$De = \frac{\lambda v}{L_{\mathrm{Char}}} \simeq \frac{\lambda_{Zimm} v}{L_{\mathrm{Char}}} = \frac{\lambda_{Zimm}\mu_{\mathrm{EOF}} E}{L_{\mathrm{Char}}} > \frac{1}{2}. \tag{5.1}$$

That is, electric fields give rise to extensional flows [147, 148], with significant coil stretching, when $De > 1/2$ [2, 103]. This equation allows the critical electric-field/voltage required for instability.

Dynamic Light Scattering experiments (Brookhaven Instruments 200SM) for 120 ppm of the HMW sample gives a hydrodynamic radius of 296 nm while the LMW sample has a radius of 137 nm. Using the experimental relationship

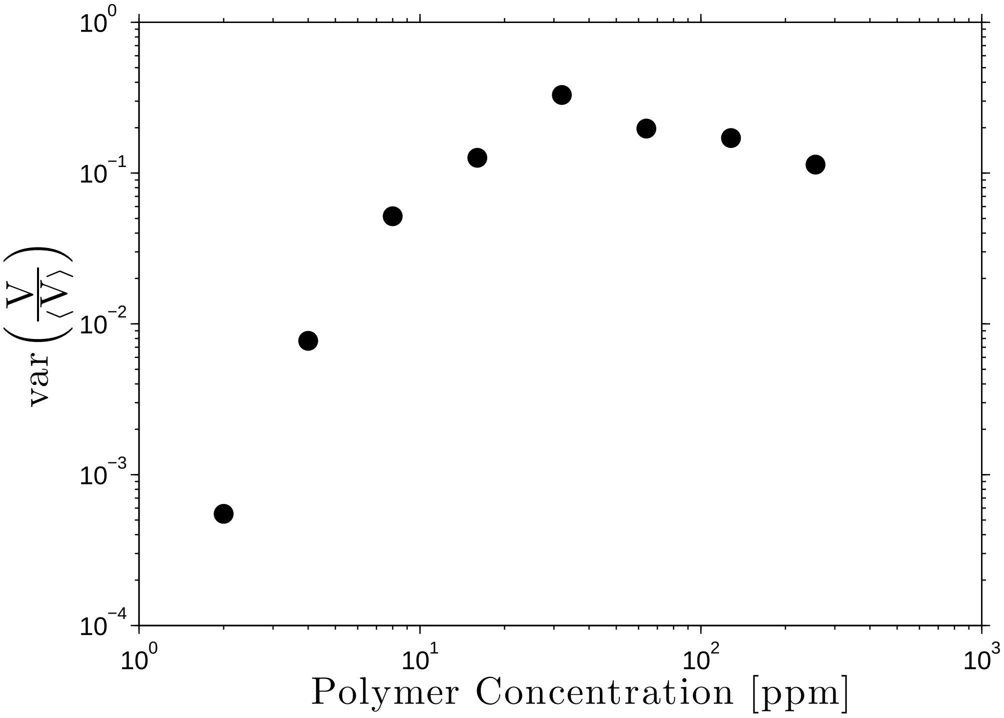

Figure 5.11: Fluctuations at various concentrations. The fluctuations in normalized PMT voltage for HMW polymer at different concentrations and 0.2 kV. It can be seen that fluctuations first increase with concentration and then rapidly peak and plateau with mild drop off; considering each polymer as independent suggests that continued growth in instability should be observed as concentration is increased. Measurement error is roughly 10% and on the order of the symbol size.

[149] between the radius of gyration R_{g} and the hydrodynamic radius R_{h} for polyacrylamide ($R_{\mathrm{h}} = 0.68R_{\mathrm{g}}$; close to the Kirkwood-Riesman prediction [150] of $R_{\mathrm{h}} = 0.665R_{\mathrm{g}}$) and the classic Zimm relaxation time equation ($\lambda_{\mathrm{Zimm}} = \eta_{\mathrm{s}}R_{\mathrm{g}}^3/k_{\mathrm{B}}T$) gives relaxation times of 0.025 and 0.0025 s for the HMW and LMW samples, respectively. Using the Mark-Houwink parameters [136] for PAAm in pure water gives relaxation times of 0.028 and 0.0029 s. The similarity in predicted relaxation times indicates that the addition of 20% MeOH has only a mild effect on the radius of gyration. The Zimm relaxation times are taken as 0.03 and 0.003s. For the HMW sample $V_{\mathrm{cr}} \approx 0.014$ kV is calculated for the system here [17]. Above this threshold instability is observed, both visually and as marked by an increase in PMT fluctuations, however below ≈ 0.05 kV bias it becomes difficult to obtain data due to diffusion rates becoming non-negligible for the low flow speeds and the fluctuation in signal approaching the noise floor.

Photomicrographs (Fig. 5.12) captured by laser excitation of the dye show the stable interface found in polymer-free flows (Fig. 5.12.a), sampling this interface with the PMT results in a smooth time trace (compare with Fig. 5.7.b). Adding polymer leads to fluctuations, of which the largest scale features are apparent in Fig. 5.12.b and c (compare with Fig. 5.8.c). The largest and dominant spatial scale of viscoelastic instabilities is determined by the system size, as for inertial instabilities [2]. There is no clear lower bound on spatial scale, with polymer size, separation, or diffusion lengths being possible cutoff lengths [31].

To better observe the transition to instability the LMW sample is used. The predicted critical driving voltage for the LMW sample is over an order of magnitude larger, $V_{\mathrm{cr}} \approx 0.28$ kV (corresponding to a critical velocity of roughly 2 mm/s), than for the HMW sample. The threshold observed in Fig. 5.13, which occurs near the predicted value, supports the hypothesis that polymer stretching drives the instability.

---

[17] The entrance length at a sudden contraction for creeping pressure driven flows is $\approx 0.63D$ [3], and has been found to be $\approx 0.57D$ for creeping electro-osmotic flows [67]. Here $L_{Char} \approx 0.6D = 12\mu$m.

The discrepancy between the observed and predicted threshold is attributed to both the relaxation time and threshold estimates and also to the existence of molecular weight distribution in polymer samples. For example, the theoretical critical Deborah number of 0.5 is approximate, and in direct experimental observation of DNA polymers in extensional flows [102] at a Deborah number of ≈ 0.4 significant stretching occurred (the latter result would reduce the estimated V_{cr} here to ≈ 0.23 kV, a velocity of 1.6 mm/s). Within the limited precision of predictions the experimentally observed instability threshold agrees well with theory.

Comparison of Fig. 5.10 and Fig. 5.13 clearly reveals the fluctuations in Fig. 5.13 are smaller. To clarify, this is due to the De numbers being an order of magnitude *smaller* in the latter figure as determined by the choice in polymer molecular weights used.

It was found that at large applied voltages globules would form which appeared to be gelled rafts of polymer (see Fig. 5.17). The observed structures retained their form while the globule remained in the field of view. These globules only formed in the HMW polymer sample, at higher voltages ($\gtrsim 0.5kV$); at lower voltages, or for the LMW sample, no indication of gel formation was observed. At the voltages reported in the present study ($\leq 0.4kV$) no visual evidence of gel formation was observed in the HMW sample, and at no voltage was gellation observed for the LMW sample. The mechanism underlying gel formation is discussed in section 5.9 and is likely electro-thermal cross-linking at the (Pt) electrode; electrogeneration of polymers at metal surfaces is an established synthesis technique that requires high current densities [151]. The possibility of contact glow electrolysis was discounted as current-voltage characteristics were linear both in the presence and absence of globules, which is not consistent contact glow electrolysis where linearity is observed only pre-ignition of the plasma [152]. Dip coating [153] the electrodes and hard drying polymer films in place could either prevent flow, or resulted in globule formation at lower voltages (0.2 kV), and removal of films again prevented globule formation at lower voltages. This result supports a high current density/thermal route to globule formation where pin hole or other imperfections in hard dried films would lead to a high local current density and subsequent heating/electron effects. It is also known that polyacrylamide will spontaneously adhere to metal and form a partial film [154], this partial film will result in higher current densities through the non-coated Pt surface relative to an pristine surface and a mildly higher surface coverage appears to arise for higher molecular weight samples [154]. This affinity for coating electrodes requires careful cleaning[18] between runs [19], while a dependence of coverage on molecular weight could account for no observed globules arising in the LMW samples for voltages observed to give rise to globules in the HMW samples. Spontaneous coating of electrodes is a rapid effect [154], on the order of 10's of seconds, and experimental setup times ensure that the coating process is complete before experiments commence. See the next section for further discussion.

Two alternative instability mechanisms must be discussed. Conductivity gradients between co-flowing streams can give rise to electrohydrodynamic (EHD) instabilities when driven by electric fields [155]. The possibility of EHD instability is ruled out, as the (otherwise identical) polymer free solutions do not show instability. It is also conceivable that dynamic polymer-wall adhesion [145] of polymer coils coating the walls could lead to a time varying μ_{EOF}, driving instabilities. This mechanism is rejected as underlying the instability, as PAAm does not adhere to glass [145]. This rejection is also supported by the similarity between μ_{EOF} measurements of polymer-free and dilute HMW polymer solutions which indicates no significant modification at the wall occurs.

An additional possible mechanism of instability is large Joule heating leading to unstable thermal convection and thus unstable flow. Joule heating is an issue in electro-osmotically pumped devices when large currents flow through the fluid, changing fluid properties [156]. As unstable temperature is observed for chips with temperatures in excess of 60 °C in ambient air [157] it is possible

---

[18] Once hard dried in place the transparent films are difficult to remove and require long hydration and careful cleaning.

[19] Once hard dried in place the transparent films are difficult to remove and require long hydration and careful cleaning to remove.

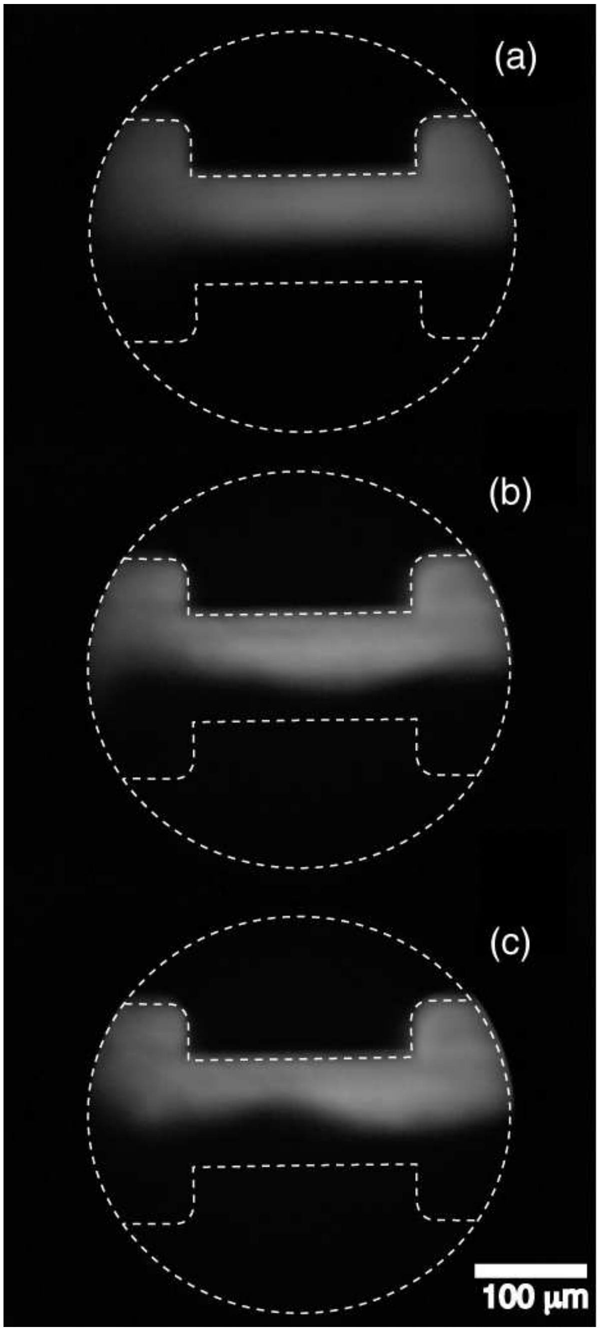

Figure 5.12: Photomicrographs of (a) no polymer and (b, c) 120 ppm HMW polymer flows at 0.2 kV. Image (c) is taken one second after (b). Dashed lines indicate field of view and microchannel constriction outline. Note that due to nonuniform illumination the dye is not excited uniformly over the field of view and there is a drop off in intensity at the edges. The scale bar is 100 μm.

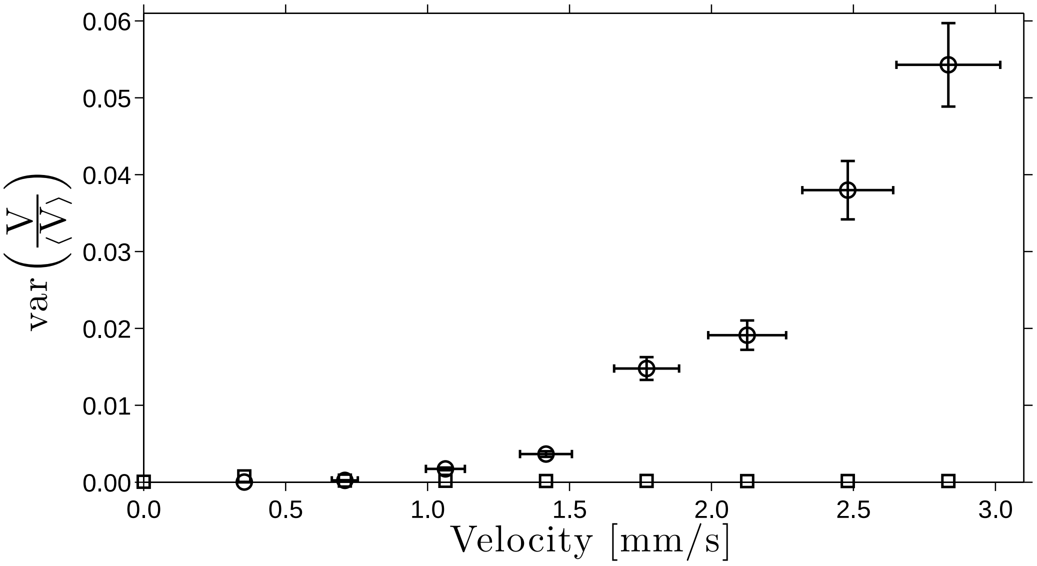

Figure 5.13: Fluctuation growth transition. The LMW sample with a predicted elastic instability at $v_{\mathrm{cr}} \approx 2$ mm/s experimentally demonstrates an instability onset at ≈ 1.5 mm/s. Above ≈ 1.5 mm/s fluctuations grow dramatically, as compared to a gentle increase below the observed threshold. While there are accepted predicted thresholds there is no generally accepted/known model for the shape of transition to instability; however a simple model that assumes that the polymer coil flux through an instability region sets instability strength suggests concave up growth, as seen here (see the next section for more discussion).

that flow is also unstable in such an regime. It is unlikely that unstable flow due to unsteady convection is occurring here, as the microchips where cool to the touch and no difference in temperature could be perceived pre- and post-run. External temperature monitoring of thin quartz capillaries (≈ 0.1 mm) in combination with simulation has established that the external wall temperature is a good proxy for the temperature at the internal wall, with a difference between the temperature of internal capillary/fluid interface and the external temperature of roughly 0.6 °C for a ≈ 50 °C increase in fluid temperature due to Joule heating [157]. Microfluidic chips have a larger mass, which will cause an increased difference between the internal and external temperature, however experiments with plastic microchips in the μTK has demonstrated that the external temperature is within a few (1-2 °C) degrees of the internal fluid temperature [25]. As plastic has a reduced thermal conductivity relative to glass (roughly 5× smaller) the observed temperature gradient of 1-2 °C in plastic chips [25] will be larger than what glass would maintain, making this offset a conservative estimate. Externally monitoring the temperature of the glass chip used here revealed no observable temperature increase from the ambient environment for a thermistor with a 0.1 °C resolution (see Fig. 5.14). In combination with the findings for plastic microchips used in conjunction with the μTK a bound on Joule heating of ≤ 2 °C can be estimated. This is consistent with no observable breaking of linearity of the current-voltage characteristics (see Fig. 5.18), whereas concave up nonlinear growth in current is a signature of Joule heating.

In summary, extensional instabilities are excited in electro-osmoticaly driven polymer flows through a 2:1 microchannel constriction. Polymer-free solutions display creeping laminar flow, while addition of high molecular weight polymer leads to instabilities above a critical flow rate corresponding to the viscoelastic instability condition for extensional flows. Electo-osmotic pumping is increasingly relevant as dimensions scale down, while viscoelastic effects become more pronounced for small dimensions due to the inverse scaling of the Deborah number with channel size (see equation 5.1). Our experimental results demonstrate instabilities can be readily excited, even in microscaled devices

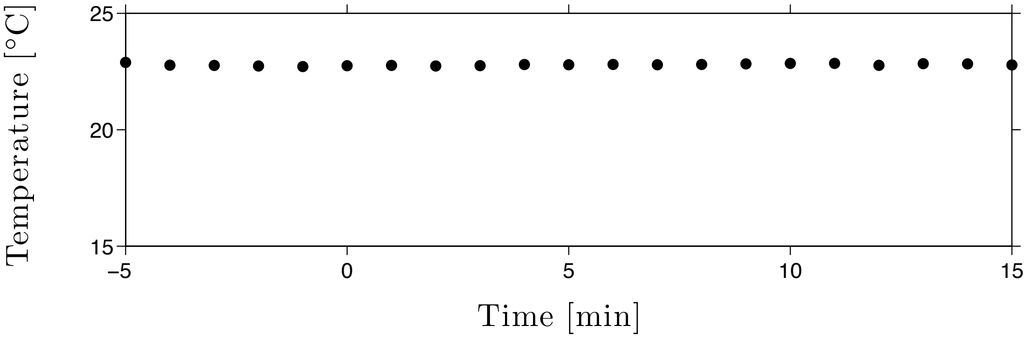

Figure 5.14: Monitored external chip temperature. To determine if large Joule heating occurred a thermistor was attached to the external surface of the chip, and the chip was run under standard operating conditions (0.2 kV, 128 ppm PAA solution). No observable heating occurred during a 10 minute run, which is roughly 10× a typical fluctuation experiment. Shown here is the 10 minute run (0-10 min), with 5 minute pre- and post- run data. As the glass is ≈ 1 mm thick any internal temperature changes will be observed after a diffusion time of roughly 3 seconds and thermal steady-state should be achieved in a few diffusion times. As no external temperature rise was observed the internal increase will be bounded by the thermistor resolution (0.1 °C) and thermal gradient maintained between the inner microchannel and the external surface. In studies of plastic microchips in a μTK a thermal gradient of 1-2 °C was observed [25], indicating that any Joule heating here will be bound by 2 °C (note that glass has a higher thermal conductivity than plastic, which will reduce the thermal gradient for the glass microchips used here). The lack of observed external temperature growth is consistent with the low current flowing through the device (order of μA), which is a consequent of low ion content (this is in contrast to the TBE buffer case).

where laminar flow normally predominates. Electro-osmotic flow can be made unstable intentionally through the addition of small amounts of chemically inert polymer, allowing the *possibility* for enhanced mixing. Our results also suggest caution when electro-osmically pumping biological or other viscoelastic samples where instabilities may arise under conditions typically assumed to be laminar.

5.8 Fluctuation growth

Inspection of Fig. 5.11 shows that fluctuations first grow with polymer concentration increase, and then peak and plateau with a gentle decrease.

Scaling properties of viscoelastic instabilities are not well understood, but the basic elements of curvature and elastic normal stress (stretching) along streamlines are well established as underlying instability [158] as these mechanisms lead to "hoop-stress" [2] allowing stretched polymers to cross streamlines, disturbing laminar flow. Fluctuations should grow with concentration (as the movement of individual polymer coils underlies the fluctuations). Changing the concentration and investigating fluctuations at a constant (0.2 kV) voltage indicates that fluctuations rapidly grow from the noise floor and then peak and plateau with a gentle decrease as concentration is increased, with fairly uniform measured fluctuations from $\approx \frac{1}{10}$X to $\approx$ 1X the overlap concentration, Fig. 5.11.

The fluctuation measure $\mathrm{var}\left(\frac{\mathrm{V}}{\langle \mathrm{V} \rangle}\right)$ takes its maximum possible value of 1 for square-wave signals; the precise maximal value for a given signal is ≤ 1 and depends on the nature of the waveform. Smooth growth in the fluctuation measure should occur until the maximum, for a given waveform with linear amplitude growth. When the maximal value is reached a sudden apparent threshold will occur and the fluctuation measure will saturate. The maximal threshold observed here is followed by a *mild decrease* rather than a strict capping and saturation; this is suggestive of a qualitative change in behavior rather than an artifact of the fluctuation measure.

Modeling the polymer solution as a colloidal solution [159], where the soft

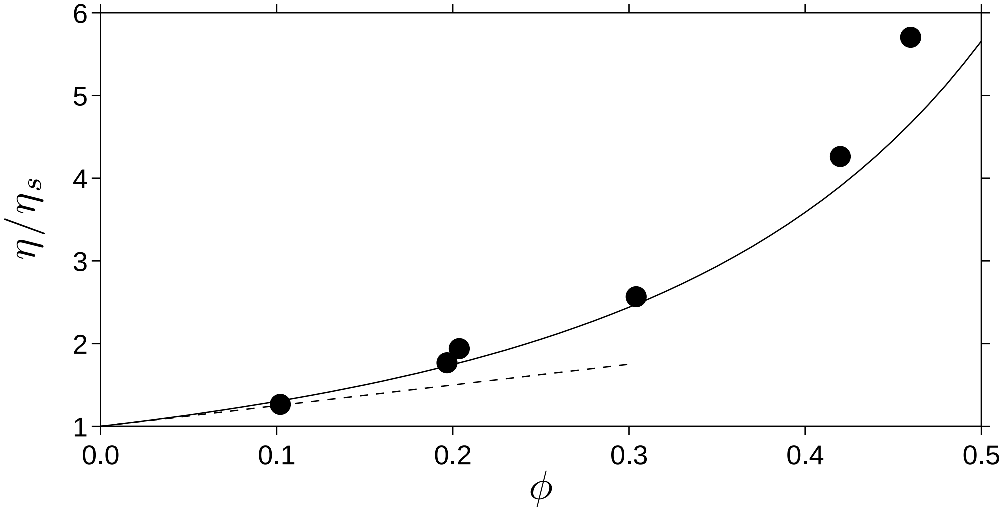

Figure 5.15: Colloidal suspension viscosity at various concentrations. Einstein [26] found the viscosity for "dilute" solutions of colloids, where dilute signifies no particle-particle interactions. Measurements [27], circles here, reveal that suspensions diverge from the Einstein prediction (dotted line) above a volume fraction of roughly $\phi \approx 0.1$; the solid curve is a theoretical extension [28] of Einstein's model that attempts to take particle crowding into account but ignores close packing effects (note that at higher concentrations, near the close packing limit, the extended model also diverges from the data)
.

polymer coils are thought of and approximated as hard colloidal spheres, one expects hydrodynamic interaction mediated *molecular crowding* effects above a volume fraction ϕ of approximately 0.1 [28], where such effects are empirically found. The presence of molecular crowding in colloids was first noted by an increase in the rate of viscosity growth with concentration due to hydrodynamic interactions leading to particle-particle interaction, resulting in viscosity "hardening" [28]; see Fig. 5.15.

To estimate the concentration when hydrodynamic interactions between polymers play a significant role one can take $\frac{c_{thresh}}{c_*} = \frac{\phi_{thresh}}{\phi_*}$, with ϕ_{thresh} empirically known [28] to be ≈ 0.1 and ϕ_* corresponding to the overlap concentration which, depending on the particular packing taken near overlap, ranges from roughly 0.5-0.7; this leads to an estimate of $c_{thresh} \approx$ 40-60 ppm for the HMW polymer used here; this estimated threshold is close in value to the observe peak in Fig. 5.11. The similarity in thresholds suggests that crowding may be the mechanism inhibiting growth in measures fluctuations; the tendency for polymer coils to deform makes the hard colloid model, which assumes polymer coils act as *hard* spheres, only approximate. It is known that molecular crowding strongly affects and reduces molecular transport [160] by hindering movement of macromoleclues; hindered movement of polymers across streamlines will limit fluctuations, as is observed here.

Compelling evidence that hydrodynamic interactions are important also comes from brownian dynamic simulations of λ-DNA, a biopolymer similar in size and nature to the HMW sample used [21], in both shear and elongational flows [29]. The simulations, that allow hydrodynamic interactions to be turned on and off, demonstrate that for $\frac{c}{c_*}$ above 0.1 including hydrodynamic interactions significantly affects calculated properties. The excellent agreement of the $\approx 0.1c_*$ threshold found in the simulation of (bio)polymers where hydrodynamic interactions become important and the peaking of fluctuations here at $\approx 0.1c_*$ supports the hypothesis that hydrodynamic interactions are limiting growth in fluctuations.

Note that below the predicted threshold, above which hydrodynamic interactions have significant affect on bulk properties, the fluctuation measure

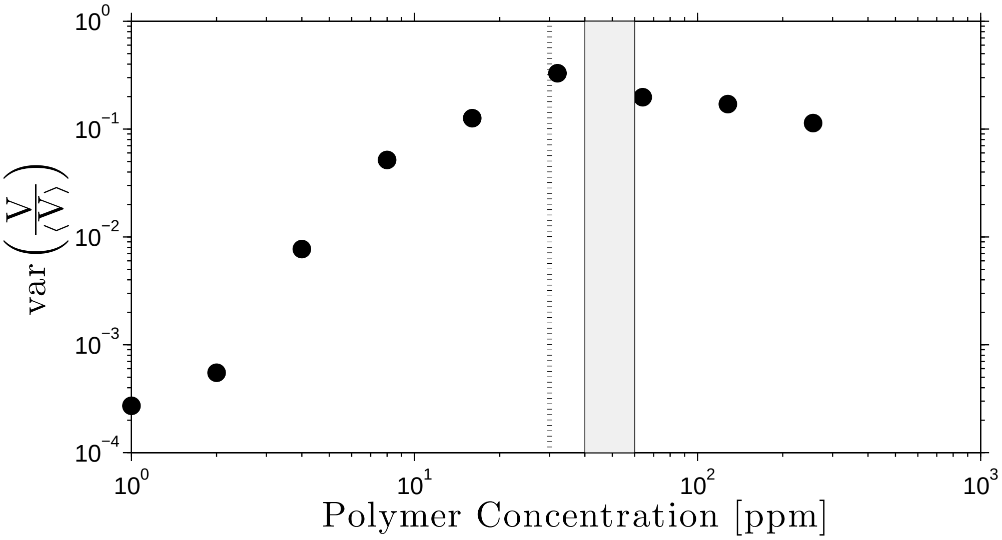

Figure 5.16: Fluctuations at various concentrations. The fluctuations in normalized PMT voltage for HMW polymer at different concentrations and 0.2 kV. It can be seen that fluctuations increase with concentration but rapidly peak and plateau well below the overlap concentration (at $\approx 0.1c_*$, where $c_*is \approx 300$ here). Modeling the polymeric solution as a hard colloidal suspension predicts a transition in behavior at c $\approx$ 40-60 ppm (grey band) due to molecular crowding. Simulations of a similar polymer [29] find a threshold of $0.1c_*$ (dotted line) above which hydrodynamic interactions between polymer coils significantly affects properties. The good agreement of both the colloidal model and the simulations with the observed peaking of fluctuation growth suggests hydrodynamic interactions and molecular crowding is the mechanism inhibiting fluctuations.

has approximate (square) power-law scaling as expected for the variance given linear growth in amplitude, which is in turn is expected if polymer coils are independent. The approximate power-scaling occurs with a concave rounding versus the strictly linear curve predicted on a log-log plot. This rounding (breaking of power-law scaling) suggests subtle polymer-polymer interactions even in quite dilute solutions; recent systematic and careful rheological studies have demonstrated [97] polymer-polymer interactions can exist for concentrations as low as 1% of the overlap concentration in elogational flows.

To summarize: the lack of true power-law scaling at low concentrations, the mild decrease in fluctuations above a threshold, and the correspondence of this observed threshold with the predicted threshold for hydrodynamic interactions in (hard) colloids and (soft) polymers indicate hydrodynamic interactions are important in nominally dilute solutions and limit fluctuation growth.

5.9 Globule formation

The unexpected formation of globules, aggregated polymer “microrafts”, arose in working samples. These polymer globules are readily apparent under fluorescent microscopy of flowing samples, where TAMRA dye is used (see Fig. 5.17).

The formation of globules occurred at lower voltages, from an inadvertent creation of dry PAA polymer (insulating) films on the electrodes due to a modification of the cleaning process[20]. The basic mechanism was one of *dip coating*: the electrodes would be emerssed into the working solution and once removed a thin sheath of (polymeric) liquid would remain which would dry into a hard coating [161].

Removal of the residual film eliminates globule formation at lower voltages. Correspondingly, films can be intentionally dried on the electrodes leading to globules, attributed to local heating at the high current density locations where the electrical insulation of the deliberate film is weakest[21]. Removal of the intentional films with vigorous cleaning again prevents the formation of the aggregates. Further, emersion of the electrode *and* its plastic insulating sleeve holding it to the experimental assembly leads to globule formation. As the space between the platinum electrode and the plastic sleeve is snug, but not liquid tight, high current densities will be present within the enclosed space and at the interface into the liquid resivour.

The controlled formation/elimination of these aggregates might be of some interest, but most importantly they pose no threat to the interpretation of the low Reynolds number unstable flows in the core experiments.

It is known that at high current densities ($i > 5\ mA/cm^2$), and in the

---

[20] Insufficient “soaking” and post-cleaning of electrodes in the cleaning process, see Appendix B, leads to formation of films.

[21] For some dried on films *no* flow was observed, indicating no defects in the polymer film surface

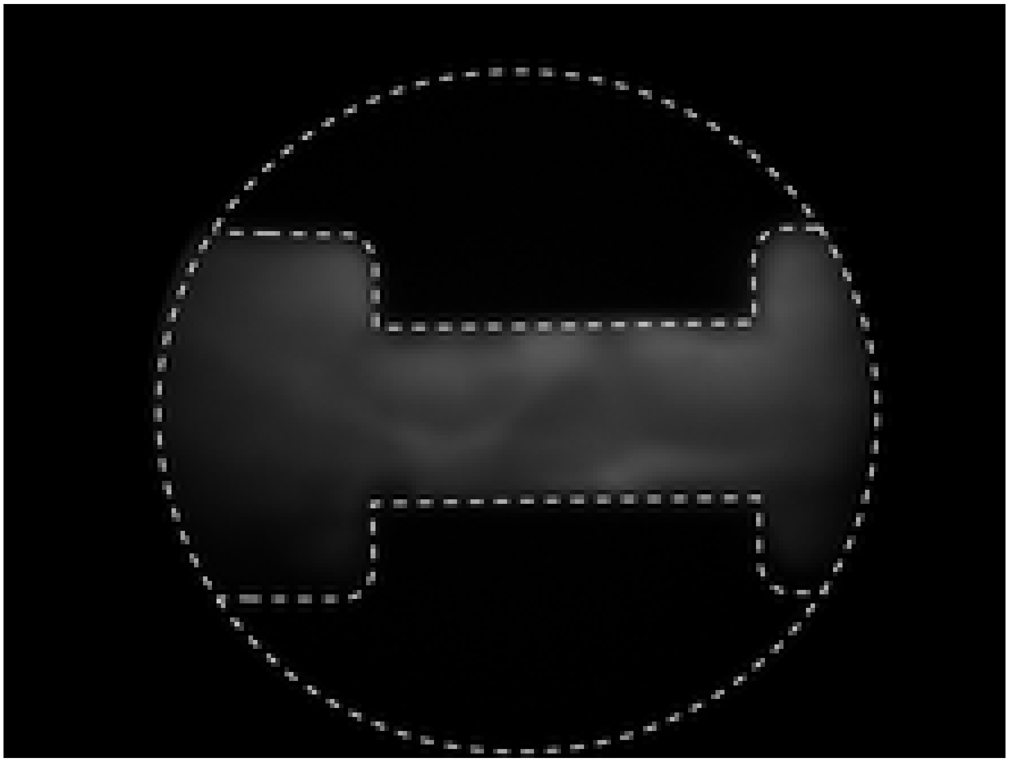

Figure 5.17: Globule formation. Globules are formed at larger applied voltages ($\geq$0.5 kV). Seen here are globules formed at 1 kV potential at a concentration of 120 ppm of the HWM sample. It was found that at larger applied voltages globules would form in the fluid with dimensions on the order of the channel, presumably due to cross linking of PAAm at the electrodes. Note that phase separation can only occur in poor solvents, and therefore is excluded from occurring here. While this effect may be of interest in making microgels [30] on demand in microfluidics, it is not explored here. This effect only occurred for the HMW polymer sample.

required presence of one of a handful of electrolytes including NO_3^-, that acrylamide will rapidly polymerize and gel in solution but at lower current densities ($i \leq 1\ mA/cm^2$) conversions less than 1% are obtained even after 3 hours [151]. The gelation occurs rapidly once polymers have built up in the system [162], the initial condition of the working samples here. A possible mechanism involved in the globule formation is decompostion of 5(6)-carboxytetramethylrhodamine (TAMRA) dye, $C_{25}H_{23}N_2O_5$, at the anode into NO_3^- in combination with the high current density due to "leaky" (cracked, pin hole, or otherwise imperfect coverage) films. However, the presence of TAMRA does not seem to be required. Driving at high currents from the nondye supply to the TAMRA resivour, by placing the TAMRA electrode at zero volts, and then running the solutions from both the TAMRA and the nondye supply to the ground, reveals a large amount of globules made visible in the dye stream, which then quickly drop off - indicating that globules are formed at the nondye electrode during the high current phase, swept into the TAMRA reservoir, and then swept to the ground during the "normal run" phase. Reducing the amount of TAMRA dye to 1/4 did not change the nature of globule formation, indicating that either TAMRA is not required or that $\approx 5\mu$M is well above the required level. This suggests TAMRA dye is not the main contributor to NO_3^-, or other reactive species, involved in the gelation process.

Further, if one of the electrodes was intentionally, or unintentionally [22], put to a low voltage flow would preferentially sweep from the high to the low voltage resivour at an higher current then in other experiments (due to reduced path distance, and hence resistance) and would often lead to globual formation. Once globules are formed at an electrode their formation tended to persist until the electrode was cleaned. Further, if runs were done at high voltages (> .5 kV) after long exposure of electrodes to solution globules would form.

These observations, in combination with the observations of Otero and Cantero, Ref. [151], where they observe the formation of a gel on anodes,

---

[22] Occasionally the control software fails to properly set the voltage on an electrode.

indicate that films can be formed either by air drying polymers onto the electrodes, or in-situ under high enough current densities (e.g. globule formation environment), or in-situ due to polymer adsorption onto the electodes (which will reduce the current for a given current density). Once formed films can lead to globule formation, due to high current densities. Further, a rough estimate of expected current densities for 1 mm of the electrode immersed into the liquid is on the order of 0.5 mA/cm^2 for a 1 μA total current, assuming roughly 90% of the electrode is covered in absorbed polymer [154]; thus for electrodes that do not have a partial hard solid film covering it the current densities are not high enough for electrogeneration of polymers [151], but the current density is close enough to the approximate value required for synthesis (> 5 mA/cm^2) that the reduction in area that would occur in the presence of a partial covering of a hard solid film plausibly could move the system into the electrogeneration regime.

Under high current densities the spontaneous formation of glow discharge can occur at anodes [152], which is known to lead to enhanced electrochemistry and polymer modification. Under heating bubbles develop around electrodes, and once completely enveloped a plasma can be ignited leading to "hot" electrons and UV emission that can result in nonfaradic- and photo- chemistry. This possible mechanism for globule formation is discounted here as experiments remained in the Ohmic regime, which persists up until significant bubble formation (transition to vapor enveloped electrode) that proceeds the eventual plasma ignition. No bubbles were observed at the electrodes, and there was also no glow observed, which would indicate the formation of plasma [152] (hence the term "glow discharge").

Kinetic studies of PAA absorption on gold [154] indicate that absorption is determined by diffusion, with 10-100 s timescale for coverage dynamics. High (> 0.9) coverage occurs rapidly once metal is emersed in a polymer solution for molecular weights in the range of 5,000 to 1,500,000 Da, using *ca.* 0.5 mm diameter platinum wires (e.g. similar to electrodes used here). Earlier thermodynamic studies [163] of PAA on gold and iron demonstrated near complete coverage of surfaces and indictated that polymers are tightly bound

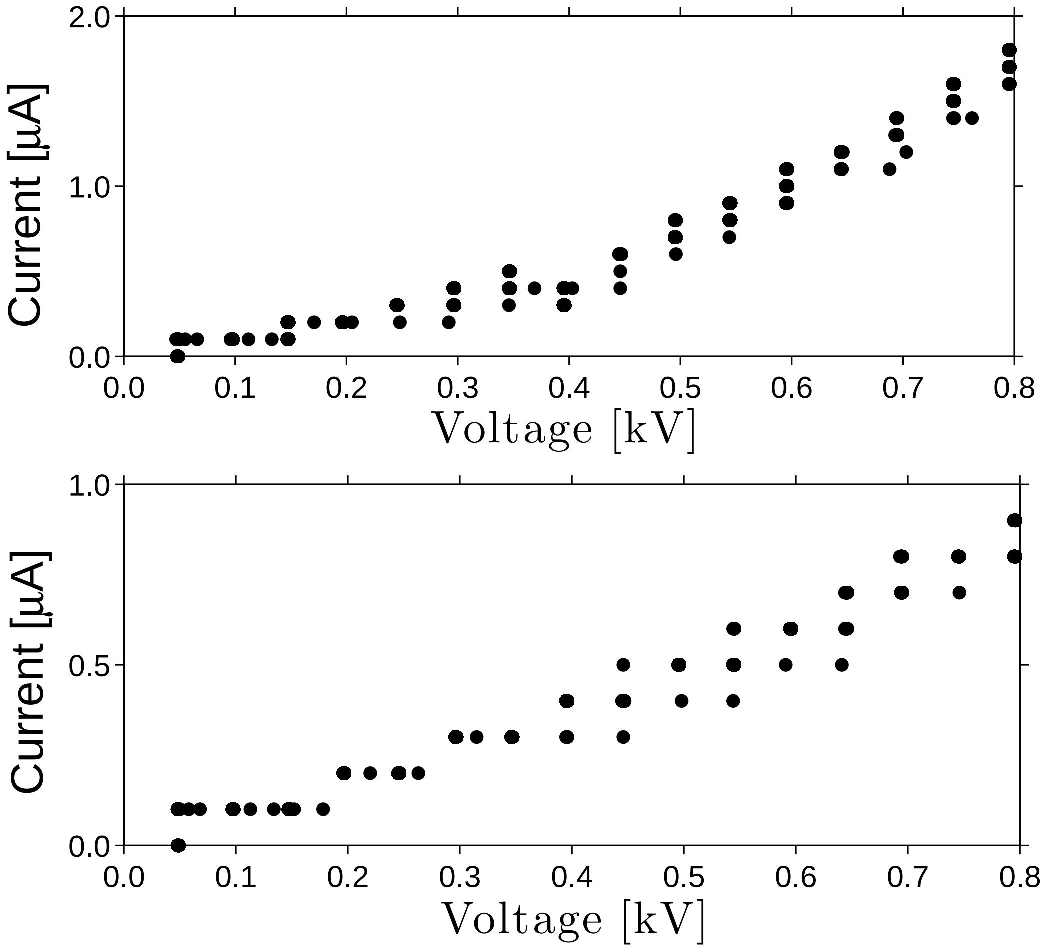

Figure 5.18: Current-voltage characteristics for 128 ppm HMW sample. Voltage is swept from 0.05 to 0.80 kV in steps of 0.05 kV, with each step lasting 100 s and current is monitored at the grounding electrode. In the top panel no globules were observed, while in the bottom panel globules formed at 0.1 kV and were (increasingly) present at each voltage step. In the top panel a kink appears above 0.4 kV, possibly due to Joule heating effects - although scatter is too large to exclude linear behaviour. In the bottom panel IV characteristics remain consistent over the entire voltage sweep, with no sudden drop or large (order one) fluctuations as seen in contact glow electrolysis. Scatter is due to device resolution (0.1 μA).

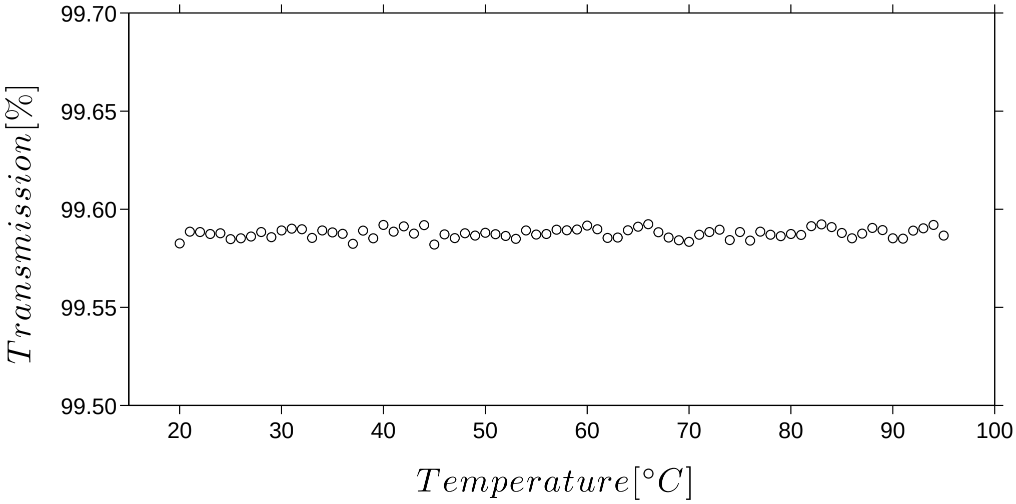

Figure 5.19: Optical transmission through a bulk sample heated in a water bath. A 128 ppm HMW PAA sample was heated up to 95 °C, and no reduction in transmission was observed using a Jasco J-810 spectrometer at 500 nm. A reduction in transmission would be expected in the presence of globules (scattering/deflection centers). Note that bubbles formed on the sidewalls, mainly at the edges of the rectangular container, and none appeared to exist in the optical path. There is no discernible threshold temperature above which decrease in transmission occurred.

and "pressed flat" against the surface at low voltages, in contrast the monomer (acrylamide) is much less strongly associated with the electrode compared to the polymer. Polyacrylamide also strongly bound to iron, and was shown to considerable inhibit corrosion, again showing strong binding to the surface. It was noted that PAA was thermally unstable at elevated temperatures (60-80 °C) with behavior consistent with polymer hydrolysis leading to radical formation and subsequent cross-linking - this thermal hydrolysis route is a plausible mechanism for the formation of globules.

Coating the electrodes with dimethyldichlorosilane (DMDCS), which prevents the adsorption of micro particles, prevented globule formation but did not not lead to a persistent and good coating and the use of nitric acid and NaOH in the cleaning process appeared to strip the coating. These coatings could be used to good effect for cleaned, then coated, electrodes.

It should be noted that electro-thermal heating effects or electron-polymer interactions (or reactions at the electrode) are indicated, as “pure” heating in a water bath did not lead to globules[23]. By immersing a sample in a water bath and monitoring optical transmission the formation of globules would be observed as reduced transmission due to scattering, elevating the temperature up to 95°C did not lead to reduction of transmitted signal (Fig. 5.19) which suggests no globules were formed; transmission of a 532 nm laser pointer beam and visual inspection also did not show any indication of large globules. However, these findings are complicated by the presence of MeOH in the sample leading to several large bubbles forming on the container walls during the heating cycle, fortuitously these bubbles did not form in the optical path. Inspection by eye post experiment showed bubbles mainly existed at edges of the rectangular container, and none appeared to be in the mid-section where the optical path was.; two separate apparatus were used and neither showed reduction in transmission. Bubbles should nucleate at imperfections, and globules would provide a likely source for bubble growth - visual inspection showed no free-floating bubbles that could indicate the presence of globules.

Finally, it must be noted that phase separation is known to occur in polymer solutions and can be induced by flow conditions. This possibility is excluded here as poor solvent conditions are a requirement for phase separation to occur [164], while the solvent here is a good solvent. Additionally the qualitative behaviour observed in phase separation is different then seen here – two *liquid* phases separate and coarsen over time [164]. Here gel-like globules rather than liquid like regions were observed and no coarsening was observed. Separation can be induced by raising the temperature, causing liquid to become cloudy [164], but raising the temperature of the sample to near the boiling point did not induce any transition. Further, solvent “holes” first appear and grow in phase separation [164] while here the globules would appear and, as the voltage was increased, the number of globules would grow.

---

[23] Although localized high temperatures could lead to a pure thermal route above the heating range explored in the water bath experiments no bubbles were observed on the electrodes or in the liquid which tends to undercut this possibility.

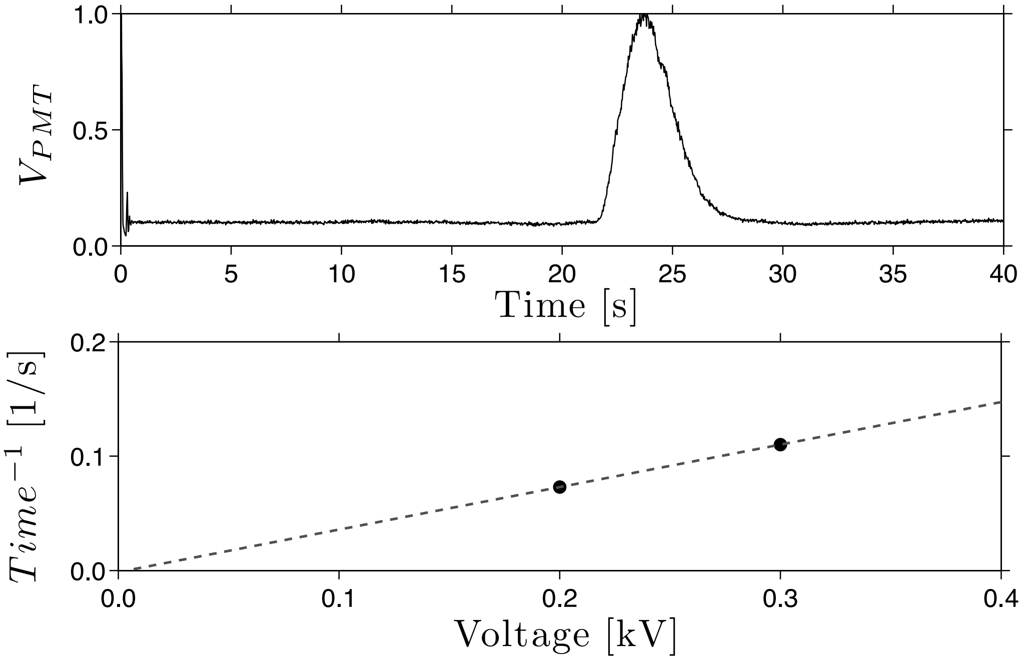

Figure 5.20: Electro-osmotic Mobility Measurement. A bolus of dye is formed by driving dye for 10 s from reservoir 1 to reservoir 2, and then driving the bolus downstream between reservoir 3 and reservoir 4 and monitoring the flow with a PMT (a). Mobility is calculated using known voltages and distances, in (b) it is seen that the inverse time versus voltage relationship is linear and within error passes through zero, as expected. The data shown is for 120 ppm of HMW polymer; in (a) the driving voltage was 0.2 kV.

5.10 Mobility measurements

The electro-osmotic mobility for solutions were measured by driving dyed solutions from reservoir 1 to reservoir 2, forming a dyed bolus at the channel intersection, and then driving fluid from reservoir 3 to reservoir 4. As in all experiments fluids in a given experimental run are identical, except for the presence or absence of dye. Focusing the laser at the bend to reservoir 4 allowed the movement of the dye bolus downstream to be timed. Using known distances and driving voltages allows mobility to be calculated. Fig. 5.20 shows a typical time trace for 120 ppm HMW polymer as well as the inverse flow time of the bolus versus voltage, which is linear if the fluid is well described by a constant mobility. For 480 ppm solutions of HMW polymer a linear relationship did not exist and the flow velocities where lower than dilute or polymer free solutions. As concentration increases above the overlap concentration polymer-polymer interactions become important and polymer will also be pushed into the wall (Debye layer); evidently mobility becomes dependent on concentration details over the overlap.

5.11 Run out instability

It was noticed that when running the solutions at high voltages for long durations that instabilities would occur of a visually differing character, and these instabilities were noted in *polymer-free* solutions. Visually checking reservoirs revealed that the input reservoirs were depleted and electrode contact was tenuous when these instabilities occurred. The instabilities were dramatic, and the PMT signal fluctuations, $\tilde{\delta}_{\mathrm{PMT}}$, were quite large - about 0.6 for the most dramatic run observed (see Fig. 5.21) and the fluctuation oscillations were much more rapid than the viscoelastic instabilities. The instabilities could last for up to about 5 minutes, but would last for indeterminate time frame and occasionally would be intermittent. The mechanism resulting in these instabilities is likely contact breaking at the electrode/liquid surface leading to oscillatory forcing of the flows, and is reminiscent of the electrokinetic instability (EKI) where oscillatory electric field forcing [165] is harnessed to promote mixing. The "run out" instability observed here was only observable for higher voltages (> 1 kV), and could not be controlled well. Visual inspection revealed that rapid span-wise oscillations were present at the junction. While time-variation was uncontrolled here one of the advantages of electrokinetic flows is the relative ease that electric fields can be switched and changed, and electrokinetic instability is an effective approach for promoting mixing [165].

5.12 Mixing: preliminary efforts

Characterization of mixing was attempted using the PMT, however this was difficult as the μTK laser feedback results in different power output between

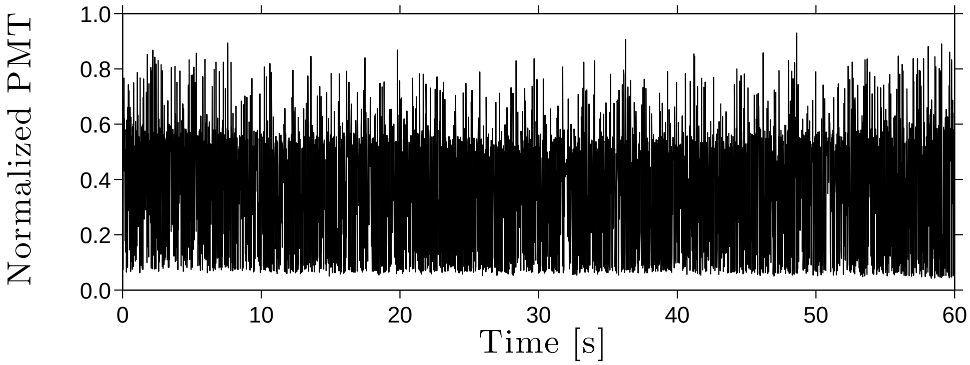

Figure 5.21: Run out instability. It was observed that after running polymer-free solutions for long times at high voltages (2 kV here) instabilities, of a different character from viscoelastic instabilities, would spontaneously arise. The signal is measured in the first constriction. Using the eye piece oscillations perpendicular to the mean flow direction were visually observed in the junction.

runs[24] limiting absolute comparison. In addition only “single pixel” sampling is possible. Attempts to estimate polymer-free mixing, by using “two-pixel” sampling (one run with the PMT focused near the top of the channel, and one run with the PMT focused near the bottom of the channel), at various distances downstream did not lead to accurate measurements and it was found that attempt-to-attempt variation was large; here focusing was attempted near the scalloped section of the channel near the edge in order to increase the distance between spots, which no doubt increased error (as the optical thickness will start to change here, so misplacement will affect measured signal).

For polymer solutions the presence of fluctuations simplifies experimental considerations - the PMT can be focused in the center of the channel, and fluctuations measured. As fluctuations should decrease as mixing progresses towards homogeneity a rough estimate of mixing may be possible. However, it is not clear how to determine how much of the decrease due to instability and what is due to diffusion and differing effective diffusion rates and instability strengths will exist at different voltages. In Fig. 5.22 it can be seen that rapid decrease in fluctuations is observed downstream.

---

[24] The laser can be turned on and left on, however due to software design the laser power is briefly interrupted and the laser restarts at the start of each run. It was found that warming up the laser would reduce the hopping between runs, but that such hopping would still occur with about 10-15% output difference.

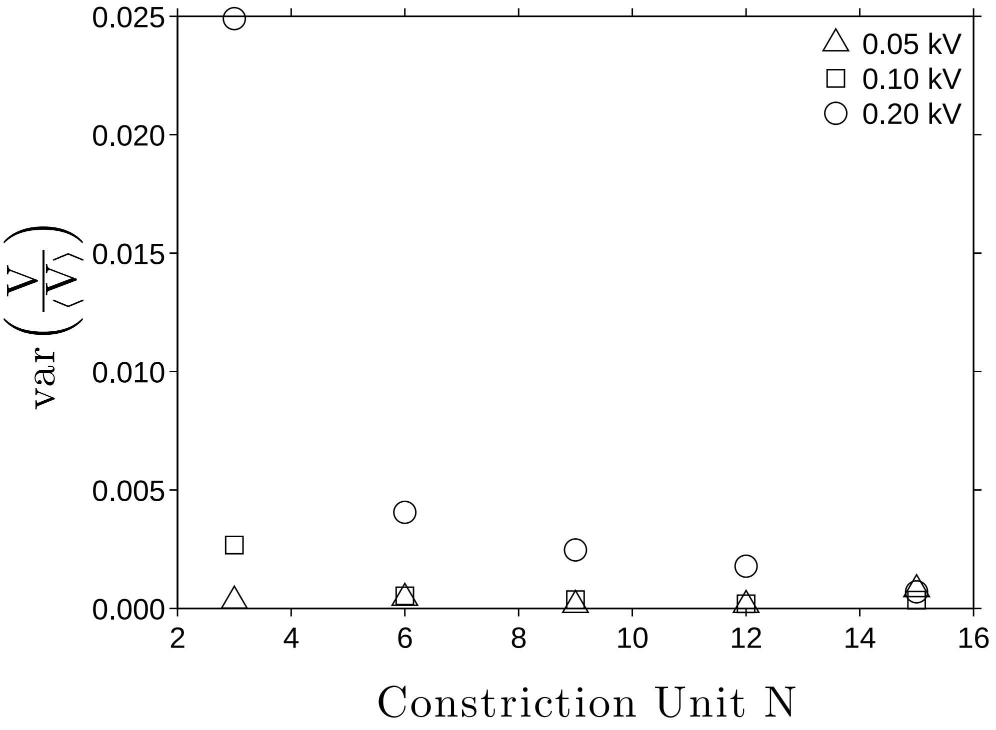

Figure 5.22: Fluctuation decay downstream. 128 ppm HMW polymer was driven downstream at different voltages and PMT signal collected in the middle of constriction units. It can be seen that the fluctuations rapidly decay as the fluid flows downstream, as expected due to instability and diffusion homogenizing the liquid. The PMT was focused in the middle of constriction. Due to difficulty in interpreting 1D "single-pixel" measurements space-time diagrams where created using video data of the flow (see the next chapter).

"Single pixel" data collection was time consuming, and results poor and/or difficult to interpret and compare with the literature. To allow mixing to be better measured the μTK was moved to another lab and an external laser was used and video data taken, allowing space-time diagrams to be created. The results of mixing is discussed in the next chapter.

5.13 Summary

Motivated by the exciting finding of elastic turbulence the possibility of such flows in electro-osmotically pumped polymeric fluids was investigated. It was found that:

- Viscoelastic elongational flow instabilities can be excited in polymeric solutions by steady electro-osmotic pumping; these instabilities occur at standard EOF velocities.
- At flows below the critical De number for elastic instability no instability is observed, while above the De number instability is seen, indicating an elastic mechanism for instability; polymer-free solutions show no instability, and lower molecular weight polymer have reduced fluctuations, again indicating an elastic mechanism.
- At semi-dilute concentrations through an y-branch geometry instabilities were observed; it appears shear thinning occurs as the Zimm relaxation time describes the experimentally observed instability. Drift occurred between input channels over longer runs, possibly due to Joule heating. It was also observed that both for polymer-doped and polymer-free solutions of (salty) TBE buffers bubbles would form at high voltages, a clear indication of Joule heating.
- Relaxation time scales with viscosity, while EOF velocity scales inversely with viscosity. For electro-osmotically pumped flows the viscosity therefore cancels out of the Weissenberg number and, as working with highly viscous solutions pose experimental difficulty due to filling and cleaning

issues, low velocities, long transient times, and significant Joule heating in high viscosity solutions, it is preferable to work with low viscosity solutions. This has the advantage of also being directly relevant to typical lab on a chip applications.

- For dilute polymeric solutions in water:methanol both external monitoring of temperature and current-voltage characteristics indicate that Joule heating is not a factor for the voltages applied.

- The flow appears chaotic in nature, however with the current experimental data true elastic turbulence cannot be established (in particular, velocity spectrum characterization must be done to determine if elastic turbulence proper occurs).

- Solid (cross-linked gel like), persistent, globules would form under some experimental conditions, with an electro/thermal mechanism indicated. These "micro-gels" may be of interest, with the electrodes forming the gels and the narrow channels acting as a size filter, allowing gels to be created and collected in the waste reservoir or be used within the microchannels themselves.

- Fluctuations first rose, then peaked and mildly dropped, as polymer concentration increased; the peak observed corresponds to the threshold in suspensions where significant hydrodynamic interaction effects occur.

- Near run out instabilities of a different character than viscoelastic instabilities were seen, even in polymer-free samples; these instabilities occurred when electrode/liquid contact was tenuous indicating that contact breaking lead to oscillatory forcing.

- PMT measured fluctuations decayed downstream, as expected for the approach to homogenization, however it was determined that space-time diagrams would constitute a better approach.

Chapter 6

Mixing in Low Reynolds Numbers

6.1 Motivation: spiking with polymers - a simple and efficient mixing scheme?

This chapter considers the use of polymers added to liquids to induce viscoelastic instabilities as a means of promoting mixing in microflow domains. Can one simply spike a sample with a low cost chemically inert polymer, excite viscoelastic instabilities, and achieve good mixing?

Shortly after elastic turbulence was established as a truly turbulent state [47] it was shown that efficient mixing[1] can be achieved [14] by including polymers in flows pushed though serpentine channels (see Fig. 6.1). This seminal work has framed and motived further research - instabilities can be easily achieved, and efficient mixing has been demonstrated. It appears that "polymers = mixing" is a good simplification, and as scaling is favorable as dimensions reduce the equation becomes "polymers = micromixing". Use of viscoelastic fluids to promote mixing has been demonstrated in microscaled Dean flows [21], where chaotic flow was established and where the earlier study of the macroscaled version of the serpentine flow geometry demonstrated true elastic turbulence [14], establishing that this is a viable scheme for promoting mixing in microdevices.

Viscoelastic flows are of practical interest for lab on a chip applications

---

[1] Efficient mixing is not well defined, as there is no standard reference, but essentially means "good, and much better than the base case".

as many biological materials of interest for biomedical testing, such as saliva [166] and blood [167], are viscoelastic in nature as are many other suspensions [109]. Several devices sort particles using laminar flow interactions [52], suggesting that viscoelastic induced instabilities can have potential undesirable effects in practice as more concentrated and complex fluids are investigated; it has already been noted that viscoelasticity in saliva testing negatively effects performance [166]. But, in addition to the detrimental effects of instabilities there is the suggestion, as noted above, that improved mixing may occur by intentionally spiking samples with polymers [14], thereby causing instability and subsequently improved mixing. As chemical reaction rate and completion depends on good mixing, and as many clinical, environmental, pharmaceutical, and other diagnostic applications require rapid and complete reactions, in particular in the presence of small concentrations of sample, efficient mixing is an important aspect in microdevice performance. The establishment of viscoelastic turbulence [47] and efficient mixing [14] along with favorable scaling properties of viscoelastic instabilities, which become easier to excite with reducing dimensions, suggests that the use of viscoelastic fluids may be a promising route to promote mixing in microfluidic devices.

In microfluidic devices the scales involved (typically O(100) μm) are such that diffusive processes are slow, yet inertial fluid instabilities are suppressed due to the small scales leading to small Reynolds numbers. This intermediate "slow scale" regime makes mixing a key issue in microfluidics [168] and various methods have been investigated in order to enhance mixing, including using bubbles [23], electrohydrodynamic instability [165], flow focusing [169], and bas-relief patterning [170]. These approaches generally rely on creating inhomogeneities to the working fluid or the microchannels. Viscoelastic fluids can exhibit flow instabilities [2], when polymer coils stretch and bend along stream lines which creates hoop-stress, allowing polymers to cross steam lines thereby disrupting laminar flow [171].

Several studies motivated by Groisman and Steinbergs' seminal work (see, for example, [21, 172, 121]) have found that viscoelastic instabilities can be excited in microdevices, however additional deformations of the flows - most

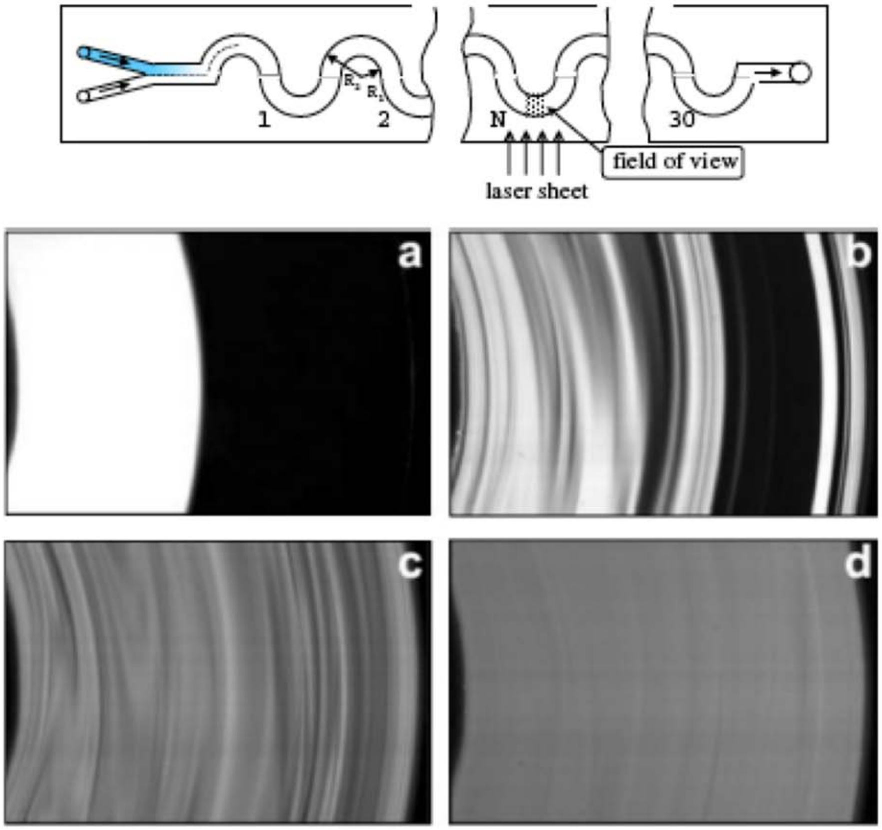

Figure 6.1: The device that originally demonstrated efficient mixing in the presence of polymer brings dyed (blue in upper panel) and undyed streams together to flow through a serpentine device with 2N half rings. For (a) pure solvent at N=29 no mixing is seen, while for polymer added at (b) N=8, (c) N=29 (compare to a), and (d) N=54 unstable flow and improved mixing is observed. Composite figure from Ref. [31]. Used with permission under a Creative Commons license.

notably shear - exists in prior work and highly viscous solvents are used, which is atypical for many lab on a chip applications. Efficient mixing - up to orders of magnitude more rapid versus the pure solvent [14] - clearly can be achieved, but it is relative to a highly viscous (orders of magnitude larger than water) solvent and in the presence of strong shear.

How is mixing affected by adding high molecular weight polymers to electro-osmotically pumped microflows? Adding low concentrations of polymer to fluids moderately increases viscosity (up to 2× the solvent viscosity) and dramatically increases elasticity, allowing microflows to undergo viscoelastic instability. Based on the relatively small increase in viscosity, the striking qualitative change in stability, and early experiments that demonstrate orders of magnitude improvement in mixing there is an expectation of dramatic increase in mixing by incorporation of polymers. By excluding shear, present in all mechanically pumped cavity flows, here it is found that contrary to such expectations absolute mixing is reduced by adding polymer to induce viscoelastic instability. These findings demonstrate that viscoelastic instabilities do not, in themselves, promote mixing and suggest that electro-osmotic flows are a good platform for studying behavior of viscoelastic instabilities and elastic turbulence.

To summarize: Here the use of electro-osmotic flow (EOF) in order to exclude shear and *solely* induce elongational viscoelastic instabilities by driving low viscosity fluids through sudden 2:1 constrictions in linear microchannels is investigated; further, mixing in unsteady viscoelastic flows is compared relative to mixing in polymer-free solutions in order to measure absolute change in mixing.

6.2 Isolating viscoelastic instabilities

Mechanically driven cavity flows[2] always have a significant shear component to the flow due to no-slip conditions; in contrast EOF has effective slip bound-

---

[2] Free surface mechanical pulling experiments also have limited shear, however due to rapid thinning these flows are short in duration making experimental investigation more difficult, but the availability of ultrahigh speed cameras are opening up these flows to study.

ary conditions and shear is confined to the Debye layer close to the channel boundary [52], further, for large polymers entropic repulsion from the walls reduces interactions of this shear regime with polymers [128]. This pumping scheme therefore excludes the shear component that is ubiquitous to mechanically pumped cavity flows, with the only shear component being due to flow focusing. In addition to deformations caused by shearing there are possible "Lagrangian chaos" effects [173], where flow fields result in chaotic trajectories which can lead to good mixing. By stacking identical constriction units equally spaced down a microchannel, symmetry is imposed as to reduce possible Lagrangian chaos effects [174]. **The device creates large instabilities, however a *reduction* in mixing over pure diffusion in simple liquids is observed, a direct experimental demonstration that viscoelastic instabilities alone do not lead to efficient mixing.**

6.3 Batchelor turbulence

Viscoelastic instabilities progress to elastic turbulence [47], a recently established turbulence that arises from elastic effects. The establishment of viscoelastic turbulence [47] and efficient mixing attributed to viscoelasticity [14] along with favorable scaling properties of viscoelastic instabilities, which become easier to excite with reducing dimensions, suggests that the use of viscoelastic fluids may be a promising route to promote mixing in microfluidic devices. Furthermore, it is well know that solution viscosity increases with polymer concentration and at the overlap concentration viscosity is only double that of the polymer-free solution [21]. In contrast to this relatively mild quantitative change in viscosity (and thus decrease in diffusion) elasticity effects have dramatic qualitative impact with polymer concentrations as low as ≈ 10 ppm leading to both large drag reduction in high Reynolds number hydrodynamic turbulent flows [175] and sizable instability and elastic turbulence in low Reynolds number flows [14].

The brief sketch is: adding polymers leads to large qualitative change in flows and large instabilities, these instabilities progress to (elastic) turbulence (and the transition to turbulence is "quicker" in elastic turbulence than in Newtonian turbulence [17]), only small decrease in diffusion mixing is expected, and huge - orders of magnitude - gains in mixing rate were observed in elastic turbulent flows [14].

However, the experimental finding of abatement of mixing found here is consistent with the understanding that strongly driven viscoelastic flows display Batchelor turbulence [176, 177]. For inertial hydrodynamic turbulence Batchelor turbulence exists below the dissipation scale. Above the dissipation scale eddies form at the integral scale set by the forcing on the fluid, and via a cascade process of eddy splitting (the "bucket brigade" moving energy to smaller scales) energy flows through a wide range of scales, eventually viscosity makes it difficult for an eddy to split and the dissipation scale (or Kolmogorov scale) occurs. Below the dissipation scale flows are smooth in terms of velocity gradients, are random in time, and energy is not efficiently coupled to smaller scales through the bucket brigade. Bachelor turbulence is thus a particularly "mild" form of turbulence. The velocity fluctuation power spectra has been experimentally found to scale faster than k^{-3} for shear flows [47] (see Fig. 6.2), where k is the wavenumber, and the steep falloff means most of the energy remains on the large scale - this contrasts with Kolmogorov's two-thirds law for inertia hydrodynamic velocity fluctuation spectra [178].

The k^{-3} scaling of the spectra found experimentally in shear flows is in agreement with theoretical derivations for 3D random flows [179], which are pure elongational flows [179, 177, 180]. This agreement, despite differing flows, arises from the primacy of elongational flows in stretching polymers which is required for instabilities and the fact that shear flows consist of rotation and elongational components (see Fig. 2.8). Note that the presence of the rotational component will lead to tumbling of polymers [131], which will somewhat suppress stretching, but otherwise the elongational mechanism underlying polymer stretching is present in shear flows. In the experimentally measured spectra there appears to be no fingerprint of shear (see Fig. 6.2. Inspection of the polymer free control (laminar flow [31]) demonstrates a "flat-line" spectra, as expected for smooth flow, and which demonstrates that shear has no gross effects on spectra. For unstable flows one again expects no contribution to the spectra from the mean shear, as only fluctuations are captured in the spectra. As both the spectra theoretically determined for elongational flow and the experimentally measured spectra for shear flows follow the same scaling behavior the underlying flow does not strongly affect the fluctuations, although there may be subtle effects in the low frequency roll-off from power-law scaling.

In Batchelor turbulence as the velocity power spectra rapidly decays the instability scale is on the order of device dimensions[3], and the flow acts like a spatially smooth flow that is random in time [177]. As such the extremal state of elastic turbulence that bounds the behaviour of viscoelastic instabilities is a particularly smooth instability regime relative to high Reynolds number turbulence, so while the transition from smooth flow to incoherent and fully developed instability is thought to occur more easily in viscoelastic solutions than for Newtonian fluids [17] the dynamics are more mild.

To create efficient mixing a bridge is needed between the relatively large scale viscoelastic instabilities and the smallest scales over which homogeneity is required; diffusion, Lagrangian chaos, or deformations such as shear can bridge these scales. In the “knead and fold” metaphor of mixing[4] [181] viscoelastic instabilities can provide the fold operation that creates large deformations of material to create striations of dis-similiar material, however additional deformations are needed to thin striations allowing diffusion to finally homogenize the fluids. In the seminal work of Groisman and Steinberg that established efficient mixing for viscoelastic fluids the viscoelastic folding is enabled by the curvilinear bends and the kneading operation is provided by the shear that stretches material as it flows down the serpentine channels [14]; the visually arresting images that work reveals of thin intricate striations, i.e. good mixing, are a result of *both* viscoelastistic instability (repeatedly applied, > 20 times) *and* persistent shear forces.

---

[3] More precisely, the scale of instabilities in Batchelor turbulence is the integral scale set by the velocity gradient scale, which in turn is set of device dimensions.

[4] As inspired by bread making.

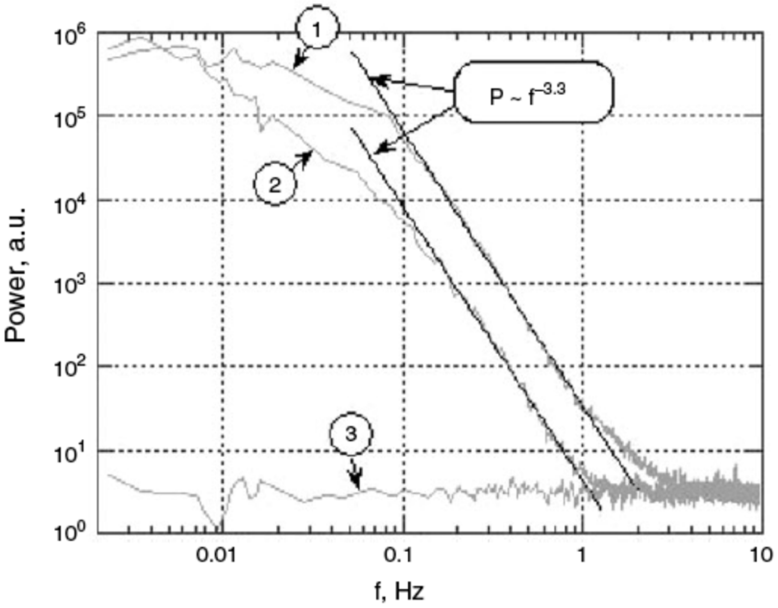

Figure 6.2: Power of velocity fluctuations for viscoelastic turbulent serpentine flow. Velocity was measured in the middle of the channel (N=12) and the spectra found; Curve 1 and 2 are of velocity fluctuations along and transverse to the main flow direction, while curve 3 is the polymer-free solvent. A rapid fall of the power was found, which dictates that fluctuations will be dominated by the integral scale (device size). Figure from Ref. [31]. Used with permission under a Creative Commons license.

6.4 What is mixing?

Mixing is intuitive, but difficult to formally capture. Following Danckwerts [182] who introduced the quantitative measurement of mixing there are two key aspects to mixing: the *scale* and the *intensity* of segregation, which correspond to convective fluid and diffusive mechanisms. Fluid instabilities stretch and deform fluids on a bulk level and result in structures with a scale determined by deformation history, while diffusion acts to reduce the intensity differential of, say, dye between nearby fluid elements. Due to wanting to know the global state of mixing in a system that has dynamics that is locally defined mixing measures are statistical in nature, with the fluid properties sampled in space/time and averaged. In practice mixing is almost always quantified by the intensity of segregation, which will more rapidly converge to a "well mixed" state if the characteristic scale is small[5] and so this measure will also implicitly contain information on scale effects. The intensity of segregation is given (originally) by

$$I = \frac{\sigma_c}{\bar{c}(1-\bar{c})}; \tag{6.1}$$

where σ_c is the standard deviation of some material concentration and $\bar{c}$ is the mean value of concentration. This measure has a value of 1 when segregation is complete, and 0 when the concentration is uniform. This basic measure has been modified in various ways but the general form (normalized variation) is used. There are different specific approaches to quantifying mixing, here I use the first moment mixing index as it is simple and does not require many assumptions:

$$M1 = \frac{\langle |c-\bar{c}| \rangle}{\bar{c}}; \tag{6.2}$$

where c is the local concentration and $\bar{c}$ is the average concentration. The value of the first moment ranges from 0 (perfect mixing) to 1 (no mixing), and can be considered a mixing efficiency η_{mix} = M1 (or, η_{mix} = 1-M1, if one

---

[5] i.e. the fluid is kneaded and folded such that *thin* tendrils of an initial "clump" of fluid is dispersed through the volume of interest

wants 1 to signify perfect mixing). The first moment mixing index is 0 for an uniform concentration profile (which describes a diffusion mixed fluid when $t >> t_{diffusion}$), 1 for a step function concentration profile (as describes two adjacent fluid streams, one dyed and one undyed), and 0.5 for a random profile (an approximate model for a well folded flow with no diffusive mixing).

6.5 The Linked Twist Map and mixing

The Linked Twist Map (LTM) is a simple model of mixing processes where fluids are alternatively subjected to 2 or more velocity fields ("blinking flow" conditions)[6], it is found that such flows can lead to Lagrangian chaos (versus the Eulerian chaos found in unsteady in time high Re turbulent fluid flows) and rapid mixing.

The basic idea behind the LTM is that nearby fluid particles must be able to diverge and separate in order for mixing to occur, which necessitates a sensitivity to initial conditions. Ideally each and every fluid element of sub-volume v should uniformly distribute into the rest of the fluid volume $\bar{v}$ [182].

As studies of mixing has matured it is becoming increasingly accepted that having two "perpendicular" flow distortions is a good strategy for mixing; see for example the now classic herringbone micromixer [183], where staggered chevron bas-relief structures manipulate fluid, and the "bend and expand" micromixer [184] that uses intermediate Reynolds number flows (inertial effects) to create rotational and jet expansion effects to mix fluids. In general, the linked twist map concept of two (plus) flow distortions and various symmetry breaking schemes are now used to inspire design efforts [168]. When turbulent ("Eularian chaos") flows are not achievable the LTM idea provides a good mental heuristic for starting design in "Lagrangian chaos" mixers, however numerical and experimental efforts are required due to sensitivity in mixing with small variations in geometry [32] (see Fig. 6.3 for an example where mixing is

---

[6] The idea of the LTM is conceptually and operationally similar to the idea behind Brownian dynamics simulations, where flow trajectories are imposed, followed by a diffusion step; this "two velocity field" (deterministic and random) stepping is repeated; likewise, *any* two (or more) fields can be repetitively applied.

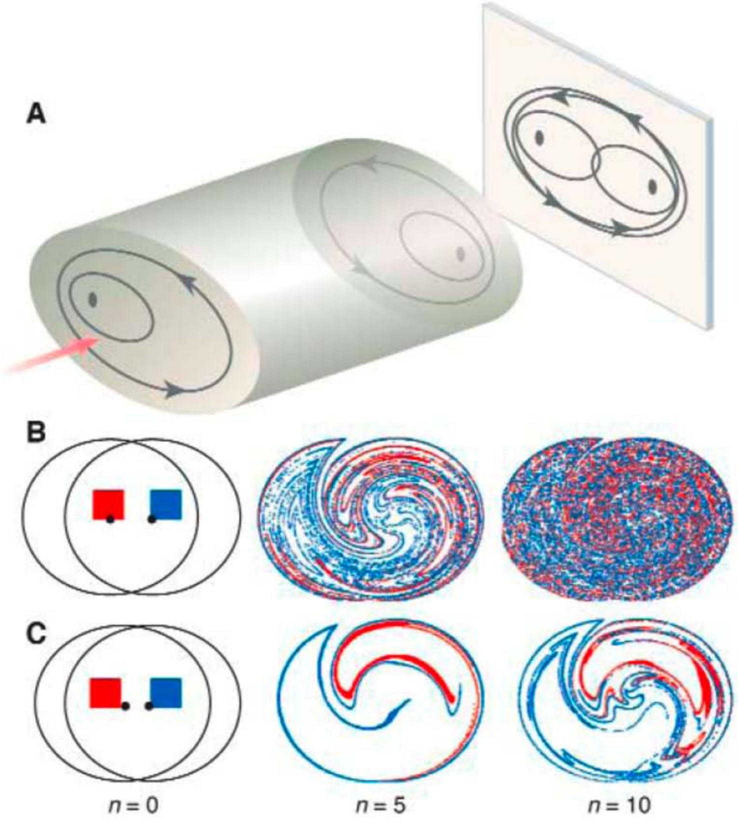

Figure 6.3: The Linked Twist Map. Crossing fluid flow lines is required for mixing, which can be achieved by diffusion or instabilities. *Blinking flows* are an alternative means of crossing flow lines where a fluid is subjected to different driving velocity fields in alternation, allowing initially nearby fluid particles to become well separated. The Linked Twist Map is a mathematical description of such flows, and is one of the few mathematically tractable approaches to mixing. Here fluid is subjected to two different velocity fields, and as can be seen in (b) and (c) mixing can be sensitive to the relative difference between the velocity fields, with 10 iterations leading to dramatically better mixing from a seemingly small difference in flow profiles. Figure from Ref. [32]. Reprinted with permission from AAAS.

sensitive to precise details of the device).

The evolving science of mixing will force a more precise language in describing low Reynolds numbers flows; with Stokes flows, laminar flows, low Reynolds numbers, steady flow, low inertia, and creeping flows being used essentially interchangeably in the past (and now). The establishment of elastic turbulence complicates the picture, with highly unstable and turbulent, but inertia “free”, flows possible, as does low inertia but chaotic flow such as in the herringbone mixer. Creeping laminar flows is a good descriptor of smooth, nonchaotic, laminar flow, as it brings to mind a slow, steady, persistent flow, however it remains to be seen which term dominates to describe these flows as low Reynolds flows in various manifestations are investigated[7]. Further complicating the issue is the field of intermediate Reynolds number microdevices were inertial effects are used well below the turbulence threshold and particle-fluid as well as particle-particle interactions are used, the nonlinear and unstable aspect of inertia can be ignored yet clearly inertia plays an important role [185].

6.6 Mixing in microflows

Instabilities are suppressed in microflows and creeping laminar flows are the norm. This results in diffusion limited mixing for most devices, which in turn limits the speed fluids can flow at in order to achieve a certain amount of mixing at a given location downstream. Mixing is a key issue in microfluidics [168] and various methods have been investigated in order to enhance mixing, including using bubbles [23], electrohydrodynamic instability [165], flow focusing [169], and zeta-potential patterning [170]. These approaches generally rely on creating inhomogeneities to the working fluid or the microchannels.

---

[7] Stokes flow is a likely candidate, although it is normally motivated as low inertia versus viscosity which, strictly speaking, allows for time varying (due to elasticity or other effects) flows.

6.7 Creeping laminar diffusion

Idealized diffusion from an initially sharp interface has an erf function like profile [186] given by

$$c = c_0(1 - erf(\frac{y}{2\sqrt{Dt}})); \tag{6.3}$$

where y=0 at the interface, D is the diffusion coefficient, and t is the contact time (t=x/V, for a flow of velocity V and making contact at x=0). This erf-like profile is used to theoretically describe diffusion between two initially unmixed coflowing creeping laminar streams.

The diffusion coefficient can be calculated using the Einstein equation

$$D = \frac{kT}{6\pi\eta r}; \tag{6.4}$$

where kT is the thermal energy (with k=$1.38x10^{-23}$ J/K, T=295K for typical room temperature), η is the viscosity of the liquid, and r is the hydrodynamic radius of the diffusing particle. For TAMRA dye $r = \frac{1.6}{2}$ nm [187] which gives D $\approx$ 270 μm^2/s; TAMRA is a small and fast diffusing particle.

To calculate mixing from experimental dye dispersions either real space or space-time images can be used. Using the space-time diagram reduces impact of possible artifacts, such as imperfections in the chip or illumination field, by selecting a small spacial region, and improves the estimate by taking numerous snapshots into account.

To estimate theoretical M1 values equation 6.2 is used assuming an ideal erf profile, equation 6.3, as plotted in Fig. 6.4. Mixing evolves approximately exponentially downstream[8], and the mixing length measured in constriction units is $\approx$ 5.7. Doubling the viscosity of the solution, which will occur at the overlap concentration (and thus captures the expected change in viscosity), will half the diffusion coefficient (see equation 6.4): this change shifts the calculated M1 values up (decreases mixing) and only slightly changes slope (the mixing length changes to 5.6). To first order increases in viscosity will simply shift M1 by a constant.

---

[8] The linear norm of residuals is $<$ 0.01.

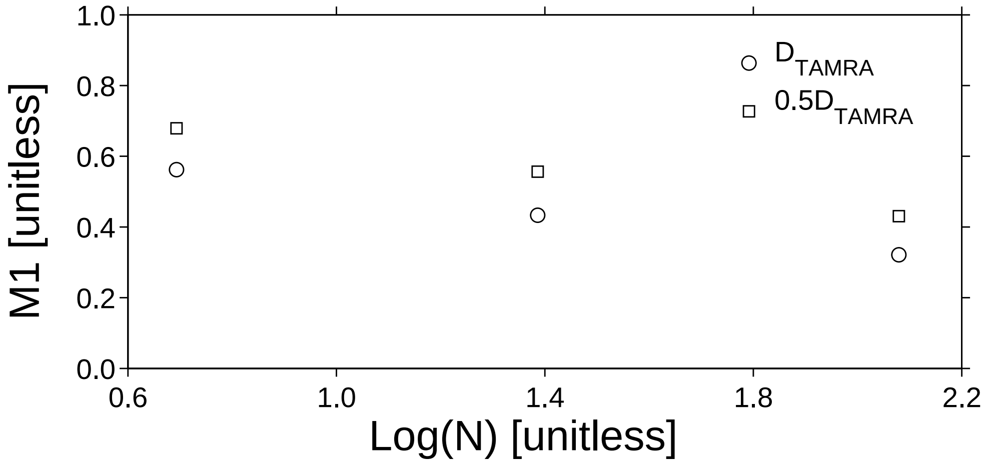

Figure 6.4: Effect of doubling solution viscosity on co-stream laminar mixing, as measured by M1 at constriction N=2, 4, 8. Idealized diffusion from an initially sharp interface has an erf-like profile allowing modeling of the flow through the corrugated channels. Mixing is seen to approximately follow exponential change, with an absolute shift up as viscosity increases (and diffusion thereby decreases). Here doubling the viscosity, which captures the change expected for adding polymer up to the overlap concentration, shifts M1 up by roughly 20% while it does not significantly effect the slope (N_{mix} changes from 5.7 to 5.6). To a first approximation it is therefore expected that increase in viscosity results in a constant shift up in the M1 curve.

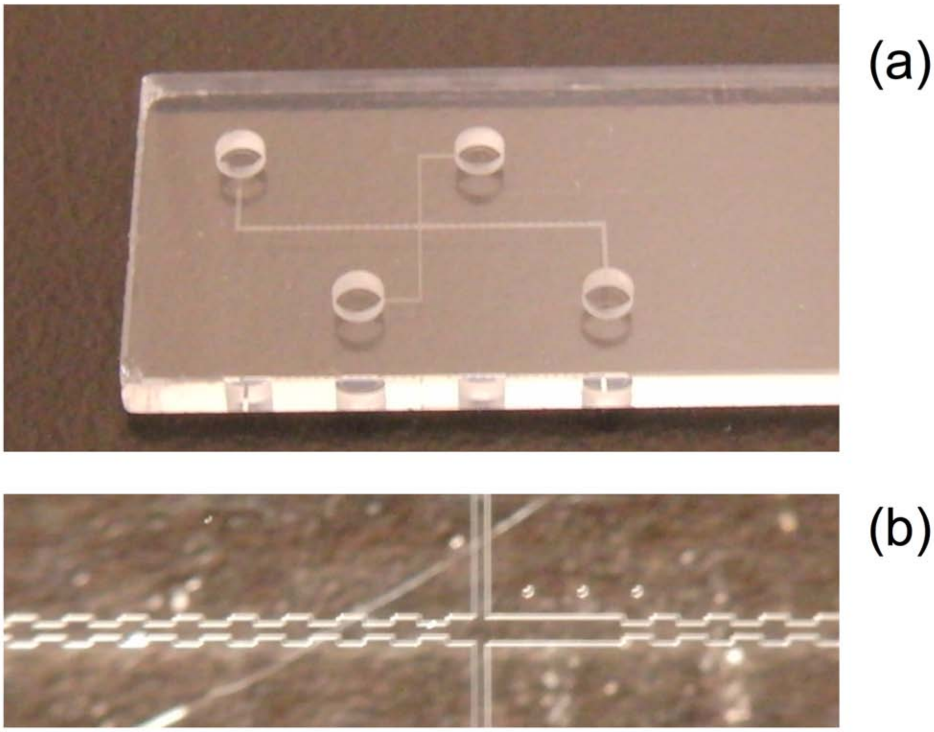

Figure 6.5: (a) Photograph of the microfluidic device, and (b) detail of the microchannels with mixing units. Fluids are electro-osmotically driven from the top and bottom wells to the left side well. Fluid in the top well contains fluorescent dye, and mixing is optically observed by exciting dye with an external 532 nm laser and collecting video data. Each 100:200 μm constriction/expansion unit creates extensional flow which induces instabilities in viscoelastic fluids with high enough Deborah number. Due to the slip conditions of electro-osmotic flow and symmetry non-viscoelastic instability mixing mechanisms are minimized. It is found that flow rates are not affected by the presence of polymer in the dilute regime and all flows are drivent with a voltage of 200 V, resulting in equal flow rates and comparable flows.

6.8 Determining mixing in flows: space-time images

Microphotographs were taken with a Casio Exilim EX-F1 camera in video mode (30 fps), by attaching the camera to the μTK via a custom machined attachment and a Scoptronix Maxview Plus optical adaptor (camera-microscope attachment). From video data space-time (xt) diagrams are created by taking a vertical cut from each video frame across the channel, horizontally centered in the constriction or expansion. Due to chemical etching side walls are scalloped, and the 20 μm nearest the channel edges are removed before analysis. Runs are nominally 100 s in duration, but the initial transient flow is excluded to prevent start up effects from influencing results.

The camera is not scientific grade and comparison of CCD intensity with true (incident) laser power reveals nonlinear characteristics; cubing the CCD values results in a linear response profile (see Fig. 6.6) allowing the optical intensity as measured to be scaled and related to the dye concentration. From video data space-time (xt) diagrams are created by taking a vertical cut from each video frame across the channel, horizontally centered in the constriction or expansion (see Fig. 6.8 and 6.9).

Polymer solutions were made by adding high molecular weight (18×10^6 Da) polyacrylamide from Polysciences Inc. to a 20:80 vol.% methanol:water mixture; again, methanol is used here to prevent aging during storage [142]. The overlap concentration c_* is ≈ 300 ppm, and to simplify the system concentrations are in the dilute regime ($c < c_*$).

In “normal” microfluidics smooth laminar flows are observed, as seen in Fig. 6.7 for the polymer-free solutions. As the fluid flows downstream the dye diffuses across the channel and eventually results in homogenously mixed fluid. We observe mixing values for polymer-free flows scale approximately exponentially as a function of distance downstream, Fig. 6.12; while perfect exponential scaling is not expected calculating M1 using the theoretical erf-profile expected [186] for laminar mixing in uniform channels results in an approximate expo-

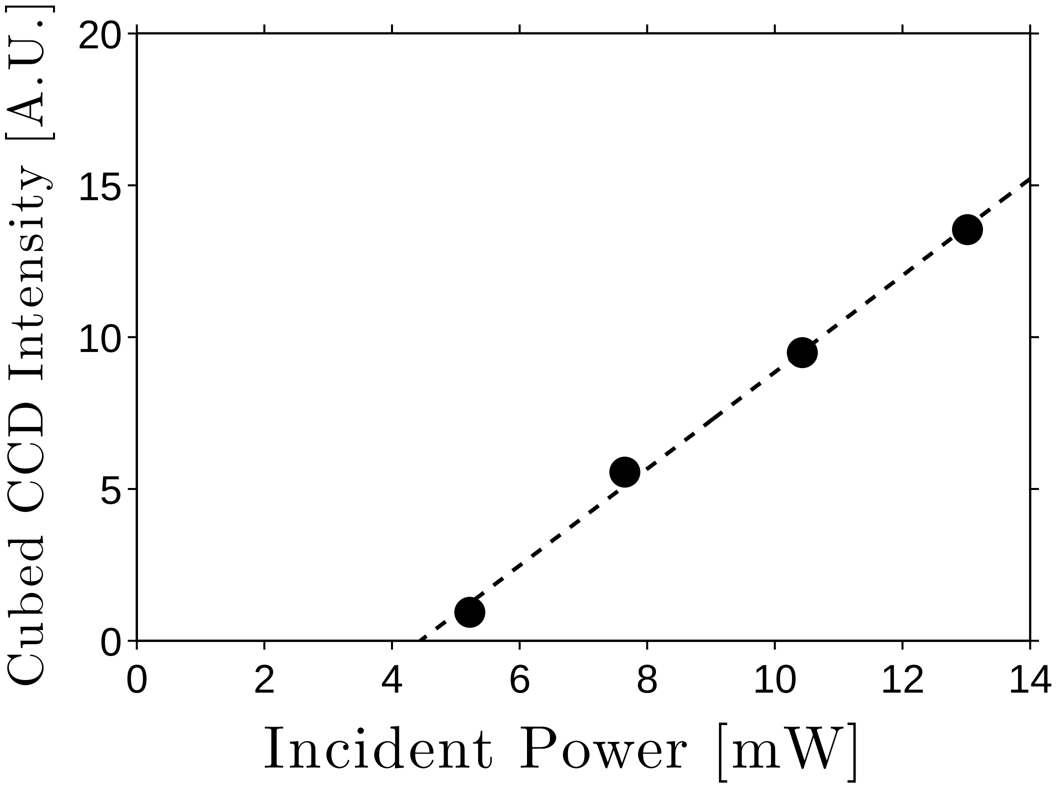

Figure 6.6: Raw CCD intensity values were nonlinear. Flowing pure dye through the microchannels and taking photomicrographs with a Casio Exilim EX-F1 camera revealed the CCD images were nonlinear versus the incident power emitted by an external 532 nm laser. Cubing the CCD intensity results in linear response with respect to incident power.

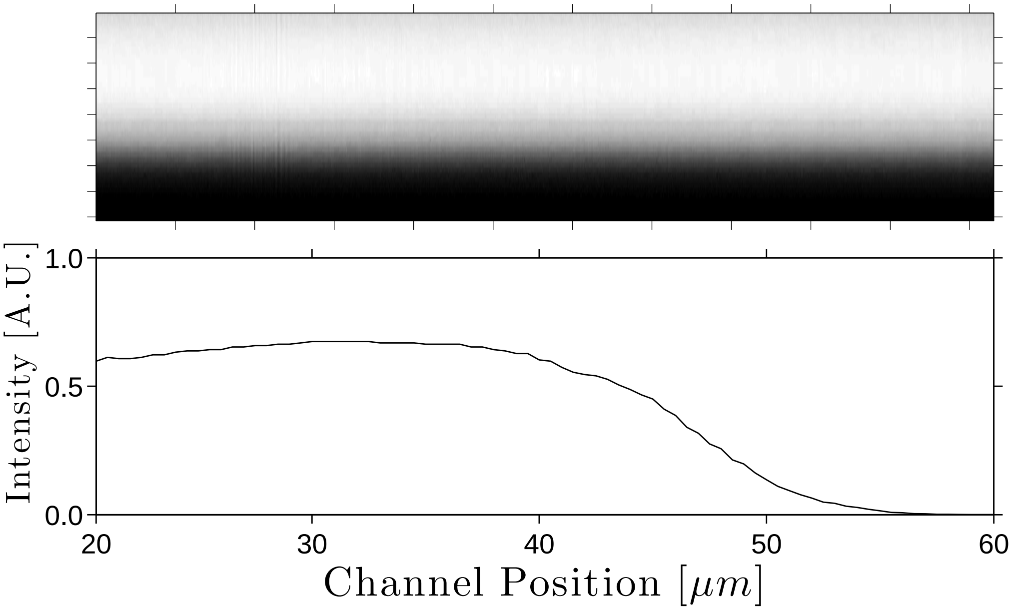

Figure 6.7: Laminar flow in the first constriction. With no polymer added creeping laminar flow with steady diffusion is observed. The top panel is a space time diagram constructed by taking a cross channel intensity profile across the middle of the constriction from each frame from video data, and is 60 μm by 75 s (see Fig. 6.8 and Fig. 6.9 for where the space-time diagram "slices" are taken). The bottom panel shows one of the cross channel intensity profiles (0.6 s from the start of the xt diagram). Note that 20 μm are trimmed from the edges (where wet etch rounding may lead to aberrations) of all xt-diagrams. An erf-like profile is observed, as expected in steady coflowing two-stream mixing.

nential drop off[9]. Error in experimental M1 values is estimated at roughly 5% of the calculated values.

Addition of polymer results in large instabilities, as can be seen in Fig. 6.8 and Fig. 6.9. The fluctuations move material transverse to the flow direction, spanning almost the entire channel. There is no dominant frequency in the flow, indicating chaotic flow [21], and the overall pattern displayed are striations with "comb-like" teeth randomly spaced which is consistent with elastic turbulences' random in time instability characteristics. Increasing the concentration from 32 to 64 ppm results in larger fluctuations and tooth spacing. As the solutions move downstream through additional elongation regions additional striations are added, as seen in Fig. 6.11, however the general pattern persists with diffusion appearing to be the dominant mixing mechanism.

Note that in contrast to high Re turbulent flows an enhanced diffusion rate, indicative of broad-band excitation of instability scales, is not observed [188] which supports the limited bandwidth visual evidence (see Fig. 6.8) that large scale instabilities dominate the instability spectrum. The lack of enhanced diffusion confirms that small scale instabilities below the camera resolution are not excited to a significant extent.

Absolute mixing is hindered by reduced diffusion, and increased by instability induced deformation of the liquid. There is therefore a tradeoff involved in adding polymer to the solution, which will allow viscoelastic instabilities yet reduces diffusion mixing. By measuring mixing (M1) in the second expansion it is found that mixing is reduced as concentration is increased (see Fig. 6.13), demonstrating that the advantage of instabilities is not dominant for mixing the dye here. However, as TAMRA dye is a small molecule (≈ 1.6 nm hydrodynamic diameter [187]) these mixing experiments are a stringent - but realistic - test. Further, as the edges of the xt-diagrams are trimmed to reduce image processing artifacts there is a possibility of artificially increased first moment mixing index M1 calculated for unstable flows, as material with

---

[9] The linear norm of residuals is < 0.01 over the range of mixing units tested, for fits to both calculated estimates and measured values, indicating exponential scaling is a close approximation of mixing behavior here.

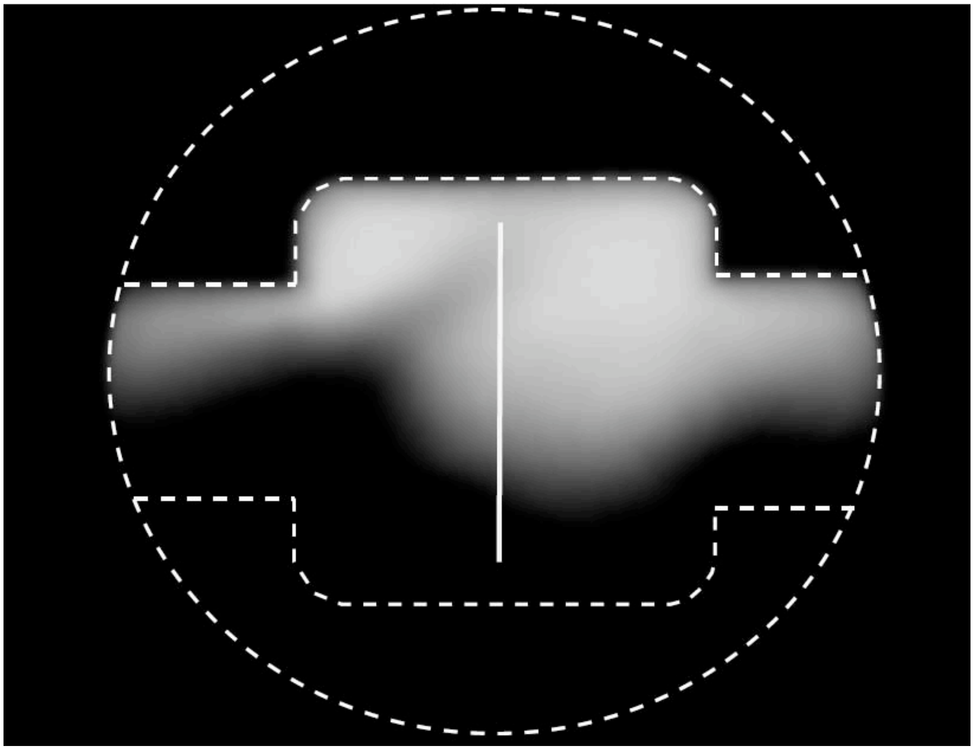

Figure 6.8: Photomicrograph of unstable flow in the second expansion for a concentration of 64 ppm high molecular weight (18×10^6 Da) polyacrylamide polymer added. It is apparent that large instabilities are excited that display a dominant scale set by the microchannel. Dashed outlines indicate field of view and microchannel outline; the solid line indicates where the space-time diagram slice was taken for the expansion regions. The instabilities in the constriction regions can also be seen here at the sides of the image; regions are centered for data collecting. See also Fig. 5.12 and Fig. 6.9.

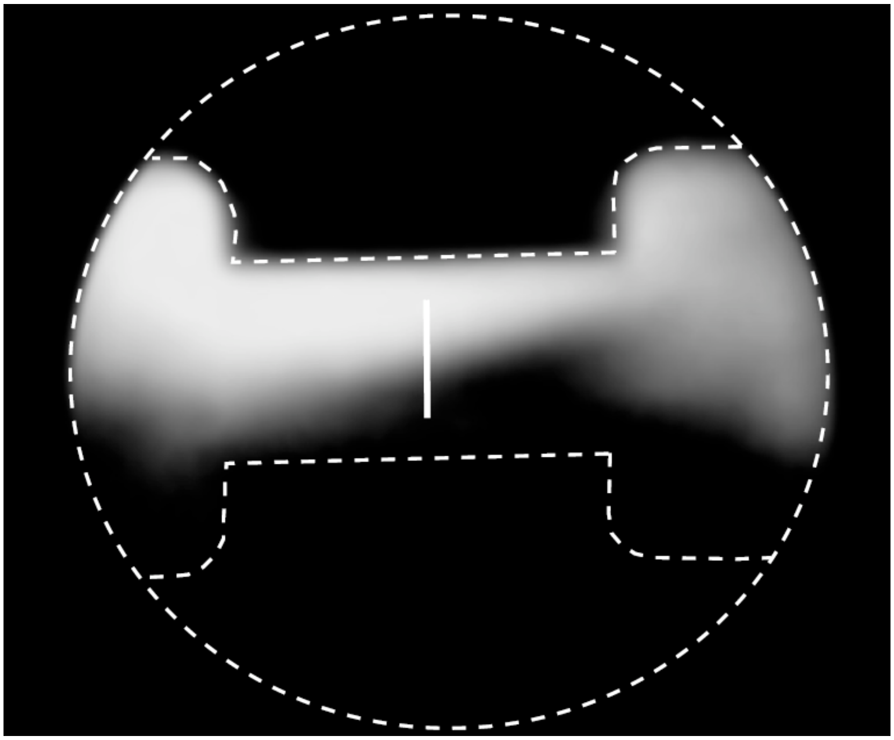

Figure 6.9: Photomicrograph of unstable flow in the second constriction for a concentration of 64 ppm high molecular weight (18×10^6 Da) polyacrylamide polymer added. Dashed outlines indicate field of view and microchannel outline; the solid line indicates where the space-time diagram slice was taken for the constriction regions.

high/low dye concentration can be injected from these regions increasing the variance seen. Looking at the change in mixing as a function of mixing unit as the fluid flows downstream will allow the role of instabilities to be better understood[10].

Finding the first moment mixing index, M1, for concentrations of 0 ppm, 32 ppm, and 64 ppm as the fluid moves downstream reveals that absolute mixing is reduced in viscoelastic solutions relative to the polymer-free sample. An increase in the rate of change in mixing downstream is observed for viscoelastic solutions. By looking at the flow at different constriction units (N=2, 4, 8) the mixing length is calculated and a mild decrease with raising polymer concentration is observed, with the mixing length reducing from 4.5 for 0 ppm to 4.2 for 32 ppm and finally 3.2 for 64 ppm. This mild decrease in mixing length can be attributed to the action of instabilities, as the simple (sharp interface) diffusion model does not result in a change in mixing length - conceptually the distortion of the interface due to instability will lead to both larger interfacial surface for diffusion in a given fluid volume and shorter required diffusion distances.

The calculated M1 values for polymer-free solutions, which assumes uniform channels, are roughly twice as large as observed for polymer-free solutions in the channels corrugated with constrictions/expansions. This enhanced mixing has been previously observed for electro-osmotic flows through constrictions/expansion units where $\approx$ 2X enhancement was found [189]. This enhancement is an open problem currently being investigated [190], but is thought to be due to the modulation of width enhancing diffusion [190] due to convective cross flow movement (e.g. periodic movement perpendicular to the main flow direction)[11].

---

[10] As discussed above, to first approximation a change in diffusion (viscosity) will result in an absolute change and a up/down shift in the mixing value; a change in slope with mixing unit will be associated with the instabilities.

[11] Naively considering the sheaves of flow lines suggests that the total distance an average particle travels as it moves downstream in a corrugated channel will be larger than the minimum distance (e.g. channel length); fluid off center will effectively “see” a longer channel and thus experience more diffusion, and one should expect enhanced overall diffusion in a given length.

In general the progression of flow from stable through unstable and chaotically unstable flows and finally to turbulent flow is thought to describe both simple and viscoelastic fluids [17]. Based on the similarity of progression, mixing might be expected to significantly improve with each step along the progression, as this is the case for simple (Newtonian) fluids. However, for chaotically unstable and (elastic) turbulent flows of viscoelastic fluids the enhancement of mixing may not be as large or easily obtained as expected from the analogy with high Re flows. While large enhancement over diffusive mixing has been found and noted in the literature this has been for *highly viscous* solutions, which are atypical of most lab on a chip applications, in the presence of strong shear components to the flow - which is absent in EOF. One of the motivations of using high viscosity solvents in studies of viscoelastic fluids is to *intentionally limit diffusion*, preventing the decay of contrast when dye is used as a marker and allowing study of instabilities and mixing effects. Further, viscoelastic fluids driven well above the viscoelastic instability threshold display elastic turbulence which has been shown to be a realization of Batchelor turbulence. One of the key characteristics of Batchelor turbulence is that instabilities are dominated by the large scale fluctuations, which are set by the system size, and therefore there will remain a mismatch between the smallest scale one wants homogeneity on and the instability which is intended to drive mixing; unlike high Re turbulence Batchelor turbulence does not excite smaller scales as readily.

Note that Lam *et al.* [191] create instabilities by driving viscoelastic fluids through abrupt 8:1 constrictions using a syringe pump, and therefore have a mechanically driven device similar to the device studied here. They observe enhancement of mixing in their liquids over deionized water at equal flow rates, demonstrating that *absolute* mixing improvements can be obtained over low viscosity Newtonian liquids (albeit for intermediate Reynolds numbers, Re $\approx$ 20). However, they use dis-similiar fluids of different viscosity, shear thinning, and elastic properties making interpreting their results difficult as flow focusing, shear thinning, and viscous thread folding [192] or other coflowing effects are physical mechanisms that all may play important roles in addition

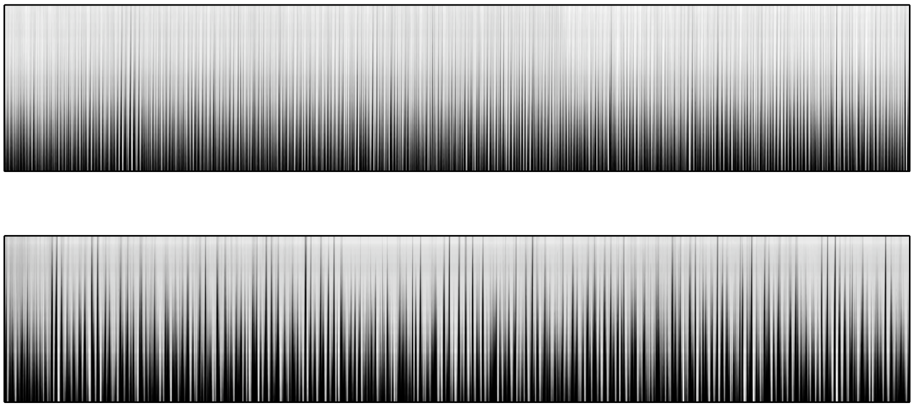

Figure 6.10: Space time diagrams of unstable flow in second constriction. Adding 32 ppm (top panel) and 64 ppm (bottom panel) results in instabilities as fluid flows through the constriction/expansion units. Visual comparison indicates that instabilities have higher average frequency for lower concentration, and that instabilities move material across the channel more with more polymer concentration. These effects are likely due to the competition between viscosity and elasticity - more polymer increases the viscosity as well as increases the number of “dispersed mixers” (polymer coils). The diagrams are 60 μm by 80 s.

to viscoelastic instabilities in promoting the mixing they observe. In particular Lam *et al.* may be observing the Kaye effect, a novelty flow disturbance where highly shear thinning liquids poured into a heap “spurts” out in a unpredictable manner, inadvertently putting it to effective use in mixing [193].

Studies of chaotic fluid mixing have found that persistent spacial patterns with slow contrast decay (due to diffusion) are associated with chaotic, versus high Re turbulent, periodic flows [174]. In the study a 2D fluid was periodically oscillated, and the recurrent spacial structure had additional striations created at each cycle. Here oscillatory flow is not imposed, however the symmetry and stacking of identical elements will create a similar environment with constriction/expansion flow fields alternating with time as the fluid flows through the structured microchannel (see Fig. 6.11, where “comb”-like xt-diagram evolves with additional fine structure, and diffusive relaxation of contrast).

It was observed that viscoelastic instabilities did not lead to rapid mixing, in contrast to earlier studies [14, 21, 121] that found up to orders of

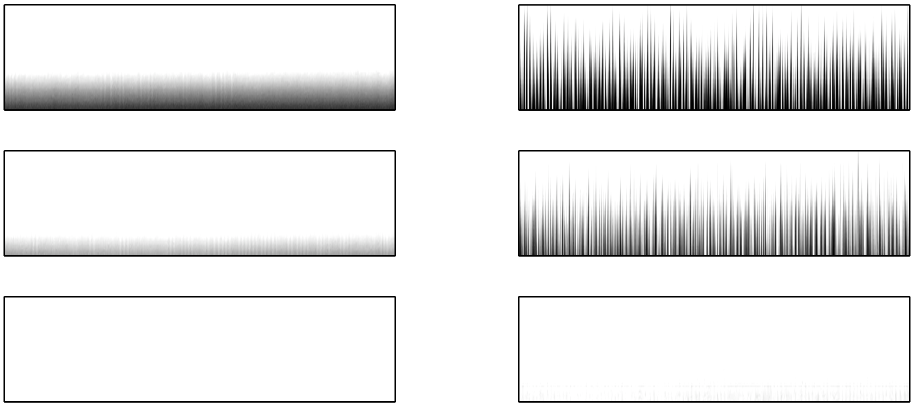

Figure 6.11: Mixing evolution. From the top to the bottom fluids pass from the 2^{nd} to the 4^{th} to the 8^{th} constriction. With no polymer (left panels) diffusion mixes the fluids, while with 64 ppm PAA added (right panels) both diffusion and instabilities lead to mixing.). The effects of diffusion are apparent, in both polymer-free and polymer-added flows, with a reduction of contrast between the 2^{nd} and the 4^{th} constriction, and finally to a visually homogeneous mixture by the 8^{th} constriction. In addition it can be seen that strong cross channel fluctuations exist in the presence of polymer, but the pattern is highly similar and a comb-like pattern persists between the 2^{nd} and the 4^{th} constriction, with addition of "teeth" but without significant pattern changing deformation. This persistence is characteristic of chaotic flows undergoing symmetric oscillatory forcing and diffusion is the dominant mechanism leading to homogeneity (mixing). The lack of enhanced diffusion for viscoelastic unstabe flows indicates that small scale instabilities are not excited. The diagrams are 60 μm by 60 s and have not been scaled, allowing comparison.

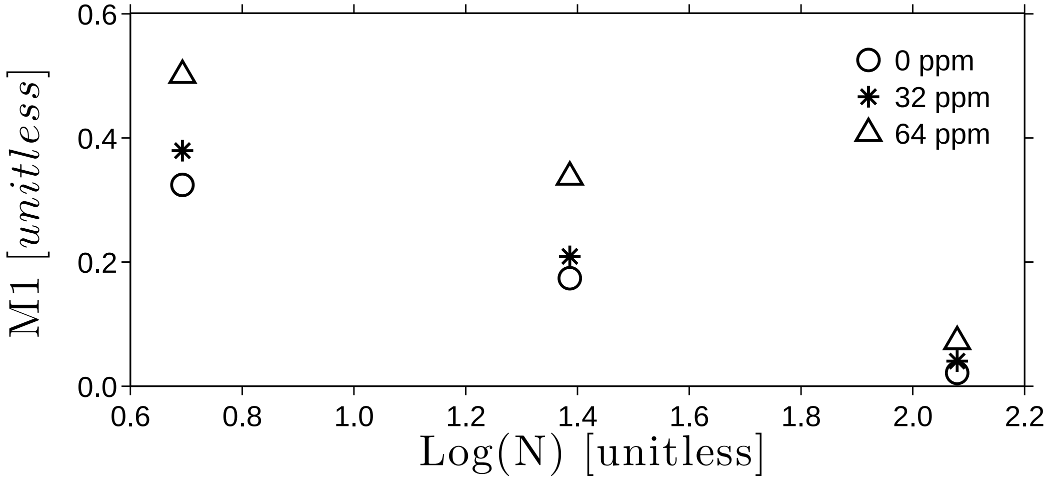

Figure 6.12: Mixing as a function of constriction unit, as measured by the first moment mixing index M1 (M1 → 0 for perfect mixing and M1 → 1 for no mixing). Using space time diagrams mixing was measured downstream of the initial junction at N=2, 4, 8. The mixing index scales exponentially, and the mixing lengths mildly reduce with concentration (4.5 for 0 ppm, 4.2 for 32 ppm, and 3.2 for 64 ppm). The vertical shift for polymer doped fluids relative to undoped fluid is due to reduced diffusion limiting the mixing, as increased polymer concentration reduces the diffusion constant by increasing viscosity. Error in M1 values is estimated to be ≈ 5%.

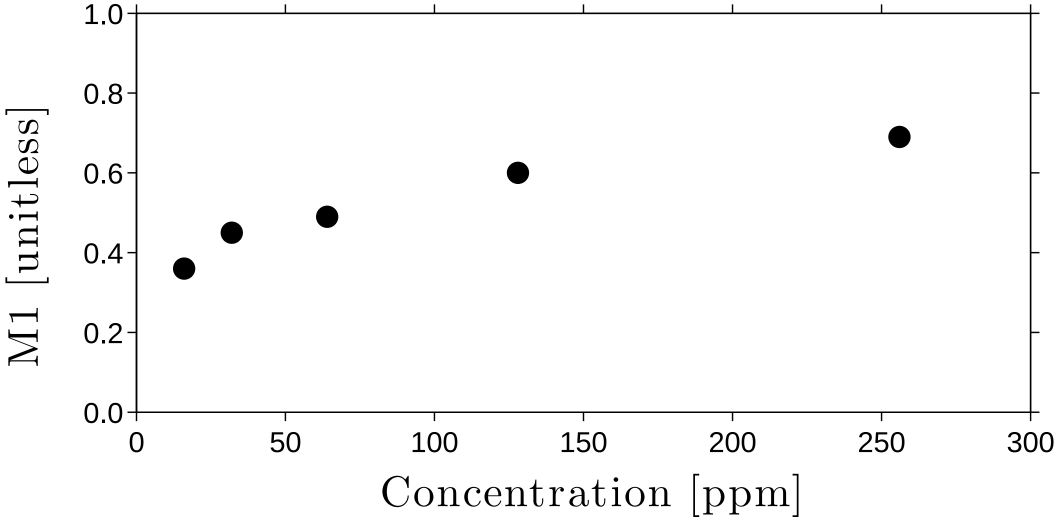

Figure 6.13: Mixing as a function of concentration in the 2^{nd} expansion unit, as measured by the first moment mixing index M1. Using space time diagrams mixing is measured for c = 16, 32, 64, 128, and 256 ppm (the overlap concentration is $c_* \approx 300$). The mixing index slowly raises with concentration in the dilute regime; this indicates that while instabilities are promoted by the presence of polymers *absolute* mixing is reduced (as diffusion is hindered by the presence of polymers).

magnitude improvement in mixing for mechanically driven flows. However, significant shear stretching is present in most prior work due to no-slip conditions. In a study of electrokinetic driven 2D sheet flow [194], which like the flows here also excludes no-slip induced shear, viscoelasticity was found to mildly suppress mixing for flows below the instability threshold, a finding that is consistent with other studies that find either mild increase [195] or decrease [196] in this regime where polymers are only weakly distorted. The results of Ref. [194] are also suggestive that mixing remains mildly suppressed, rather than enhanced, in viscoelastic liquids above the instability threshold, as it is shown that stretching fields are reduced in these flows and by comparing a low stretching Newtonian fluid with a high stretching shear thinning and viscoelastic fluid stretching trends are shown to be likely correlated with mixing trends. The mixing performance of low stretching Newtonian versus low stretching, yet unstable, viscoelastic flows, was not presented; this control would provide stronger support for correlation - while the hypothesis that stretching fields are intimately linked with mixing is coherent and conceptually compelling evidence is still lacking, due to the ability to measure stretching fields being a recent addition to the experimental toolkit (i.e. Ref. [194] is one of the few works in this exciting area). Both the results here which demonstrate reduced mixing and the evidence of low stretching fields [194] in unstable viscoelastic flows are consistent with the understanding that viscoelastic fluids driven well above the viscoelastic instability threshold progress towards elastic turbulence which has been shown to be a realization of Batchelor turbulence [176, 177].

One of the key characteristics of Batchelor turbulence is that instabilities are dominated by the large scale fluctuations, which are set by the system size, and therefore there will remain a mismatch between the smallest scale one wants homogeneity on and the instability which is intended to drive mixing. In Batchelor turbulence it has been established that the velocity decays rapidly (the wavenumber k scales as k^{-x}, where x has experimentally been found to be in the range 3.3 to 3.6 [177]) which leads to weak coupling between scales, in sharp contrast to high Reynolds number turbulence with its "bucket brigade", and the resulting flows are random in time yet spatially smooth and strongly correlated on the integral scale [177]. This results in instabilities dominated by large scale fluctuations, which are set by the system size [177], and therefore there will remain a mismatch between the smallest scale one wants homogeneity on and the instability which is intended to drive mixing. Note that the smooth flow characteristics of Batchelor turbulence are consistent with the observations here (see, for example, Fig. 6.9 where the large scale nature of the instability can be visually observed) and, without some other mechanism (such as shear) to further modify flow, are at odds with enhanced mixing.

The observed highly unstable yet diffusion limited flows has potential to be harnessed in applications which depend on large interfacial area; for example, in membraneless fuel cells [197] or for use in combination with the liquid junction potential [198]. In membraneless fuel cells a large interfacial area is wanted, while rapid mixing is not desired, and the liquid junction potential can be used to drive ions across interfaces, so LJP effects in combination with viscoelastic instabilities could lead to rapid mixing of ionic species.

While it has been shown that viscoelastic instabilities alone will not lead to efficient mixing the microfluidic platform here represents in some sense a worse-case situation (if rapid mixing is the goal; on the other hand EOF devices are good platforms for study of viscoelastic instabilities, as other effects can be limited allowing the isolation of viscoelastic instability and controlled application of other effects), where only viscoelastic instabilities ("folding") and fast diffusion occur.

Can mixing never-the-less be improved? By including designed stretching elements ("kneading"), by breaking symmetries [174], or by including other deformation elements in addition to the elongational units mixing may be improved [181, 199]. The science of mixing is still poorly understood, but recent frameworks using dynamical systems [199] and the linked twist map [181], where two (or more) flow fields alternatively affect the flow, are gleaning insight and inform design. As viscoelastic instabilities progress towards Batchelor turbulence, a previously experimentally inaccessible regime [176], they offer an additional experimental tool for exploring basic instability and mixing mechanisms, as well as potential application for enhanced mixing schemes.

Using the “knead and fold” metaphor of mixing [181] viscoelastic instabilities provide the fold operation that creates large deformations of material to create striations of dis-similiar material, and additional deformations are needed to thin striations allowing diffusion to finally homogenize the fluids. One means of improving mixing would be to add shear (i.e. co-pressure pumping; electro-osmotic flows can be used to isolate viscoelastic instabilities, and combined pressure/EOF driven flows [200] enable controlled application of shear allowing detailed investigation of flow evolution and mixing) or break the symmetry of the microchannel patterning: instead of centering constrictions in the mid axis random location of the 100 μm constriction center within the 200 μm channel may lead to improved mixing by increasing the deformation across the flow direction for a given element, in addition by adding “jitter” to the spacing between constrictions the time-periodic nature of the flow field would be broken, where the time-periodic aspect leads to[12] persistent patterning [174].

6.9 Summary

To summarize, the addition of high molecular weight polyacrylamide to liquids leads to striking viscoelastic instabilities in extensional electro-osmotic flow, thereby breaking the laminar flow typical of flows in microchannels. The strategy to promote instabilities discussed here is simple. The addition of polymer is facilitated if pre-solvated polymer mixtures are added to working fluids[13]. The use of high viscosity solvents or concentrated polymer is *not* required: low viscosity, lightly polymer doped liquids undergo instability under typical electro-osmotic flow conditions. The breaking of laminar flow for dilute low viscosity viscoelastic fluids has implications for device design as laminar flow

---

[12] Intuitively, the flow is distorted periodically, and therefore returns to a similar state, leading to persistence - by breaking the period close by trajectories will separate quicker, increasing mixing.

[13] Initial solvation of *dried* polymer is time intensive, but once solvated mixtures of a specific concentration can be rapidly mixed together with additional fluid (the sample of interest) to give a specified final concentration. Also, alcohol, as used in the samples here, is not required unless long term storage of polymers is intended [142].

is often assumed in microflows; as lab on a chip applications move towards more complex fluids this assumption must be checked. The loss of the simplicity that steady laminar flow affords does not, however, mean that highly efficient mixing is gained. The results here show that for flows of low viscosity solutions through unoptimized geometries mixing is *reduced* over purely diffusive mixing, despite the excitation of large viscoelastic instabilities: shear free viscoelastic unstable flows are essentially diffusion limited. As viscoelastic instabilities progress to Batchelor turbulence relatively "smooth" flows are expected and care must be taken in designing and incorporating deformations of such smooth flows to promote mixing. **Both the results found here, and earlier electrokinetic stretching of 2D sheets of liquid polymer [194], demonstrate that electro-osmotic flows can be used to isolate viscoelastic instabilities, by "turning off" shear, and that such flows are effectively diffusion limited**. Combined pressure/EOF driven flows [200] enables controlled application of shear allowing possibility for detailed investigation of flow evolution and mixing.

It is found that:

- Adding high molecular weight polymer leads to instability, with higher concentration leading to larger and slower oscillations,
- Even polymer-free solutions experience enhanced mixing versus uniform pipe flow; this finding has been previously noted in the literature,
- Increased concentration leads to absolute less mixing at a given location in the microchannel, and (slightly) shorter mixing length (i.e. slope in mixing as a function of mixing unit) due to instability. In contrast to the heuristic expectation that "polymer=mixing" it is found that the slight quantitative increase in viscosity dominates over the striking qualitative viscoelastic instability mechanism - in this sense (purely) viscoelastic unstable flows are diffusion limited, as diffusion is the dominant and limiting factor,
- To repeat: efficient mixing, relative to polymer-free solutions, was *not*

observed in shear-free unstable flows, demonstrating that viscoelastic instabilities do not, by themselves, lead to good mixing. This finding is consistent with earlier studies of 2D shear-free flows that found a mild decrease in mixing due to viscoelasticity,

- The observed highly unstable, yet diffusion limited, flows has potential for applications which make use of large interfacial area. Some speculative applications include use in membraneless fuel cells, or for use in combination with the liquid junction potential to enhance ionic mixing,
- Symmetry in the microchannel patterning will tend to reduce the mixing rate, breaking this symmetry will help improve mixing rates; the Linked Twist Map and rational design may lead to efficient mixing where the Bachelor turbulence, that viscoelastic instabilities progress to, provides the “fold” operation and other means will be required to “knead” the fluids. Use of co-pressure flows would enable controlled application of shear, allowing systematic investigation of viscoelastic instability-shear effects,
- As EOF flows are shear-free, while shear is a significant component of all mechanically driven cavity flows, EOF devices are a good platform for the study of viscoelastic instabilities and elastic turbulence in isolation and with controlled introduction of additional deformations (such as those noted above).

Chapter 7

Conclusions and Outlook

As device dimensions shrink and more complex fluids are investigated electro-osmotic flows of nonNewtonian fluids will become increasingly important, making these flows of practical interest. As a means to enable mixing the addition of polymers to fluids is enticing, as various instabilities and even elastic turbulence have been observed in some flow systems. By adding inert polymers to fluids instabilities can be excited in devices that require no special (multistep) fabrication processes, and it was found that viscoelastic instabilities can be excited in microchannels using standard electro-osmotic pumping rates. It was also observed that electrode effects can create globule microgels in polyacrylamide solutions. This means that both intentional excitation can be achieved by doping a working fluid with high molecular weight polymers, and also that unintentional effects (i.e. nonlaminar flow, globules) may be observed when working with biological or other material, requiring care.

The mixing rate was found to be *reduced* in studies of fast diffusing dye in shear-free flow through symmetric microchannels; purely viscoelastic unstable flows are effectively diffusion limited. Breaking microchannel structure symmetry may allow for optimization of mixing, as it has previously been found that persistent spacial structure with slow decay occurs in periodic forcing of chaotic flows. Adding other fluid deformation elements may also improve mixing, as the efficient mixing in pressure pumped serpentine flows suggests (where shear provides a persistent stretching element). Due to the exclusion of shear the use of EOF devices enables the fundamental study of viscoelastic unstable and elastic turbulence in isolation of other mechanisms, and the controlled application of fluid deformations, allowing instabilities and mixing to be studied.

A key “competitor” to viscoelastic fluids as a means to enhance mixing is “bubble fluidics” [201]: by pushing trains of bubbles through microchannels secondary flows and rapid mixing can be achieved, and - like viscoelastic fluids flows where memory and control has been demonstrated [202] - logic and control has been shown for bubble flows [203]. By having aqueous droplets in oils compartmentalized reaction chambers can be achieved in this system, high repeatability is achieved, and effective mixing has been demonstrated [204]. The main limitation of bubble fluidics is its use of pressure flows for pumping in most schemes. Despite the advantages of bubble fluidics viscoelastic flows has the advantage of being a single phase system which has a simple protocol for experimental use - presolvated polymer solution can be mixed X:Y with a sample to be investigated to give a required polymer concentration and rapidly mixed and used; additionally a given material under study may be viscoelastic itself, which necessitates understanding possible nonNewtonian effects.

In addition to the experimental findings on viscoelastic instabilities, it was found that the predicted concentration fluctuation instability[1] for dilute polymer solutions corresponds to the viscoelastic instability. This co-incidence may have “masked” the earlier discovery of density fluctuation instabilities, which have only recently been discovered in simple fluids where they are difficult to excite, and may lead to continued difficulties in modeling and understanding polymeric instabilities[2].

Discovery and investigation of density fluctuation instabilities is in its infancy, but has promise for both application (i.e. mixing enhancement) as well possible negative effects (i.e. breaking expected laminar flow when design depends on it), and, of course, fundamental investigations. In general complex

---

[1] Complex fluid analogue of density fluctuation instability.

[2] The “High Weissenberg Number Problem” is a well known inability to computationally track flows above the instability threshold; various numerical techniques will fail at different particular values of the Weissenberg number, but all approaches ultimately fail relatively close to the threshold of (physical) instability.

fluids often have concentration/viscosity variation on the order of the velocity gradients[3] which makes finite-sized/granalarity interaction with flow fields a distinct possibility that could lead to unstable flow; this structure-gradient consideration provides a simple conceptual model as to why concentration fluctuation instabilities could be expected to be excited in complex fluids[4]. As was seen for viscoelastic fluids in the studies here, diffusion will be reduced relative to macromolecular-free solutions, and depending on the nature of the instability mixing may remain diffusion limited.

It was also discovered that correlations in tracer particles in unstable polymer flow can be used to extract the relaxation time *without fitting to a model and within a given experimental setup.* The first, and possibly the second, order relaxation time was observed, in prior rheological studies clear observation of relaxation time is not obtained and model fits are required. The availability of in-situ relaxation time measurements is desirable, and as various model fits and assumptions are typically used to estimate relaxation time this approach allows for testing for systematic errors of a given fitting procedure. Despite the promise of this technique it must be pointed out that there is a requirement to sample much faster than the relaxation time, as a cross-over must be determined, which limits the smallest measurable relaxation time for a given imaging system, and the addition of tracer particles themselves will change the underlying fluid.

Finally, poly(ether sulfone) films were found to have negative resist properties and the ability to use PES as an etch-mask was demonstrated for both plasma and chemical etching. As PES films are robust there is possibility of incorporation in devices. A key limitation here is writing time, which will limit feasible structures.

7.1 What next?

There are a number of projects that can be be pursued.

---

[3] "Structured fluids" is yet another term for complex fluids, and this phrase is due to the similarity in structure-forcing size.

[4] E.g. the continuum assumption can clearly break down for complex fluids.

- Further study of poly(ether sulfone) films for fluidic applications. PES was found to be a negative resist, limiting feasible structures to small sized features. However, sparse structures (such as pillars in a 2D array) or “nanofluidic” channels would have reasonable write times allowing investigation of PES for microfluidics. As PES is both transparent and hydrophilic microfluidic applications are facilitated, further PES is food grade which indicates that it will not release or capture material (e.g. a concern for PDMS).

- Electron beam studies of sulfone polymers, as both positive and now negative resist action have been observed in sulfones, indicating versatility.

- Using fluorescent microspheres velocity profiles can be obtained, which would establish if true elastic turbulence occurs.[5]

- Investigation of micro-gels. Dynamics were complex when globules formed, and while it appeared that rapid mixing occurred for the liquid between the globules the inhomogeneity of the micro-gels prevents a simple mixing value from being found from either PMT or space-time images. Investigation using chemical reactions is one possible means of probing mixing rates.

- The BEM method has been coded into MatLab and allows fairly rapid numerical calculations[6], and average flow was confirmed against both physical expectations and Schwarz-Christoffel calculated flows; however due to a poor geometry input procedure that requires geometry files to be encoded by hand it is difficult to modify geometries in order to reduce discretizations and related distortion in calculated fields. Improving the code and creating a toolbox, for example by including a GUI in order to allow geometry to be created, automatic discretization refinement, and

---

[5] Note that due to EP effects particle velocity will not be solely set by fluid flow, complicating analysis.

[6] Unoptimized code ran at comparable speeds to the Schwarz-Christoffel toolbox, albeit with large discretization on the boundary.

MatLab optimization (such as "vectorization"), would be valuable as no such toolbox currently exists.

- Better control of the elongation rate can be obtained by using hyperbolic constrictions, which have constant elongation rate through the constriction [205]. Having long sections of constant elongation rate would allow entry effects to be studied; additionally by modulating the hyperbolic constrictions with hyperbolic expansions long regions of constant elongation can be achieved, allowing for continuous deformation of fluids.
- Investigation of entry effects in EOF, in particular confirming shear-free flow. Entry effects, caused by a rapid change in boundary geometry, are often ignored in electro-osmotic flows. Investigating how and to what extent flows are changed from potential flow, both experimentally and numerically, is important to establish the precise flow conditions. It is argued here that the Helmholtz decomposition theorem should hold, as entry effects appear to be a pure pressure effect [8], and thus flows affected by entry effects should remain irrotational (shear-free). However, a full multi-physics simulation allowing flow rotation to be calculated would be valuable in order to confirm, or repudiate, if this is indeed the case.
- Symmetry in the microchannel patterning will tend to reduce the mixing rate; breaking the symmetry may enhance mixing and studying viscoelastic Lagrangian chaos effects may enable rapid mixing to be achieved.
- Investigation use of the liquid junction potential in viscoelastic unstable flows, where increased interface is created, for enhanced ionic mixing.
- Investigation of viscoelastic *and* shear thinning[7] liquids to promote mixing in EOF pumped flows; to obtain strong thinning behaviour in polyacryamide solutions $c > c_*$ is required, which will create steric polymer-

---

[7] Shear thinning is caused by entwined polymer-polymer coils unraveling from each other and in elongational flows such unraveling should also occur. Thinning is a more suitable term here.

polymer repulsion and tend to push coils into the Debye layer and thus complicate flows. Note that it has been found that shear thinning viscoelastic fluids have demonstrated good mixing in 2D experiments, while purely viscoelastic fluids had reduced mixing [194].

- Investigation of highly shear thinning liquids to study if one can harness the Kaye effect [193] to promote mixing at microchannel expansions for intermediate Reynolds numbers, a possible interpretation of the results in Ref. [191]. Mechanically driven flows would be more suitable here, in order to limit Joule heating and globule effects at the high velocities (voltages) required and in order to induce both shear and elongational thinning. Currently the Kaye effect is a “novelty” [193], demonstrating an application of the effect would be fruitful in gaining more insight and promoting further investigation into the mechanisms involved.

- Studies of colloidal mixtures is of interest, for if concentration instabilities exist they should also be present in colloidal fluids. Using fluorescent microspheres (or using a mixture of non- and dyed microspheres for high concentrations) would allow imaging of instabilities and the collection of velocity profiles.

- Investigation of the similarity between bubbles and polymers may lead to an useful mesoscopic numerical model, where individual polymers are simply modeled by bubbles with surface tension selected to give the required relaxation time[8].

- Further investigation of Detrended Fluctuation Analysis to find relaxation times, particularly investigating the possibility of extracting higher order relaxation modes from experimental data.

- As EOF allows the isolation of viscoelastic instabilities fundamental mixing studies are enabled; combined pressure and EOF pumped flows would enable shear to be introduced in a controlled manner.

---

[8] Bubbles can be incorporated into many CFD codes.

- Mechanically pulled elongation experiments also have low shear. While these flows are short in duration, due to rapid thinning and eventual filament breaking, the availability of ultrafast cameras is opening up experimental opportunities here.

Bibliography

[1] D. Acheson, *Elementary Fluid Mechanics*. Clarendon Press, 1990.

[2] R. B. Bird, R. C. Armstrong, and O. Hassager, *Dynamics of Polymeric Liquids*, vol. 1. Wiley, second ed., 1987.

[3] N.-T. Nguyen and S. Wereley, *Fundamentals and Applications of Microfluidics*. Artech House, 2002.

[4] O. Reynolds, "An experimental investigation of the circumstances which determine whether the motion of water shall be direct or sinuous, and of the law of resistance in parallel channels," *Philosophical Transactions of the Royal Society*, vol. 174, pp. 935–982, 1883.

[5] R. E. Goldstein, I. Tuval, and J.-W. van de Meent, "Microfluidics of cytoplasmic streaming and its implications for intracellular transport," *Proceedings of the National Academy of Sciences of the United States of American.*, vol. 105, no. 10, pp. 3663–3667, 2008.

[6] P. H. Paul, M. G. Garguilo, and D. J. Rakestraw, "Imaging of pressure- and electrokinetically driven flows through open capillaries," *Analytical Chemistry*, vol. 70, pp. 2459–24671, 1998.

[7] D. P. Barz and P. Ehrhard, "Model and verification of elctrokinetic flow and transport in a micro-electrophresis device," *Lap Chip.*, vol. 5, pp. 949–958, 2005.

[8] N. Sylvester and S. Rosen, "Laminar flow in the entrance region of a cylindrical tube: Part 1. newtonian fluids," *AlChE J.*, vol. 16, pp. 964–966, 1970.

[9] A. Chorin and J. Marsden, *A mathematical introduction to fluid mechanics*. Springer, 2000.

[10] D. Smith, H. Babcock, and S. Chu, "Single polymer dynamics in steady shear flow," *Science*, vol. 283, p. 1724, 1999.

[11] T. A. Driscoll, "A matlab toolbox for schwarz-christoffel mapping," *ACM Trans. Math. Soft.*, vol. 22, pp. 168–186, 1996.

[12] P. Doyle, B. Ladoux, and J. Viovy, "Dynamics of a tethered polymer in shear flow," *Phys. Rev. Let.*, vol. 84, pp. 4769–4772, 2000.

[13] R. Larson, "Fluid dynamics - turbulence without inertia," *Nature*, vol. 405, pp. 27–28, 2000.

[14] A. Groisman and V. Steinberg, “Efficient mixing of liquids at low reynolds numbers using polymer additives,” *Nature*, vol. 410, pp. 905–908, 2001.

[15] P. Pakdel and G. McKinley, “Elastic instability and curved streamlines,” *Phys. Rev. Lett.*, vol. 77, pp. 2459 – 2462, 1996.

[16] G. McKinley, P. Pakdel, and A. Oztekin, “Rheological and geometric scaling of purely elastic flow instabilities,” *J. Non-Newtonian Fluid Mech.*, vol. 67, p. 1947, 1996.

[17] A. Morozov and W. van Saarloos, “An introductory essay on subcritical instabilities and the transition to turbulence in visco-elastic parallel shear flows,” *Physics Reports*, vol. 447, pp. 112–143, 2007.

[18] T. Perkins, S. Quake, D. Smith, and S. Chu, “Relaxation of a single dna molecule observed by optical microscopy,” *Science*, vol. 264, pp. 822–826, 1994.

[19] A. Groisman and V. Steinberg, “Elastic turbulence in a polymer solution flow,” *Nature*, vol. 405, pp. 53–55, 2000.

[20] A. Groisman and V. Steinberg, “Efficient mixing of liquids at low reynolds numbers using polymer additives,” *Nature*, vol. 410, p. 905, 2001.

[21] T. Burghelea, E. Segre, I. Bar-Yosef, A. Groisman, and V. Steinberg, “Chaotic flow and efficient mixing in microchannel with a polymer solution,” *Phys. Rev. E*, vol. 69, p. 066305, 2004.

[22] W. Cleveland, *The elements of graphing data.* Hobart Press, 1994.

[23] P. Garstecki, M. Fischbach, and G. Whitesides, “Design for mixing using bubbles in branched microfluidic channels,” *APL*, vol. 86, p. 244108, 2005.

[24] J. Filliben, *Exploratory Data Analysis, in Engineering Statistics Handbook.* NIST/SEMATECH, 2006.

[25] T. Sikanen, T. Zwinger, S. Tuomikoski, S. Franssila, R. Lehtiniemi, C.-M. Fager, T. Kotiaho, and A. Pursula, “Temperature modeling and measurement of an electrokinetic separation chip,” *Microfluidics and Nanofluidics*, vol. 5, pp. 1613–4982, 2008.

[26] A. Einstein, “Eine neue bestimmung der molekuldimensionen,” *Ann. Phys.*, vol. 19, pp. 289–306, 1906.

[27] R. Roscoe, “The viscosity of suspensions of rigid spheres,” *Br. J. Appl. Phys.*, vol. 3, pp. 267–269, 1952.

[28] P. C. Hiemenz and R. Rajagopalan, *Principles of Colloid and Surface Chemistry.* CRC, 1997.

[29] C. Stoltz, J. de Pablo, and M. Graham, “Concentration dependence of shear and extensional rheology of polymer solutions: Brownian dynamics simulations,” *J. Rheol.*, vol. 50, pp. 137–167, 2006.

[30] M. Das, H. Z. H, and E. Kumacheva, "Microgels: Old materials with new applications," *Annual Review of Materials Research*, vol. 36, pp. 117–142, 2006.

[31] A. Groisman and V. Steinberg, "Elastic turbulence in curvilinear flows of polymer solutions," *NJP*, vol. 6, p. 29, 2004.

[32] J. Ottino and S. Wiggins, "Designing optimal micromixers," *Science*, vol. 305, pp. 485–486, 2004.

[33] H. Newton, *Timeslab: A time series analysis laboratory.* Wadsworth, 1988.

[34] W. Beveridge, "Wheat prices and rainfall in western europe," *Journal of the Royal Statistical Society*, vol. 85, pp. 412–447, 1922.

[35] M. V. Dyke, *Album of Fluid Motion.* Parabolic Press, 1982.

[36] C. Pozrikidis, *Little Book of Streamlines.* Academic Press, 1999.

[37] M. Samimy, M. Breuer, L. Leal, and P. Steen, *Gallery of Fluid Motion.* Cambridge Press, 2004.

[38] *http://pof.aip.org/pof/gallery.*

[39] W. Loose and S. Hess, "Rheology of dense model fluids via nonequilibrium molecular dynamics: shear thinning and ordering transition," *Rheologica Acta.*, vol. 28, pp. 91–101, 1989.

[40] J. N. Israelachvili, "Measurement of the viscosity of liquids in very thin films," *J. Colloid Interface Sci.*, vol. 110, p. 263, 1986.

[41] P. M. J. N. Israelachvili and A. Homola, "Dynamic properties of molecularly thin liquid films," *Sceince*, vol. 240, pp. 189–191, 1998.

[42] C. Neto, D. R. Evans, E. Bonaccurso, H.-J. Butt, and V. S. J. Craig, "Boundary slip in newtonian liquids: a review of experimental studies," *Reports on Progress in Physics*, vol. 68, pp. 2859–2897, 2005.

[43] J. Koplik and J. R. Banavar, "Slip, immiscibility, and boundary conditions at the liquid-liquid interface," *Physical Review Letters*, vol. 96, p. 044505, 2006.

[44] M. G. el Hak, "Liquids: The holy grail of microfluidic modeling," *Physics of Fluids.*, vol. 17, p. 100612, 2005.

[45] A. Bejan, *Entropy Generation Through Heat and Fluid Flow.* John Wiley & Sons Inc, 1982.

[46] B. Hof, A. de Lozar, D. Kuik, and J. Westerweel, "Repeller or attractor? selecting the dynamical model for the onset of turbulence in pipe flow," *Phys. Rev. Lett.*, vol. 101, p. 214501, 2008.

[47] A. Groisman and V. Steinberg, "Elastic turbulence in a polymer solution flow," *Nature*, vol. 405, pp. 53–55, 2000.

[48] A. Furukawa and H. Tanaka, "Violation of the incompressibility of liquid by simple shear flow," *Nature*, vol. 443, pp. 434–438, 2006.

[49] N. Alleborn, K. Nandakumar, H. Raszillier, and F. Durst, “Further contribution on the two dimensional flow in a sudden expansion,” *J. Fluid Mech.*, vol. 330, pp. 169–188, 1997.

[50] E. Purcell, “Life at low reynolds number,” *American Journal of Physics*, vol. 45, pp. 3–11, 1977.

[51] L. Leger, “Friction mechanisms and interfacial slip at fluid-sold interfaces,” *J. Phys.: Condens. Matter*, vol. 15, pp. S19–S29, 2008.

[52] T. Squires and S. Quake, “Microfluidics: Fluid physics at the nanoliter scale,” *Rev. Mod. Phys.*, vol. 77, pp. 977–1026, 2005.

[53] S. Ghosal, “Fluid mechanics of electroosmotic flow and its effect on band broadening in capillary electrophoresis,” *Electrophoresis*, vol. 25, pp. 214–228, 2004.

[54] P. M. Monk, *Fundamentals of Electroanalytical Chemistry.* John Wiley and Sons, 2001.

[55] V. Tandon and B. Kirby, “Zeta potential and electroosmotic mobility in microfluidic devices fabricated from hydrophobic polymers: 2. slip and interfacial water structure,” *Electrophoresis*, vol. 29, pp. 1102–1114, 2008.

[56] R. Probstein, *Physicochemical hydrodynamics: an introduction.* Wiley-Interscience, 2003.

[57] X.-H. N. Xu and E. Yeung, “Long-range electrostatic trapping of single-protein molecules at a liquid-solid interface,” *Science*, vol. 281, pp. 1650–1653, 1998.

[58] V. Heleg-Shabtai, N. Gratziany, and Z. Liron, “Separation and detection of vx and its methylphosphonic acid degradation products on a microchip using indirect laser-induced fluorescence,” *Electrophoresis*, vol. 27, pp. 1996–2001, 2006.

[59] G. de Marsily, *Quantitative Hydrogeology: Groundwater Hydrology for Engineers.* Academic Press, 1986.

[60] S.-S. Hsieh, H.-C. Lin, and C.-Y. Lin, “Electroosmotic flow velocity measurements in a square microchannel,” *Colloid Polym Sci*, vol. 282, pp. 1275–1286, 2006.

[61] E. Cummings, S. Griffiths, R. Nilson, and P. Paul, “Conditions for similitude between the fluid velocity and electric field in electroosmotic flow,” *Analytical Chemistry*, vol. 72, pp. 2526–2532, 2000.

[62] J. Santiago, “Comments on the conditions for similitude in electroosmotic flows,” *Journal of Colloid and Interface Science*, vol. 310, pp. 675–677, 2007.

[63] G. Randall and P. Doyle, “Dna deformation in electric fields: Dna driven past a cylindrical obstruction,” *Macromolecules*, vol. 38, pp. 2410–2418, 2005.

[64] V. Kolar, “Vortex identification: New requirements and limitations,” *International Journal of Heat and Fluid Flow*, vol. 28, pp. 638–652, 2007.

[65] C. Pozrikidis, *Numerical Computation in Science and Engineering.* Oxford University Press, second ed., 2008.

[66] K. Ang, "Introducing the boundary element method with matlab," *Int. J. of Math. Ed.*, vol. 39, pp. 505–519, 2006.

[67] Y. H. Zhang, R. W. Barber, and D. R. Emerson, "Creeping electroosmotic flow through microchannels," *Proc. 13th Micro-Mechanics Europe Workshop (MME02)*, pp. 153–156, 2002.

[68] R.-J. Yang, L. M. Fu, and C.-C. Hwang, "Electroosmotic entry flow in a microchannel," *Journal of colloid and Interface Science*, vol. 244, pp. 173–179, 2001.

[69] J. Kirchner and E. H. Jr., "Dispersion of solute by electrokinetic flow through post arrays and wavy-walled channels," *Anal. Chem*, vol. 77, pp. 1140–1146, 2005.

[70] M. Rubinstein and R. H. Colby, *Polymer Physics.* Oxford University Press, 2003.

[71] P. de Gennes, "Coil-stretch transition of dilute flexible polymers under ultrahigh velocity-gradients," *J. Chem. Phys.*, vol. 60, pp. 5030–5042, 1974.

[72] T. Yamaguchi, H. Namatsu, M. Nagase, K. Yamazaki, and K. Kurihara, "Nanometer-scale linewidth fluctuations caused by polymer aggregates in resist films," *Applied Physics Letters*, vol. 71, pp. 2388–2390, 1997.

[73] H. Namatsu, M. Nagase, T. Yamaguchi, K. Yamazaki, and K. Kurihara, "Influence of edge rougness in resist patterns on etched patterns," *Journal of Vacuum Science & Technology B.*, vol. 16, pp. 3315–3321, 1998.

[74] R. Bryce, M. Freeman, and M. Aktary, "Poly(ether sulfone) as a negative resist for electron-beam lithography," *Appl. Phys. Lett.*, vol. 90, p. 203110, 2007.

[75] R. Bryce, M. Freeman, and M. Aktary, "Poly(ether sulfone) as a negative resist for electron-beam lithography," *Virtual Journal of Nanoscale Science and Technology*, 2007.

[76] P. Rai-Choudhury, ed., *Handbook of Microlithography, Micromachining, and Microfabrication*, vol. 1. SPIE, 1997.

[77] A. Broers, A. Hoole, and J. Ryan, "Electron beam lithography - resolution limits," *Microelectron Eng*, vol. 32, pp. 131–142, 1996.

[78] J. Fujita, Y. Ohnishi, Y. Ochiai, and S. Matsui, "Ultrahigh resolution of calixarene negative resist in electron beam lithography," *Appl Phys Lett*, vol. 68, pp. 1297–1299, 1996.

[79] L. Thompson, L. Stillwagon, and E. Doerries, "Negative electron resists for direct fabrication of devices," *J Vac Sci Technol*, vol. 15, pp. 938–943, 1978.

[80] S. Hart, G. Maskaly, B. Temelkuran, P. Prideaux, J. Joannopoulos, and Y. Fink, "External reflection from omnidirectional dielectric mirror fibers," *Science*, vol. 296, pp. 510–513, 2002.

[81] J. Goodberlet, J. Hastings, and H. Smith, "Performance of the raith 150 electron-beam lithography system," *J Vac Sci Technol B*, vol. 19, p. 24992503, 2001.

[82] P. Mali, A. Sarkar, and R. Lal, "Facile fabrication of microfluidic systems using electron beam lithography," *Lab on a Chip*, vol. 6, pp. 310–315, 2006.

[83] S. Tachi, K. Tsujimoto, and S. Okudaira, "Low-temperature reactive ion etching and microwave plasma-etching of silicon," *Appl Phys Lett*, vol. 52, pp. 616–618, 1988.

[84] H. Ku and L. Scala, "Polymeric electron beam resists," *J. Electrochem. Soc.: Solid State Science*, vol. 116, p. 980, 1969.

[85] G. Underwood, "private communication," *Private communication*, 2006.

[86] L. Ocola, D. Tennant, G. Timp, and A. Novembre, "Lithography for sub-60 nm resist nanostructures," *J. Vac. Sci. Technol. B*, vol. 17, pp. 3164–3167, 1999.

[87] M. Bowden and L. Thompson, "Electron-irradiation of poly(olefin sulfones) - application to electron-beam resists," *J. of App. Poly. Sci.*, vol. 17, pp. 3211–3221, 1973.

[88] S.-I. Kuroda, A. Nagura, K. Horie, and I. Mita, "Degradation of aromatic polymers .3. crosslinking and chain scission during photodegradation of polysulfones," *Eur. Poly. J*, vol. 25, pp. 621–627, 1989.

[89] M. Bowden, L. Thompson, and J. Ballantyne, "Poly(butene-1 sulfone) - highly sensitive positive resist," *J. Vac. Sci. Technol.*, vol. 12, pp. 1294–1296, 1975.

[90] M. Bowden and L. Thompson, "Poly(styrene sulfone) - sensitive ion-millable positive electron-beam resist," *J. Electrochem. Soc.*, vol. 121, pp. 1620–1623, 1974.

[91] K. Christe, "A renaissance in noble gas chemistry," *Angew. Chem. Int. Ed.*, vol. 40, p. 1419, 2001.

[92] P. Dubos, P. Charlat, T. Crozes, P. Paniez, and B. Pannetier, "Thermostable trilayer resist for niobium lift-off," *J. Vac. Sci. Technol. B*, vol. 18, pp. 122–126, 2000.

[93] S. Garner, J. Cites, M. He, and J. Wang, "Polysulfone as an electro-optic polymer host material," *Appl. Phys. Lett.*, vol. 84, pp. 1049–1051, 2004.

[94] I. Teraoka, *Polymer Solutions: An Introduction to Physical Properties.* John Wiley & Sons., 2002.

[95] Y. Heo and R. G. Larson, "The scaling of zero-shear viscosities of semidilute polymer solutions with concentration," *J. Rheol.*, vol. 49, pp. 1117–1128, 2005.

[96] R. Larson, "The rheology of dilute solutions of flexible polymers: Progress and problems," *J. Rheol.*, vol. 49, pp. 1–70, 2005.

[97] C. Clasen, J. Plog, W.-M. Kulicke, M. Owens, C. Macosko, L. Scriven, M. Verani, and G. McKinley, “How dilute are dilute solutions in extensional flows?,” *J. Rheol.*, vol. 50, pp. 849–881, 2006.

[98] A. Lindner, D. Bonn, E. C. Poire, M. B. Amar, and J. Meunier, “Viscous fingering in non-newtonian fluids,” *J.Fluid Mech.*, vol. 469, pp. 237–256, 2002.

[99] G. Harrison, J. Remmelgas, and L. Leal, “The dynamics of ultradilute polymer solutions in transient flow: Comparison of dumbbell-based theory and experiment,” *J. Rheol.*, vol. 42, pp. 1039–1058, 1998.

[100] J. Reddy and D. Gartling, *The Finite Element Method in Heat Transfer and Fluid Dynamics*. CRC, second ed., 2000.

[101] P. Arratia, C. Thomas, J. Diorio, and J. Gollub, “Elastic instabilities of polymer solutions in cross-channel flow,” *Phys. Rev. Lett.*, vol. 96, p. 144502, 2006.

[102] T. T. Perkins, D. E. Smith, and S. Chu, “Single polymers in elongational flow,” *Science*, vol. 276, p. 2016, 1997.

[103] R. Larson and J. Magda, “Coil-stretch transitions in mixed shear and extensional flows of dilute polymer solutions,” *Macromolecules*, vol. 22, pp. 3004–3010, 1989.

[104] A. Y. Malkin, “The state of the art in the rheology of polymers: Achievements and challenges,” *Polymer Science. Ser. A*, vol. 51, pp. 80–102, 2009.

[105] R. G. Owens and T. N. Phillips, *Computational Rheology*. World Scientific Publishing Company, 2002.

[106] C. Schroeder, H. Babcock, E. Shaqfeh, and S. Chu, “Observation of polymer configuration hysteresis in extensional flow,” *Science*, vol. 301, pp. 1515–1519, 2003.

[107] S. Gerashchenko and V. Steinberg, “Critical slowing down in polymer dynamics near the coil-stretch transition in elongational flow,” *Phys. Rev. E*, vol. 78, p. 040801, 2008.

[108] R. Fattal and R. Kupferman, “Constitutive laws for the matrix-logarithm of the conformation tensor,” *J. Non-Newtonian Fluid Mech.*, vol. 123, pp. 281–285, 2004.

[109] R. Larson, *The Structure and Rheology of Complex Fluids*. Oxford University Press, 1998.

[110] S.Berti, A. Bistagnino, G. Boffetta, A. Celani, and S. Musacchio, “Small-scale statistics of viscoelastic turbulence,” *Europhysics Letters*, vol. 76, pp. 63–69, 2006.

[111] I. Kosztin and K. Schulten, *Nonequilibrium statistical mechanics lecture notes (PHYCS 498SM)*. http://www.ks.uiuc.edu/ kosztin/PHYCS498NSM/, 2000.

[112] P. Attard and S. J. Miklavcicn, “Effective spring constant of bubbles and droplets,” *Langmuir*, vol. 17, pp. 8217–8223, 2001.

[113] E. Degand and K. Walters, "On the motion of a sphere falling through an elastic liquid containing a tightly-filling cylindrical container," *J. Non-Newtoninan Fluid Mech.*, vol. 57, pp. 103–115, 1995.

[114] A. Acharya, R. A. Mashelkar, and J. Ulbrecht, "Flow of inelastic and viscoelastic fluids past a sphere. part ii: Anomalous separation in the viscoelastic fluid flow," *Rheologica Acta*, vol. 15, pp. 471–478, 1976.

[115] S. Chen and J. P. Rothstein, "Flow of a wormlike micelle solution past a falling sphere," *J. Non-Newtonian Fluid Mech.*, vol. 116, pp. 205–234, 2004.

[116] M. Kameda, T. Katsumata, and M. Ichihara, "Deformation of bubbles in highly viscous pipe flow," *Fluid Dynamics Research*, vol. 40, pp. 576–584, 2008.

[117] A. Groisman, M. Enzelberger, and S. R. Quake, "Microfluidic memory and control devices," *Science*, vol. 300, pp. 955–958, 2003.

[118] A. Groisman and S. R. Quake, "A microfluidic rectifier: Anisotropic flow resistance at low reynolds numbers," *Phys. Rev. Lett.*, vol. 92, p. 094501, 2004.

[119] M. Denn, "Fifty years of non-newtonian fluid dynaimcs," *AIChE J.*., vol. 50, pp. 2335–2345, 2004.

[120] S. Berti, A. Bistagnino, G. Boffetta, A. Celani, and S. Musacchio, "Two-dimensional elastic turbulence," *PRE.*, vol. 77, p. 055306, 2008.

[121] J. Pathak, D. Ross, and K. Migle, "Elastic flow instability, curved streamlines and mixing in microfluidic flows," *Phys. Fluids*, vol. 16, p. 4028, 2004.

[122] H. Gan, Y. Lam, and N. Nguyen, "Polymer-based device for efficient mixing of viscoelastic fluids," *APL*, vol. 88, p. 224103, 2004.

[123] K. Helton and P. Yager, "Interfacial instabilities affect microfluidic extraction of small molecules from non-newtonian fluids," *Lab Chip*, vol. 7, pp. 1581–1588, 2007.

[124] A. Leshansky, A. Bransky, N. Korin, and U. Dinnar, "Tunable nonlinear viscoelastic focusing in a microfluidic device," *Phys. Rev. Lett.*, vol. 98, p. 234501, 2007.

[125] L. Rodd, T. Scott, D. Boger, J. Cooper-White, and G. McKinley, "The inertio-elastic planar entry flow of low-viscosity elastic fluids in micro-fabricated geometries," *J. Non-New. Fluid Mech.*, vol. 129, pp. 1–22, 2005.

[126] A. Groisman, M. Enzelberger, and S. Quake, "Microfluidic memory and control devices," *Science.*, vol. 300, pp. 955–958, 2003.

[127] H. Park and W. Lee, "Helmholtz-smoluchowski velocity for viscoelastic electroosmotic flows," *J. Colloid and Inter. Sci.*, vol. 317, pp. 631–636, 2008.

[128] F.-M. Chang and H.-K. Tsao, "Drag reduction in electro-osmosis of polymer solutions," *Appl. Phys. Lett.*, vol. 90, p. 194105, 2007.

[129] M. Olivares, L. Vera-Candioti, and C. Berli, "The eof of polymer solutions," *Electrophoresis*, vol. 30, pp. 921–929, 2009.

[130] V. Steinberg, A. Uvkev, R. Kompaneets, and G. Morfill, "Shear instability in fluids with a density-dependent viscosity," *Phys. Rev. Lett.*, vol. 100, p. 254502, 2008.

[131] D. Smith, H. Babcock, and S. Chu, "Single polymer dynamics in steady shear flow," *Science*, vol. 283, pp. 1724–1727, 1999.

[132] D. Pine, J. Gollub, J. Brandy, and A. Leshansky, "Chaos and threshold for irreversibility in sheared suspensions," *Nature*, vol. 438, pp. 997–1000, 2005.

[133] R. Larson, "The rheology of dilute solutions of flexible polymers: Progress and problems," *J. Rheol.*, vol. 49, pp. 1–70, 2005.

[134] K. Hu, P. Ivanov, Z. Chen, P. Carpena, and H. Stanley, "Effect of trends on detrended fluctuation analysis," *PRE.*, vol. 64, p. 011114, 2001.

[135] A. Frankel, "How does the ground shake?," *Science*, vol. 283, pp. 2032–2033, 1999.

[136] R. A. Orwoll and Y. S. Chong, *Polyacrylamide, Polymer Data Handbook.* Oxford University Press, 1999.

[137] D. Allen and G. Pernica, "Control of floor vibration," *Construction Technology Update*, vol. 22, 1998.

[138] P. E. Arratia, G. A. Voth, and J. P. Gollub, "Stretching and mixing of non-newtonian fluids in time-periodic flows," *Phys. Fluids*, vol. 17, p. 053102, 2005.

[139] X. Huang, M. Gordon, and R. Zare, "Current-monitoring method for measuring the electroosmotic flow rate in capillary zone electrophoresis," *Anal. Chem.*, vol. 60, pp. 1837–1838, 1988.

[140] P. de Gennes, *Scaling Concepts of Polymer Physics.* Cornell University Press, 1979.

[141] C. Petrie, "Extensional viscosity: A critical discussion," *J. Non-Newton. Fluid*, vol. 137, pp. 15–23, 2006.

[142] J. C. W. McGary, "Degradation of poly(ethylene oxide)," *J. Poly. Sci.*, vol. 46, pp. 51–57, 1960.

[143] P. B. Wright, A. S. Lister, and J. G. Dorsey, "Behavior and use of nonaqueous media without supporting electrolyte in capillary electrophoresis and capillary electrochromatography," *Anal. Chem.*, vol. 69, pp. 3251–3259, 1997.

[144] S. H. Behrens and D. G. Grier, "The charge of glass and silica surfaces," *J. Chem. Phys.*, vol. 115, no. 14, pp. 6716–6721, 2001.

[145] J. Horvath and V. Dolnik, "Polymer wall coatings for capillary electrophoresis," *Electrophoresis*, vol. 22, no. 4, pp. 644–655, 2001.

[146] M. N. Albarghouthi, B. A. Buchholz, P. J. Huiberts, T. M. Stein, and A. E. Barron, "Poly-n-hydroxyethylacrylamide *polyduramide*^{TM}: A novel, hydrophilic, self-coating polymer matrix for dna sequencing by capillary electrophoresis," *Electrophoresis*, vol. 23, pp. 1429–1440, 2002.

[147] Y.-J. Juang, S. Wang, X. Hu, and L. J. Lee, "Dynamics of single polymers in a stagnation flow induced by electrokinetics," *Phys. Rev. Lett.*, vol. 93, p. 268105, 2004.

[148] G. C. Randall and P. S. Doyle, "Electrophoretic collision of a dna molecule with an insulating post," *Phys. Rev. Lett.*, vol. 93, p. 058102, 2004.

[149] P. M. Patterson and A. M. Jamieson, "Molecular weight scaling of the transport properties of polyacrylamide in water," *Macromolecules*, vol. 18, pp. 266–272, 1985.

[150] C. M. Kok and A. Rudin, "Relationship between the hydrodynamic radius and the radius of gyration of a polymer in solution," *Makromol. Chem. Rapid Commun.*, vol. 2, pp. 655–659, 1981.

[151] T. Otero and I. Cantero, "Electropolymerization of acrylamide at high current density in aqueous media," *Journal of Electroanalytical Chemistry*, vol. 395, pp. 75–81, 1995.

[152] A. Hickling and M. Ingram, "Contract glow-discharge electrolysis," *Transactions of the Faraday Society*, vol. 60, pp. 783–793, 1964.

[153] S. Sakka and T. Yoko, "Sol gel-derived coating films and applications," *Structure and Bonding*, vol. 77, pp. 89–118, 1992.

[154] D. Chamovska, M. Cvetkovska, and T. Grchev, "The kinetics of polyacrylamide adsorption on polycrystalline gold," *Croatica Chemica Acta*, vol. 81, pp. 461–466, 2008.

[155] J. R. Melcher and G. I. Taylor, "Electrohydrodynamics: a review of the role of interfacial stresses," *Annu. Rev. Fluid. Mech.*, vol. 1, pp. 111–146, 1969.

[156] C. Evenhuis and P. Haddad, "Joule heating effects and the experimental determination of temperature during ce," *Electrophoresis*, vol. 30, pp. 897–909, 2009.

[157] T. Nishikawa and H. Kambara, "Temperature profile of buffer-filled electrophoresis capillaries using air convection cooling," *Electrophoresis*, vol. 17, pp. 1115–1120, 1996.

[158] G. McKinley, P. Pakdel, and A. Oztekin, "Geometric and rheological scaling of purely elastic flow instabilities," *J. Non-Newt. Fluid Mech.*, vol. 67, pp. 19–48, 1996.

[159] Y. Heo and R. G. Larson, "The scaling of zero-shear viscosities of semidilute polymer solutions with concentration," *J. Rheol.*, vol. 49, pp. 1117–1128, 2005.

[160] P. Bernado, J. G. de la Torre, and M. Pons, "Macromolecular crowding in biological systems: hydrodynamics and nmr methods," *Journal of Molecular Recognition*, vol. 17, pp. 397–407, 2004.

[161] K. Tang and Z. Zhang, “Dissolution equation of polymer,” *Journal of Polymer Science Part B - Polymer Physics*, vol. 34, pp. 1175–1180, 1996.

[162] S. N. Bhadani and Y. K. Prasad, “Anodic gel polymerization of acrylamide,” *Journal of Polymer Science: Polymer Letters Edition*, vol. 15, pp. 721–728, 1977.

[163] T. Grchev, M. Cvetkovska, T. Stafilov, and J. Schultze, “Adsorption of polyacrylamide on gold and iron from acidic aqueous solutions,” *Electrochimica Acta*, vol. 36, pp. 1315–1323, 1991.

[164] H. Tanaka, “Viscoelastic phase separation,” *J. Phys.: Condens. Matter*, vol. 12, pp. R207–R264, 2000.

[165] C. Chen, H. Lin, S. Lele, and J. Santiago, “Hydrodynamic focusing on a silicon chip: mixing nanoliters in microseconds,” *J. Fluid Mech.*, vol. 524, p. 263303, 1998.

[166] K. Helton and P. Yager, “Interfacial instabilities affect microfluidic extraction of small molecules from non-newtonian fluids,” *Lab Chip*, vol. 7, pp. 1581–1588, 2007.

[167] G. Thurston, “Viscoelasticity of human blood,” *Biophysical Journal*, vol. 12, pp. 1205–1217, 1972.

[168] J. M. Ottino and S. Wiggins, “Introduction: mixing in microfluidics,” *Phil. Trans. R. Soc. Lond. A*, vol. 362, pp. 923–935, 2004.

[169] J. Knight, A. Vishwanath, J. Brody, and R. Austin, “Hydrodynamic focusing on a silicon chip: mixing nanoliters in microseconds,” *Phys. Rev. Lett.*, vol. 80, pp. 3863–3866, 1998.

[170] A. Stroock, S. Dertinger, A. Ajdari, I. Mezic, H. Stone, and G. Whitesides, “Chaotic mixer for microchannels,” *Science*, vol. 295, pp. 647–651, 2002.

[171] P. Pakdel and G. McKinley, “Elastic instability and curved streamlines,” *Phys. Rev. Lett.*, vol. 77, pp. 2459 – 2462, 1996.

[172] P. Arratia, C. Thomas, J. Diorio, and J. Gollub, “Elastic instabilities of polymer solutions in cross-channel flow,” *Phys. Rev. Lett.*, vol. 96, p. 144502, 2006.

[173] M. Funakoshi, “Chaotic mixing and mixing efficiency in a short time,” *Fluid Dynamics Research*, vol. 40, pp. 1–33, 2008.

[174] D. Rothstein, E. Henry, and J. Gollub, “Persistent patterns in transient chaotic fluid mixing,” *Nature*, vol. 401, pp. 770–772, 1999.

[175] P. Virk, “Drag reduction fundamentals,” *AlChE Journal*, vol. 21, pp. 626–656, 1975.

[176] A. Groisman and V. Steinberg, “Elastic turbulence in curvilinear flows of polymer solutions,” *NJP*, vol. 6, p. 29, 2004.

[177] T. Burghelea, E. Segre, and V. Steinberg, “Elastic turbulence in von karman swirling flow between two disks,” *Phys. Fluids*, vol. 19, p. 053104, 2007.

[178] P. Davidson, *Turbulence: An Introduction for Scientists and Engineers.* Oxford University Press, 2004.

[179] A. Fouxon and V. Lebedev, "Spectra of turbulence in dilute polymer solutions," *Physics of Fluids*, vol. 15, pp. 2060–2072, 2003.

[180] G. Batchelor, "Small scale variation of convected quantities like temperature in turbulent fluid," *J. Fluid Mech.*, vol. 5, p. 113, 1959.

[181] R. Sturman, J. Ottino, and S. Wiggins, *The Mathematical Foundations of Mixing.* Oxford University Press, 2006.

[182] P. Danckwerts, "The definition and measurement of some characteristics of mixtures," *Appl. Sci. Res.*, vol. 3, pp. 279–296, 1952.

[183] A. D. Stroock, S. Dertinger, A. Ajdari, I. Mezic, H. Stone, and G. Whitesides, "Chaotic mixer for microchannels," *Science*, vol. 295, pp. 647–651, 2002.

[184] A. Sudarsan and V. Ugaz, "Multivortex micromixing," *Proc. Nat. Acad. Sci.*, vol. 103, pp. 7228–7233, 2006.

[185] D. D. Carlo, "Inertial microfluidics," *Lab Chip*, vol. 9, pp. 3038–3046, 2009.

[186] J. Cank, *The Mathematics of Diffusion.* Oxford, Great Britain: Clarendon Press, second ed., 1975.

[187] A. Michelman-Ribeiro, F. Horkay, R. Nossal, and H. Boukari, "Probe diffusion in aqueous poly(vinyl alcohol) solutions studied by fluorescence correlation spectroscopy," *Biomacromolecules*, vol. 8, pp. 1597–1600, 2007.

[188] G. Taylor, "Diffusion by continuous movements," *Proc. London Maths Soc*, vol. 20, pp. 196–211, 1921.

[189] S.-S. Hsieh and Y.-C. Huang, "Passive mixing in micro-channels with geometric variations through μpiv and μlif measurements," *J. Micromech. Microeng.*, vol. 18, p. 065017, 2008.

[190] E. Yariv and K. Dorfman, "Electrophoretic transport through channels of periodically varying cross section," *Physics of Fluids*, vol. 19, p. 037101, 2007.

[191] Y. Lam, H. Gan, N. Nguyen, and H. Lie, "Micromixer based on viscoelastic flow instability at low reynolds number," *Biomicrofluidics*, vol. 3, p. 014106, 2009.

[192] T. Cubaud and T. Mason, "Folding of viscous threads in diverging microchannels," *Phys. Rev. Lett.*, vol. 96, p. 114501, 2006.

[193] L.Courbin, E. Denieul, and H. A. Stone, "Drag reduction fundamentals," *J. Stat. Mech: Theory and Exp.*, p. N10001, 2006.

[194] P. Arratia, G. Voth, and J. Gollub, "Stretching and mixing of non-newtonian fluids in time-periodic flows," *Physics of Fluids*, vol. 17, p. 053102, 2005.

[195] T. Niederkorn and J. Ottino, "Mixing of a viscoelastic fluid in a time-periodic flow," *J. Fluid Mech.*, vol. 256, pp. 243–268, 1993.

[196] C. Leong and J. Ottino, "Increase in regularity by polymer addition during chaotic mixing in two-dimensional flows," *Phys. Rev. Lett.*, vol. 64, p. 874877, 1990.

[197] E. Kjeang, N. Djilali, and D. Sinton, "Microfluidic fuel cells: A review," *J. Power Sources*, vol. 186, pp. 353–369, 2009.

[198] M. Munson, C. Cabrera, and P. Yager, "Passive electrophoresis in microchannels using liquid junction potentials," *Electrophoresis*, vol. 23, pp. 2642–2652, 2002.

[199] J. Ottino, *The Kinematics of Mixing.* Cambridge University Press, 1989.

[200] H. Park and W. Lee, "Effect of viscoelasticity on the flow pattern and the volumetric flow rate in electroosmotic flows through a microchannel," *Lab Chip*, vol. 8, pp. 1163–1170, 2008.

[201] K. Jensen and A. Lee, "The science and applications of droplets in microfluidic devices," *Lab Chip*, vol. 4, pp. 31N–32N, 2004.

[202] A. Groisman, M. Enzelberger, and S. R. Quake, "Microfluidic memory and control devices," *Science*, vol. 300, pp. 955–958, 2003.

[203] M. Prakash and N. Gershenfeld, "Microfluidic bubble logic," *Science*, vol. 315, pp. 832–835, 2007.

[204] S. Teh, R. Lin, L. Hung, and A. Lee, "Droplet microfluidics," *Lab Chip*, vol. 8, pp. 198–220, 2008.

[205] M. Oliveira, M. Alves, F. Pinho, and G. McKinley, "Viscous flow through microfabricated hyperbolic contractions," *Experiments in Fluids*, vol. 43, pp. 437–451, 2007.

[206] C.-K. Peng, S. Buldyrev, S. Havlin, M. Simons, H. Stanley, and A. Goldberger, "Mosaic organization of dna nucleotides," *PRE*, vol. 49, pp. 1685–1689, 1999.

[207] R. Nagarajan and R. Kavasseri, "Minimizing the effect of sinusoidal trends in detrended fluctuation analysis," *International Journal of Bifurcation and Chaos.*, vol. 15, pp. 1767–1773, 2005.

[208] Y. Liu, P. Cizeau, M. M. M, C. Peng, and H. Stanley, "Correlations in economic time series," *Physica A*, vol. 254, pp. 437–440, 1997.

[209] S. Leistedt, M. Dumont, J.-P. Lanquart, F. Jurysta, and P. Linkowski, "Characterization of the sleep eeg in acutely depressed men using detrended fluctuation analysis," *Clinical Neurophysiology.*, vol. 118, pp. 940–950, 2007.

[210] M. Kurnaz, "Detrended fluctuation analysis as a statistical tool to monitor the climate," *J. Stat. Mech.*, vol. 68, p. P07009, 2004.

[211] R. Govindan and H. Kantz, "Long-term correlations and multifractality in surface wind speed," *EPL*, vol. 68, pp. 184–190, 2004.

[212] K. Ivanova, M. Ausloos, E. Clothiaux, and T. Ackerman, "Break-up of stratus cloud structure predicted from non-brownian motion liquid water and brightness temperature fluctuations," *EPL*, vol. 52, pp. 40–46, 2000.

[213] A. Bashan, R. Bartsch, J. Kantelhardt, and S. Havlin, "Comparison of detrending methods for fluctuation analysis," *Physica A*, vol. 295, pp. 5080–5090, 2008.

[214] A. Goldberger, L. Amaral, L. Glass, J. Hausdorff, P. Ivanov, R. Mark, J. Mietus, G. Moody, C.-K.Peng, and H. Stanley, "Physiobank, physiotoolkit, and physionet: components of a new research resource for complex physiologic signals," *Circulation*, vol. 101, pp. e215–e220, 2000.

[215] M. Newman, "Power laws, pareto distributions and zipf's law," *Contemporary Physics*, vol. 46, pp. 323–351, 2005.

[216] K. W. K. and D. Francis, "Tempting long-memory - on the interpretation of dfa results," *Physiol. Meas.*, vol. 24, pp. N1–N7, 2003.

[217] D. Maraun, H. Rust, and J. Timmer, "Tempting long-memory - on the interpretation of dfa results," *Nonlinear Processes in Geophysics*, vol. 11, pp. 495–503, 2004.

[218] G. Smyth, "Employing symmetry constraints for improved frequency estimation by eigenanalysis methods.," *Technometrics.*, vol. 42, pp. 277–289, 2000.

[219] C. Chatfield, *The Analysis of Time Series.* Chapman & Hall, 2003.

[220] C. Granger and A. Hughes, "A new look at some old data: The beveridge wheat price series," *Journal of the Royal Statistical Society Series A-General*, vol. 134, pp. 413–28, 1971.

[221] J. Kantelhardt, E.Koscielny-Bunde, H. Rego, S. Havlin, and A. Bunde, "Detecting long-range correlations with detrended fluctuation analysis," *Physica A*, vol. 387, pp. 441–454, 2001.

Appendix A

Finding characteristic times with detrended fluctuation analysis

Finding characteristic response times is an important aspect in understanding a system. Due to the significance of finding such natural response times many techniques exist to measure characteristic times, with spectral and the related correlation methods being widely used approaches. A key advantage of Detrended Fluctuation Analysis is its ability to find crossovers between response time regimes and it is found that polymer relaxation times can be extracted from fluctuation data. Detrended Fluctuation Analysis also allows the identification of periodic signals, a familiar ability of spectral methods, and the frequency of waves emanating from a vibrating cylinder in a water tank are extracted. Due to the simplicity and power of Detrended Fluctuation Analysis this technique is an useful tool for finding characteristic times.

Detrended Fluctuation Analysis (DFA) measures the scaling behaviour of fluctuations in a time series [206]. The profile of a time series is created by integrating the time series (cumulatively summing prior values), and the fluctuations are calculated by dividing the profile into boxes with n samples (varying time windows) and finding the root-mean-square deviation from the local least-squares fit. Calculating the fluctuation F(n) over differing box size n and creating the log-log plot of F(n) versus n allows the scaling behaviour to be observed[1]. Linear regions correspond to power law scaling, $F(n) \propto n^{\alpha}$, with the scaling exponent α characterizing the correlation (e.g. $\alpha = \frac{1}{2}$ indicates white noise, $\alpha = \frac{3}{2}$ brown noise, $1 > \alpha > \frac{1}{2}$ positive correlation, etc.). The key property often sought by users of DFA is evidence for "fractal" behaviour, as characterized by α. However, crossovers between differing power law regimes can also be observed [206] and give characteristic measures of a signal (e.g. spacial scales or characteristic times). It has been found that oscillatory trends do effect DFA leading to crossovers [134, 207], which can be used to find the characteristic frequency of sinusoidal signals in a time series. Here, we study the use of DFA in finding characteristic times of time series data.

There has been increasing use of DFA since its original introduction to study subtle correlations in noncoding DNA sequences [206]. For example, markets [208], physiological processes such as brain waves [209], climate [210], wind speed [211] and cloud dynamics [212] have been studied by DFA. While novelty has been one reason for the increased application of DFA the beneficial factors include reduced sensitivity to various non-stationary effects [134] with simple and computationally inexpensive application. There has been several modifications to the method, however the original methodology performs well, can be compared to more studies in the literature, and is generally applicable and has results comparable to the various modifications [213]. Here we use the original method [206, 214] due to its simplicity and lack of assumptions.

The current focus on using DFA to measure power law scaling is due to its historic introduction [206] for this purpose and its apparent superiority to competing methods. However, like other power law studies [215], claims of fractal properties [216], power law behaviour [217], and long-memory [217] are often not fully supported by DFA and are instead assumed from impartial evidence. While DFA is more robust to trends than some methods correlation properties can be effected by trends [134] and care must be taken in analyzing

---

[1] Often to make use of log transformations variables are made dimensionless by dividing by a characteristic scale. However, in DFA this is not typically done and as pointed out by Cleveland [22] taking logs of values containing units is often done. In DFA scaling by a constant does not affect results, as differences between "boxed data" is probed.

data. Moreover, linear scaling on log-log graphs is not sufficient to demonstrate power law behaviour and, for example, log-normal distributions are not simple to distinguish from power law distributions and accurate determination of scaling parameters is difficult [215]. For these reasons (trend distortion of scaling behaviour, difficulty in establishing true power law behaviour, difficulty in extracting accurate scaling parameters) the use of DFA to characterize time series is not as clear and simple as initial promise suggests; in Ref. [216] it has been shown that spectral analysis of heart rate variability for diagnosing cardiovascular disease give results consistent with DFA yet is more easily interpreted, this despite a widely believed improvement in prognosis via DFA. The difficulty in robustly characterizing scaling behaviour with DFA suggests it is best used in conjunction with other information and approaches with its utility found on a case-by-case basis. These considerations suggest that DFA is more robust for finding crossovers and their associated characteristic times, as crossover locations depend on a *change* in scaling properties with the specific type and measured fluctuation values being unimportant.

The characteristic time t_{Char} is determined by finding the crossover c_x between power law scaling regimes on the log-log plot of the fluctuations versus box size and mapping it to the time domain:

$$t_{Char} = \Delta t 10^{c_x}, \tag{A.1}$$

where $1/\Delta t$ is the sampling rate of the times series.

A.1 Polymer relaxation times

The relaxation time of a polymeric liquid is a characteristic parameter that describes the elasticity by identifying the time it takes for stress to decay in the fluid [70, 2]. Measurement is typically done with macroscopic rheometers; particular experimental conditions can often differ from rheometric flows.

The elastic stress is caused by stretching of polymer coils which are transported in the fluid, introducing nonlinear memory effects that can give rise to instabilities [2]. It has been found that these instabilities can manifest themselves as (elastic) turbulence [31] and chaotic flows [21]. In Ref. [21] chaotic flow was observed in flows of polymeric liquids through serpentine channels, under steady forcing. By seeding the liquid with microspheres flow velocity data was collected (see Fig. 4.3, inset) which displays dramatic fluctuations.

DFA of the velocity data (Fig. 4.3) shows a linear scaling regime for large bin sizes. Visual inspection allows direct estimation of a crossovers at (1.2 ± 0.1) s between the linear region for large bins and a nonlinear region for small bins. Within this nonlinear region there is some suggestion of a crossover at (0.36 ± 0.04) s, however it is difficult to interpret the nonlinear region. The experimentally determined [21] relaxation time is 1.1 s, agreeing within error with the crossover between linear and nonlinear scaling. A slight divergence from power law like scaling can be seen between 2.0 and 2.5 in Fig. 4.3, and is likely a weak sinusoidal signal (see below and Ref. [134]) which may be due to vibrations in the experimental setting [135].

The first order (slowest mode) relaxation time is normally used to characterize polymeric liquids, due to experimental difficulties in finding higher order relaxation times, however a spectrum of relaxation times are expected. Zimm polymer theory [70] predicts that the p-th mode relaxation time λ_p is given by:

$$\frac{\lambda_p}{\lambda_1} = (\frac{1}{p})^{3\nu} \tag{A.2}$$

where λ_1 is the first order relaxation time and ν is the Flory solvent parameter (0.588 for a good solvent, and 0.5 for a theta solvent [70]). Assuming good solvent conditions [21], and using the first order relaxation time determined here, the second order relaxation time is calculated to be 0.35 s, in close agreement with the 0.36 s value found for the possible crossover within the nonlinear region. This agreement indicates a possible ability of DFA to find higher mode relaxation times. The theta solvent case of 0.42 s cannot be excluded, although our error is likely overestimated. The third order and higher relaxation times cannot be determined here due to the sampling rate and limited resolution of data.

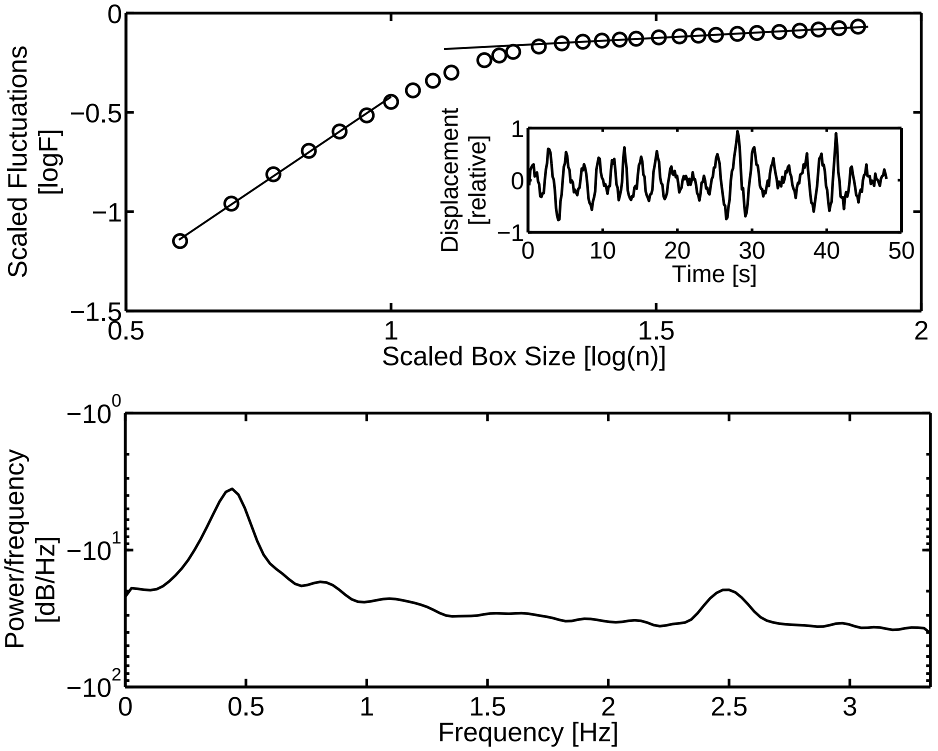

Figure A.1: Water waves. Vertical displacement of waves (top, inset) emanating from a cylinder suspended in a water tank, sampled every 0.15 s as reported in Ref. [33]. Detrended fluctuation analysis (top panel) of the displacement data indicates three power law regimes, with crossovers at 1.4 and 2.5 s. These crossovers correspond to peaks in the power spectrum (bottom panel) at 1.2 and 2.3 s. The high frequency peak is due to noise [33], and is below the resolution of detrended fluctuation analysis.

A.2 Oscillatory signals

To study the ability of DFA to find oscillatory signals we use data of waves emanating from a cylinder suspended in a water tank, measured by finding relative displacement [33]. Crossover times of (1.31 ± 0.84) s and (2.43 ± 0.23) s are found using linear regression on the DFA data, however here it is found that linear scaling does not well describe the middle regime and nonlinear curvature exists here. Visual inspection reveals that divergence from the linear regimes occurs at crossovers of (1.35 ± 0.15) s and (2.5 ± 0.4). Calculating the power spectrum using Welch's method reveals peaks at 2.3, 1.2, 0.9, and 0.4 s; the first two peaks agree with the values obtained by DFA, while the 0.4 s peak is below the resolution imposed on DFA by the requirement of boxing several data points together to enable fluctuations to be calculated. The peak at 0.9 s is broad and weak relative to the other peaks in the spectrum, but does not appear to be spurious. In Ref. [218] a number of characteristic times are given for this data, with values at (2.44 ± 0.13) s and (1.29 ± 0.08) s obtained by eigenanalysis with imposed symmetry constraints. Further values at roughly 4.85, 1.94, 0.87, and 0.43 s were found; the DFA results agree, however only two of the 6 reported values are revealed. The power spectrum finds 4 of the 6 values, the additional peaks found in Ref. [218] may be artifacts of the algorithms used, e.g. (0.87, 0.43) and (4.85, 2.44) form possible "Nyquist pairs". These additional peaks underscore the need of complementary tools and measures in time series analysis.

Using synthetic data we determine DFA can find sinusoidal signals in Gaussian noise with signal-to-noise ratios down to SNR $\approx 1/8$ (Fig. A.2). It can be seen in Fig. A.2 that when sinusoidal oscillations introduce a crossover in the DFA plot of noisy data that additional crossovers are introduced on either side of the crossover associated with the harmonic period, and that a bump shape appears in the plot which can be used to identify harmonics in noise (see Fig. 4.3); a careful discussion and analysis of the crossovers induced by harmonics can be found in Ref. [134].

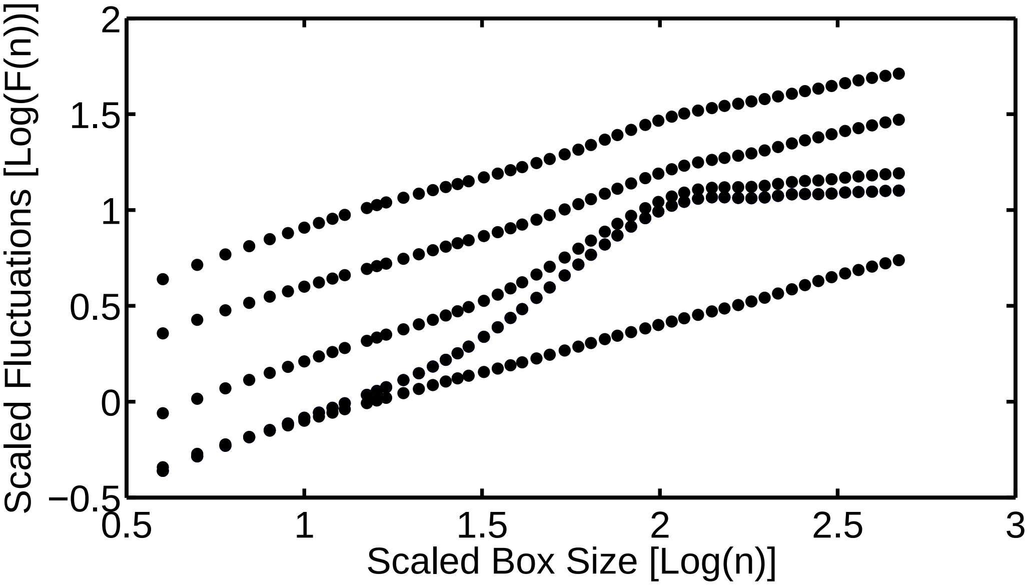

Figure A.2: Fluctuation scaling of noisy sinusoidal signals. DFA can accurately find periodic signals within noise with signal-to-noise ratios down to roughly 1/8. Here $sin(2\pi t) + \delta(t)$, with $\delta(t)$ being Gaussian noise with zero mean and unity standard deviation, Δt=0.01s, and time traces were 20 s long. From the bottom up: profile is of pure noise (SNR=0), SNR=1:2, SNR=1:8, SNR=1:50, SNR=1:200.

A.3 Oscillatory signals?

Time series analysis can be notoriously difficult [219]. A good historical example is Beveridge's wheat index data [33]. The index value itself is somewhat questionable, being an aggregate value that is only partially documented, never-the-less some 20 periods were identified [34] with an emphasized finding being an ≈ 15 year oscillatory cycle which is identified as a rainfall cycle. Later analysis [220] instead found this to be a 13.3 year period, and about 5 relevant peaks were identified. A difficulty is detrending the data without inducing artifacts in the spectrum as well as the visual identification of important spectral peaks. Investigating this data using DFA (see Fig. A.3) indicates the existence of two crossovers, corresponding to characteristic times of roughly 8 and 25 years, neither of which were identified as important in spectral studies. The

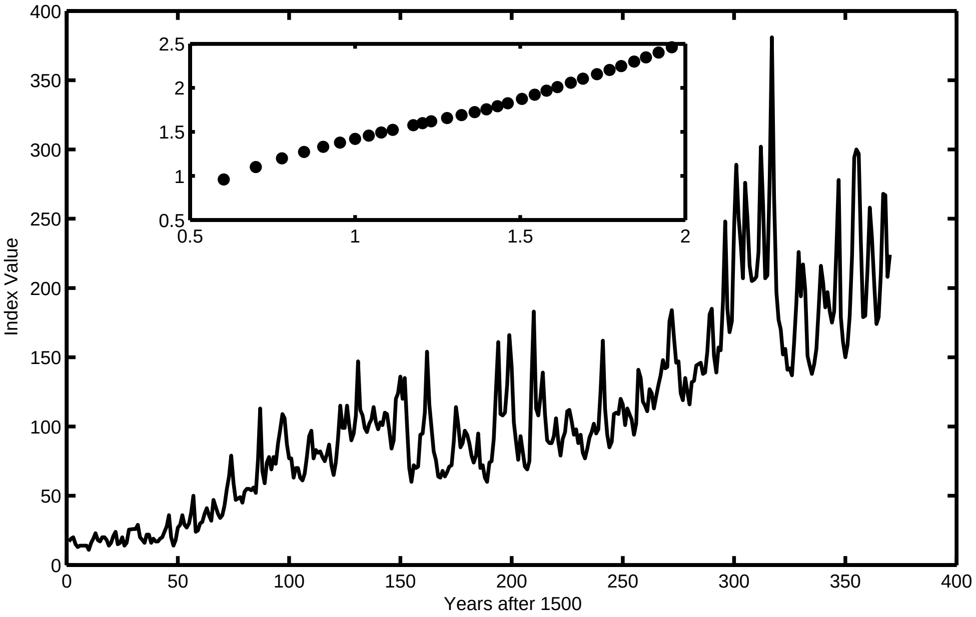

Figure A.3: Price of wheat in Europe aggregated in an index over the years 1500-1869. Using DFA (see inset) we find here that crossovers occur at roughly 8 and 25 years, neither of which correspond to peaks identified by spectral analysis. The 8 year value identified appears to correspond to the average time between spikes in the index value. This classic data [34] demonstrates the difficulty in interpretation of time series analysis.

mechanisms underlying these characteristic times is unclear[2], however the inability to identify times that spectral studies find suggests that the significance of the spectrally identified cycles is marginal.

A.4 Discussion

As DFA measures scaling behaviour of fluctuations instead of signal harmonics, properties such as polymer relaxation time can been seen, as observed in Fig. 4.3, despite the power spectrum not displaying any peaks [31]. This complimentary information is a key advantage of using DFA in conjunction with other techniques. As seen in Fig. A.1 strong harmonics can also be identified, due to the effect of the sinusoidal trend on the fluctuation calculation,

---

[2] Simply counting index spikes in the data over time intervals suggests they occur roughly every 8 years.

and compared with the power spectrum in finding the strongest frequency components. Such dual identification can help reduce subjectivity and bias.

The possible ability to find higher order relaxation mode times directly from experimental data is a particularly desirable feature, as competing methods require assumptions and data fitting procedures [2] in order to estimate higher order relaxation times. It must be stressed that this possibility is not well supported, and must be considered only suggestive and more investigation is required to establish if this possible crossover is legitimate, or simply a visual artifact that agrees with the second order relaxation time by coincidence.

Note that previous studies [213, 221] on synthetic data found that DFA overestimated crossovers of noisy sinusoidal time series, requiring scaling by about exp(-0.25) in order to agree with true crossover times [213]. The scaled polymer relaxation time of 0.93 s is within the error bounds here, however our error is likely overestimated due to the shallow change in slope between regimes, simply finding crossovers and estimating error "by eye" gives similar values but with error $\approx 4\times$ smaller, which excludes the scaled value. Inspection of Fig. A.2 suggests that the scale factor of exp(-0.25) required to find true crossovers in Ref. [213] results from a differing methodology in selecting the crossover. We fit in linear regions away from the crossover and find the intersection. Due to curvature near the crossover and "overshoot" in the fluctuation scaling before settling back to a linear section the crossover location suggested visually occurs at a later time than the intercept selected crossover. This overshoot indicates that having sufficient data on both sides of the characteristic time of a harmonic is important, but can be accurately estimated using the scaling factor determined in Ref. [213] by finding the peak of the overshoot.

A weakness of DFA is the requirement for consistent power law scaling over a wide range of box sizes (time windows), and significant change in scaling behaviour, in order to establish a crossover. If processes are not characterized by such scaling finding crossover points becomes difficult, although the shape of the fluctuation scaling profile gives valuable information. A further weakness is that characteristic times are found from crossovers that are raised to a power, equation A.1, resulting in amplification of error and limiting achievable accuracy.

A.5 Conclusion

The use of Detrended Fluctuation Analysis to find characteristic system times is straightforward [206]. The ability shown here to measure polymer relaxation times from fluctuation data is a valuable addition to the existing techniques, as it allows a robust estimate of relaxation time in experimental conditions without the use of any free parameters or assumptions. The ability to find oscillatory signals, akin to Fourier analysis, is useful when a small number of dominant frequencies exist and provides information to compare with spectral approaches. Extracting characteristic times of waves from water tank data was achieved with DFA, and it was found that DFA is comparable to Fourier approaches in finding the most significant oscillatory components. Using synthetic data demonstrates DFA can find sinusoidal signals in noise with signal-to-noise ratios down to $\approx 1/8$. A key difficulty in using DFA is discriminating where crossovers occur. As DFA is simple to perform and can be compared and contrasted to other approaches the technique is an useful tool for exploratory data analysis and characterization of systems.

Appendix B

Cleaning Process

> *It is important to have clean surfaces in order to obtain a consistent working environment, prevent optical distortion, and reduce the possibility of contamination of samples. All glassware and related items were cleaned prior to use, and special care was taken to clean the microchannels before and after experiments.*

Cleaning of microchips consisted of an external cleaning (isopropyl alcohol followed by water) to ensure dust or other debris or residue would not lead to poor optical views, followed by microchannel/electrode cleaning.

To clean microchannels a simple acid:base protocol was used, where two water fill of resivours and channels, then (roughly 1 M) nitric acid, then NaOH (roughly 1 M), then two more water fills. Each fill step was followed by a ≈ 5 minute "soak" of the microchip and with electrodes lowered into the resivours and then followed by a vacuum pump out step. Finally a gentle wipe of electrodes with wetted then dry lab tissue was done. The final dry wipe is used in order to wick any water left between the electrode and the plastic holding sleeve. Water was "overfilled" until water beaded up in the resivours, to ensure that no harsh acid or base was left behind. Cleaning was done both before and after use of the μTK.

Plastic resivours made by cutting plastic pipette tips off at the base and epoxying the base to the glass microchip were used for longer runs, these plastic resivours received the same cleaning protocol and when first attached were left for a minimum of 12 hours to ensure complete setting of the quick dry epoxy.

Rigorous cleaning is required in order to prevent the formation of bubbles upon fill of final working fluid, repeatability of electroosmotic flow conditions, and post cleaning to prevent polymer dying on the inner microchannel surface (initial solvation of dry polymer takes on the order of a day, leading to fairly robust dried films if polymer doped solutions are left to dry on electrodes, glass, etc.).

All glassware used was cleaned prior to use with alcohol and repeatedly with distilled water and dried.

Occasional running flows with polymer-free solutions was performed to allow flow to be visually checked, to ensure slow plaguing of surfaces did not occur and to "burn off" any possible absorbed polymer films from electrodes.

Appendix C

Microfluidic Toolkit: the μTK

> *Electro-osmotic experiments were undertaken with a MicraLyne Inc. microtoolkit (μTK) apparatus. This "off the shelf" platform electrically pumps liquids, has a microscope objective allowing visual interrogation of flows, and is controlled via provided software.*

The μTK is a platform for electrokinetic microfluidics, used for driving electrophoretic and electroosmotic flows. The apparatus consists of an high voltage power supply that supplies a voltage (up to 6 kV) to platinum electrodes located on a lowerable assembly. A microchip can be set in a machined plexiglas holder below the electrode assembly, below which a 40X microscope objective is positioned allowing imaging of microchannels. The optics module consists of an epiluminescent confocal microscope allowing fluorescent excitation and either visual inspection by eye or by a photomultiplier tube (PMT)[1] which can be swung and held in the optical path. Removing the eyepiece allows a camera to be attached using a custom machined connector and an optical adaptor (camera-to-microscope).

During use the μTK was placed on an anti-vibration table to prevent mechanical environmental noise from affecting optical measurements.

The optical module has an internal 532 nm diode laser[2], a beam splitter, and various lenses in an enclosure. Opening the module for dusting and cleaning of optics has the hazard of possibly throwing the laser feedback set point

---

[1] Hamamatsu H5773-03 PMT

[2] Alternatively, an 635 nm laser option option existed

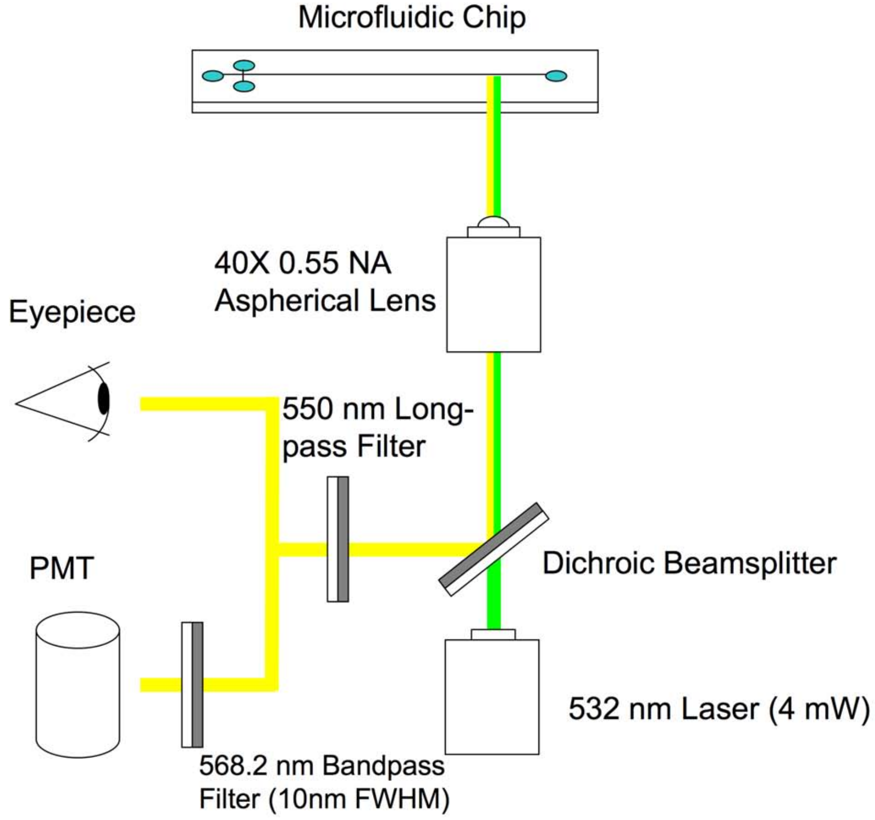

Figure C.1: MicroTool Kit Optics Diagram. The MicraLyne Inc. μTK allows optical observation either by eye piece or with a PMT.

off, as the optical diode used to provide feedback is sensitive to position and can be easily jarred during dismantling the optics module.

The internal laser can be either focused into an ≈ 10 μm beam waist focal spot, or expanded to ≈ 300 μm wide beam for broad illumination of channels. Due to dust on the expansion lens, lens imperfections, and high modulation of the Gaussian like field use of an external laser for illumination of channels was used for creating xt-diagrams.

The software provided allows electrode voltages to be set to a given level for a given time duration, with the ability to set multiple steps. The internal laser and PMT can be turned on/off, with a constant bias on the PMT. The data collection frequency can be selected between 25 and 50 Hz (higher rates are possible, however the PMT only outputs at 50 Hz making the higher rates irrelevant). On turning on the laser feedback is initiated, with the precise output power of the laser being locked-in to a level that can differ between runs. Data can be output in a text file; an error in the software inserts blank lines in the electrode potential value field occasionally, resulting in offset which must be corrected with a script or by hand. Occasionally[3] setting feedback on an electrode fails and the potential will be low (positive, but near 0 V) - this makes long multistep control programs prone to failure.

Micralyne Inc. has discontinued distribution and dedicated support of the μTK.

---

[3] perhaps a 5 % chance

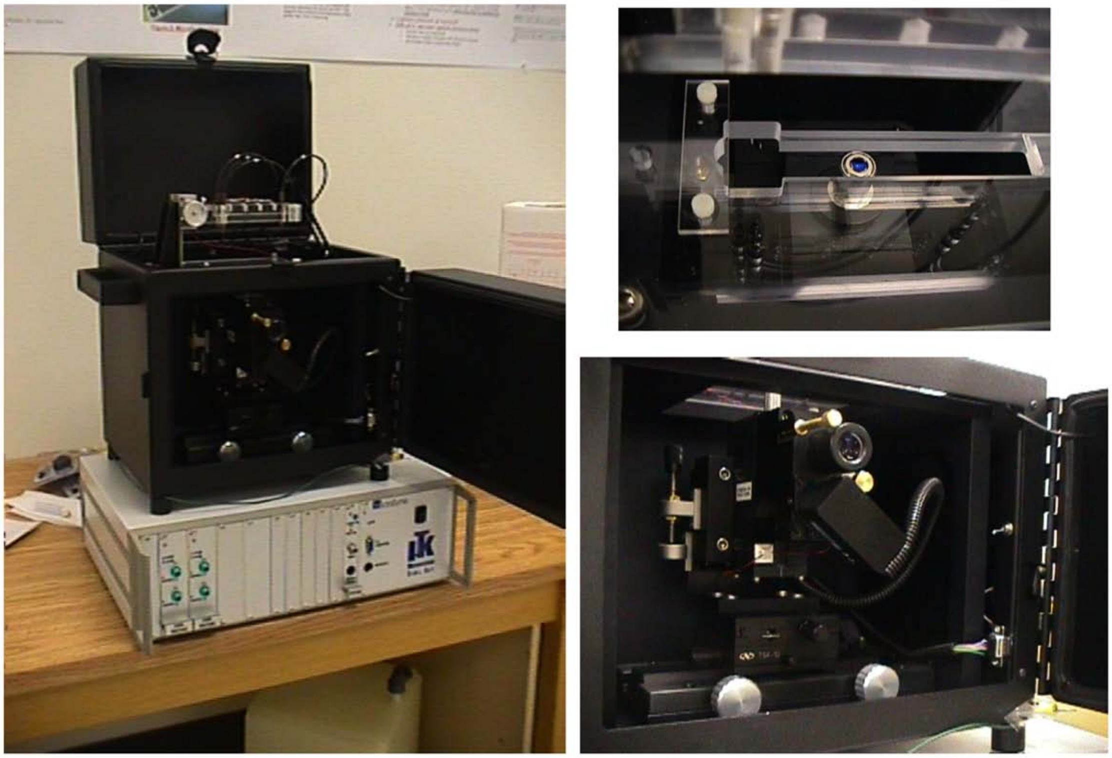

Figure C.2: The μTK Apparatus. The μTK is a platform for electrokinetic microfluidics. The apparatus consists of an high voltage power supply that supplies a (software) set voltage to platinum electrodes which are located on a lowerable assembly. A microchip is set in a machined plexiglas holder below the electrode assembly, below which a 40X microscope objective is positioned allowing imaging of microchannels. The optics module is an epiluminescent confocal microscope allowing fluorescent excitation (images courtesy of Micra-Lyne Inc.).

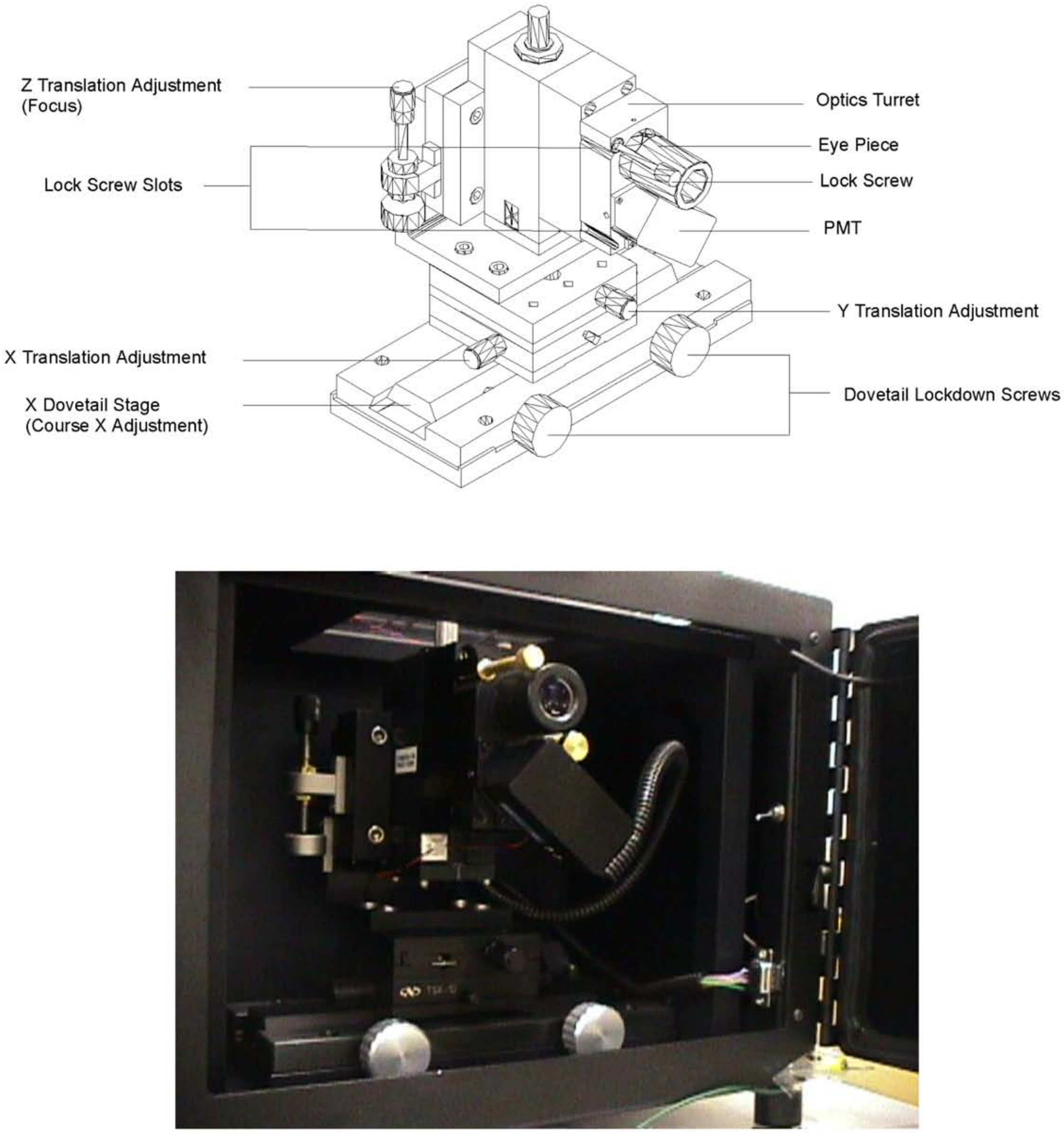

Figure C.3: The μTK optics module. The observation heart of the μTK is the epiluminescent confocal microscope which induces and captures laser induced fluorescence detection by exciting TAMRA dye via a 532 nm laser (schematic and image courtesy of MicraLyne Inc.).